THE ~~STRUCTURE~~ STUDY OF ~~THE~~ SLUMP SHEETS IN THE LUDLOW SERIES OF EAST CENTRAL WALES

BY

NIGEL HOWARD WOODCOCK

A thesis submitted for the degree of
Doctor of Philosophy in the University of London

Department of Geology
Imperial College
London S.W.7

September 1973

ABSTRACT

A review of previously published literature on submarine slumping reveals that slump structures have been inadequately described and that their directional significance has been poorly understood. The aim has been to clarify these points with reference to the Ludlovian slump structures of East Central Wales and the adjacent Borderland, particularly by analogy with structures formed by tectonic processes.

The slump deposits are grouped into two main sequences, which have been analysed by regional sampling and detailed local field mapping. Each sequence comprises interlayered slumped and undisturbed sediments. The slumped units display a range of internal structure from which a sequence of development has been deduced. The slump folds show a similar range of shape and style to tectonic folds and are commonly recumbent with sub-horizontal axes. There has been a significant buckling component during their formation. Folds sometimes have an axial plane cleavage. The slumped units also show conjugate cleavages which are attributed to compaction after deformation. The attitude of all structures is symmetrically related to the depositional datum. Methods of estimating the palaeoslope trend and direction are applied to the sheets, and their accuracy and reliability are examined. These provide confimation that the two slump sequences lay on opposite sides of the 'Montgomery Trough' of Ludlow times.

Theoretical analysis shows that earthquakes would have been necessary to induce failure of slump sheets. Subsequent downslope movement would only have occurred in sheets with porosities higher than a certain critical value. Only a small proportion of these sheets would then have travelled appreciable distances before reaching velocities sufficient for transformation into turbidity currents. Most remaining sheets would have been brought to rest on, or at the base of, the slope, with the consequent formation of a 'rise' area. Field evidence suggests that turbidity currents must have flowed along-slope on the rise, and some theoretical justification for this is provided.

ACKNOWLEDGEMENTS

The slump structures of Central Wales were first brought to my attention by Dr. J.E. Treagus of Manchester University. He put me in touch with Dr. R.J. Bailey of the University College of North Wales, whose suggestion of suitable slump localities in the region was a great help during the initial stages of field work.

The project has been supervised by Prof. J.G. Ramsay, for whose inspiration in the field of Structural Geology I am extremely grateful.

My thanks also go to Dr. and Mrs. C.G. Johnson for providing accommodation in the field, to Dr. W. Owens of Birmingham University for determining magnetic anisotropies, to M. Casey and Dr. A. Siddans for help with parts of the computing, and to these and other colleagues at Imperial College, especially Dr. P. Cobbold, I. Allison and R. Kerrich, for valuable discussion of my research. Finally, without the constant support of my wife Toni, this work would not have been possible.

CONTENTS

PART I INTRODUCTION 1

CHAPTER 1 THE SCOPE AND ORGANISATION OF THE THESIS 2

CHAPTER 2 SLUMPING - A LITERATURE REVIEW 3

2.1 Introduction 3

2.2 The origin of the slumping concept 3

2.3 The slump controversy in Britain 7

2.4 Slump structure types 9

2.5 Directional data from slump sheets 17

2.6 Evidence for slumping on the present sea floor 22

2.7 Conclusion 23

CHAPTER 3 THE CENTRAL WELSH LUDLOVIAN SLUMPS - AN INTRODUCTION 26

3.1 General geology 26

3.2 Regional structure 27

3.3 The basin slumps 28

3.4 The shelf slumps 31

3.5 Basin geometry 32

PART II FIELD STUDIES - THE INTERNAL STRUCTURE OF THE SLUMP SEQUENCES 36

CHAPTER 4 THE EASTERN SEQUENCE : CWM BLITHUS 37

4.1 Location and description of the succession 37

4.2 Thickness of the constituent units 43

4.3 Orientation of structures 45

4.4 The estimation of palaeoslope trend and its variability 49

4.5 Determination of slump movement direction 54

4.6 Fold attitude and size 58

4.7 Fold style : surface shapes 61

4.8 Fold style : layer geometry 66

4.9 Deformed lineations and minor structures 69

4.10 Lineations 73

4.11 Fabrics 77

CHAPTER 5 THE EASTERN SEQUENCE : OTHER AREAS 81

5.1 The area within and to the west of the Wye Valley 81

5.2 The area between the Wye Valley and Radnor Forest 84

5.3 Cwm-y-Bont 85

5.4 The Radnor Forest area 91

5.5 The Bishops Castle area 94

CHAPTER 6 THE WESTERN SEQUENCE 95
6.1 The Teme Valley section : an introduction 95
6.2 Orientation of structures 96
6.3 Estimation of palaeoslope attitude 100
6.4 Fold geometry 101
6.5 Lineation and cleavage 105
6.6 Other localities in the Western Sequence 108
6.7 Slump sheets near Llangunllo 110

CHAPTER 7 THE SHELF SLUMPS 113
7.1 Mode of occurrence 113
7.2 The Gatley Coppice sequence 114

CHAPTER 8 SUMMARY AND DISCUSSION OF FIELD RESULTS 116
8.1 Summary of results 116
8.2 The sequence of development of structures 117
8.3 Criteria for distinguishing slump structures from tectonic structures 122

PART III THEORETICAL STUDIES - THE TRANSLATION OF SLUMP SHEETS 126

CHAPTER 9 INITIAL STATE OF THE SEDIMENT 127
9.1 Values of sediment parameters 127
9.2 Notes on parameter estimates 127
9.3 Estimation of excess pore pressure due to sedimentation 129

CHAPTER 10 THE INITIATION OF SLUMPING 133
10.1 Mode of slump failure 133
10.2 Slope stability 134
10.3 Influence of earthquakes 136
10.4 Field evidence supporting earthquake initiation 138

CHAPTER 11 POST-FAILURE MOVEMENT OF A SLUMP SHEET 142
11.1 Equations of motion 142
11.2 Critical porosity 143
11.3 Development of the rigid sheet model 146
11.4 Criticism of the rigid sheet model 148

CHAPTER 12 THE FINAL POSITION OF THE SHEETS 150
12.1 Introduction 150
12.2 Distance of travel for the slope/floor profile model 150
12.3 True profile of the Montgomery Trough 153

CHAPTER 13 SUMMARY OF THEORETICAL ANALYSIS OF SHEET MOVEMENT 157
13.1 Summary of results 157

APPENDICES 159

APPENDIX 1 THE ACCURACY OF FIELD ORIENTATION MEASUREMENTS 160

A1.1 Introduction 160

A1.2 Theoretical determination of accuracy 160

A1.3 Practical tests of accuracy 169

A1.4 Conclusion 173

APPENDIX 2 GRAPHICAL REPRESENTATION OF ORIENTATION DATA 174

A2.1 Introduction 174

A2.2 The Watson method 174

A2.3 Synoptic plot of distribution attitude 175

A2.4 Synoptic plot of distribution shape 177

APPENDIX 3 THE DATA ANALYSIS PROGRAM - STATIS 182

A3.1 Program capability 182

A3.2 Program design 182

A3.3 Data input instructions 183

A3.4 Storage and time requirements 185

A3.5 Program listing 186

LIST OF REFERENCES 208

PART I

INTRODUCTION

CHAPTER ONE

THE SCOPE AND ORGANISATION OF THE THESIS

Rock structures have traditionally been subdivided according to their relative time of formation: 'sedimentary structures' are formed during or shortly after deposition of sediments, while 'tectonic structures' are formed after their burial and consolidation. Consequently 'slump structures' - formed by deformation of unconsolidated sediment on a depositional slope - are classified as sedimentary structures. This is unfortunate because they have little morphological similarity to depositional sedimentary structures, and are formed by a fundamentally different mechanism. They do appear, however, to be analogous to some tectonic structures. The aim of this thesis is to explore this analogy, with particular reference to the Ludlovian slump structures of East Central Wales and the adjacent Borderland.

The remaining chapters of Part I describe the previous research on slumping in general, and on the slumps and regional geology of the Central Welsh Ludlovian in particular. Part II comprises a detailed description of the geometry of the slump structures. Emphasis has been placed on the fold styles, and on the relationship of structure orientation to the palaeoslope. Although examples of structures are taken from most of the good slump exposures in the region, this is not intended as a comprehensive guide to slump localities. A regional map is provided (Enclosure 1) which fulfils this purpose. The field studies give little information on the bulk translation of slump sheets. Part III attempts to analyse this theoretically, and examines the consequences of sheet movement on basin geometry. Three appendices deal with the field measurement of orientation data and their subsequent analysis and representation.

The descriptions adhere to the structural terminology of Ramsay (1967, Chap. 4) except where otherwise stated. Lower hemisphere equal area projections have been used throughout.

CHAPTER TWO

SLUMPING - A LITERATURE REVIEW

2.1 INTRODUCTION

Slumping is the failure and downslope gravity transport of sheets of unconsolidated sediment, in which the primary sedimentary structures are more or less deformed, but not totally destroyed. Slumping was first invoked as a possible geological process at the beginning of this century, but its importance was not generally recognised until the late 1930s. With the upsurge of interest in basin analysis in the last twenty years, slump structures have assumed a new importance as palaeoslope indicators.

The resultant mass of literature has, of necessity, been reviewed selectively. Emphasis has been placed on the historical evolution of the slumping concept and on subsequent field observations of slump structures. Recent theoretical work on the mechanics of slumping has not been reviewed. This is adequately described in papers by Terzaghi (1957), Moore (1961), Dott (1963), Morgenstern (1967) and Sturm (1971). No mention is made of structures whose slump origin is doubtful. These include convolute lamination, almost certainly a syn-depositional structure, and deformed cross bedding, which probably originates mainly by current drag (Allen et al. 1972). Lastly only important contributions have been selected from the early German literature, much of which is cited by Beets (1946).

2.2 THE ORIGIN OF THE SLUMPING CONCEPT

Although nineteenth century geologists described zones of complex folding within otherwise undeformed sedimentary sequences, they generally regarded these as minor tectonic structures. Logan (1863), though supporting a tectonic origin for structures at Cape Gaspé, Quebec (Fig. 2.1), did recognise the penecontemporaneous nature of the deformation. He deduced that the layers "after their deposit had been contorted by lateral pressure, the underlying strata remaining undisturbed, and had then been worn smooth before the deposition of the next bed".

A penecontemporaneous origin was also postulated by McGee (1891) for Devonian structures in Iowa. He advanced "a useful even though far-fetched hypothesis" that (p. 323) "the fresh formed sediments upon

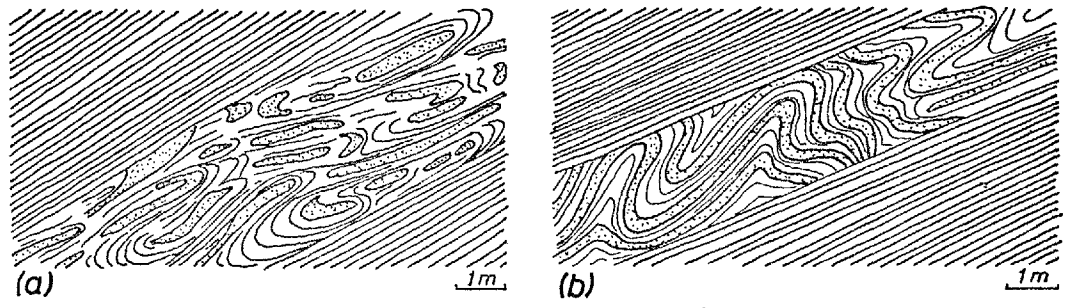


FIGURE 2.1 Slumped units in the Devonian Gaspé Limestone, Quebec (after Logan 1863).

the sloping flanks.....settled slightly seaward down the prevailing slope". He deduced that (p. 351) "the strata at some distance from the shoreline must have been compressed horizontally, perhaps buckled and crumpled, and thrown into anticlinal and synclinal folds concentric with the shore". This was apparently the first explicit statement of the slumping process.

The process of submarine slumping remained virtually unrecognised until interest was aroused by descriptions of slumping in recent sediments. Milne (1897) recorded the severing of submarine telephone cables, and attributed this to 'submarine landslides' triggered by earthquakes. Heim (1908) described two recent slides of Swiss lake sediments. Although the slides were probably mudflows rather than

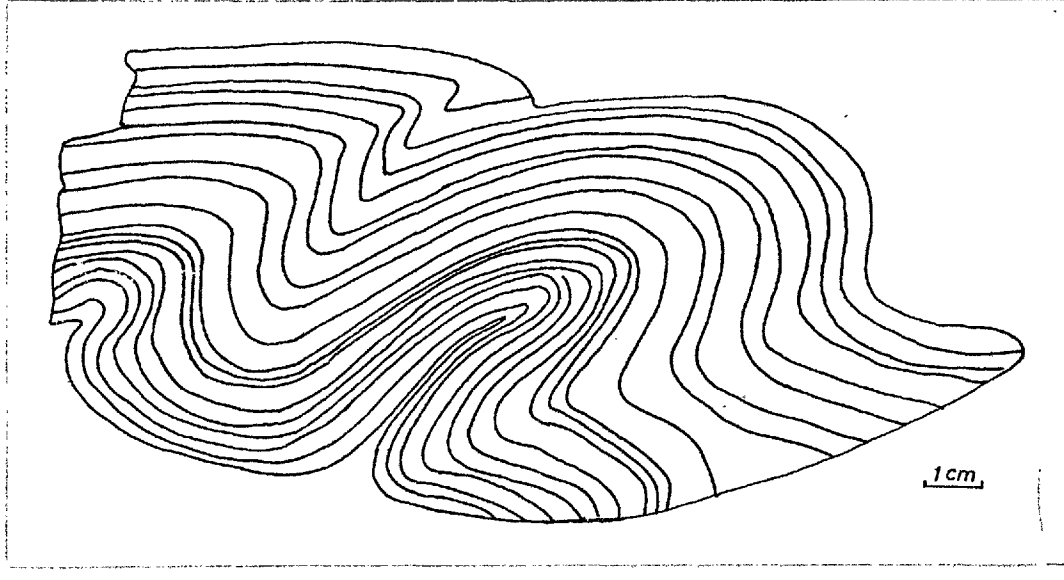


FIGURE 2.2 A slump fold from the Miocene marls of Oeningen (after Heim 1908, plate XIII).

true slumps, they provided clear evidence that unconsolidated sediments could be unstable on very gentle slopes (in these cases as low as 2.5°). Heim figured structures from the Miocene marls of Oeningen (Fig. 2.2) which he attributed to this 'submarine solifluction' process.

Heim's description stimulated the re-interpretation of other 'intraformational contortions'. Reis (1909) recognised the slumps in the German Muschelkalk (Fig. 2.3). Grabau (1913, p. 782) correctly re-interpreted Logan's Cape Gaspé structures (Fig. 2.1). Hahn (1913) recognised as typical slump structures the folds in the Trenton Limestone, New York (Fig. 2.4), previously attributed by Miller (1908) to the effects of thrusting. Brown (1913) and Norton (1917) recognised the slump origin of some breccias and conglomerates.

The explanation of intraformational folds by slumping was not unopposedly accepted. Miller (1915,1922) still supported a tectonic origin for the Trenton Limestone structures, and even for structures

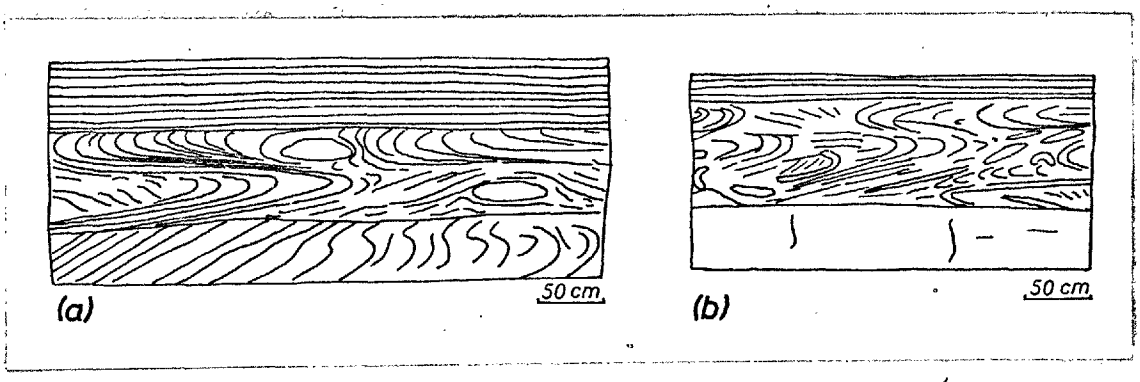


FIGURE 2.3 Slump sheets in the Muschelkalk of Germany (after Reis 1909).

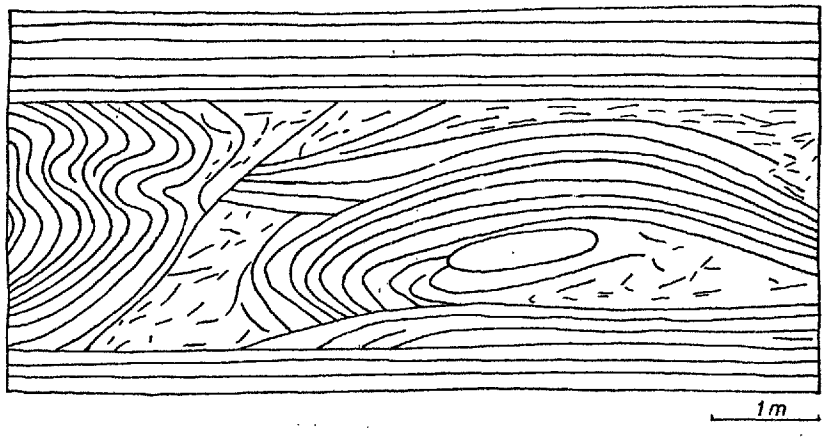


FIGURE 2.4 Slump folds in the Trenton Limestone, New York (after Miller 1908, Fig. 1).

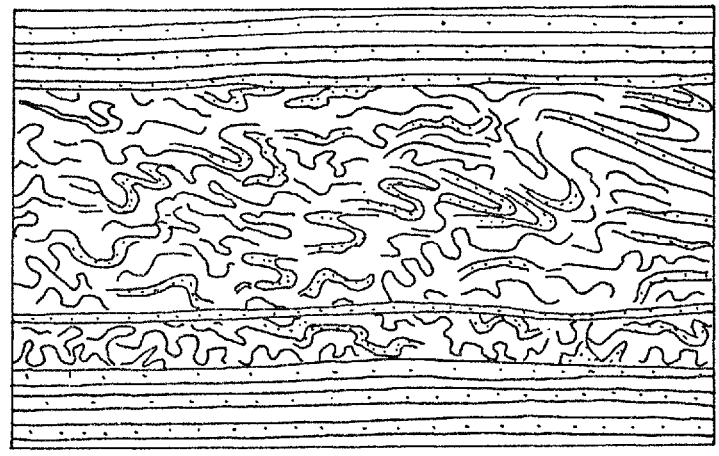


FIGURE 2.5 Slump structures in Pleistocene varved clays and silts, Northampton, Mass. (after Miller 1922, Fig. 6).

in Pleistocene varved clays (Fig. 2.5) could see no evidence for penecontemporaneous deformation:- "It seems impossible to explain intraformational contorted clays.....except as a result of differential movements after the clays overlying the contortions were deposited". Such structures had also been attributed to grounding of ice-flows or to glacier advance (e.g. Sussmilch et al. 1920). This controversy continued for another 25 years (see review by Fairbridge 1947), before the slump origin of many Pleistocene structures was generally accepted.

The other contemporary misinterpretation of slump structures (e.g. Bradley 1931, p. 26) was as products of "the differential movements and readjustments within and between beds after burial, and during compaction of the sediments".

By the early 1930s, however, the importance of submarine slumping was widely recognised by American and Continental geologists and De Terra (1931) and Hadding (1931) gave the first analyses of the initiation and deformation of slump sheets. British geologists at this time were still virtually unaware of the idea. E.B. Bailey et al. (1928) did apply a 'submarine landslip' hypothesis to breccias near Quebec City, and (Bailey et al. 1932) to Kimmeridge conglomerates in Sutherland, as did Henderson (1935) to Ordovician structures in the Girvan district. But the hypothesis of submarine slumping was to be brought forcefully to the attention of British geologists by a controversy over the origin of 'intraformational disturbances' in the Welsh Silurian.

2.3 THE SLUMP CONTROVERSY IN BRITAIN

In 1922 L.J. Wills had recorded 'internal crumpling' in Ludlow rocks near Llangollen, North Wales, and noted that "a bed preserves its upper and lower surfaces subparallel and seemingly undisturbed, while within there is folding and even overfolding". Wedd et al. (1927 p. 100) thoght it "most probable that.....folding and contortion were produced soon after deposition", but admitted that " they may have been brought about by the cleavage movements". P.G.H. Boswell (1926, p. 568, 1928 p.706) noted similar structures in Denbighshire, but had no doubt that they were tectonic. In 1932, Boswell described a thick sequence of these disturbed beds which had apparently been thrust over underlying beds, to produce a Schuppen or imbricate structure.

At this time S.H. Straw was mapping an area of Ludlow rocks, near Builth in Central Wales, which contained intraformational folding. In 1933 he showed these structures to O.T. Jones, who noticed that the folds were truncated at the upper surface of the deformed unit, which showed an erosional contact with the overlying undisturbed bed (Fig. 2.6). This conclusively proved that the deformation was penecontemporaneous with deposition. When Boswell (1935a,b) published photographs of the Denbighshire structures, Jones noticed their similarity to those at Builth, and a field examination confirmed this. Jones could not convince Boswell of their non-tectonic origin, and began mapping the area himself to obtain further evidence.

Jones read the results of his investigation in June 1936, and



FIGURE 2.6 Undisturbed unit between two slumped units. The upper contact of the lower unit is erosional. Ludlovian south of Builth, Central Wales (Llandewi'r Cwm, SO 036488).

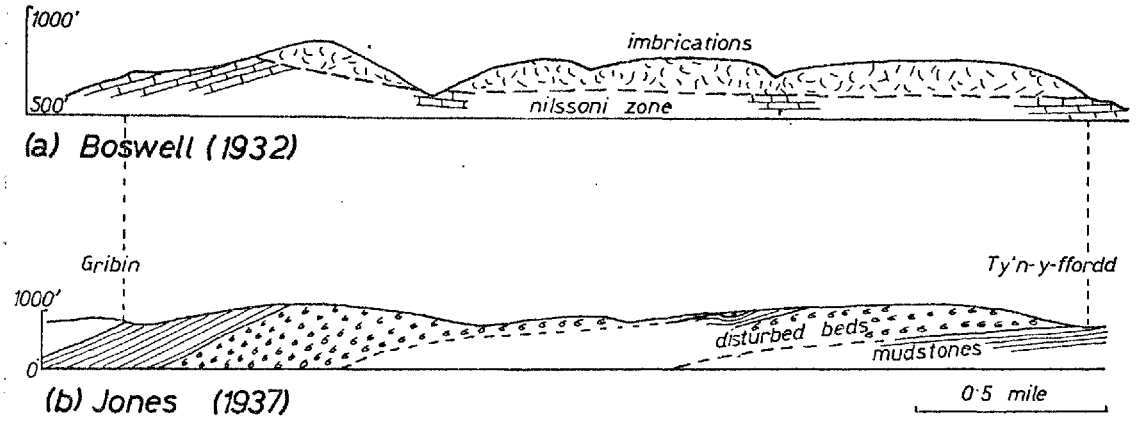


FIGURE 2.7 Two conflicting interpretations of the 'disturbed series' near Llangerniew, Denbighshire (A) after Boswell (1932) (B) after Jones (1937).

concluded "that the disturbed beds are primarily the result of recurrent sliding or slumping of the mudstones on the sea-floor during the Lower Ludlow period, and that they now occur as intercalations at several horizons in a great stratigraphical sequence of Lower Ludlow mudstones". He showed how the slump sheets could be mapped as distinct lithological units within an otherwise monotonous sequence. Jones' interpretation was completely incompatible with Boswell's 'thrust tectonics' hypothesis, as is clearly shown by comparison of their respective cross-sections of the main disturbed zone (Fig. 2.7). Boswell (in discussion, Jones 1936) remained convinced that the structures were tectonic.

In December 1936 Straw read his description of the slump structures of the Builth area (Straw 1937). In the discussion (p. 454) Boswell agreed that the structures were non-tectonic and were probably due to "penecontemporaneous or contemporaneous sliding", but they appeared to him "to differ in character from the disturbances.....of north west Denbighshire".

Boswell presented the evidence against the slump hypothesis in January 1937. While not explicitly rejecting his thrust tectonics hypothesis he admitted (1937, p. 299) that "the passage upwards from normal deposits into highly disturbed beds is gradual and suggests that the strata were in a plastic condition when they were disarranged". He suggested that some of the structures were produced by tectonic compression of 'soft' sediments, others by deformation associated with dip-slip faults, and some small scale examples by "what may be

interpreted as contemporaneous slipping of sediments due either to sliding.....or to differential compaction".

During the next three years Boswell showed some limited acceptance of the slump hypothesis. Describing other areas in Denbighshire he thought (Boswell et al. 1938, p. 292) the disturbances "in part at least to be contemporaneous with the formation of the deposits", and observed (Boswell et al. 1940, p. 185) "it is often difficult to distinguish the effects of later movements from those due to contemporaneous sliding". After Earp (1938) had described extensive slump deposits in Central Wales, Boswell admitted (p. 159) that the evidence "seemed definitely to rule out tectonics as a cause of the disturbance", and in reply to a new study by Jones (1940) of the Colwyn Bay area in Denbighshire, recognised the presence of slumps and only differed from Jones "as regards the scale of the movement". In 1942 Boswell himself found a new area of disturbed beds, which he attributed to a combination of slumping and later movements, and noted new evidence for, as well as against, the slump hypothesis.

If Boswell was not, by this time, convinced of the importance of submarine slumping, most other British geologists were. Lamont (1936a, b,1938,1941) and Shackleton et al. (1940) had described Palaeozoic slumps in Ireland and Rice (1939) an example from the Trias of Cheshire. Brown (1938), Baldry (1938) and Hudson et al. (1940) however, had thought that slump deformation took place under some load of sediment. This provoked Jones to say (1940 p. 381) "he wished to make it as clear as words could make it that.....the upper contacts proved decisively and beyond argument that the tops of the slumped beds were the actual sea bottom where they happened, and they had no load upon them other than the sea water above".

The controversy between Boswell and Jones continued intermittently for at least another decade (Boswell 1943,1949,1953, Jones 1943,1947, 1953a,1953b) but only concerning points of detail. Jones had substantially proved his thesis, and his detailed mapping of slump structures provided the basis for the large number of subsequent studies which are described in the following sections.

2.4 SLUMP STRUCTURE TYPES

The development of the turbidity current hypothesis in the 1950s revealed that 'slumping' is only one of a range of possible subaqueous gravity induced processes. There have been a number of attempts to

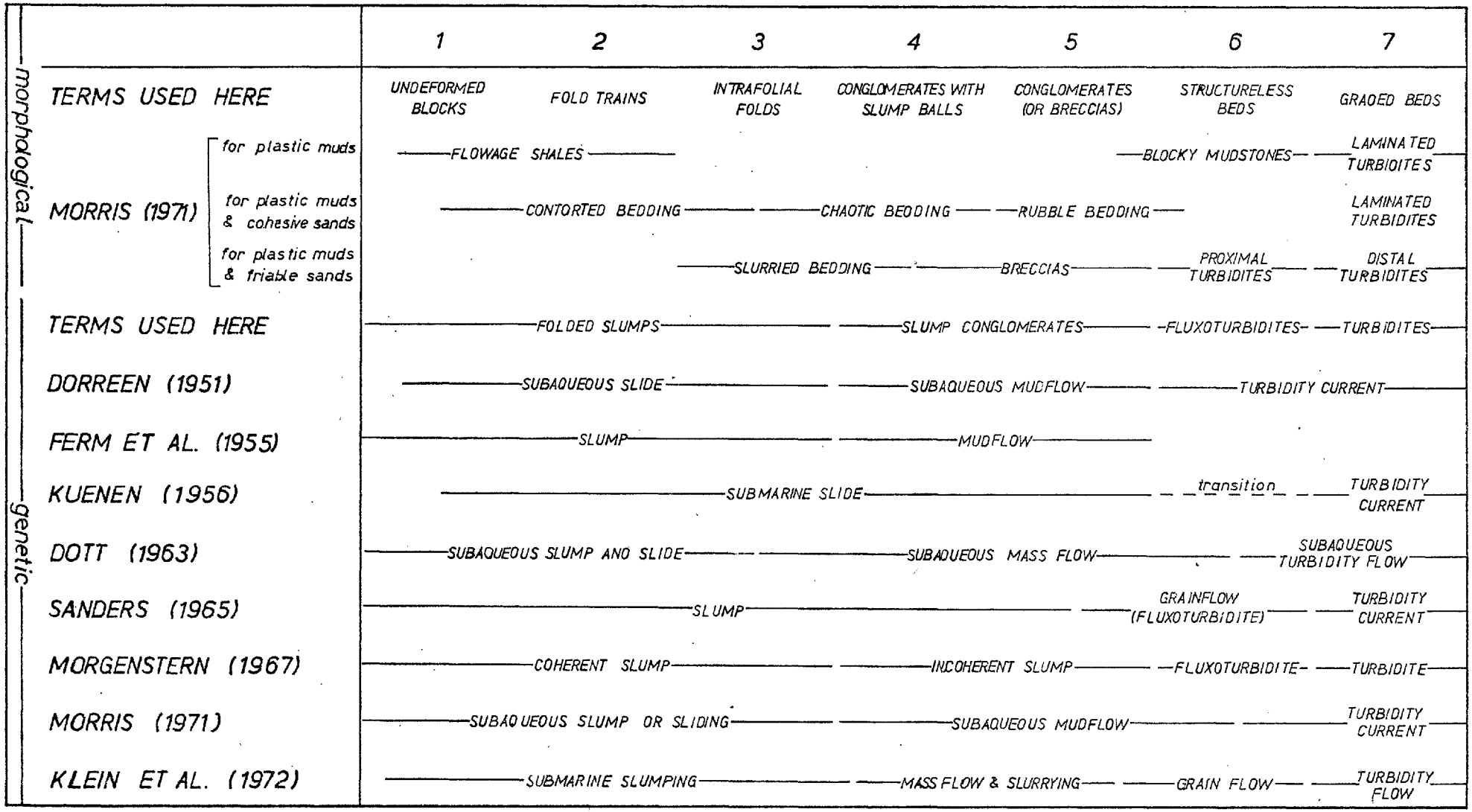


FIGURE 2.8 Classification of slumping and related phenomena.

classify these processes, but few attempts to classify the structures in which they result. For the purposes of description structures are grouped into seven categories in the chart in Fig. 2.8. The categories are arranged in order of increasing destruction of initial structure. This does not imply that this is the sequence of development of structures with time in all or any case. The approximate correlation is shown between these categories and the terms used by Morris (1971). Also indicated is the approximate correspondence with genetic terminology which has been proposed, though each structural type may actually be polygenetic. The following sections describe the characteristics of each category, omitting turbidites and fluxo-turbidites which fall outside any definition of 'slumping'. It should be emphasised that a complete gradation exists between the categories in reality.

Group 1 - Undeformed blocks

Structures corresponding to the initial stages of slumping are rarely observed. A few cases are recorded (Gray et al. 1952, Williams et al. 1965, Laird 1968, Cline et al. 1968) of essentially undeformed blocks which have been displaced along a discrete slip surface (Fig. 2.9). These examples were all formed in deltaic or swamp environments and all have more or less circular slip surfaces. Incipient slumps on the continental slope would probably have more planar slip surfaces. 'Rotated packets' of undeformed strata noted by Hoorn (1970) and 'wedge structures' described by Newell et al. (1953) are possible examples from this environment.

Group 2 - Fold trains

In the early stages of slumping the sedimentary layering is

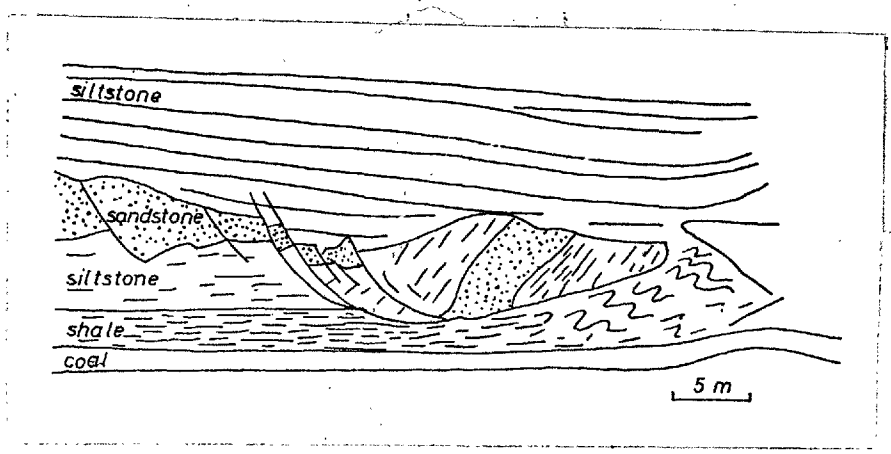


FIGURE 2.9 Rotational slumping of internally undeformed blocks, Coal Measures, Pennsylvania (from Williams et al. 1965, Fig. 3(c)).

commonly folded. Layers can be traced along a 'train' of folds, in contrast to later stages, where folds become isolated as 'intrafolial folds' or 'fold remnants'.

The style of folding shows wide variation, even within one slumped unit. Folds are most commonly rounded, but show a complete range of tightness from gentle to elasticas shapes (Fig. 2.10). The more open folds have upright or steeply inclined axial surfaces (when referred to a datum parallel to the slump unit boundaries). This is a necessary consequence of the original horizontal layering, as is the tendency for fold hinge lines to lie approximately in the plane of the slumped unit. Tighter folds show a wider variation in axial surface

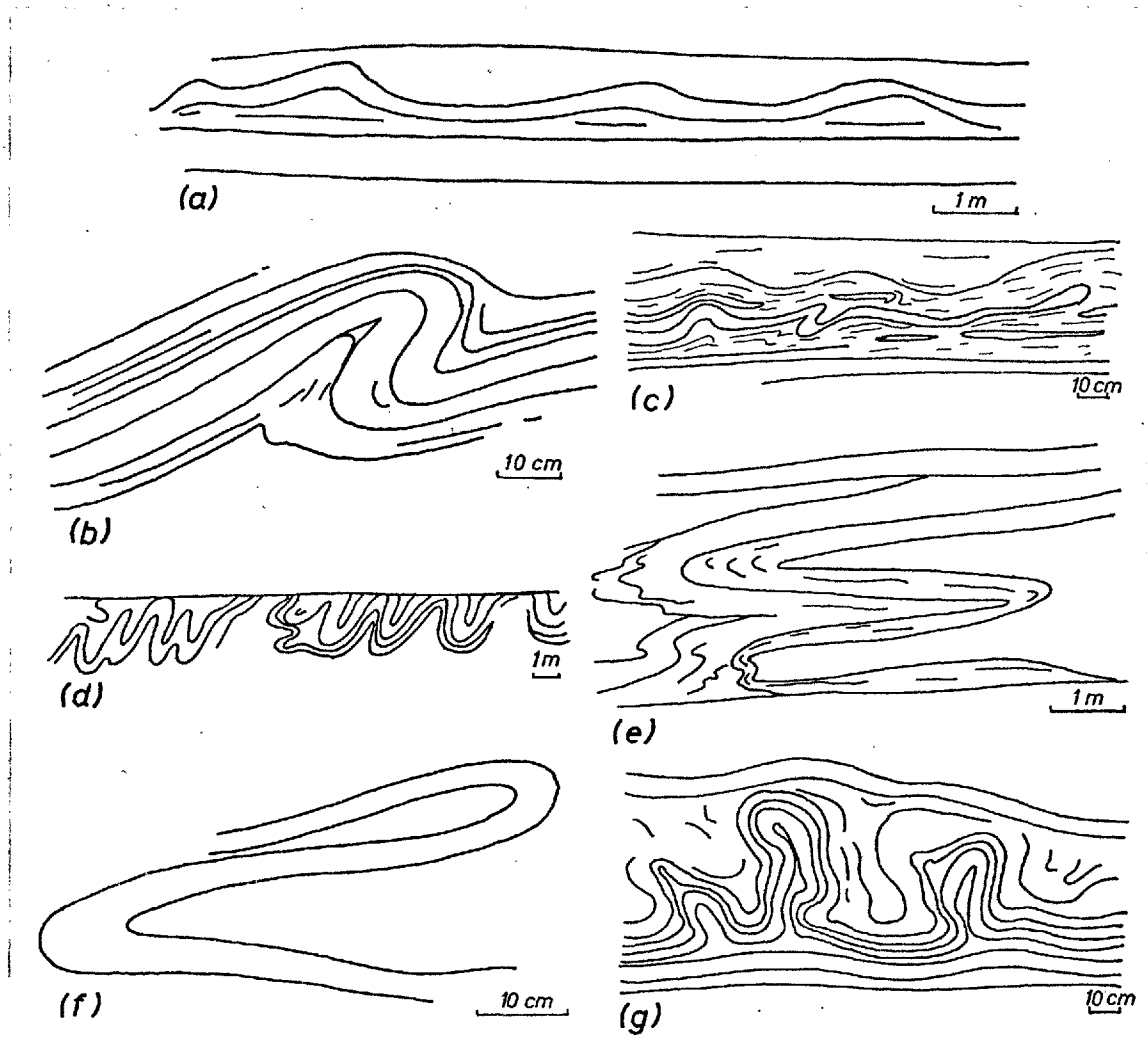


FIGURE 2.10 Examples of folded slumps A) from Beets 1946, Fig. 2, B) & F) from Fairbridge 1947, plate III, C) from Newell et al. 1953, Fig. 42, D) from Scott 1966, Fig. 5, E) from Blanc 1972, Fig. 7, G) from Straaten 1950, Fig. 3.

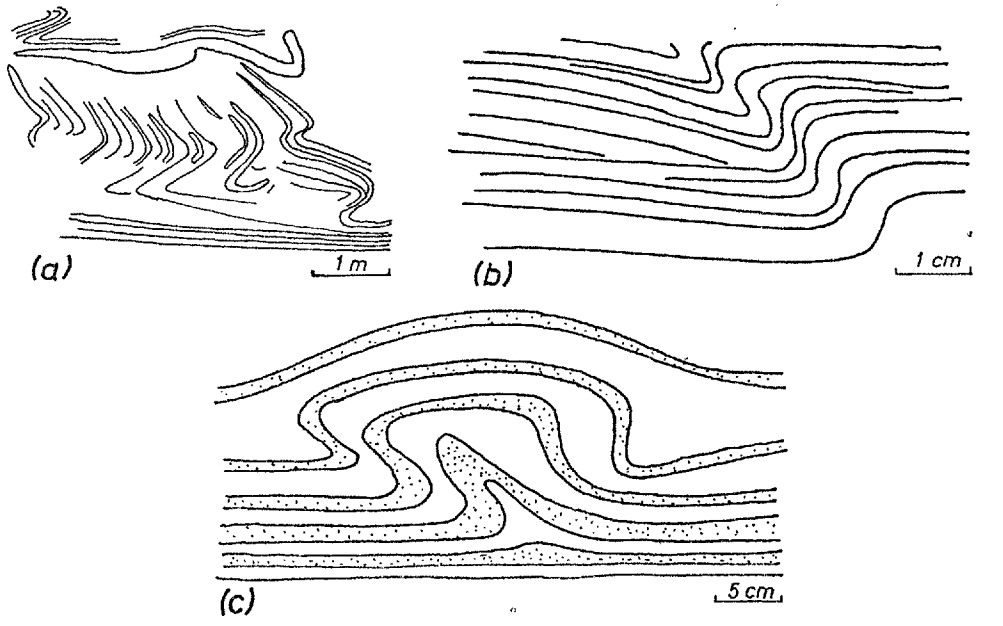


FIGURE 2.11 Slump folds A) after Scott 1966, Fig. 5, B) after Sheridan 1972, plate 10, C) after Williams et al. 1969, Fig. 4B.

attitude, though gently inclined or recumbent attitudes are common. Hinge lines still tend to be coplanar with the sheet. Folds are usually strongly non-cylindrical and characteristically show no consistent asymmetry sense.

The rounded-hinged folds are particularly common in glacial lake sediments (Fig. 2.10c,f,g). Fairbridge (1947) has reviewed such occurrences and other examples a e figured by Straaten (1950) and Nichols (1960). They are also common in lagoonal sediments (e.g. Hallam 1960, Daley 1972) and shelf sediments (e.g. Dunnington 1945, Grant-Mackie et al. 1964, Spreng 1967). In 'flysch basin' environments folds usually occur as isolated remnants, though fold trains may sometimes be preserved (e.g. Crowell 1957, Radomski 1958, Scott 1966).

Though slump folds most commonly have rounded hinge zones, recumbent chevron folds have been described by Scott (1966), angular box folds by Williams et al. (1969) and Kuenen (1948), and kink structures by Sheridan (1972) (Fig. 2.11).

In early descriptions slump folds were often assigned a 'similar' geometry. This resulted from the erroneous idea that 'incompetent' unconsolidated sediments could only fold by inhomogeneous simple shear. Shackleton et al. (1940) however, noted slump folding with a more 'parallel' style, evidencing some component of flexural slip. Later Work has confirmed that slump folds show a wide range of styles.

Horne (1970) found folds of all five of Ramsay's (1967) classes, and Waterhouse et al. (1957) and Nagtegaal (1963) have noted a predominance of more parallel folds.

Slump folds do not usually have a related cleavage. This fact has been used as evidence for their non-tectonic origin (Rettger 1935, Fairbridge 1947, Helwig 1970). Recent work (Williams et al. 1969, Yagishita 1971, Corbett 1973) suggests that there may be an axial planar fabric associated with some slump folds.

A lineation associated with slump folding has been noted in some of the Welsh Silurian slumps (e.g. Straw 1937, Jones 1937,1939, Earp 1938, Williams et al. 1957). Similar lineations have been observed elsewhere (Newell et al. 1953, Rigby 1958, Morris 1971, Corbett 1973). The lineations are apparently due to a crenulation of the fine sedimentary layering.

Group 3 - Intrafolial folds

In many slump deposits there is a characteristic lack of continuity of the sedimentary layering. Individual folds are clearly distinguishable, but are isolated from one another, either by planar discontinuities (Fig. 2.12a) or by regions where the original layering has been destroyed (Fig. 2.12b). A range of fold styles occurs, similar to that previously described, though there is a tendency for folds to be fairly tight with gently inclined axial planes.

Slump sheets with intrafolial folds have most commonly been described from 'flysch basin' environments (e.g. Jones 1939, Radomski 1958, Ballance 1964, Szulczewski 1968, Corbett 1973). They are also fairly common in shelf deposits (Hubbard et al. 1965, Spreng 1967) but occur less frequently in continental or transitional environments (Kuenen 1948, Hallam 1960).

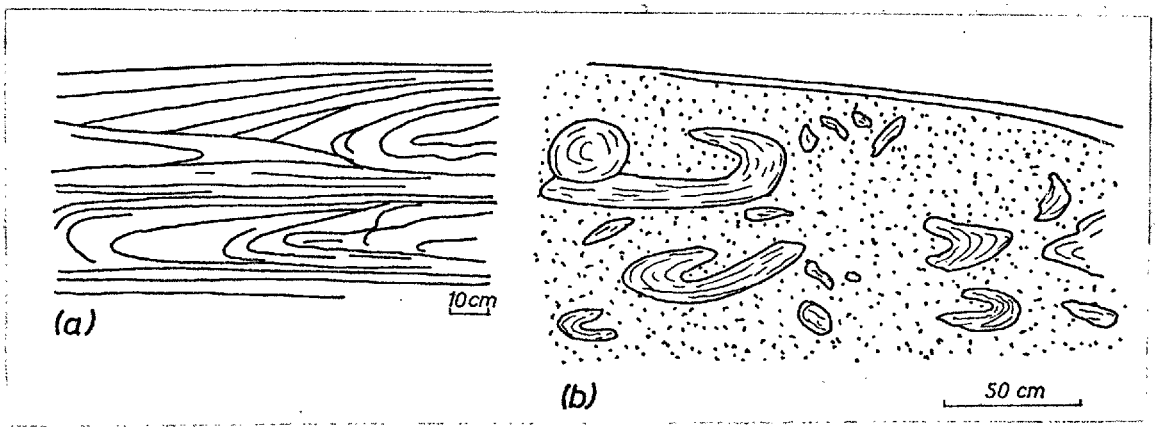


FIGURE 2.12 Intrafolial slump folds A) from Newell et al. 1957, Fig. 44d, B) from Ksiazkiewicz 1958, Fig. 9.

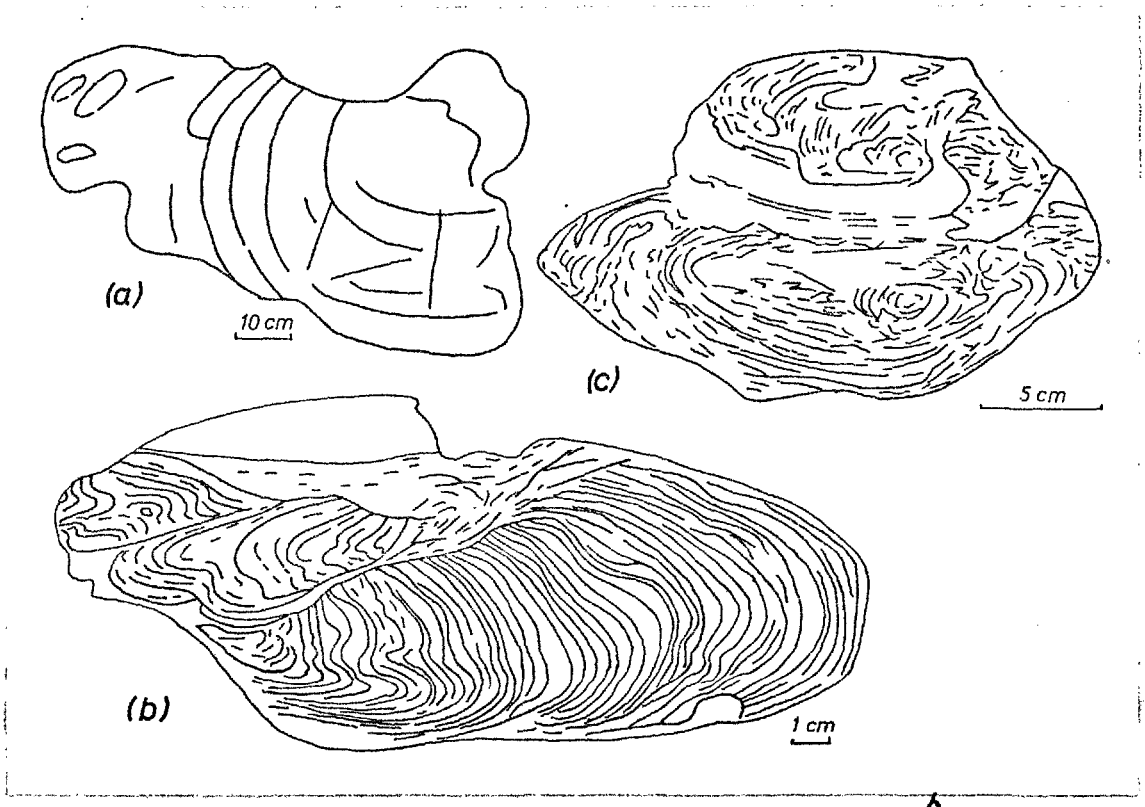


FIGURE 2.13 Slump balls a) after Ksiazkiewicz 1958, b) after Kelling 1966, Fig. 8, c) after Kuenen 1948, Fig. 6d.

Group 4 - Conglomerates with slump balls

Slump units of this type are characterised by more or less rounded fragments enclosed in a matrix. In section, the fragments show remnants of a sedimentary layering. The internal structure of these slump balls may range from recognisable fragments of slump folds (Fig. 2.13A,B) to rolled up layers (Fig. 2.13C). Conglomerates with slump balls are most important in basin environments (Jones 1939, Grzybek et al. 1958, Dzulynski et al. 1958, Marschalko 1961,1964, Dimitrijevic et al. 1970, Baranowski 1971), though examples from other environments are commonly described (Kuenen 1948, Radwanski et al. 1962, Allen 1963, Lindsay 1966, Hallam 1966).

Group 5 - Conglomerates

Conglomerates in which the clasts have no internal structure probably represent the most disturbed deposits still attributable to a slumping mechanism. In fact these, and conglomerates containing slump balls, are often regarded as the products of a separate 'mudflow' mechanism (e.g. Ferm et al. 1958, Radomski 1958, Morris 1971).

The mechanisms which operate in the transition from true slumping

to true turbidity flow are the subject of much present research (Stauffer 1967, Fisher 1971, Klein 1972). Massive structureless beds attributable to these mechanisms are commonly associated with both slumps and turbidites (Dzulynski et al. 1958, Radomski 1958, Morris 1971).

Conglomerates thought to have formed by slumping are common in both basin and shelf sediments (Radomski 1958, Dzulynski 1958, Horne 1970, Robinson 1967, Mikulenko 1967).

The frequency of slumping in different environments

It has already been noted that some types of slump structure are more common in certain environments than in others. To investigate this effect a sample of 69 descriptions of slump structures has been chosen from the literature. These are marked with an asterisk in the list of references. This is in no way a random sample, but rather comprises the better documented descriptions of slump structures. It is nevertheless adequate to show the general relationship of structure to environment.

The examples have been assigned to one of three groups of environment:- a) continental or transitional (i.e. fluvial, lacustrine, paludal, deltaic, lagoonal or littoral), b) marine shelf, c) marine basin. Nearly 60% of the examples come from marine basins (Fig. 2.14).

The types of structure present in each environment are shown in Fig. 2.15. The histograms clearly show the dominance of the 'less disturbed' structures in continental and transitional environments, and of the 'more disturbed' structures in marine environments. The frequency of turbidites and fluxoturbidites is shown, though, because the sample only includes references to slump structures in particular, their relative frequency in basin environments is grossly underestimated.

Basin slopes are clearly the most favourable environment for slumping in general, and for the development of highly deformed deposits in particular. It is therefore from basin environments that

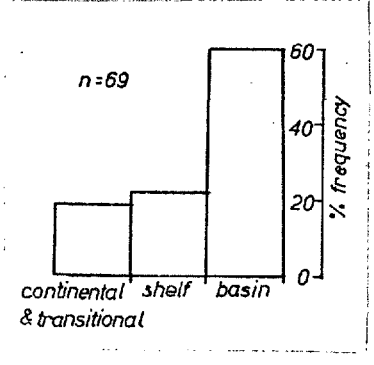


FIGURE 2.14 Histogram showing the frequency of slumping in different environments, based on references starred in list of references.

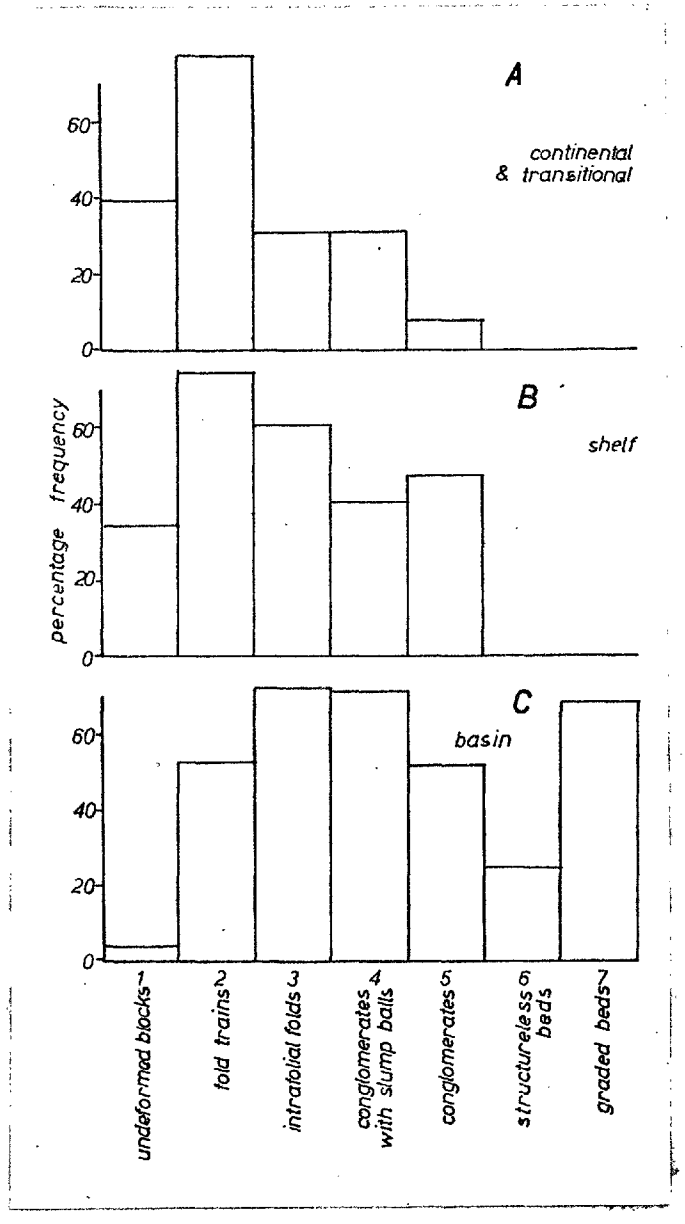


FIGURE 2.15 Histograms showing the frequency of various types of slump structure in three different environments.

most directional data from slump sheets are obtained. These data are reviewed in the next section.

2.5 DIRECTIONAL DATA FROM SLUMP SHEETS

There have been few studies of the orientation of structures in slump deposits, perhaps because of their apparently chaotic arrangement. A table has been compiled (Fig. 2.16) of studies which give directional information. A distinction is made between the results apparently based on actual measurement, and those which are more subjective.

Hinge lines of slump folds are the most commonly measured structure. Data are usually presented only as azimuths, the implication being that

		STRUCTURES MEASURED							RELATIONSHIP OF AXES TO CURRENT DIRECTION		
		hinge lines	bedding	axes of pebbles or slump balls	lineation	axial planes	fold asymmetry	fold closure	parallel	oblique	perpendicular
1937	Jones	o					o				
1937	Straw	o					o	o			
1939	Jones	o	+								
1948	King	o					o				
1950	Rich	+									
1952	Chenoweth	+									
1953	Newell et al.	+									
1957	Crowell	o						o			o
1957	Williams et al.	+			+		+				
1958	Dzulynski et al.	o						o	o		o
1958	Ksiazkiewicz	+		+				+		+	+
1958	Rigby	+									
1959	Haaf	+									+
1959	Holland				o		o				
1960	Allen	+		o		o	o				+
1960	Hallam	o		o							
1960	Nichols					o					
1961 1964	Marshalko	o							o		o
1961	Matthews	o									o
1962	McBride	o					o				
1962	Murphy et al.	+							+		
1962	Prentice	+							+		
1962	Scott et al.	+							+		+
1962	Whitaker	o			o						
1963	Dzulynski	o				o					
1964	Bailey	+							+		
1964	Ballance	+									+
1966	Crowell et al.	+				o	+		+		
1966	Hubert	+							+		+
1966	Kelling et al.	+		+			+	+			
1966	Scott	+							+		
1967	Spreng	o					o				
1969	Gregory	+									
1969	Jones	+									+
1969	Kelling	+							+		
1969	Rice	+									
1969	Williams et al.	+				o	+				
1970	Dimitrijevic et al.	+							+		
1970	Helwig	+				o	+		+		
1970	Hoorn	+							+		
1970	Horne	+				o	+				o
1970	Shawa	+							+		+
1971	Morris	o							o		
1972	James	+							+	+	
1972	Tyler	+					+				+
1973	Corbett	+							+		

+ studies based on measurement o more subjective studies

FIGURE 2.16 Summary of studies of directional structures in slump deposits.

the hinge lines are parallel to the bounding surfaces of the slump sheet (i.e. the regional bedding). The few studies in which the three dimensional orientation of hinge lines has been measured (Williams et al. 1969, Helwig 1970, Horne 1970) show hinge lines which are fairly dispersed about the regional bedding (Fig. 2.17). There is therefore a significant loss of information in the rose diagram form of representation (Fig. 2.18), though this does permit direct comparison

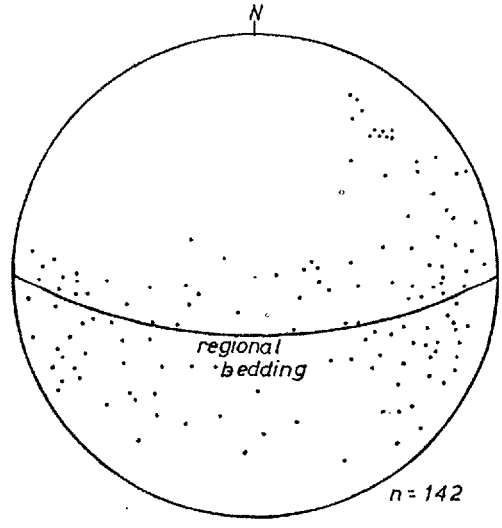


FIGURE 2.17 Slump fold hinge lines from Farmer's Head, Newfoundland (from Horne 1970, Fig. 10A).

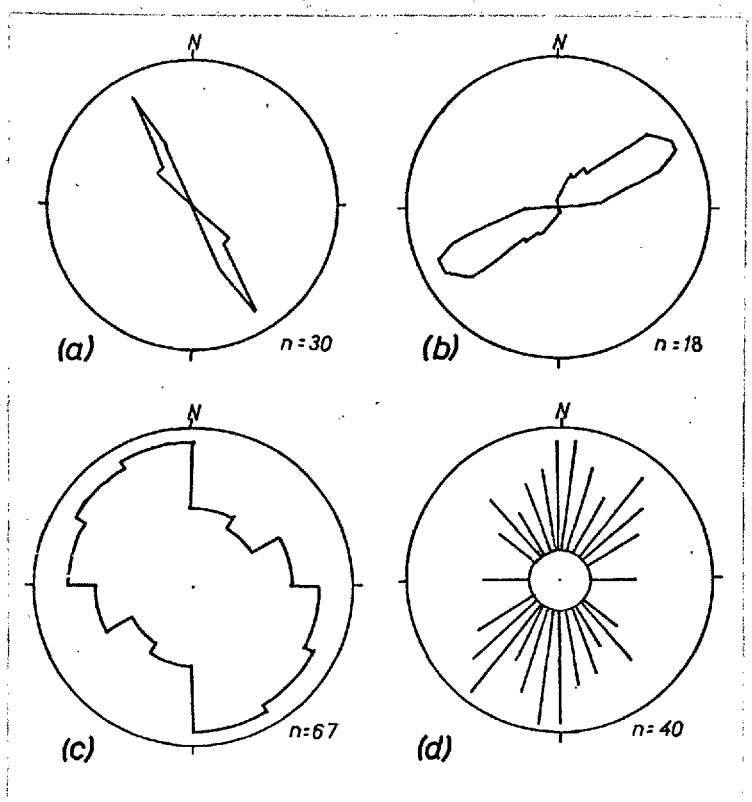


FIGURE 2.18 Rose diagrams of slump fold axis orientations A) from Newell et al. 1953, B) from Chenoweth 1952, Fig. 14, C) from Dimitrijevic 1970, Fig. 15, D) from Gregory 1969, Fig. 15a.

with palaeocurrent data.

Hinge line distributions with no preferred orientation have been noted (e.g. Newell et al. 1953, Crowell 1957, Hallam 1960, Morris 1971), though only in more subjective studies. Measured distributions always show some preferred orientation. Occasionally the hinge lines are well aligned (Fig. 2.18A,B) but more usually they show dispersed patterns (Fig. 2.18C,D). In some regions this dispersion is due to combining data from several areas having markedly different distributions, but generally the dispersion is a feature of the geometry on all scales. The mean axial orientation is assumed to indicate the strike of the palaeoslope.

The dip direction of the palaeoslope can usually be deduced from the regional geology. Horne (1970) has successfully deduced this from the sense of fold asymmetry, but in other studies (e.g. Crowell et al. 1966, Williams et al. 1969, Helwig 1970) asymmetry has given inconclusive results. Attempts to use the direction of fold closure as a slope direction indicator have also proved inconclusive (Straw 1937, Crowell 1957, Ksiazkiewicz 1958).

Structures other than folds have occasionally been analysed. Williams et al.(1957) measured a lineation shown to be due to micro-folding, and showed it to be approximately parallel to the major slump folds. Ksiazkiewicz (1958), Kelling et al. (1966) and James (1972) measured the long axes of slump balls or pebbles in slump conglomerates. Jones (1939) recorded the attitude of deformed bedding within a slump sheet, and showed that it had a fairly constant strike which was taken to indicate the palaeoslope strike.

The directional relationship of slump structures to palaeocurrent structures is an important guide to the total geometry of a depositional basin. The most common relationship is with the mean fold axis parallel to current indicators (Fig. 2.19). This pattern implies turbidity or traction current flow across rather than down slope. Crowell et al. (1966) and Dimitrijevic (1970) were reluctant to accept this possibility, and attributed the folding to turbidity current impact rather than to slumping. Similarly Corbett (1973) invoked 'local slopes' formed by faulting perpendicular to the regional palaeoslope deduced from current directions. The less common pattern, with the mean fold axis approximately perpendicular to the current indicators,is taken to indicate a downslope current (Fig. 2.20). Both types of pattern may be present within one area (e.g. Marschalko 1961, 1964) or in different areas within the same region (Hoorn 1970). The

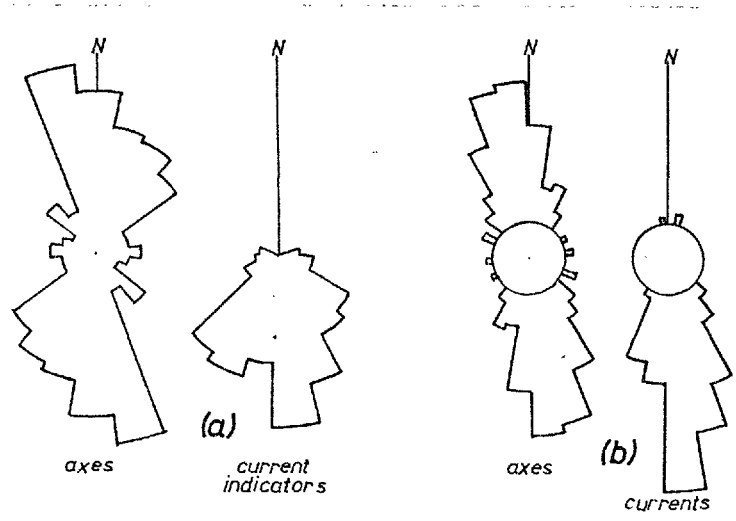


FIGURE 2.19 Rose diagrams of associated slump fold axes and current indicators a) from Murphy et al. 1962, Fig. 7, b) from Scott 1966, Fig 3.

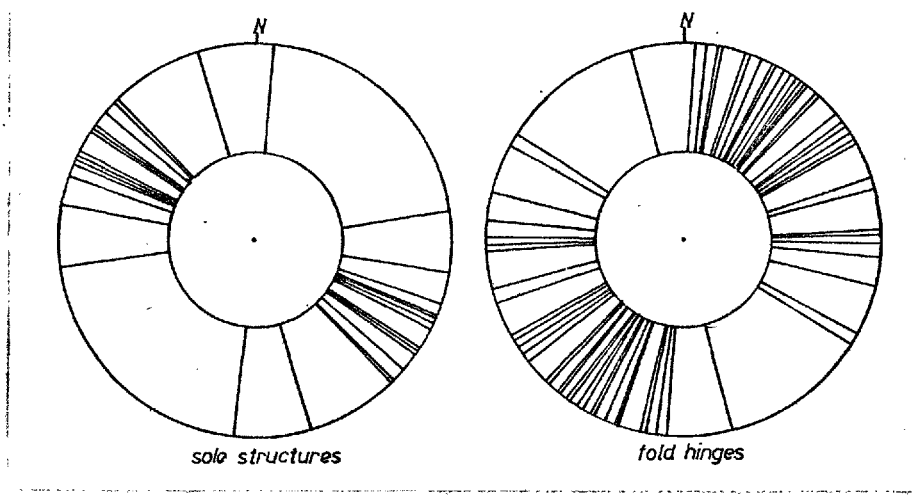


FIGURE 2.20 Rose diagrams of associated slump fold hinge lines and current indicators from Ballance 1964, Fig. 14.

relationship of palaeocurrents to palaeoslopes has been the subject of much controversy (see reviews by Hubert 1968, Walker 1970).

In addition to the studies on geological examples of subaqueous slumps, directional data have been collected from two recent subaerial slides. Hansen (1965,1971) measured hinge line orientations and asymmetry sense of folds in a tundra landslide and Lajoie (1972) hinge lines in a snow slump sheet. The hinge lines show a wide dispersion in the plane of the sheet (Fig. 2.21), but retain an approximately symmetrical relationship to the slope strike and sheet movement direction. These patterns provide useful models to compare with orientation data from true slumps.

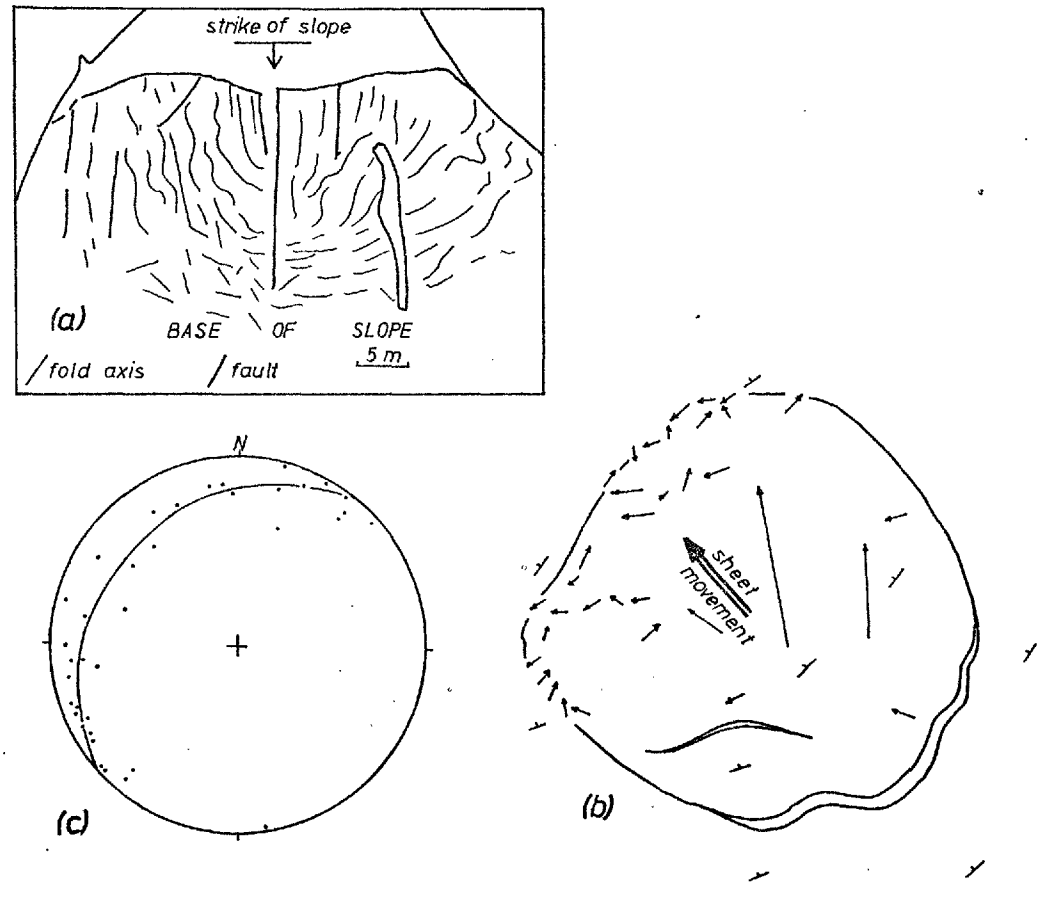


FIGURE 2.21 a) plan of a snow slump from Lajoie 1972, b) plan of a tundra landslide showing fold hinge line attitudes, from Hansen 1971, Figs. 15,17, c) equal area plot of hinge lines in b).

2.6 EVIDENCE FOR SLUMPING ON THE PRESENT SEA FLOOR

Since the early observations of Heim (1908) and Milne (1897) much additional evidence has been found of recent subaqueous mass movement of sediment. However, direct observations of these movements are restricted to those occurring at or near the present shores (e.g. Koppejan et al. 1948, Terzaghi 1957, Coulter et al. 1966, Andresen et al. 1967). Though such slides probably have analogs in the geological record, they are clearly not comparable with slumps formed in 'shelf' or 'slope' environments.

Sediment movement has also been directly observed in submarine canyons (Dill 1964), though an avalanche or sandflow mechanism is probably dominant in this case. True slumping is also thought to occur in canyons (Shepherd 1951, Emery et al. 1956, Chamberlain 1964) and is evidenced by seismic profiler surveys (Uchupi 1968, Belderson et al. 1969, Roberson 1964). Geological examples of slump structures in

submarine canyon heads have been described by Whitaker (1962).

Evidence of mass movements on the continental slope and rise is provided by the systematic series of submarine cable breaks recorded after some large earthquakes, notably the 1929 Grand Banks earthquake. Though these breaks have been attributed to progressive slumping by Jones (1954) and Van der Lingen (1959) they are generally thought to have been due to a turbidity current (Heezen et al. 1952, Kuenen 1952). However Heezen et al. (1964) have shown evidence that the Grand Banks earthquake produced both a slump and a turbidity current. This close relationship between slumps and turbidity currents has also been shown by Ryan et al. (1965).

The use, first of echo sounders, and later of continuous seismic profilers, has revealed sea floor structures which can be attributed to various forms of slumping. Such structures have been recognised from the continental margins of Eastern America (Ballard 1966, Moore et al. 1963, Gealy et al. 1955, Ewing et al. 1966, Rowa et al. 1967, Uchupi 1967), Western America (Curray 1965, Ross et al. 1965, Scholl et al. 1966) and Europe (Roberts et al. 1968, Stride et al. 1969, and Roberts 1972). However the disturbed sheets have thicknesses in the order of hundreds of metres, and are thus on a larger scale than most geological examples.

Slumping of much thinner sheets of sediment has been described by Lewis (1971), from the continental slope to the east of New Zealand. The seismic profiles (Fig. 2.22) show slump sheets between 25 and 50 metres thick on a slope varying from one to four degrees. Distinct structural zones have been recognised within each sheet (Fig. 2.22) and the areal extent of each zone has been mapped (Fig. 2.23). The size of the slump sheets is within the range commonly observed in geological examples, and they therfore provide the best model for slumping on the continental slope yet described.

2.7 CONCLUSION

The widespread importance of slump structures is now well established, and their potential in basin analysis has been recognised if not yet fully exploited. However several gaps are immediately obvious in our understanding of slumping.

Firstly the morphology of slump structures has been inadequately described. In particular the styles of slump folds have not been specified in detail. Such descriptions might enable slump folds to be more easily distinguished from tectonic folds. Helwig (1970) and

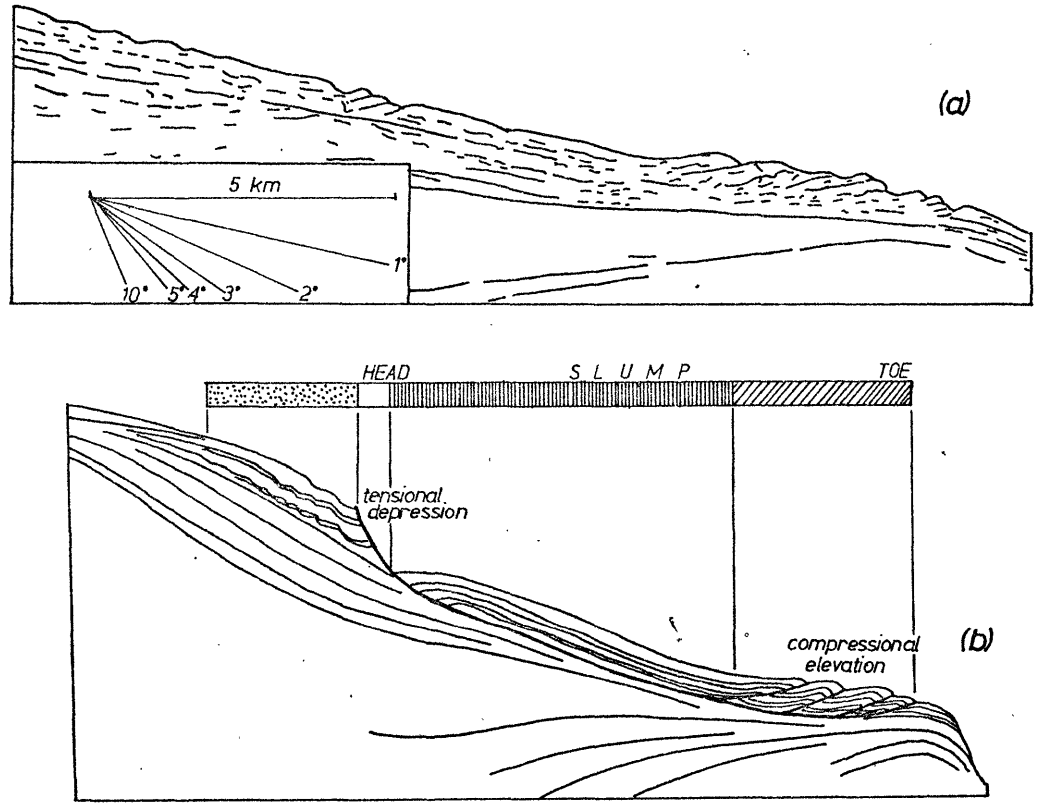


FIGURE 2.22 A) seismic profiler trace from the continental slope east of New Zealand, B) Interpretation as a slump sheet. From Lewis 1971, Figs 2,3.

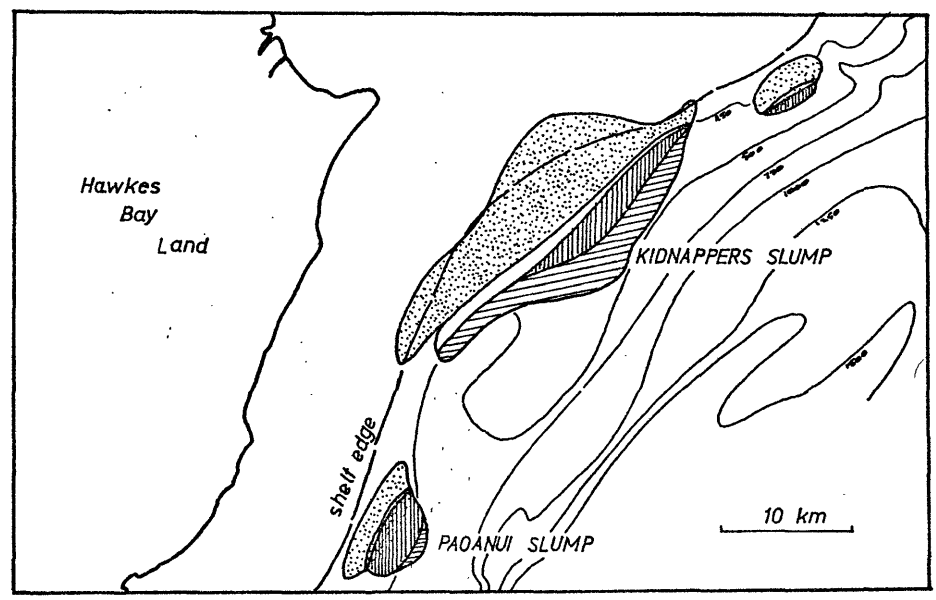


FIGURE 2.23 Chart of the area off Hawkes Bay, New Zealand, showing the form of the slump sheets in Fig. 2.22. From Lewis 1971, Fig. 1.

Wright (1969) have both identified as slumps the 'first phase' structures in their areas, and the same situation might exist elsewhere.

Secondly the prediction of palaeoslope orientation from directional slump data is still of doubtful validity, especially when based on a small nunber of readings from a wide area. Lajoie (1972) has recently concluded that it seems "premature to use slump fold axes as palaeoslope indicators". The use of the sense of fold vergence or closure to determine movement direction is also suspect. It is important for future studies to establish the validity and limitations of these techniques.

Only when the geometry of slump sheets is more fully documented will a greater understanding of the mechanics of slumping be possible.

CHAPTER THREE

THE CENTRAL WELSH LUDLOVIAN SLUMPS - AN INTRODUCTION

3.1 GENERAL GEOLOGY

Rocks of the Ludlow Series occupy an area of about 1100 square kilometres in East Central Wales and the adjoining Borderland (Fig. 3.1). Slump structures are absent or poorly developed in the Wenlock Edge area to the north-east and the Mynydd Bwlch-y-Groes strip to the south-west. These areas, and the outlying Long Mountain area to the north, have not been included in the present study. The remaining area

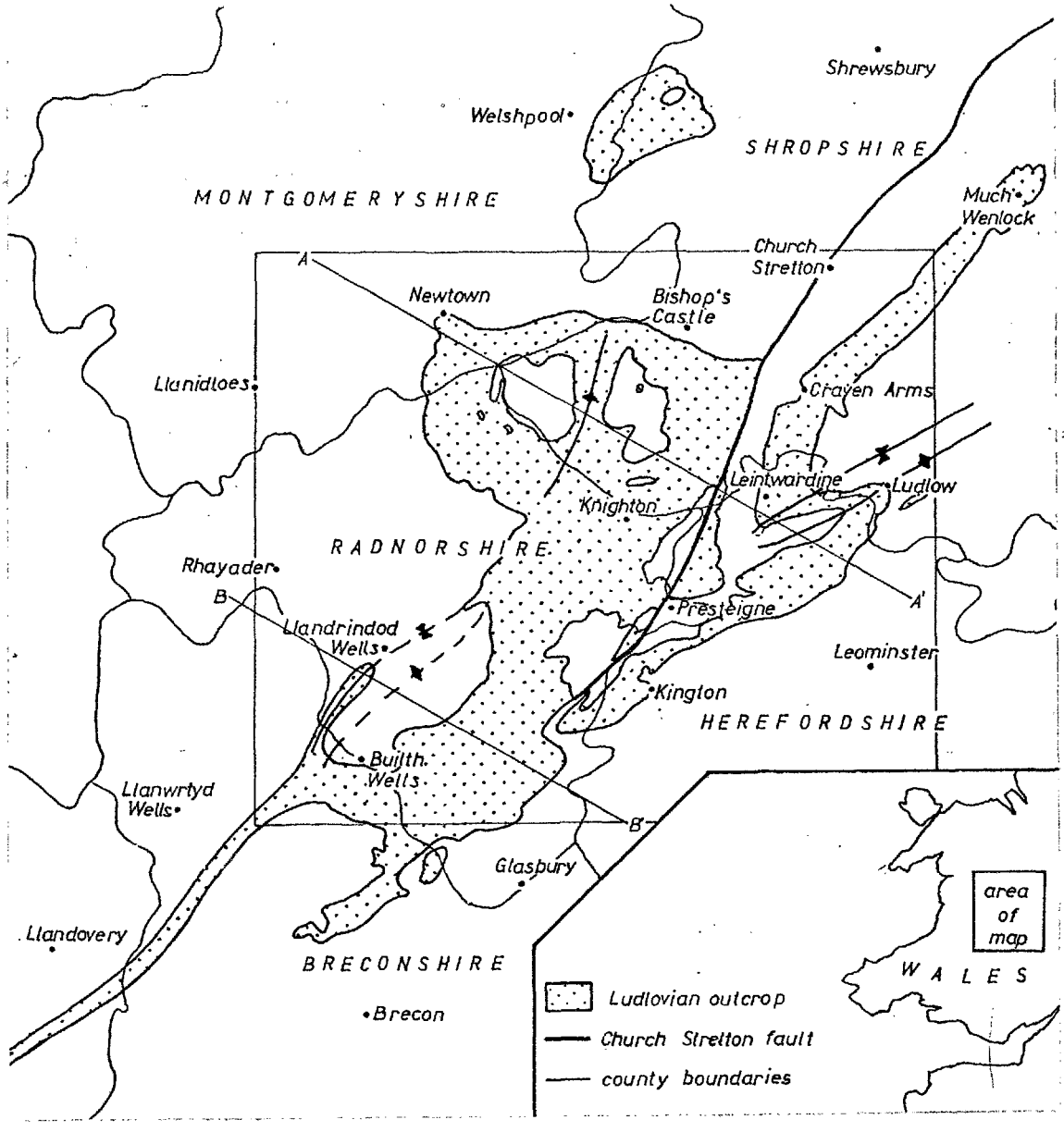


FIGURE 3.1 Map of the main Ludlovian outcrop in Central Wales and the Borderland, showing the area covered by the main map (Enclosure 1).

comprises some 900 square kilometres of Ludlow Series rocks (Enclosure 1).

The region has been a focus of Ludlovian stratigraphical research since Murchison (1839) established the type succession in the Ludlow area. This research has been reviewed by Lawson et al. (1956), up to the formation of the Ludlow Research Group in 1951. The programme of research initiated by this group, and reviewed in part by Bassett (1963), has provided better stratigraphical control throughout the area. The results have been summarised in the Silurian Correlation Paper (Cocks et al. 1971).

The stratigraphical work has shown that, throughout most of the Series, there is a clear distinction between a shelf sequence to the east and a basin sequence to the west. The shelf sequence comprises up to 300 metres of calcareous silts with flaggy or massive limestones. By contrast the basin sequence is up to 1900 metres thick, and predominantly composed of less-calcareous siltstones and mudstones with graptolitic shales.

Jones (1927) noted that the Church Stretton fault zone approximately coincides with the shelf/basin facies change, and suggested that sedimentation had been influenced by contemporary fault movements. This view has been supported by Greig et al. (1968) and Ziegler (1970) but disputed by Dean (1964). Accurate delimitation of the shelf margin by Holland et al. (1963) has shown that it follows a complicated line apparently unrelated to the fault zone (see Fig. 3.6), and moreover that its position changed markedly through the Ludlow period.

The stratigraphical work has been augmented in recent years by several sedimentological studies. These will be reviewed in conjunction with the related work on basin analysis (Sec. 3.5).

3.2 REGIONAL STRUCTURE

The detailed structure of the area is poorly known, and even the major structural elements are ill-defined (Fig. 3.1).

The simple structure in the east of the area is complicated by the Ludlow Anticline and the complimentary Brown Clee Syncline. In this area these folds plunge at between 5 and 10 degrees to the east-north-east, with a slight asymmetry to the north-north-west and an interlimb angle of about 150 degrees. To the west the Church Stretton fault zone trends NNE-SSW across the region, being replaced to the south by an essentially anticlinal zone, the Brecon Anticlinal of Kirk (1952).

The Church Stretton zone is flanked to the west by a zone about

10 kilometres wide, which is gently folded on undulating NNE-SSW axes. In the south this zone is succeeded westward by the broadly anticlinal region comprising the Builth Volcanic Series, and then by a synclinal belt containing Ludlow rocks. In the north a linear belt of more intense folding trends SSW from Clun Forest. Pugh (in discussion Jones 1947) thought this to be a continuation of the Builth anticlinal zone, but it possibly replaces the Builth structure en echelon.

The north-west of the area comprises the open Bettws-y-crwyn basin, with some more intense folding in the extreme north-west.

Cleavage is generally absent throughout the area. Sporadic development of a 'fracture' cleavage occurs in the most highly deformed areas. Cross-sections of the region (Fig. 3.2) emphasise that the major folds are mostly open, with fairly angular hinge zones and steeply inclined axial surfaces. The style of these tectonic folds is in direct contrast to the slump structures in the area.

3.3 THE BASIN SLUMPS

Slump sheets are a common feature throughout the Ludlow Series, but are particularly abundant in the basin facies. A succession of intercalated slump sheets and undisturbed beds is here termed a slump sequence. Jones (1939) used the term 'slump series' in the same sense. The major slump sequences which have been recognised as a result of this and previous work are shown on the map of Enclosure 1. Their boundaries in some areas have not been accurately mapped, and are shown approximately.

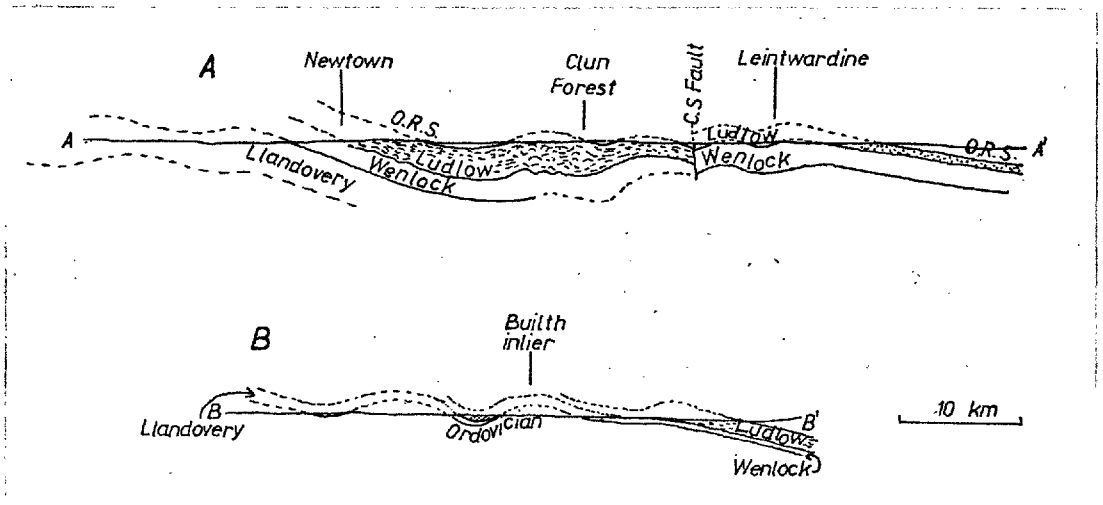


FIGURE 3.2 Rough sections through east-central Wales along the lines indicated in Fig. 3.1.

The slump structures in the area were not recognised as such until the 1930s. Murchison (1839), De la Beche (1846) and Wood (1900) had all described parts of the slump sequence near Builth, but had interpreted the structures as concretionary. In 1933 the Llandewi'r Cwm locality (SO 036488) provided O.T. Jones and S.H. Straw with the first clear evidence of the slump origin of the disturbed beds (see Sec. 2.3 and Fig. 2.6).

Straw subsequently traced out the slump sequence south of Builth and described (Straw 1937) the main features of the slump deformation; the interbedded disturbed and undisturbed layers, the wide range of fold styles and the 'characteristic corrugation of the bedding surfaces with a corresponding internal puckering of the laminae'.

A broadly similar sequence was described by Earp (1938,1940) from the western part of Clun Forest. He demonstrated that the slump sequence formed an integral part of the stratigraphic succession in the area, but that it apparently wedged out towards the southeast.

Jones (1947) described the region to the northwest of Straw's area, and found further slump development in the Ludlow rocks, as well as some more chaotic slumping in the uppermost Wenlock rocks. The south-westerly continuation of the Builth slump sequence was later recognised by Straw (1953) at Cwm Graig Ddu, and a possible north-westerly continuation by Kirk (1947,1951) to the east of Radnor Forest.

The Knighton area, in between the Clun Forest and Radnor Forest/ Builth areas, was described by Holland (1959a,b). He found only minor slump development. More extensive slump structures were mapped by Allender (1959, also Allender et al. 1960) in the Bishops Castle area to the north of Clun Forest.

To this date only Straw (1937) had tried to determine the palaeoslope orientation from the basin slumps. He noted that the slump fold axes most commonly trend NE-SW in the Builth area, and from the sense of fold overturning deduced a palaeoslope facing to the north-west. Bailey (1962,1964) confirmed Straw's estimate by statistical analysis of measured fold axes. He also found a broadly similar pattern of axial trends throughout the other slump sequences, including a newly described sequence to the west of Radnor Forest (Fig. 3.3). Bailey also described a slump conglomerate occurring at a fairly constant horizon throughout the area.

The approximate stratigraphical horizons of the basin slump sequences are shown in Fig. 3.4

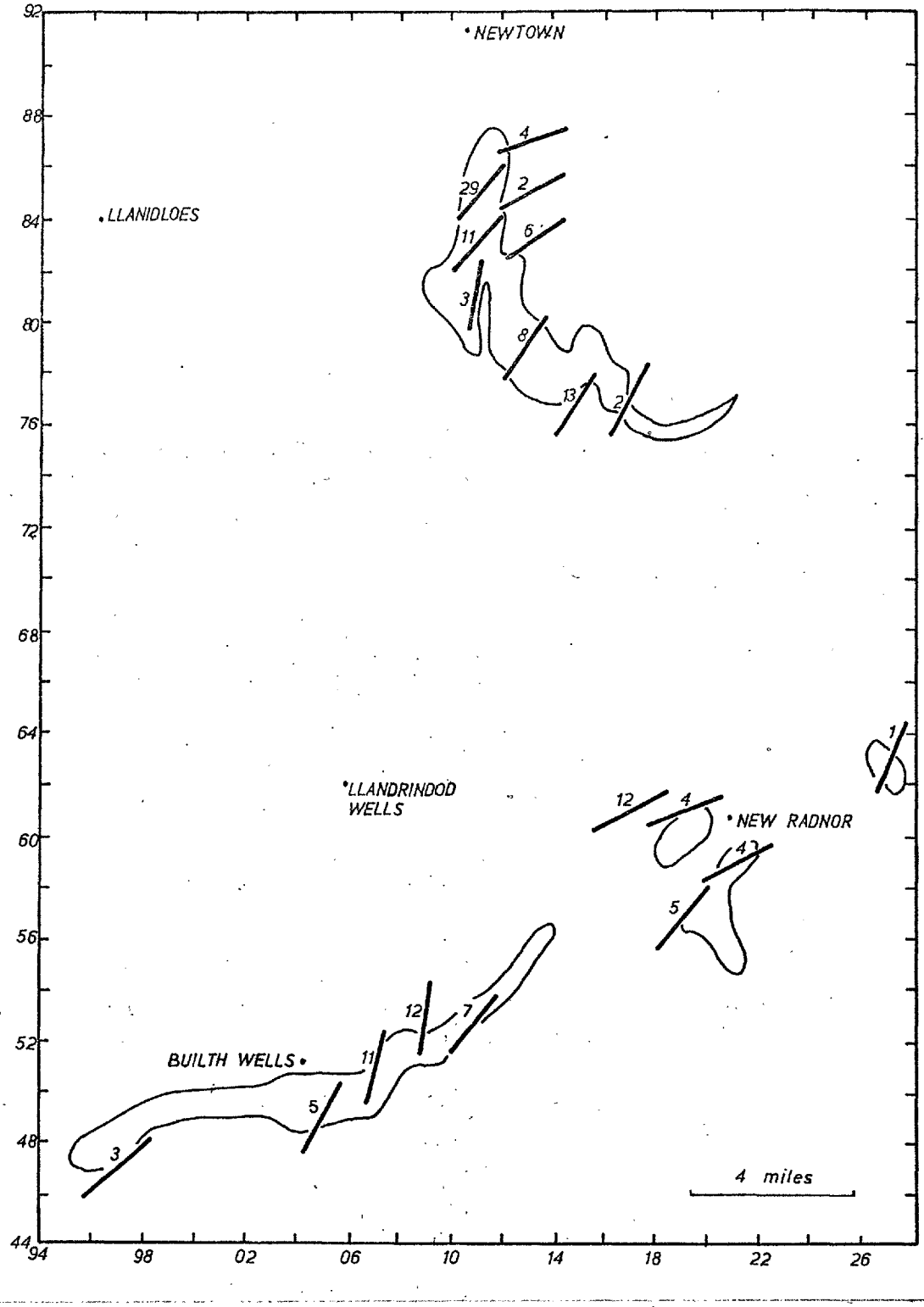


FIGURE 3.3 The outcrops of the main slump facies with mean slump fold axis orientations. Numbers of readings are indicated by each symbol. National grid is indicated. From Bailey 1964, Fig.2.

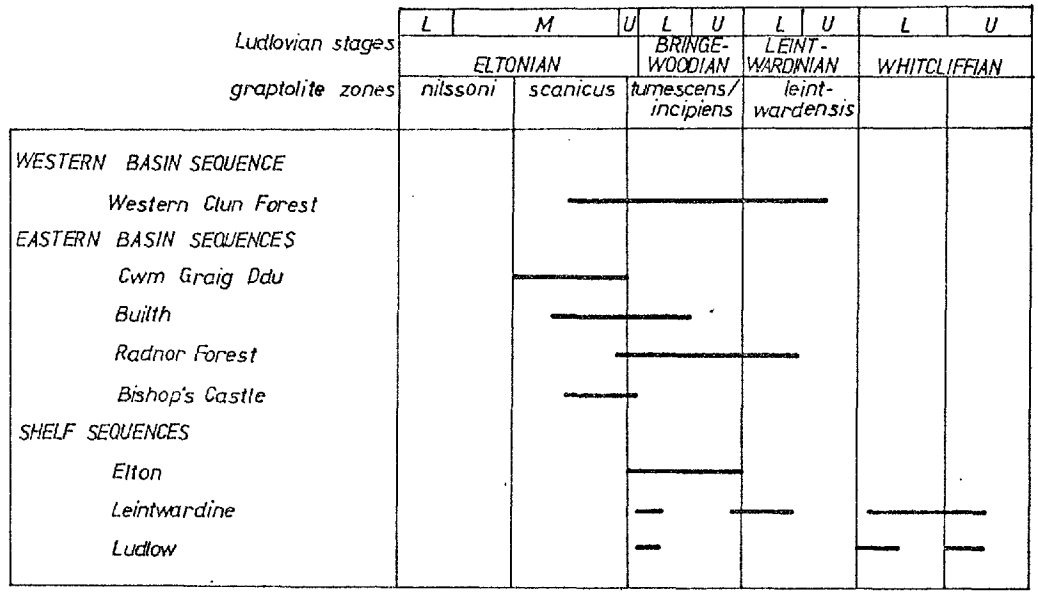


FIGURE 3.4 The approximate stratigraphical horizons of the Ludlovian slumps.

3.4 THE SHELF SLUMPS

Slump structures in the shelf facies are more sparsely developed than in the basin facies. They usually occur as isolated sheets rather than as part of a slump sequence comprising a number of sheets.

Alexander (1936) first described the slump structures of the Leintwardine area. These slumps were later shown by Whitaker (1962) to occur near to the edge of the shelf. Some are restricted to 'channels' which Whitaker interpreted as the heads of submarine canyons cut into the shelf edge.

Williams et al. (1957) also mapped slump folds occuring near to the shelf edge, in the Elton area to the south. They attributed the westerly increase in the intensity of the slump deformation to a transition towards the basin environment. Slump folds indicated a north or west sloping palaeoslope. 'Crinkle marks' on slumped bedding surfaces were shown to be due to microfolding, and to indicate the palaeoslope in the same way as larger slump folds.

Slump structures were noted by Holland et al. (1963) from the shelf sequence west of Ludlow. The palaeoslope indicators gave inconclusive results.

The approximate stratigraphical horizons of the shelf slumps are shown in Fig. 3.4.

3.5 BASIN GEOMETRY

Jones (1938) gave the first synthesis of the data on Welsh Silurian sedimentation. He suggested that the Silurian sediments were deposited in, or on the margins of, an elongate 'geosynclinal' basin trending NE-SW. The Builth slumps marked the position of the basin's southeastern margin, and those in Denbighshire its northwestern margin. Field evidence of movement direction from these two sequences supported Jones' interpretation. The movement direction in the Clun Forest sequence was unknown (see also Pugh 1950).

Straw (in discussion Kirk 1951) suggested that the basin margin may have trended north-south between Builth and Clun Forest, inferring that slumps in both these areas should show a westerly movement direction. In 1956 Jones refined his earlier interpretation, using isopachyte maps to define the basin geometry (Fig. 3.5A). His maps supported the hypothesis that the Clun Forest sheets moved westward.

Jones' interpretation was soon revised by Cummins (1957,1959a,b). He recognised that turbidites were a major element in the basin sequence, and used their current direction indicators to show that two distinct depositional troughs existed in Wales throughout much of the Silurian (Fig. 3.5B). In Central Wales the 'Montgomery Trough' had northward axial turbidity current flow, while in the north the

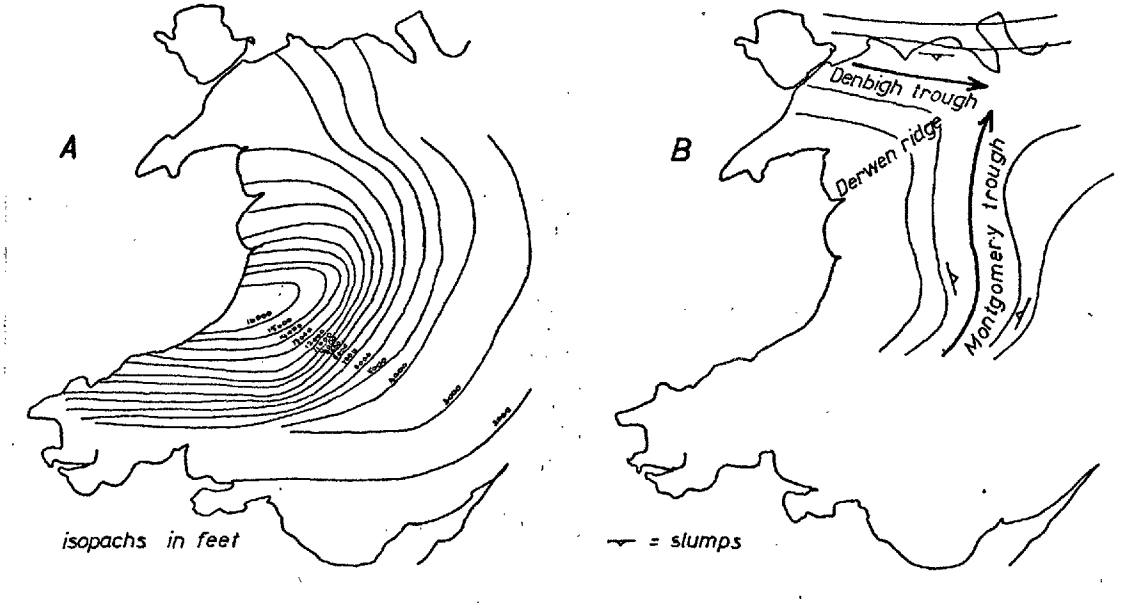


FIGURE 3.5 Interpretations of the Silurian basin geometry A) from Jones 1956, pl. XVII, B) from Cummins 1959, Fig. 4C.

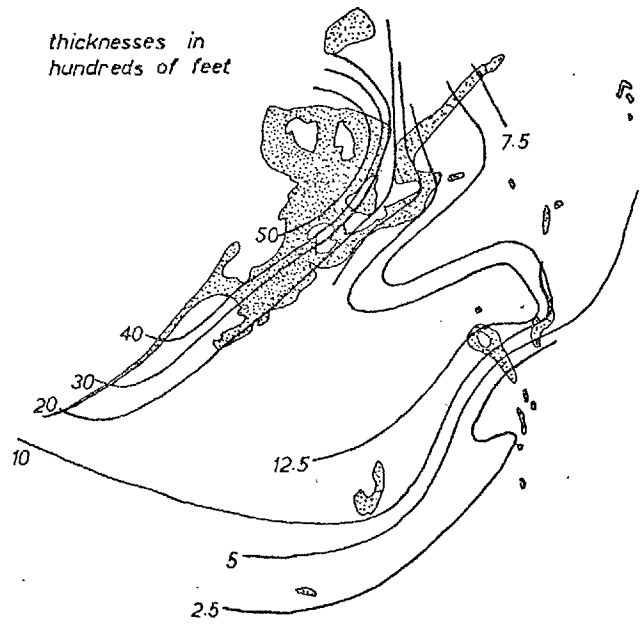


FIGURE 3.6 Selected isopachs for the Ludlow Series in Central Wales and the Borderland, from Holland et al. 1963, Fig. 15.

'Denbigh Trough' had northward axial turbidity current flow. The Builth slumps clearly marked the eastern margin of the Montgomery Trough, and Cummins proposed that the Clun Forest sheets marked its western margin, and therefore moved to the east.

Jones' 'geosynclinal' model was also opposed by Boswell (1961), who envisaged a series of more equidimensional basins of deposition.

Holland et al. (1963) constructed isopachyte and facies maps for the Ludlovian in East Central Wales and the Borderland. The maps clearly show the contrast between the shelf and basin deposits, in facies and particularly in thickness (Fig. 3.6). The results were more compatible with Cummins' basin model than with that of Jones, but Holland et al. did not comment on the existence of a western margin to the Montgomery Trough.

More positive support for Cummins' interpretation came from Bailey (1962,1964,1969), whose analysis of the facies within the basin sequence assumed eastward movement of the Clun Forest slumps off the 'Derwen Ridge' to the west (Fig. 3.7). Cummins (1969) thought this ridge to have been a relatively sudden development in the late Lower Ludlow, whereas Bailey (in discussion Cummins 1969) envisaged its more gradual development, associated with an eastward shift of the Montgomery Trough axis. Bailey (1964) confirmed the dominant

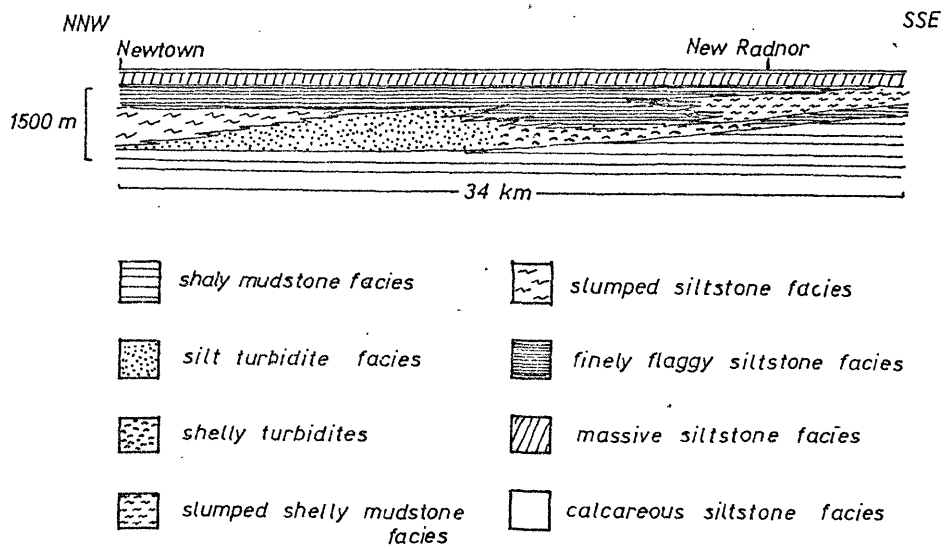


FIGURE 3.7 Schematic section of facies relationships in the Central Welsh Ludlovian, from Bailey 1969, Fig. 59b.

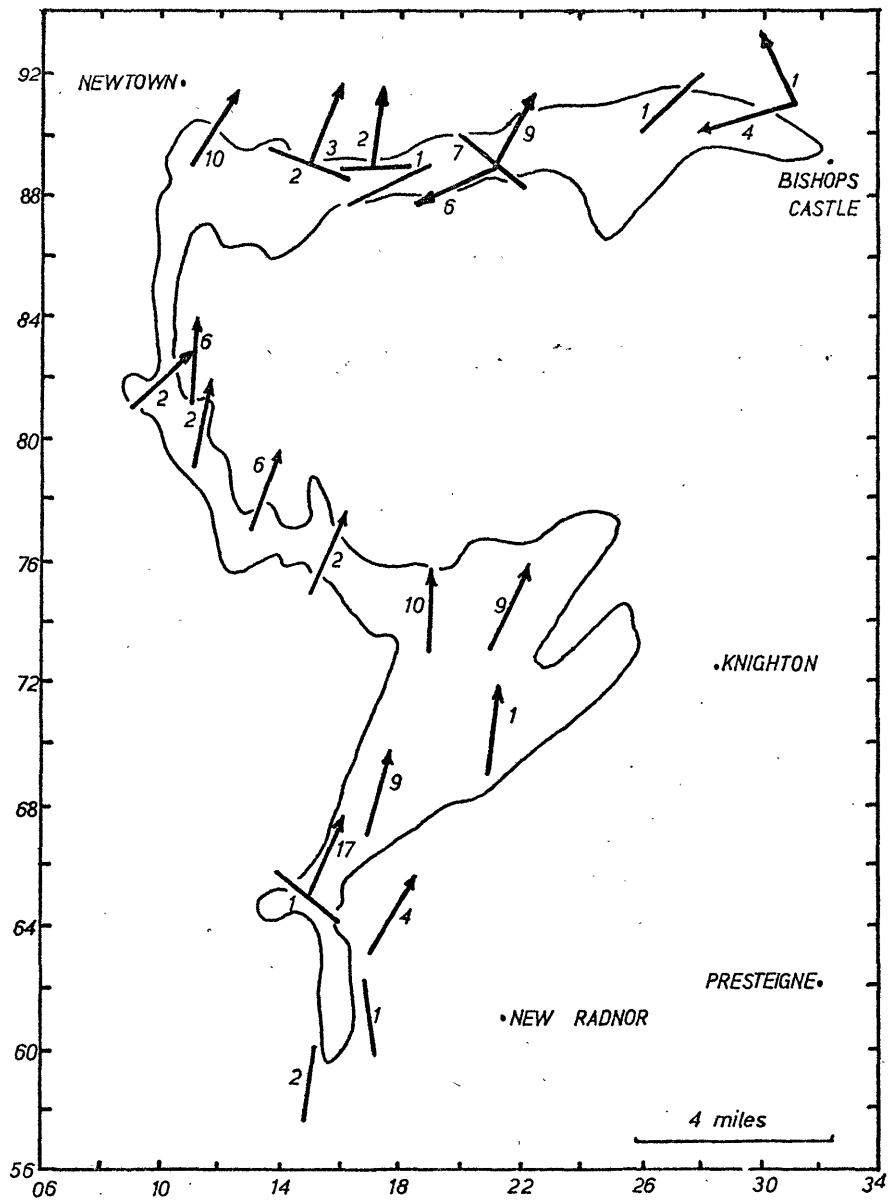


FIGURE 3.8 The outcrop of the 'silt turbidite' facies showing mean palaeocurrent trends and sense where known, from Bailey 1964 Fig. 3.

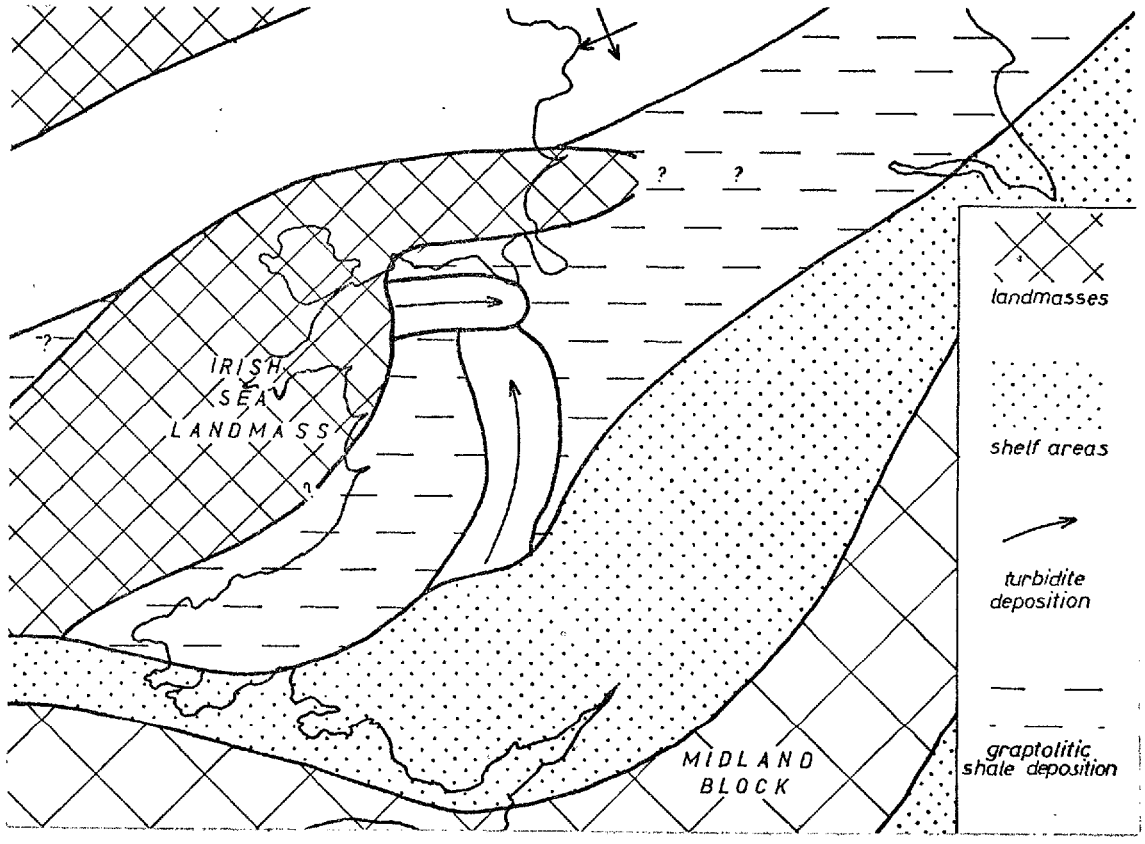


FIGURE 3.9 Early Ludlow palaeogeography, from Ziegler 1970, Fig.7.

axial transport determined by Cummins, but gave evidence for local lateral transport in the north of the area (Fig. 3.8).

Holland (1969) and Ziegler (1970) have recently shown that the models of Cummins and Jones are not entirely incompatible. Ziegler has incorporated Cummins' troughs within a 'geosynclinal' basin between the Irish Sea Landmass and the Midland Block (Fig. 3.9). This provides the most satisfactory palaeogeographical interpretation currently available for the Central Welsh Ludlovian.

In the following chapters the basin slump sequences will be referred to by their positions relative to the Montgomery Trough. Thus the sequence extending from Builth Wells to New Radnor is termed the 'Eastern Slump Sequence' and that to the west of Clun Forest the 'Western Slump Sequence' (see Enclosure 1).

PART II

FIELD STUDIES

THE INTERNAL STRUCTURE OF THE SLUMP SEQUENCES

CHAPTER FOUR

THE EASTERN SEQUENCE : CWM BLITHUS

4.1 LOCATION AND DESCRIPTION OF THE SUCCESSION

The first area to be described is probably the most informative section through any Ludlovian slump sequence in Central Wales. As such it will be treated here as a 'type locality' with which other sequences in the region will be contrasted and compared (Chaps. 5,6,7). In addition to the detailed description of the slump deformation at this locality, this chapter also considers related problems of data collection and analysis which are of relevance to all slump sequences.

The steep gully of Cwm Blithus (SO 166615 to SO 168611), off the Mithil Brook 1km ENE of Llanevan Farm, provides a continuous section through some 200 metres of the slump sequence forming the western edge of the Radnor Forest plateau (Fig. 4.1). This comprises almost the total thickness of the sequence in this area. The sequence is part of the 'slumped shelly mudstone facies' of Bailey (1962, 1964, 1969), who dated it as mid-Eltonian to early Leintwardinian (that is within the scanicus, tumescens/incipiens and leintwardinensis graptolite zones; see Fig. 3.4).

No detailed maps of the area have been published. Mapping of the sequence in the immediate vicinity of Cwm Blithus (Fig. 4.2) reveals the simple tectonic structure of the area, with bedding dipping gently eastward. However lack of exposure prevents the succession in Cwm Blithus from being traced laterally in detail, and its features are



FIGURE 4.1 View of Cwm Blithus looking south.

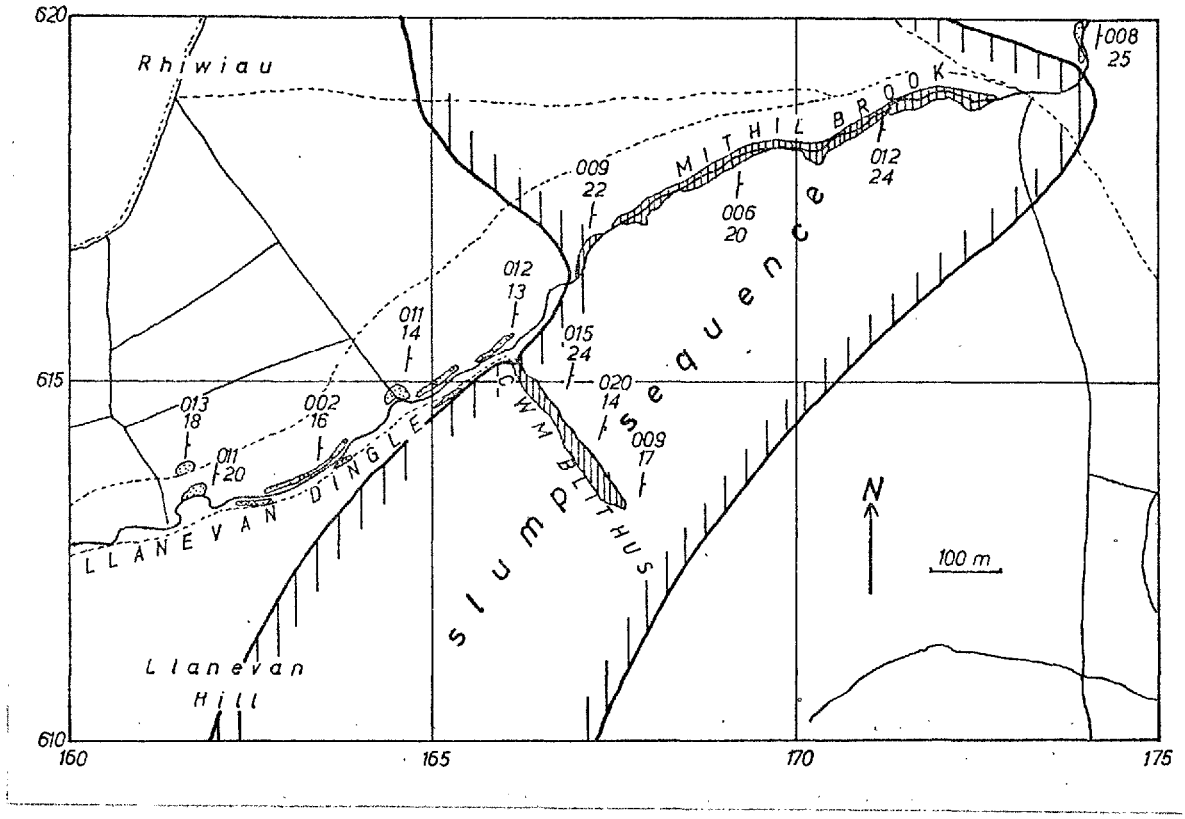


FIGURE 4.2 Geological map of the area around Cwm Blithus. Bedding orientation is marked.

thus better represented on a section than on a map. An accurately measured section (Enclosure 2) has been constructed to show the structural composition of the sequence. Despite the possibility that the gully is fault controlled, there is no discernible displacement across it, and the section therefore combines information from both its eastern and from its western wall.

The succession exposed in Llanevan Dingle below Cwm Blithus comprises finely flaggy muddy siltstones with some silt turbidite beds (Fig. 4.3). There is no trace of slumping. The first major slump sheet outcrops at the foot of Cwm Blithus, and this horizon is taken as the base of the slump sequence. Above this level the sequence has been divided into segments of four main structural types (Enclosure 2).

Undisturbed segments comprise the sediments which were deposited in between slump episodes. They are, therefore, the 'autochtonous' units of the succession. The lithology is almost identical to that below the slump sequence, except that the occasional structureless 'fluxoturbidite' bed is present (as in Unit 27, see Fig. 4.4). The original bedding is everywhere unslumped (Fig. 4.5), but some convolute lamination occurs in the turbidite beds.



FIGURE 4.3 Undisturbed muddy siltstones in Llanevan Dingle (SO 162613) below the slump sequence.

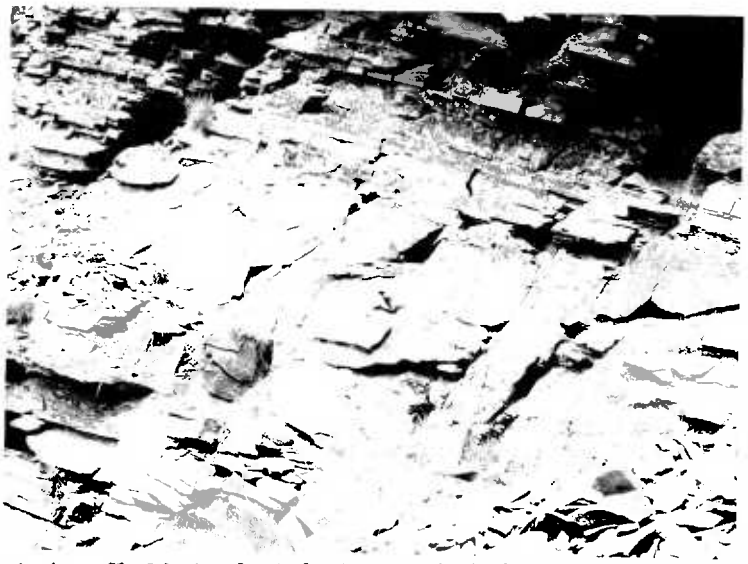


FIGURE 4.4 Undisturbed beds containing a massive 'fluxoturbidite' member (Unit 27).



FIGURE 4.5 Undisturbed segment within the main slumped sequence (Unit 25).



FIGURE 4.6 A folded slumped segment within Unit 5.

Folded slumped segments show deformation of the original bedding without its obliteration (Fig. 4.6), and individual beds can be traced through a series of adjacent folds. The lithology is apparently similar to that in the undisturbed units. Some turbidite beds are involved in the slump folds in addition to the laminated silts.

Slumped segments with intrafolial folds show an almost total destruction of the original bedding on the scale visible in outcrop, with folds, sometimes barely discernible, occuring as isolated remnants (Fig. 4.7). The areas where the original bedding has apparently broken down show a laminated or phacoidal structure in outcrop. Splitting surfaces, both in the laminated areas and within the folds, may show a lineated surface. The slumped segments with intrafolial folds grade into the 'laminated slumped segments'.



FIGURE 4.7 An intrafolial fold isolated within laminated sediment (Unit 18).

Laminated slumped segments show the complete replacement of visible bedding by the laminated (Fig. 4.8) or phacoidal (Fig. 4.9) structure, and show no trace of folding. Lineated surfaces are common (Fig. 4.10).

The undisturbed units divide the sequence into a number of slumped units, each comprising various combinations of the different types of slumped segment. Many of these units probably represent an individual slump sheet, that is a sheet introduced during one discrete slump episode. Each slump sheet may therefore contain several different structural segments as distinguished in the field. However it is probable that some units are composite, being composed of sheets from several episodes, without any intervening undisturbed unit.



FIGURE 4.8 A laminated slumped segment (Unit 30).



FIGURE 4.9 Phacoidal structure developed in Unit 30.

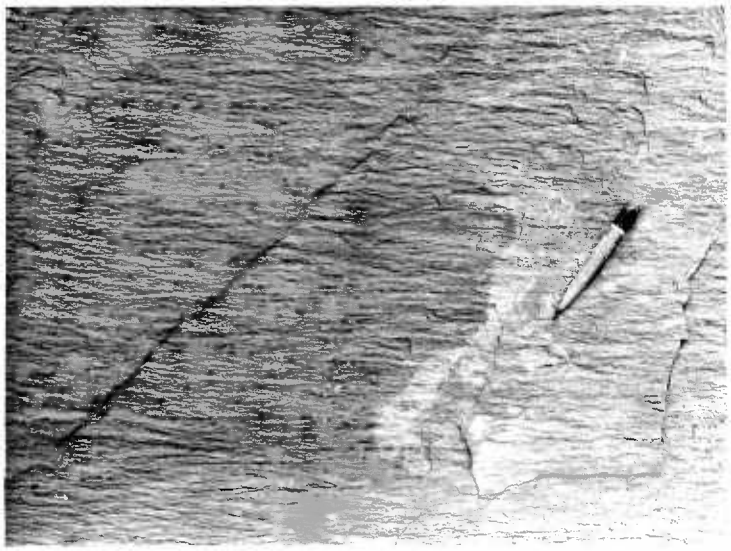


FIGURE 4.10 A lineated lamination surface within slumped Unit 17.

The contacts between adjacent structural segments are most usually gradational. This is especially true of 'contacts' between laminated slumped segments and slumped segments with intrafolial folds, which represent a rather arbitrary division of what is clearly a continuum of structural types. Distinct contacts do occur however at the upper margins of some of the slumped units (e.g. above Units 7, 11, 18; Enclosure 2). Folds in the slumped unit are truncated by a sharp erosional surface, and are directly overlain by undisturbed strata. Such contacts conclusively prove that deformation occurred before deposition of the overlying unit. Where the upper section of a slumped unit is laminar, the exact position of the contact with the overlying undisturbed unit is often uncertain. The lower contacts



FIGURE 4.11 Lower contact of slumped Unit 5.

of slumped units are always gradational, usually through a zone with a laminar structure (Fig. 4.11).

One clear example has been seen of a contact between two slump sheets without any intervening autochthon (above Unit 17). Folds in the lower unit are clearly truncated and overlain by a laminated slumped segment of the succeeding sheet (Fig. 4.12). This again suggests that some of the other slump units may be composite, but without clearly recognisable sheet contacts.

The top of the slump sequence is not exposed in Cwm Blithus, but apparently lies only a short way above the highest exposures in the gully (Fig. 4.2).



FIGURE 4.12 Contact between two slumped units (Units 17 and 18).

4.2 THICKNESS OF THE CONSTITUENT UNITS

Of the 32 exposed units (totalling 205 metres), 29% comprise undisturbed units, 5% folded slumped segments, 34% slumped segments with intrafolial folds and 32% laminated slumped segments. Slumping was clearly the most important depositional process in this part of the basin, over the long period represented by the slump sequence. A better idea of the pattern of slump deposition through time is, however, obtained by considering the thickness of individual units.

A thickness frequency histogram for the unslumped units is positively skewed with a mode of about 3 metres and a mean of 3.8 metres (Fig. 4.13). The data have been fitted to a gamma distribution

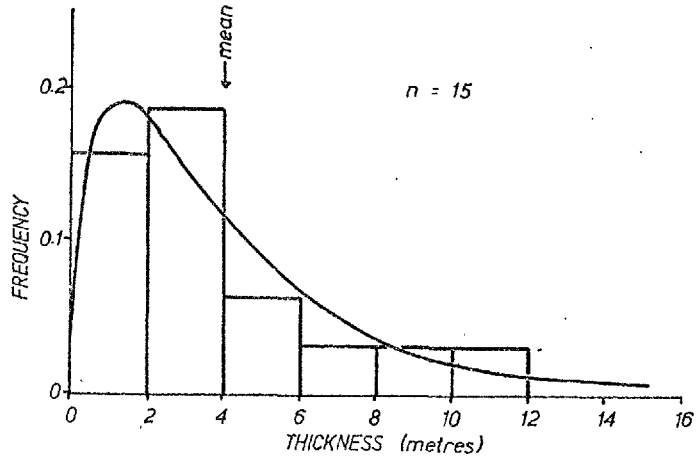


FIGURE 4.13 Thickness frequency histogram for the unslumped units.

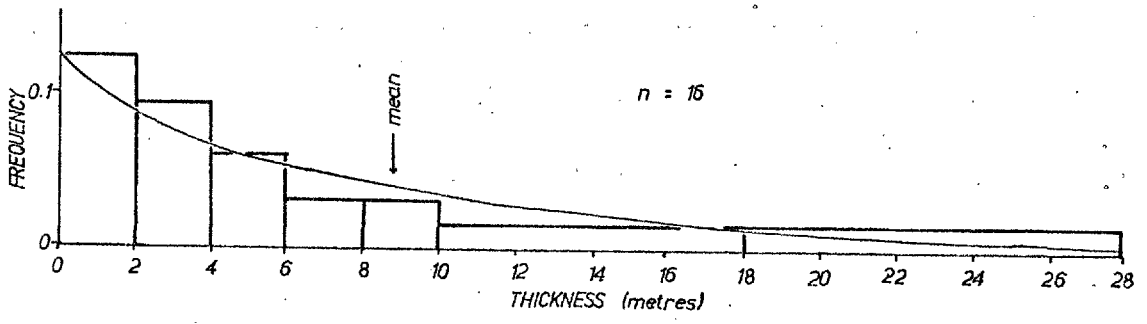


FIGURE 4.14 Thickness frequency histogram for the slumped units.

of the form

$$f(x) = \left(\frac{k}{\mu}\right)^k \cdot \frac{x^{(k-1)} \cdot e^{-kx/\mu}}{\Gamma(k)}$$

where μ is the mean and k is a skewness parameter (see Cox et al. 1966, p. 137-8). The estimated k value is about 1.52. The analogous histogram for slumped unit thicknesses (Fig. 4.14) is strongly positively skewed, and fits a gamma distribution with a mean (μ) of 8.8 metres and a k value of 0.96. This approximately corresponds to an exponential distribution (obtained with k = 1).

The significance of these histograms will be fully discussed in Sec. 10.4. However some estimate of the frequency of slump episodes can be made here by assuming that the thickness of an undisturbed unit is proportional to the time between successive episodes. Assuming a sedimentation rate of 20 cm/1000yr (Sec. 9.2), the modal interval between slump sheet incursions was about 15,000 years, and the mean about 19,000 years.

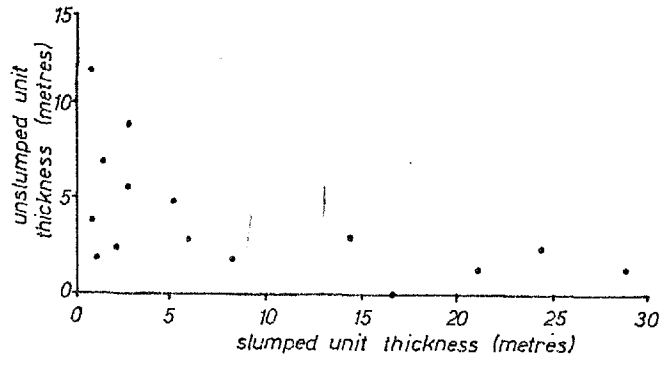


FIGURE 4.15 Plot of the slumped unit thickness against the thickness of the underlying unslumped unit.

If, as is likely, some of the slumped units are composite, the histograms in Figs. 4.13 and 4.14 would be modified slightly. The mean thickness of the slumped units would be reduced, and their distribution would become less positively skewed with a higher 'k' value. The extra very thin, or missing, unslumped units would lower the mean unslumped thickness and lower the 'k' value, to give a more positive skew.

It might be expected that the thickness of each slumped unit would correlate with the thickness of the underlying undisturbed unit. Both might reflect the same time interval; the slumps of deposition in the source area of slumping, and the autochthon of deposition in the basin. However, no such correlation exists (Fig. 4.15), suggesting that more than one source area, perhaps at different distances up the marginal basin slopes, was operative during deposition of this sequence.

4.3 ORIENTATION OF STRUCTURES

Orientation data from the entire slump sequence have been combined, and are plotted in Fig. 4.16.

The bedding in the undisturbed succession below the slump sequence dips regularly eastward at about 10 to 20 degrees (Fig. 4.16A). The undisturbed units within the slumped sequence have essentially the same bedding orientation (Fig. 4.16B), but with slightly more dispersion of poles. This regularity of the bedding orientation throughout the sequence enables the orientation of slump structures from different units to be validly compared without prior correction. The mean undisturbed bedding trace is marked on Figs. 4.16C-F as a reference datum.

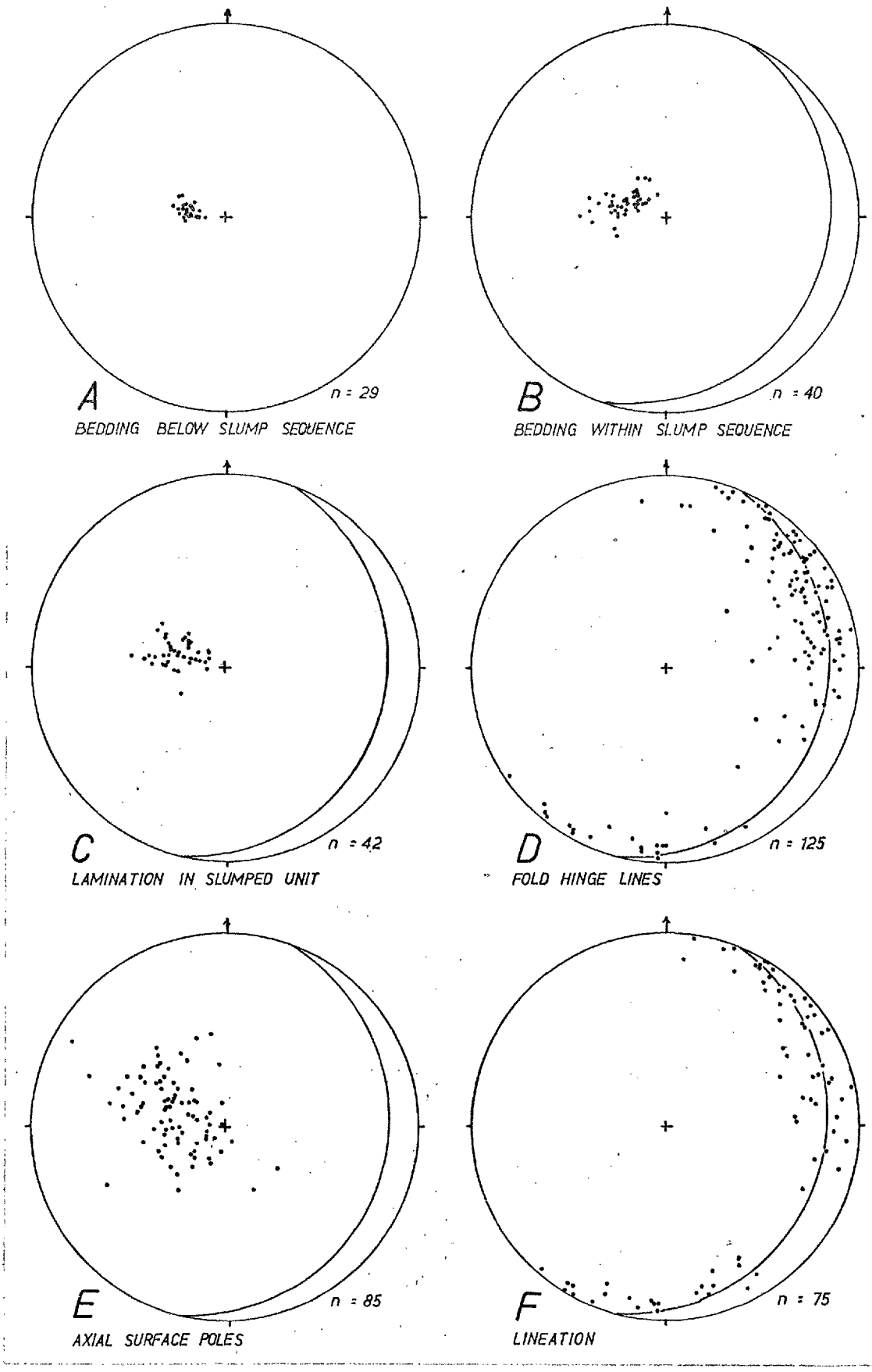


FIGURE 4.16 Projections of orientation data from within and below the slump sequence. The trace of the mean bedding within the sequence is marked on projections B to F.

Within the slumped units the most regular structure is the lamination, which is approximately parallel to the bedding in the undisturbed units, and consequently parallel to the gross attitude of each sheet (Fig. 4.16C). Anomalous attitudes of the lamination occur in Unit 9 and the lower part of Unit 11. These are plotted separately in Fig. 4.17. The dips of bedding in the intervening undisturbed Unit 10 are also anomalous, suggesting a tectonic rather than a slump origin. Data from this restricted part of the sequence have been ignored in plotting Figs. 4.16D,E & F.

The hinge lines of folds form a great circle girdle approximately in the plane of the slump sheets (Fig. 4.16D). There is a tendency to cluster in the northeast quadrant of the plot. Fold axial planes tend to lie in the plane of the sheets, though with some dispersion about an axis approximately parallel to the mean fold axis direction (Fig. 4.16E). The crinkled lineations present on many lamination surfaces within the slumped units also define a girdle within the plane of the sheets (Fig. 4.16F). Some lineations are demonstrably axial to folds in the field, and all have a tendency to cluster in the northeast quadrant in a similar manner to the fold axes.

The relationships between distributions of the different structures are more clearly revealed by using the synoptic plotting techniques described in Appendix 2. The plot of principal axes of the six distributions (Fig. 4.18) emphasises their symmetrical relationship to

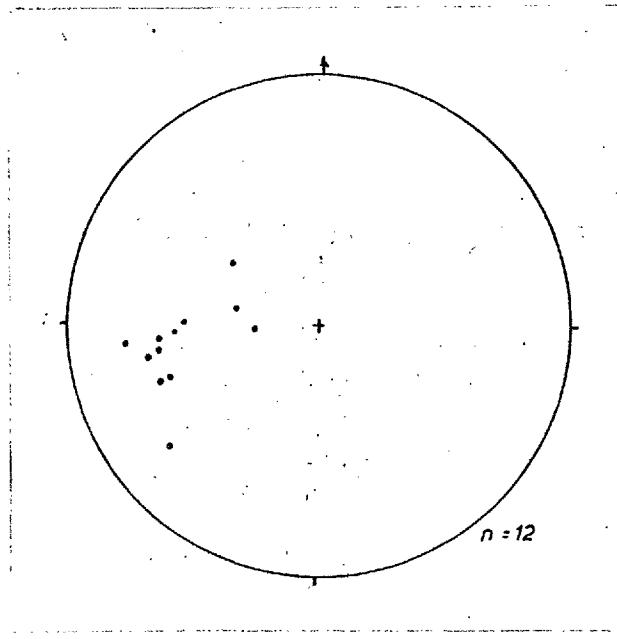


FIGURE 4.17 Anomalous attitudes of bedding and lamination in Unit 9, 10 & 11.

the gross attitude of the sequence, and hence to the original depositional datum. The near coincidence of the fold axis mean, the lineation mean, and the pole to the girdle of axial plane poles is also apparent. The deduction of slump movement direction from this diagram is discussed in Sec. 4.4. The forms of the six distributions are summarised on an eigenvalue ratio plot (see Appendix 2) in Fig. 4.19.

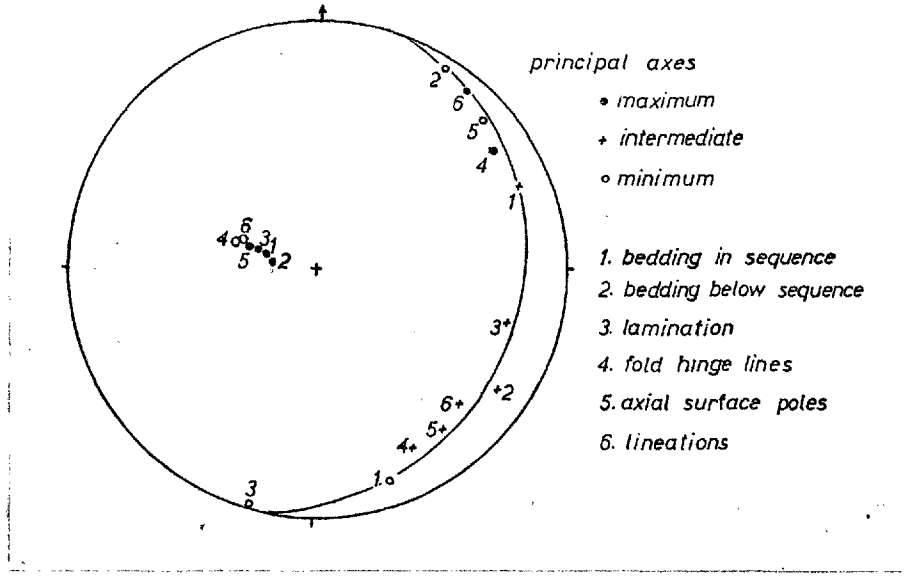


FIGURE 4.18 Plot of the principal axes of the distributions in Fig. 4.16.

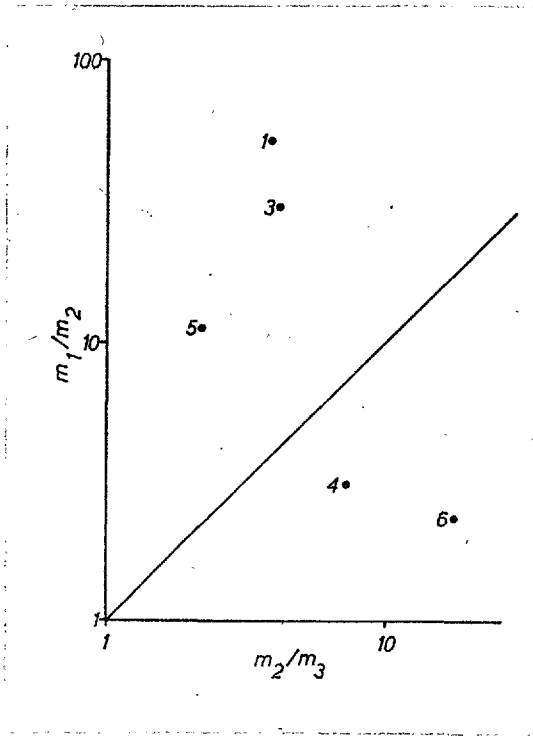


FIGURE 4.19 Ratio plot of the distributions in Fig. 4.16. The points are numbered according to the scheme in Fig. 4.18.

4.4 THE ESTIMATION OF PALAEOSLOPE TREND AND ITS VARIABILITY

A complete determination of the palaeoslope orientation involves firstly an estimate of its trend, which will be derived in this section, and secondly the determination of the direction of slope, which is the subject of Sec. 4.5.

The relationship of structure orientation to the palaeoslope is most clearly seen if distributions are referred to the depositional datum. The synoptic plot of principal axes (Fig. 4.18) has therefore been rotated in Fig. 4.20 to refer to the mean bedding attitude in the slump sequence. Circles representing the confidence limits about the mean directions at the 95% confidence level have been plotted. Comments on the validity of this procedure are given later in this section.

The usual assumption that the mean fold axis indicates the palaeoslope trend yields an estimate of about 060°. A broadly similar figure of about 040° is derived from the mean lineation trend, and of about 050° from the pole to the girdle of axial surface poles. These estimates are compatible with the independent evidence of palaeoslope trends from isopachs (Fig. 3.6), and agree with Bailey's (1964) estimate based on slump fold axis measurements in the same area. However the significant divergence of trend estimates based on different structures questions their accuracy. The two main factors which may influence the accuracy are the sample size and possible heterogeneity of the sample.

Sample heterogeneity could, in this area, be due to significant variation in the attitude of structures between different slumped

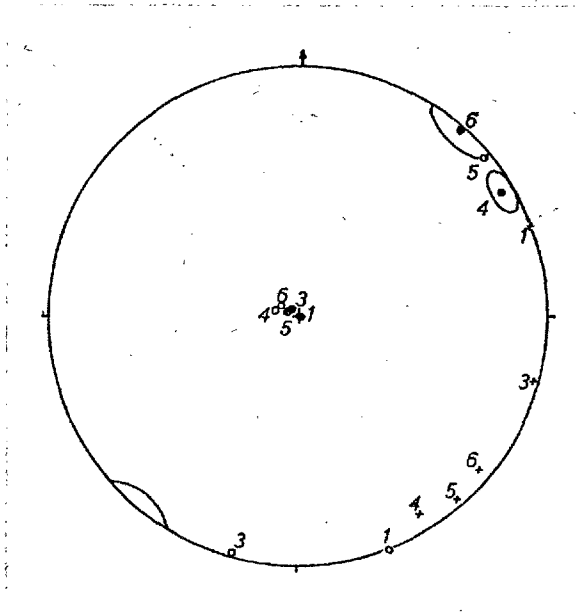


FIGURE 4.20 Principal axis plot as in Fig. 4.18 but corrected for tectonic tilt. 95% cones of confidence are given for lineations and fold hinge lines.

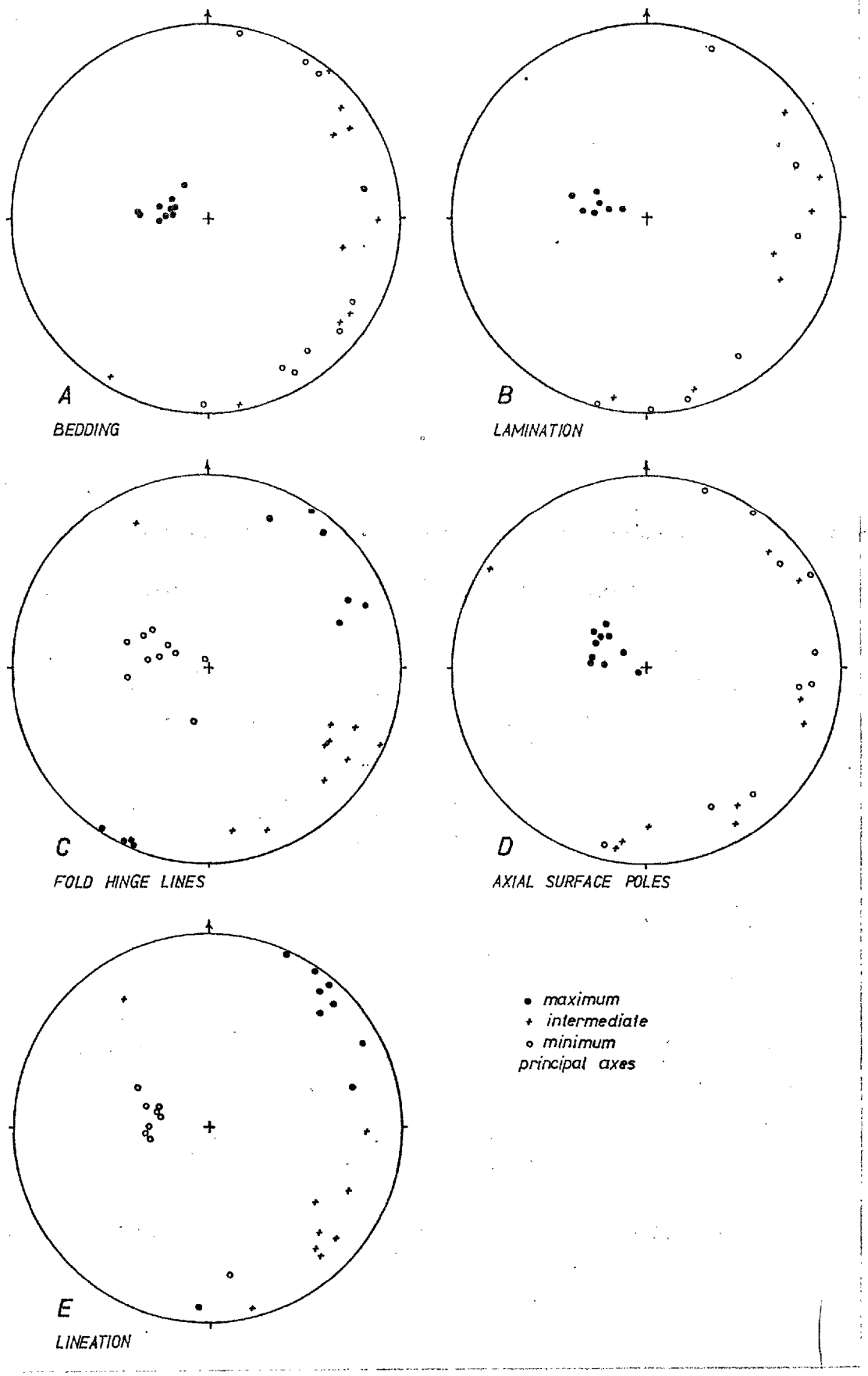


FIGURE 4.21 Plots of the principal axes of the distributions of structures from each slumped unit in the sequence.

units. This possibility has been investigated by analysing separately the data from each unit of the slump sequence. Synoptic plots of the principal axes of the distributions of each type of measurement are given in Fig. 4.21, and the shapes of the distributions are summarised on an eigenvalue ratio plot in Fig. 4.22. One principal axis of most distributions plots almost vertically. This confirms the symmetrical relationship of all structures to the original depositional datum throughout the sequence, and determines that the other two axes lie essentially in the plane of the mean bedding. Those for the bedding and lamination (Fig. 4.21A,B) have no preferred orientation within this plane, since the distributions are essentially axially symmetrical (see ratio plot, Fig. 4.22). Those for the axial planes (Fig. 4.21D) also show no preferred orientation, but the maximum principal axes for hinge lines and lineations (Fig. 4.21C,E) show a tendency to cluster in the NE and SE of the plot.

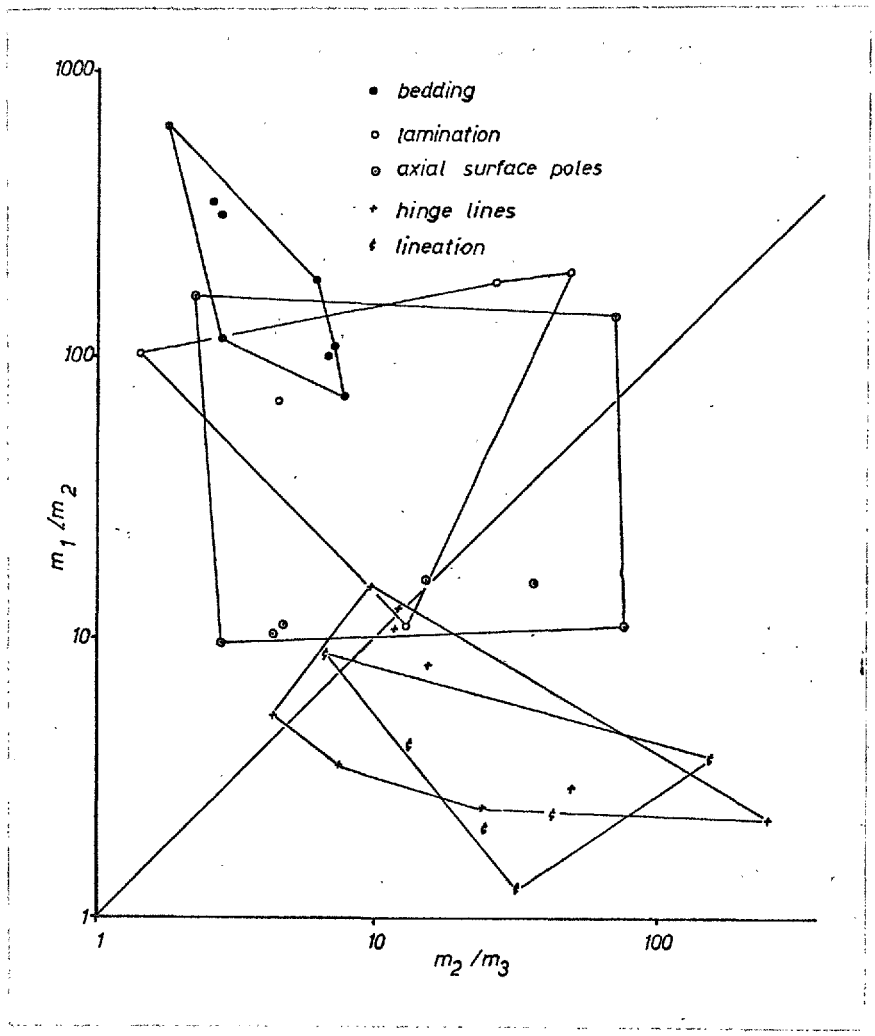


FIGURE 4.22 Ratio plot of the distributions of structures from each slumped unit within the sequence. The lines mark the fields corresponding to each structure.

Much of the apparent variation between units evidenced in Figs. 4.21 and 4.22 is probably attributable to the small samples obtainable (Fig. 4.23). This effect can be tested by computing confidence limits about the mean in the same way as shown in Fig. 4.20. This procedure is only strictly valid for data distributed according to Fisher's (1953) distribution (i.e. for axially symmetrical unimodal clusters), but, in the absence of any other statistic, provides a useful estimator of the accuracy of the mean for other unimodal distributions. It will, in general, underestimate the error in trend, and overestimate the error in plunge, of a mean in a similar orientation to those considered here.

The azimuthal estimates of palaeoslope trend, and their angular confidence limits at the 95% level, are plotted in Fig. 4.24 for hinge lines and lineations from each individual slumped unit. The azimuths have been corrected for tectonic tilt. The plots reveal the rather large uncertainty (usually greater than $\pm$ 20°) in the estimates of

UNIT NO.	SAMPLE SIZES			
	lamination	hinge lines	axial planes	lineation
32	4	1	0	2
30	8	10	11	13
28	0	0	0	0
26	2	0	0	2
24	0	0	0	0
22	0	0	0	0
20	7	5	3	15
18	1	6	4	6
17	14	6	3	20
15	2	5	3	6
13	0	0	0	0
11	12	4	4	8
9	1	1	1	2
7	0	9	4	1
5	0	71	52	0
3	0	2	2	1
1	1	6	3	2

FIGURE 4.23 List of sample sizes from the slumped units.

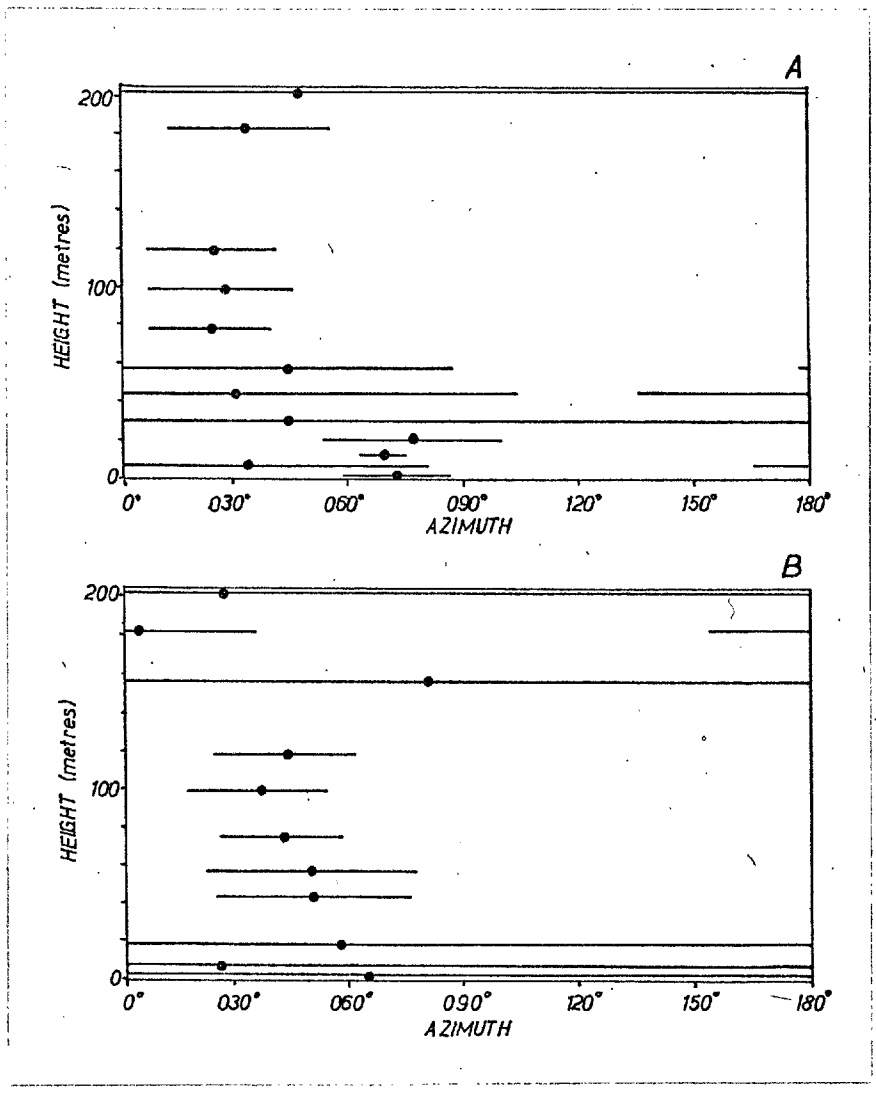


FIGURE 4.24 Plot of mean azimuthal estimates of palaeoslope trend and their 95% confidence interval for A) fold hinge lines and B) lineations, against height in the slump sequence.

palaeoslope trend. If any consistent pattern exists in the means, it is a tendency towards a more northerly azimuth in the higher levels of the sequence. This accounts for the difference in mean trend of the lineations and hinge lines from the total sequence (Fig. 4.20), since more hinge line measurements were taken in the lower, and more lineation measurements in the upper, part of the sequence (Fig. 4.23). If the northerly shift in palaeoslope trend is a real effect, however, it is unlikely to have been of more than local importance.

The correlation of sample size and accuracy of the palaeoslope trend estimate is shown in Fig. 4.25. Estimates with accuracy better than $\pm$ 10°, at the 95% confidence level, can only be obtained with samples larger than about n = 100. It is important to realise, therefore, that any palaeoslope estimates based on samples from

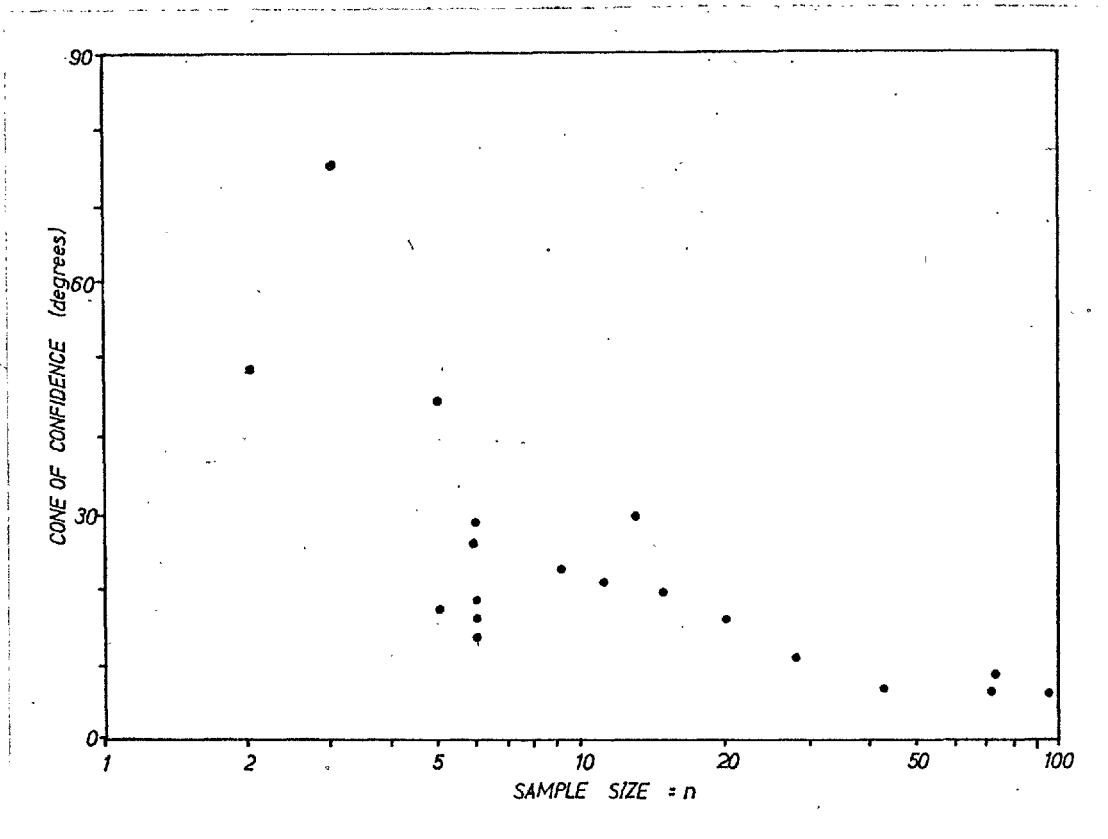


FIGURE 4.25 Plot of sample size against the semi-apical angle of the 95% cone of confidence for the mean, for all hinge line and lineation samples.

dispersed populations of fold hinge lines are subject to large errors. Large samples are often unobtainable from slump sheets, due to their limited thickness, partial destruction of folds and, in Central Wales, their poor exposure, so the resultant inaccuracy must be admitted and preferably quantitatively estimated.

4.5 DETERMINATION OF SLUMP MOVEMENT DIRECTION

Fold axis orientation only gives an estimate of the trend of a palaeoslope and not of its slope direction. In some cases regional evidence clearly indicates one of the two opposing possibilities. This is so in Cwm Blithus. Facies studies and isopach maps (Chap. 3) show that the area lay on the southeastern side of the Montgomery Trough, and that the palaeoslope must have faced towards the northwest. However, in the western slump sequence, to be described in Chapter 6, regional evidence is inconclusive. In this section, therefore, various techniques for estimating slump movement direction will be assessed prior to their use for the Clun Forest slumps.

The closure directions of folds have been used by several authors (see Fig. 2.16) to determine transport directions, usually with little success. The assumption has been that isolated slabs of more competent sediment turned over at their leading edges by some unspecified mechanism, and that folds should therefore close in the direction of transport. This hypothesis has been tested by plotting the closure direction of each fold as the normal to the hinge line within the axial plane (Fig. 4.26). A solid circle has been used if the fold closes into the lower hemisphere, and an open circle if into the upper. Data have been corrected for tectonic tilt. They have also been summarised in an azimuthal histogram which includes, in addition to the stereographically plotted data, the closure directions of folds with unknown axial plane orientation. Both graphs show that there is no predominance either of northwesterly or of southeasterly closure. This technique is therefore unreliable as a transport direction indicator.

An intuitively sounder indicator is the sense of fold asymmetry. This has been used successfully by several authors (see Fig. 2.6), but has the disadvantage in this area that the asymmetry sense of most folds cannot be determined. However, consistent results are obtained

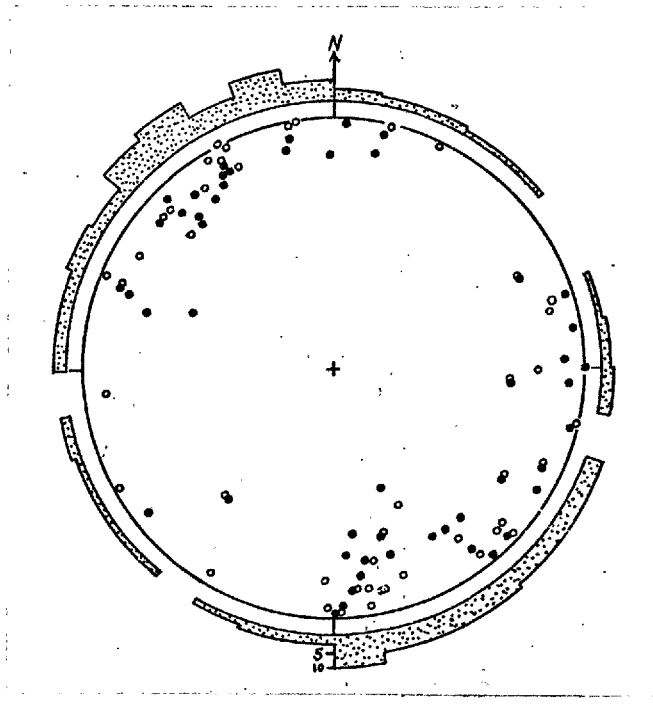


FIGURE 4.26 Projection of fold closure directions. A solid circle indicates closure into the plot, and an open circle out of the plot. An azimuthal frequency histogram summarises that data, which have been corrected for tectonic tilt.

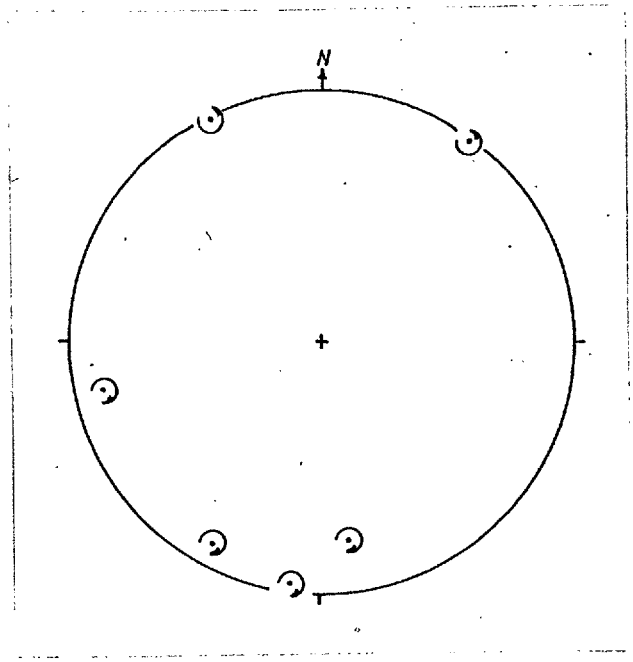


FIGURE 4.27 Rotation sense of asymmetric folds. Data corrected for tectonic tilt.

from the few folds to exhibit a clear asymmetry (Fig. 4.27), and these are compatible with a northwesterly transport direction. A similar technique has been applied to the microfolding responsible for much of the lineation in the slumped units. Though results are not wholly consistent, the majority of microfolds also indicate a northwesterly facing slope (Fig. 4.28).

One other useful, and previously unused, direction indicator is

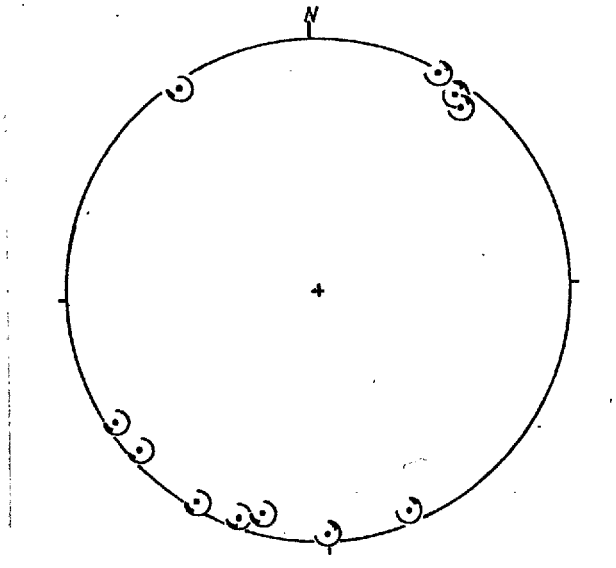


FIGURE 4.28 Rotation sense of asymmetric microfolds associated with the lineation. Data corrected for tectonic tilt.

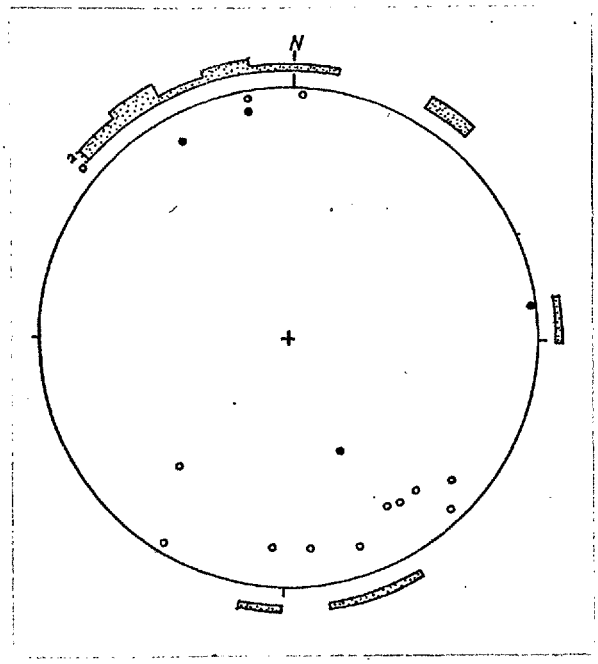


FIGURE 4.29 Projection of fold facing directions, with similar conventions to Fig. 4.26.

the direction of fold facing - their younging direction along the axial surface. The facing directions were difficult to determine in the field, but could often be determined on cut and polished profile sections. This necessarily limited the number of determinations which could be made. A similar form of representation to the closure plot has been used (Fig. 4.29), and shows a predominant facing towards the northwest. The presence of southeast facing folds can only be attributed to 'rolling' of folds about their axes, evidence for which is commonly seen. Nevertheless facing direction seems a reliable indicator of transport direction.

It was noted (Sec. 4.3) that the orientation of all structures is symmetrically related to the depositional datum as determined from the undisturbed bedding. In fact (see Fig. 4.20) there is a slight, and consistently directed, deviation of the 'vertical' principal axis of each distribution from that of the bedding. This 'imbrication' of axial surfaces, lamination, and the hinge line and lineation girdles is consistent with a northwest facing slope. Although, in the present case, this effect is too small to be statistically significant, it may nevertheless be a real effect which could be of more positive use in other areas.

4.6 FOLD ATTITUDE AND SIZE

The total attitude of folds is best described according to the scheme of Fleuty (1964). Though Fleuty's diagram relating axial plunge and axial surface dip was devised as an aid to classification of fold attitudes, it can also serve as a graph for summarising data. In Fig. 4.30 the axial plunge and axial surface dip of the Cwm Blithus folds have been plotted. The resulting plot loses any azimuthal information, but clearly reveals the total attitude of the folds. The data have been transformed to refer to the original depositional datum, and on this basis most folds have sub-horizontal or gently plunging axes, with recumbent or gently inclined axial surfaces.

The specification of fold dimensions by the usual wavelength and amplitude parameters is not possible for the Cwm Blithus slump folds because of their isolated 'intrafolial' geometry (Fig. 4.7). Instead the 'length' and 'breadth' of each fold packet was recorded (Fig. 4.31A). These parameters clearly lack the genetic significance of wavelength

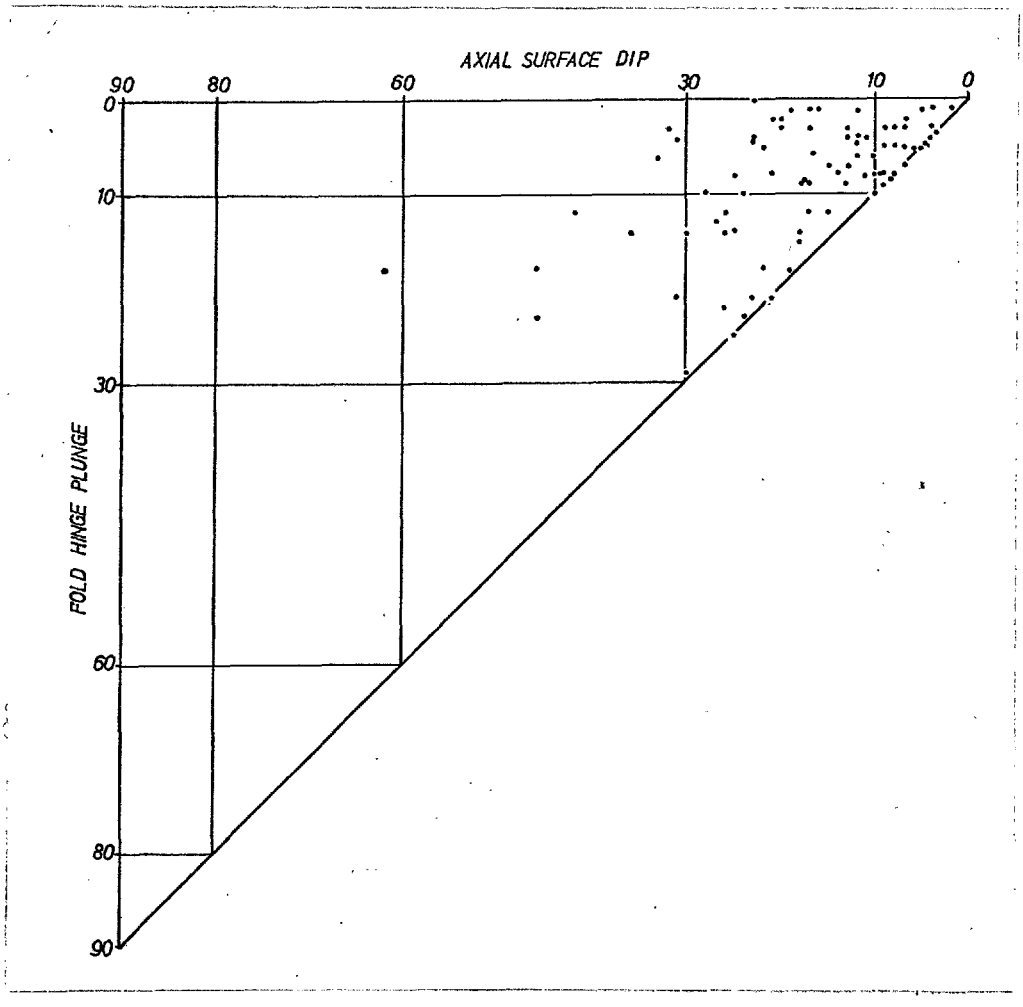


FIGURE 4.30 Plot of fold axial plunge against axial surface dip (cf. Fleuty 1964). Attitudes have been corrected for tectonic tilt.

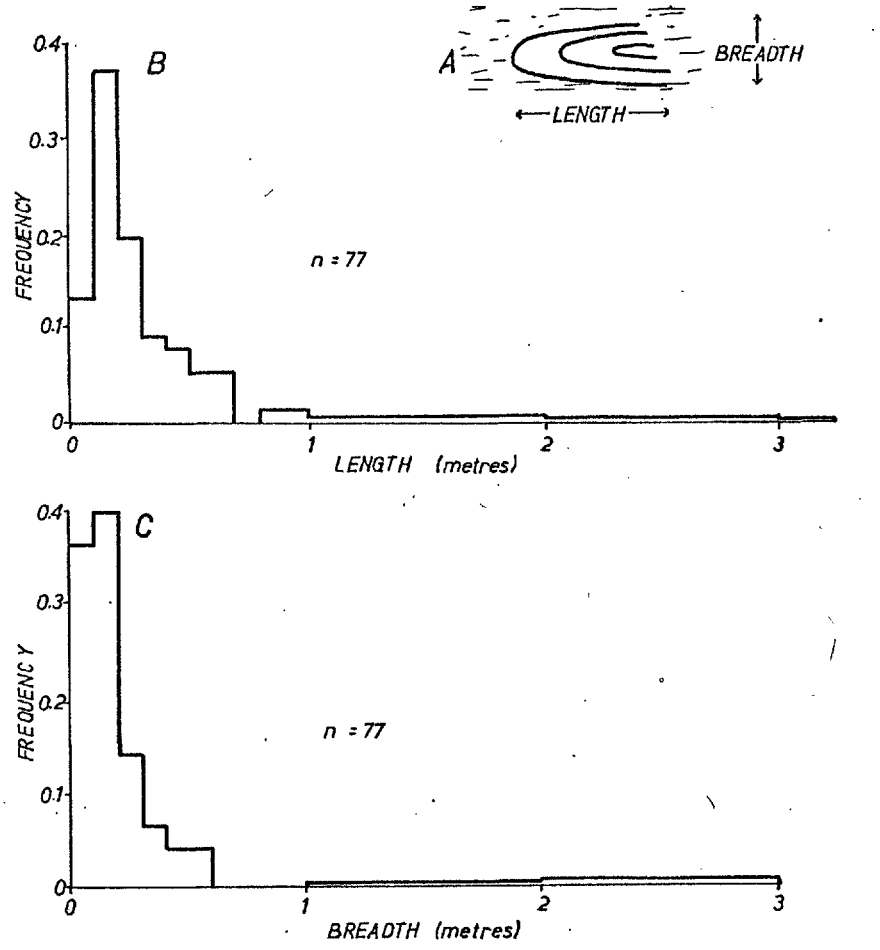


FIGURE 4.31 Frequency histograms of 'length' and 'breadth' of fold packets from the whole sequence.

and amplitude, but are the only objective measure of fold size available in this situation. Histograms of length and breadth frequency (Fig. 4.31B,C) do, however, show a similar positive skew to wavelength and amplitude histograms of tectonic folds recorded by Hudleston (1973c), and approximate to lognormal distributions. Separate histograms (Fig. 4.32) constructed for Units 5 & 7 (of 'folded' type) and for the remainder of the sequence (of 'intrafolial fold' type) reveal the relatively smaller size of folds in the former units. The distinctive character of these 'folded' units has already been apparent from the abundance of folds which they contain (Figs. 4.6, 4.23), and they will also be seen to differ in the fold styles exhibited.

A plot of the length against the breadth of each fold (Fig. 4.33) is approximately linear, and reveals a similar range of length/breadth ratios for folds of all sizes.

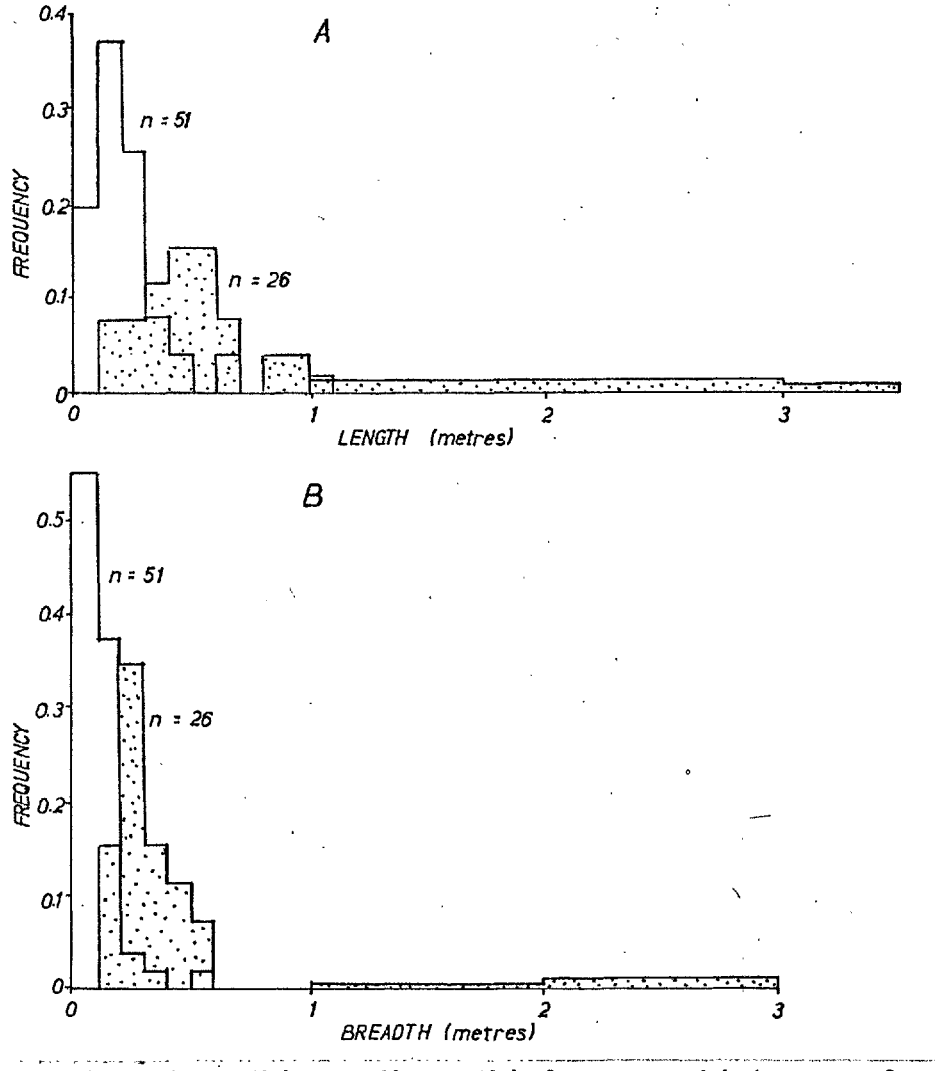


FIGURE 4.32 'Length' and 'breadth' frequency histograms for Units 5 & 7 (plain) and for the remainder of the sequence (stippled).

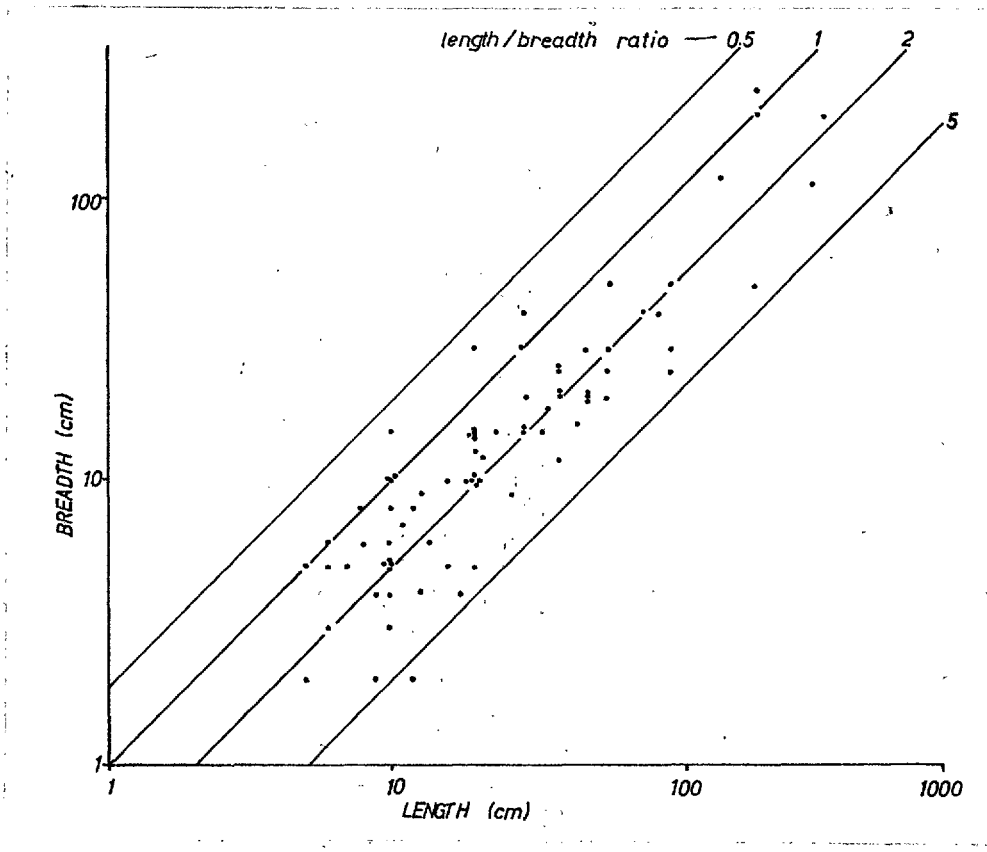


FIGURE 4.33 Plot of 'length' against 'breadth' of folds.

4.7 FOLD STYLE : SURFACE SHAPES

The first elements of fold style to be considered are those connected with the shape of single surfaces within folds.

Interlimb angles of folds were recorded in the field and also measured on collected hand specimens. Histograms of interlimb angle frequency in the total sequence (Fig. 4.34) show essentially similar distributions from both sampling methods, with modes close to 0° and with means between 20° and 30°. Comparison of field results from Units 5 & 7 with those from the remainder of the sequence (Fig. 4.35) reveals smaller and less variable interlimb angles in these 'folded' units.

The isolated 'intrafolial' occurrence of many of the measured folds reduces the accuracy of interlimb angle determinations, since

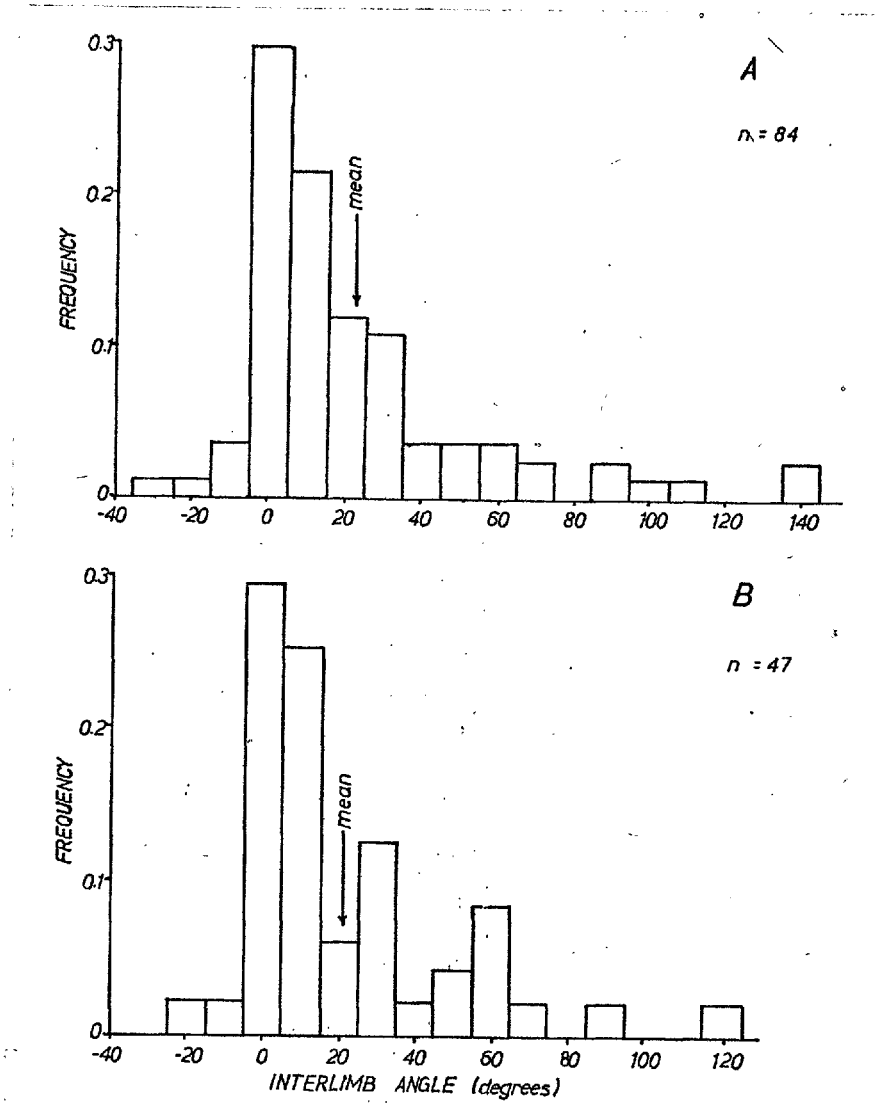


FIGURE 4.34 Frequency histograms of fold interlimb angles measured A) in the field and B) on hand specimens.

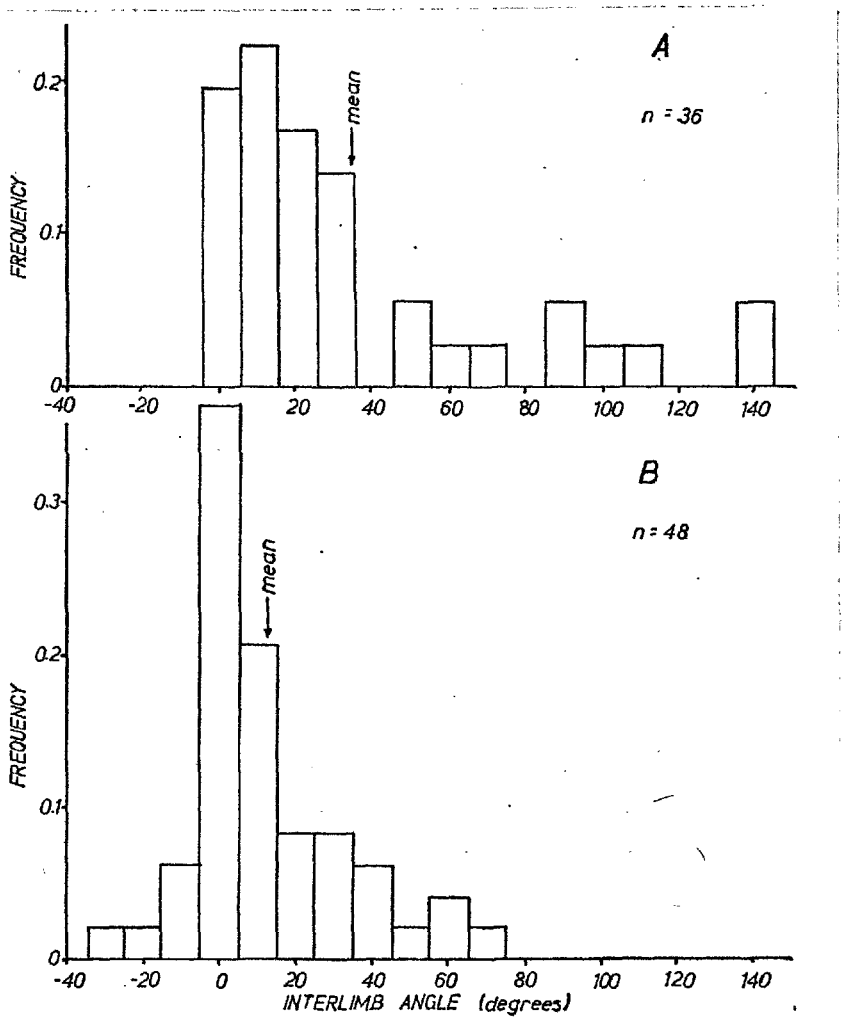


FIGURE 4.35 Frequency histograms of fold interlimb angles measured in the field within A) Units 5 & 7 and B) the remainder of the sequence.

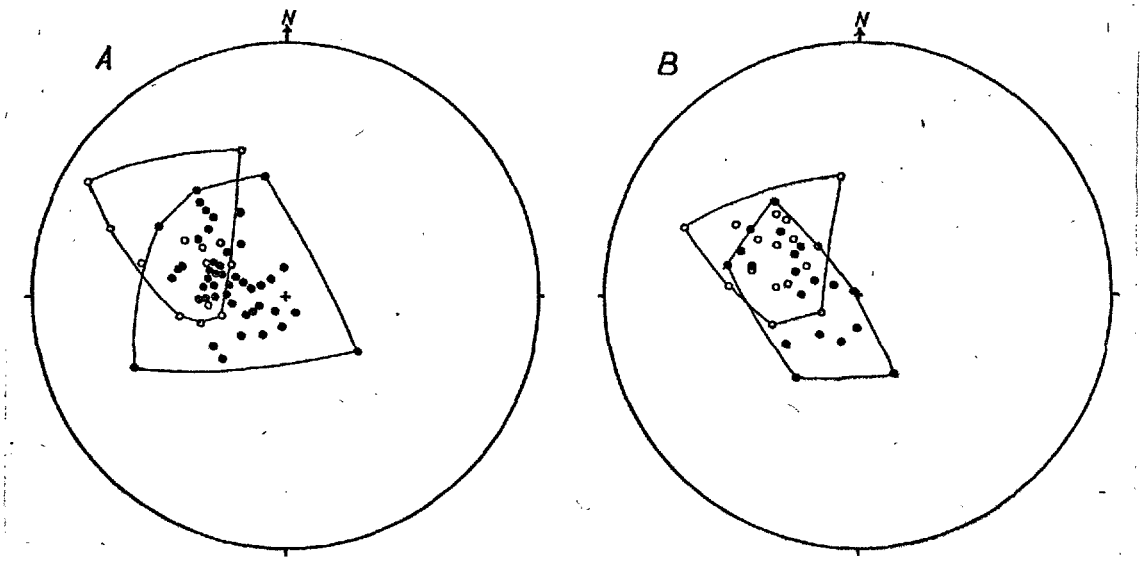


FIGURE 4.36 Poles to axial surfaces of folds having interlimb angles above the mean (solid circles) and below the mean (open circles), A) from field measurements, B) from hand specimens.

inflexion points cannot be determined. The angle recorded for a fold was therefore the minimum interlimb angle visible anywhere within it. Elimination of any errors inherent in the data would lower the mean angle. In fact the errors are probably small, since the folds most prone to large errors (those with large interlimb angles) are usually among the few whose true angle can be verified.

There is a broad correlation between interlimb angle and axial surface attitude, revealed in Fig. 4.36. The more open folds tend to have steeper axial planes, compatible with a tightening of folds during progressive deformation.

The interlimb angle defines only one aspect of the shape of a folded surface. A more complete specification is provided by Fourier analysis of surfaces. The method used is fully described by Hudleston (1973a). Folded surfaces are divided into quarter-wavelength segments. Each segment is fitted to a function of the form

$$f(x) = \tfrac{1}{2}a_0 + \sum_{n=1}^{\infty} a_n.\cos nx + \sum_{n=1}^{\infty} b_n.\sin nx$$

By suitable choice of reference axes the coefficients a_0, a_n, and b_{2n} become zero, and the layer shape can be fully specified by the coefficients b_1, b_3, b_5...etc. The first two of these are sufficient to define the shape of most folds with moderate accuracy.

In order to specify the quarter-wavelength units, the hinge and inflexion points must be determinable. The only folds which meet this requirement in Cwm Blithus are those in Unit 5, and Fourier analyses are restricted to this Unit. The determinations made are represented on a graph of b_1 vs b_3 (Fig. 4.37), which is calibrated with the equal 'shape' and 'amplitude' lines derived by Hudleston. The plot reveals a clear trend of shape/amplitude variation, from variable but predominantly angular shapes at low amplitude, towards semi-elliptical or double-hinged shapes at high amplitude. The trend is better shown on a plot of b_1 (approximating to amplitude) against b_3/b_1 (equivalent to shape)(Fig. 4.38A), and the variation is represented pictorially in Fig. 4.38B. The trends are very similar to those determined by Hudleston (1973b) from experimental folds and (1973c) from tectonic folds. Hudleston showed that the trend of fold shapes observed probably also defines the shape change of any single fold during progressive deformation.

In units other than Unit 5 a qualitative visual matching of shapes suggested that most folds fall in the field delineated in Fig. 4.37, or its extrapolation to higher amplitudes. Hence folds with angular hinge zones are rare throughout the sequence, except for some low amplitude folds.

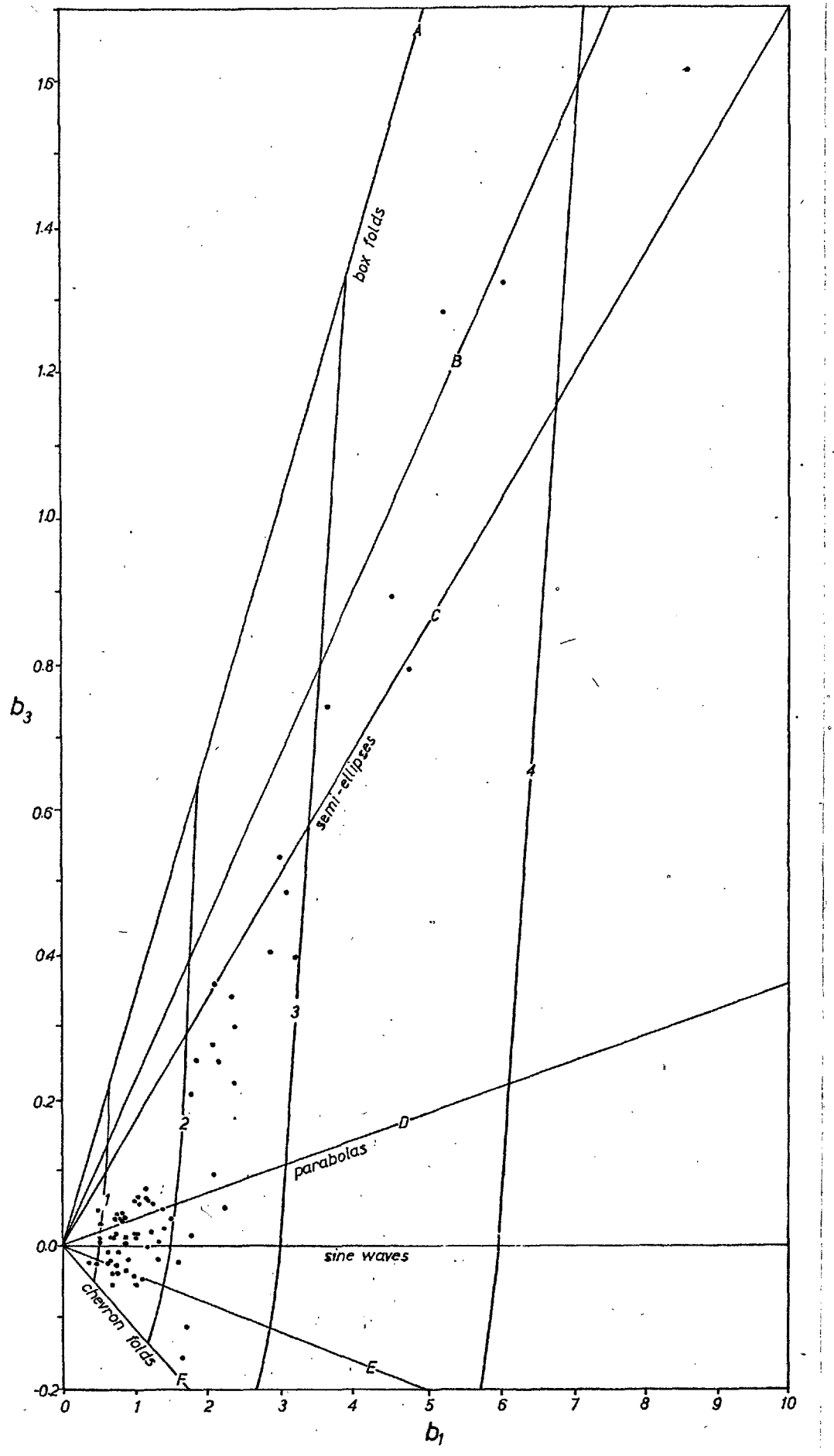


FIGURE 4.37 Plot of the Fourier coefficients b_1 vs b_3 for fold shape. The plot is calibrated following that of Hudleston (1973a).

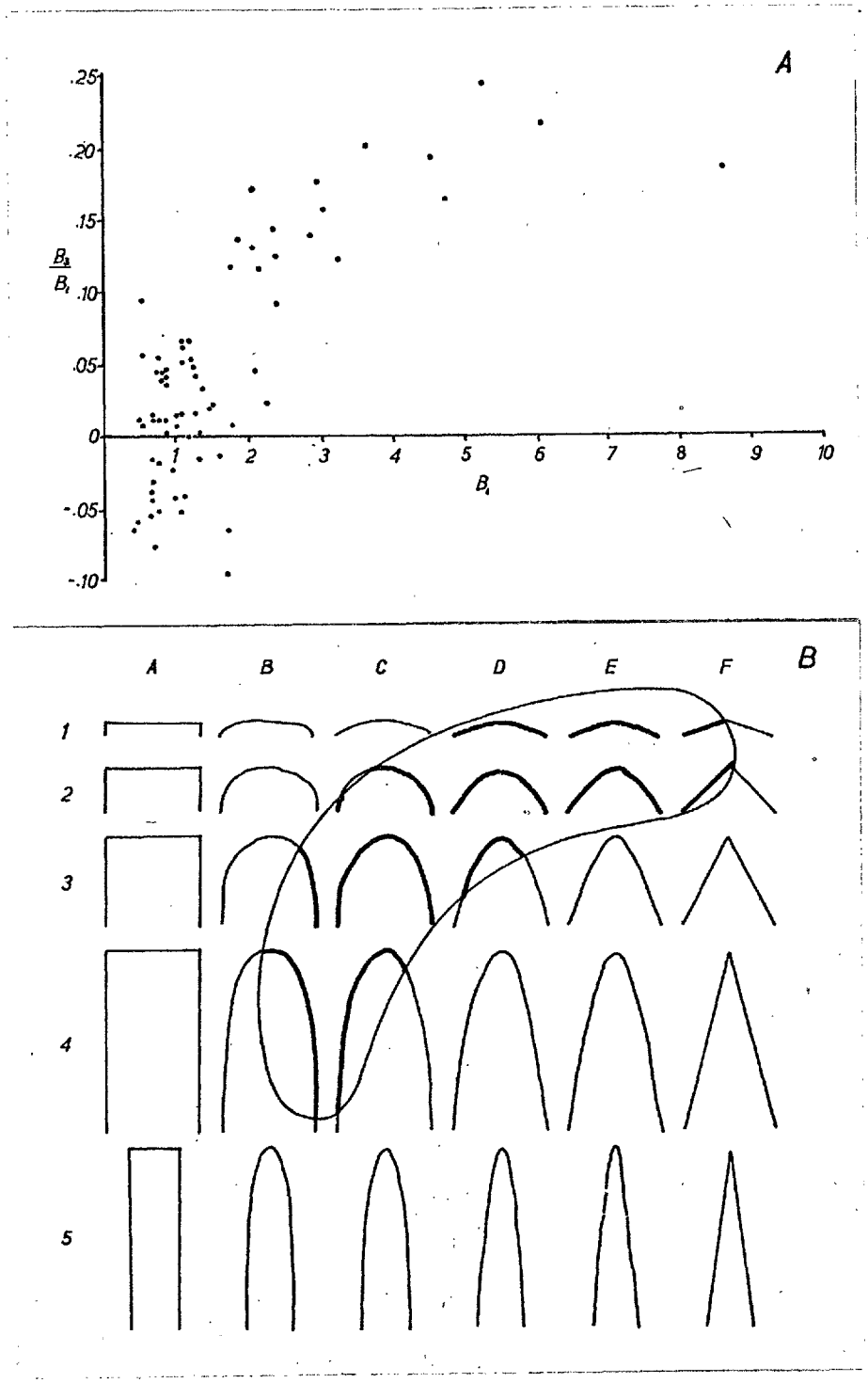


FIGURE 4.38 A) Plot of b_3/b_1 (representing 'shape') against b_1 (approximating to 'amplitude'). B) Pictorial representation of fold shapes after Hudleston 1973a showing the approximate trend evidenced in Fig. 4.37.

4.8 FOLD STYLE : LAYER GEOMETRY

Layer shapes in the slump folds were studied on cut and polished profile sections of hand specimens. Photographs of folds in outcrop were generally inadequate for this purpose, due to the indistinct bedding and the weathering characteristics of the rock.

The folds have been analysed by constructing dip isogons on the profile section (Ramsay 1967). In many of the slump folds, however, there is an initial problem in selecting mechanistically significant folded 'surfaces' for the isogon construction. The fold in Fig. 4.39 illustrates the problem. Two sets of isogons have been drawn; one for a 'coarse' layering and one for a 'fine'. On the basis of the coarse isogons alone the main coarse layer would be classified as Class 1C (approaching Class 2). On the finer scale, however, the layers within this coarse layer vary from Class 1B on the outer arc, to Class 3 towards the core. This is, of course, a reflection of the strain distribution within the coarse layer. An additional feature of the fine layering is the inconsistent sense of refraction of isogons across layer boundaries, as the layer is followed along its length. This probably implies a low competence difference between adjacent layers, and suggests that the deformation was, on this scale, controlled by the bulk anisotropy of the stack of layers rather than by individual layer behaviour. This may also be the case for the coarse layering in Fig. 4.39, though in folds of this scale it exhibits a more consistent layer geometry than the fine layering. The conclusion must be that the choice of surfaces for isogon construction in multilayer sequences of



FIGURE 4.39 Fold with convergent isogons (Class 1C) from Unit 5.

4.8 FOLD STYLE : LAYER GEOMETRY

Layer shapes in the slump folds were studied on cut and polished profile sections of hand specimens. Photographs of folds in outcrop were generally inadequate for this purpose, due to the indistinct bedding and the weathering characteristics of the rock.

The folds have been analysed by constructing dip isogons on the profile section (Ramsay 1967). In many of the slump folds, however, there is an initial problem in selecting mechanistically significant folded 'surfaces' for the isogon construction. The fold in Fig. 4.39 illustrates the problem. Two sets of isogons have been drawn; one for a 'coarse' layering and one for a 'fine'. On the basis of the coarse isogons alone the main coarse layer would be classified as Class 1C (approaching Class 2). On the finer scale, however, the layers within this coarse layer vary from Class 1B on the outer arc, to Class 3 towards the core. This is, of course, a reflection of the strain distribution within the coarse layer. An additional feature of the fine layering is the inconsistent sense of refraction of isogons across layer boundaries, as the layer is followed along its length. This probably implies a low competence difference between adjacent layers, and suggests that the deformation was, on this scale, controlled by the bulk anisotropy of the stack of layers rather than by individual layer behaviour. This may also be the case for the coarse layering in Fig. 4.39, though in folds of this scale it exhibits a more consistent layer geometry than the fine layering. The conclusion must be that the choice of surfaces for isogon construction in multilayer sequences of



FIGURE 4.39 Fold with convergent isogons (Class 1C) from Unit 5.

4.8 FOLD STYLE : LAYER GEOMETRY

Layer shapes in the slump folds were studied on cut and polished profile sections of hand specimens. Photographs of folds in outcrop were generally inadequate for this purpose, due to the indistinct bedding and the weathering characteristics of the rock.

The folds have been analysed by constructing dip isogons on the profile section (Ramsay 1967). In many of the slump folds, however, there is an initial problem in selecting mechanistically significant folded 'surfaces' for the isogon construction. The fold in Fig. 4.39 illustrates the problem. Two sets of isogons have been drawn; one for a 'coarse' layering and one for a 'fine'. On the basis of the coarse isogons alone the main coarse layer would be classified as Class 1C (approaching Class 2). On the finer scale, however, the layers within this coarse layer vary from Class 1B on the outer arc, to Class 3 towards the core. This is, of course, a reflection of the strain distribution within the coarse layer. An additional feature of the fine layering is the inconsistent sense of refraction of isogons across layer boundaries, as the layer is followed along its length. This probably implies a low competence difference between adjacent layers, and suggests that the deformation was, on this scale, controlled by the bulk anisotropy of the stack of layers rather than by individual layer behaviour. This may also be the case for the coarse layering in Fig. 4.39, though in folds of this scale it exhibits a more consistent layer geometry than the fine layering. The conclusion must be that the choice of surfaces for isogon construction in multilayer sequences of

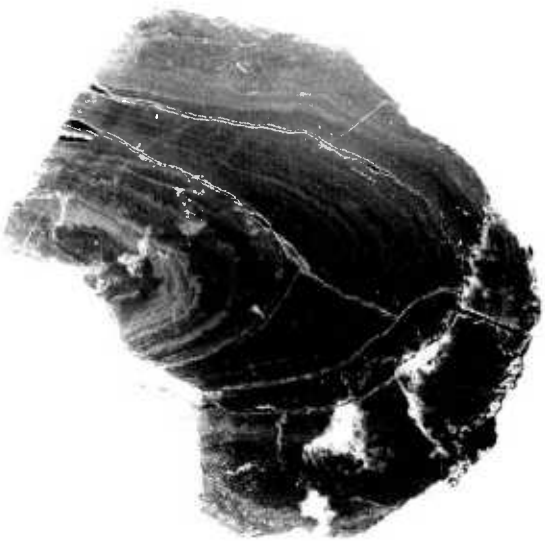


FIGURE 4.39 Fold with convergent isogons (Class 1C) from Unit 5.

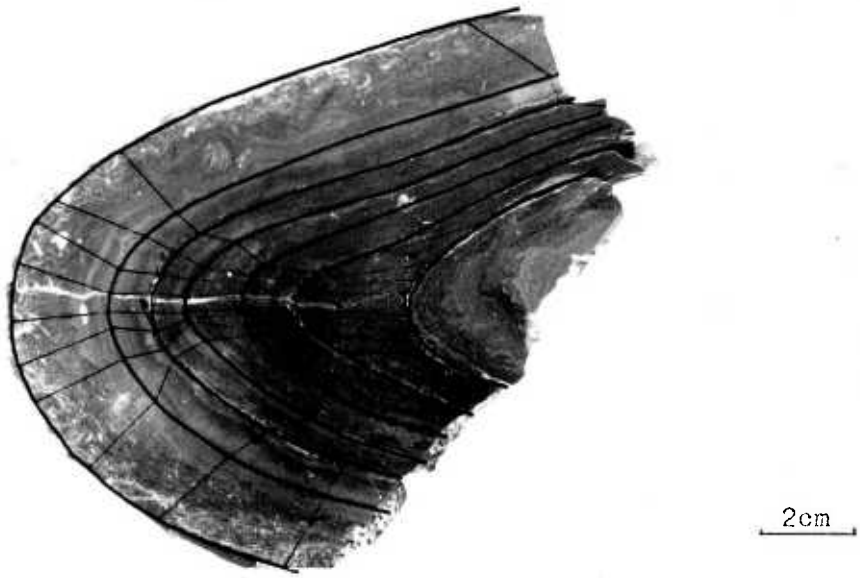


FIGURE 4.40 Fold with convergent isogons (Class 1C) from Unit 5.



FIGURE 4.41 Fold with convergent isogons (Class 1C) from Unit 13.

this type is not critical, unless single layers show sufficient competence contrast with the adjacent layers to significantly influence the deformation.

The fold in Fig. 4.39 exemplifies the dominant style throughout the slump sequence. Further examples of this weakly convergent (Class 1C) isogon pattern can be taken both from the basal 'folded' sheets (Fig. 4.40) and from the higher sheets with intrafolial folds (Fig. 4.41). The former example shows well the transition from a Class 1B (parallel) geometry on the outer arc towards a Class 2 (similar) geometry in the core. An approximate Class 2 geometry is, of course, a geometrical necessity if the fold is continuous for some distance along its axial surface trace in profile, and such styles are

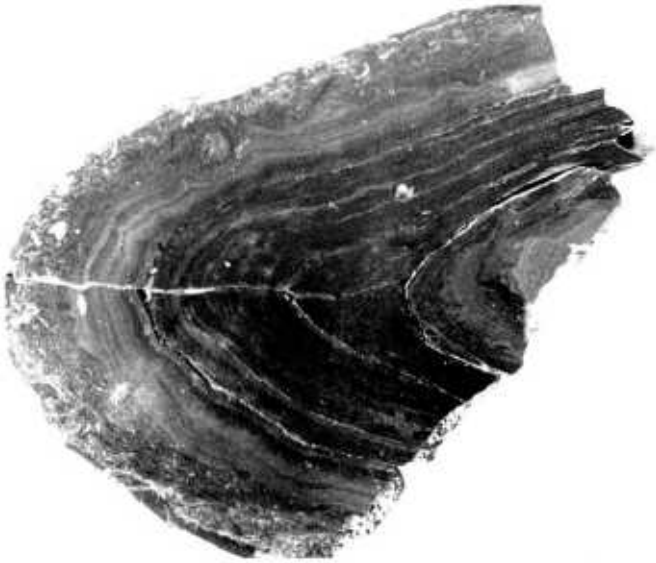


FIGURE 4.40 Fold with convergent isogons (Class 1C) from Unit 5.



FIGURE 4.41 Fold with convergent isogons (Class 1C) from Unit 13.

this type is not critical, unless single layers show sufficient competence contrast with the adjacent layers to significantly influence the deformation.

The fold in Fig. 4.39 exemplifies the dominant style throughout the slump sequence. Further examples of this weakly convergent (Class 1C) isogon pattern can be taken both from the basal 'folded' sheets (Fig. 4.40) and from the higher sheets with intrafolial folds (Fig. 4.41). The former example shows well the transition from a Class 1B (parallel) geometry on the outer arc towards a Class 2 (similar) geometry in the core. An approximate Class 2 geometry is, of course, a geometrical necessity if the fold is continuous for some distance along its axial surface trace in profile, and such styles are



FIGURE 4.42 Fold with approximate similar (Class 2) geometry from Unit 9.



FIGURE 4.43 Fold with geometry close to the Class 1B (parallel) model from Unit 5.

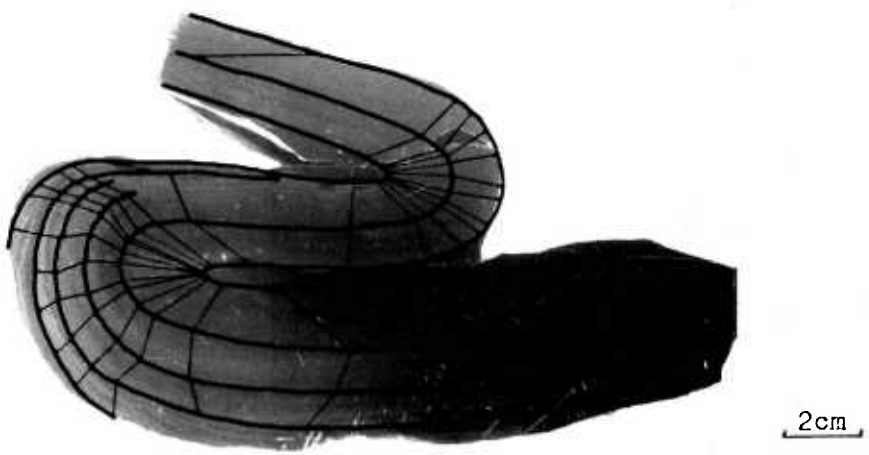


FIGURE 4.44 Fold with geometry close to the Class 1B (parallel) model from Unit 5.



FIGURE 4.42 Fold with approximate similar (Class 2) geometry from Unit 9.



FIGURE 4.43 Fold with geometry close to the Class 1B (parallel) model from Unit 5.



FIGURE 4.44 Fold with geometry close to the Class 1B (parallel) model from Unit 5.

occasionally developed (Fig. 4.42). A more common feature is the presence of a core of shell debris (Fig. 4.49). Individual shells in slump folds are always completely undeformed, a convincing testimony to the soft-sediment origin of the structures.

In the basal folded sheets (Units 5 & 7) some folds (e.g. Figs. 4.43, 4.44) exhibit a Class 1C geometry which is closer than most folds to the parallel model (Class 1B). These folds usually involve layers which apparently differed significantly in competence from the adjacent sediment. The incompetent material in the cores is 'squeezed out'.

The most significant result of the fold geometry determination is the comparitive rarity of similar (Class 2) folds. This suggests that folding did not occur wholly by simple shear parallel to the fold axial surfaces, as has commonly been implied (Chap. 2). It seems certain that there has been a significant buckling component in the formation of the folds. However, the isogon patterns also suggest some homogeneous 'flattening' in the plane of the axial surface. Several lines of evidence, to be introduced in the following sections, suggest that this flattening may be mainly due to compaction of the slump sheets after the true slump deformation had ceased. The gently inclined or recumbent axial surfaces of most folds (Fig. 4.30) will approximately coincide with the flattening plane of the compaction strain ellipsoid. If significant compaction strains were generated, the fold styles visible at the present may differ markedly from those immediately after slumping (see Sec. 8.2).

4.9 DEFORMED LINEATIONS AND MINOR STRUCTURES

The linear structure which is developed during the slump deformation, while normally axial to slump folds, is occasionally deformed by them. The character and origin of the lineations will be considered in the next section (Sec. 4.10), but for the present purpose it is sufficient to note that prior to deformation they are usually rectilinear on the scale of the hand specimen. The loci of the deformed lineations should therefore be a guide to the variation in finite strain within the folds (Ramsay 1967, Chap. 8).

Typical lineation loci are shown in Figs. 4.45 - 8. The loci are all plotted in the conventional way, with reference to a north-south horizontal axis and a vertical axial plane, but the fold profiles are drawn in their correct attitudes. The most significant feature of all plots is the marked discontinuity of the locus across the axial surface.

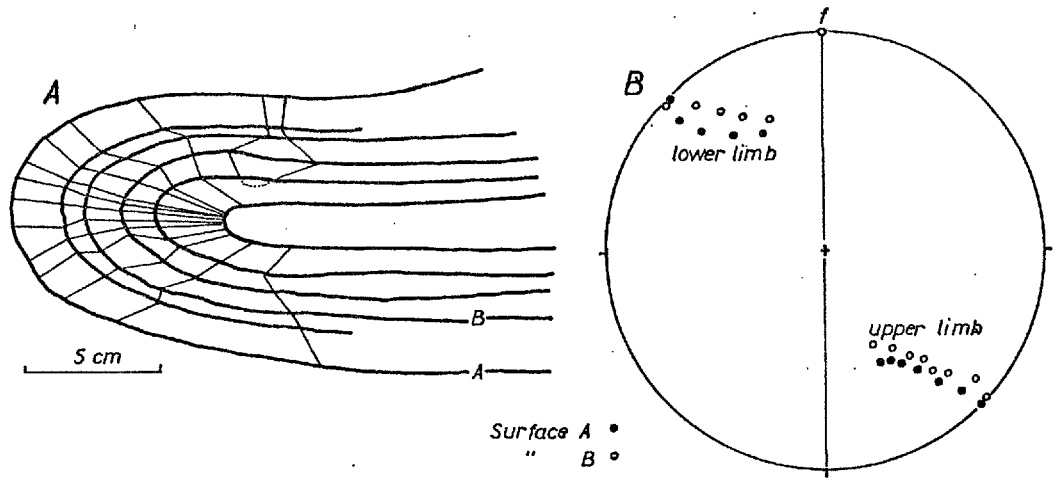


FIGURE 4.45 see below.

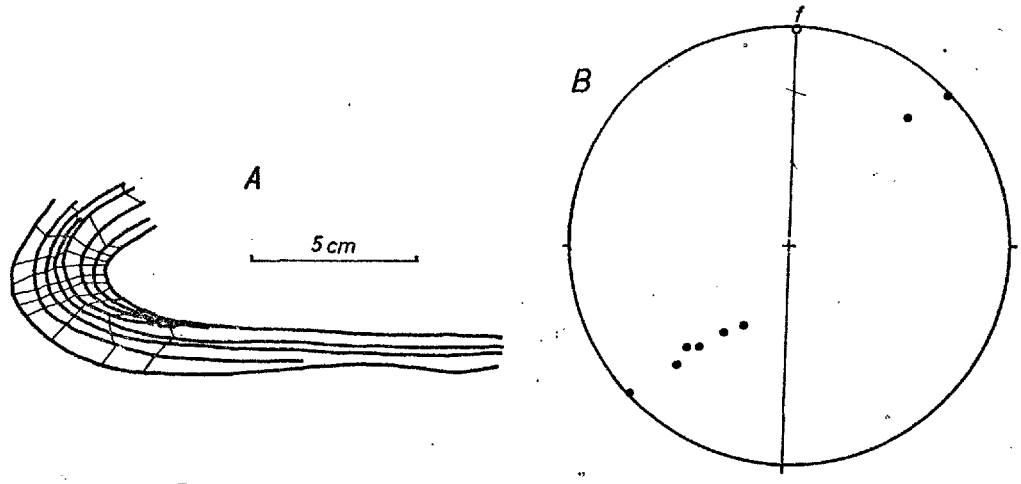


FIGURE 4.46 see below.

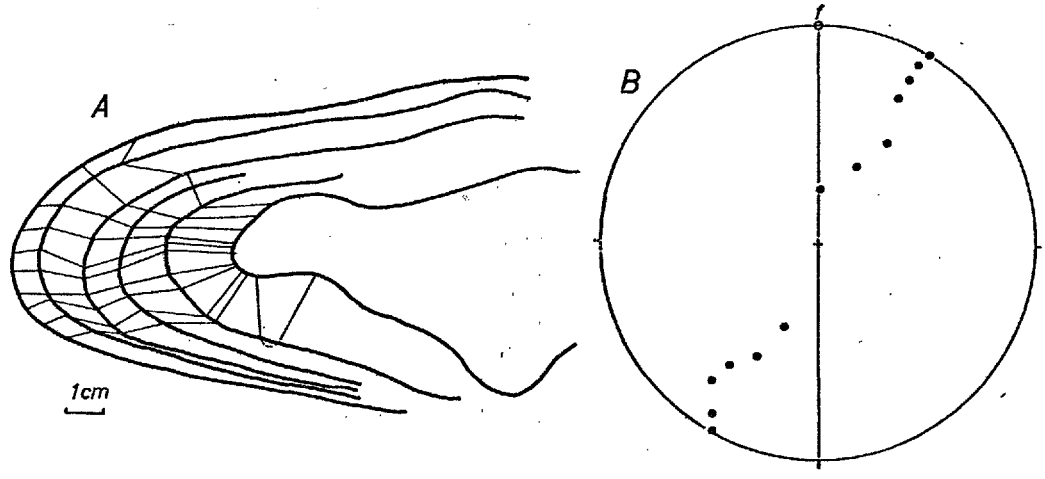


FIGURE 4.47 see below.

FIGURES 4.45/6/7 Fold profiles with isogons at 15° intervals and deformed lineation loci (from outer surface except where indicated). From Unit 5.

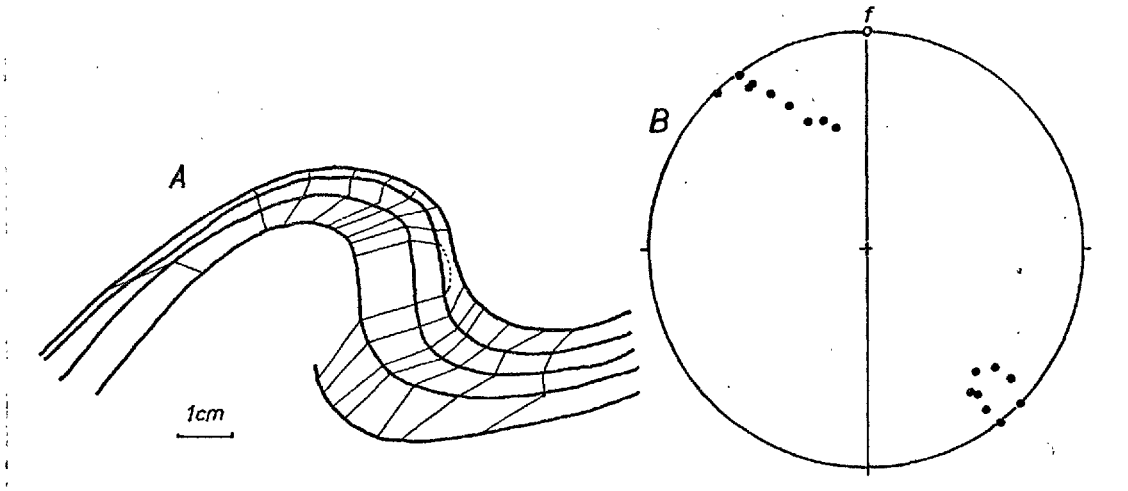


FIGURE 4.48 Fold profile with isogons at 15 degree intervals and deformed lineation locus from the outer surface. From Unit 5.

This indicates that buckling was an important mechanism in fold formation, as heterogeneous simple shear alone would generate a continuous great circle locus. This compliments the evidence for buckling from isogon patterns (Sec. 4.8).

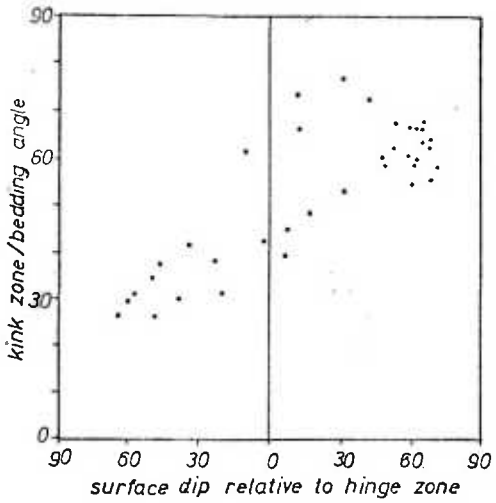
The well developed bedding lamination in most folds suggests that the deforming sediments had a marked anisotropy, and that flexural slip parallel to the lamination would be an important mode of buckling. Some loci (e.g. Fig. 4.45) approximate to the small circle pattern characteristic of pure flexural slip, but the majority (e.g. Figs. 4.46, 4.47) show marked deviations from this pattern. These could, in part, be due to a compactional flattening, but probably imply a significant heterogeneous simple shear component during slump deformation.

Further features of potential use in determining the mechanism of folding are the small kink folds occasionally seen in the fine lamination. These imply a high anisotropy (Cobbold et al. 1971), and again suggest that flexural slip on the layering may have been important in the formation of the larger folds. The kink folds are apparently deformed by the normal slump folds in places. The reality of this impression can be tested by plotting the angle between the kink zones and the lamination against the dip of the lamination (Ramsay 1967 Ch. 9). Typical plots (Figs. 4.49,50,51) show a systematic variation in dihedral angle with dip which can only be a result of deformation. However, the patterns cannot confidently be matched to the theoretical patterns for particular fold mechanisms (Ramsay 1967, pp. 501,507). This could, in any case, be unreliable, because the kink zones were probably not passive during the later folding.



FIGURE 4.49 see below

1cm



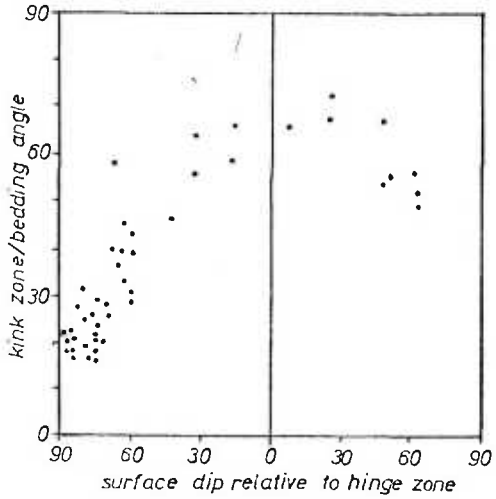
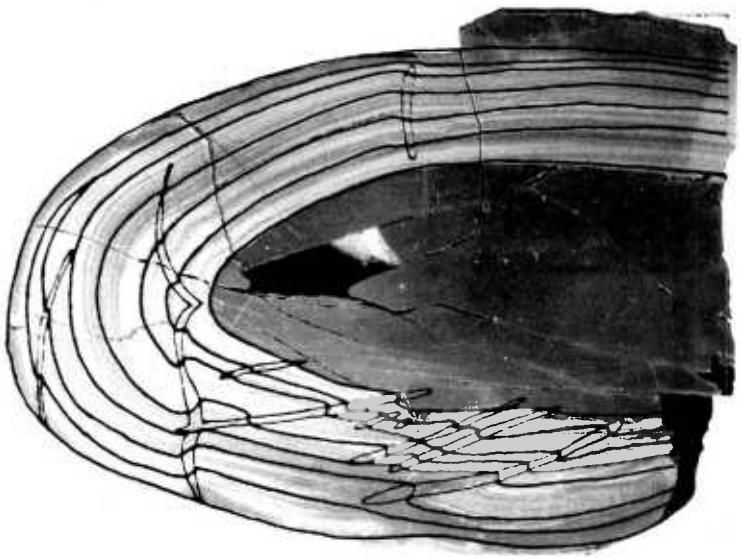


FIGURE 4.50 see below

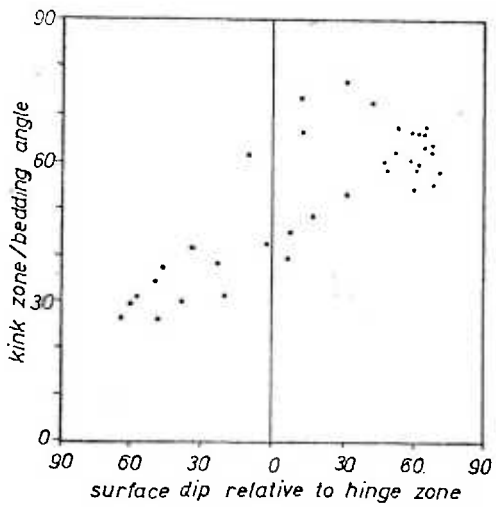
1cm



FIGURES 4.49/50 Folds from Unit 5 with deformed kink zones. Plots show the variation with dip of the angle between kink zones and lamination.

FIGURE 4.49 see below





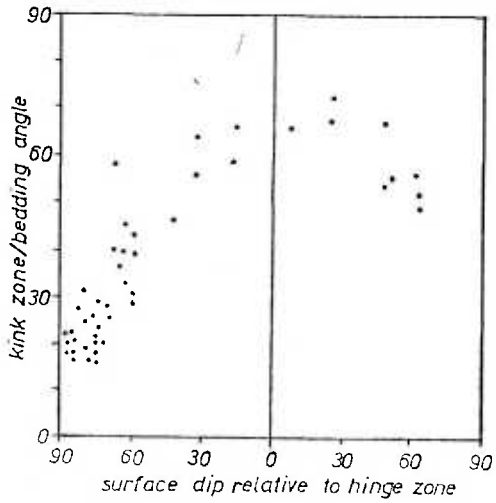
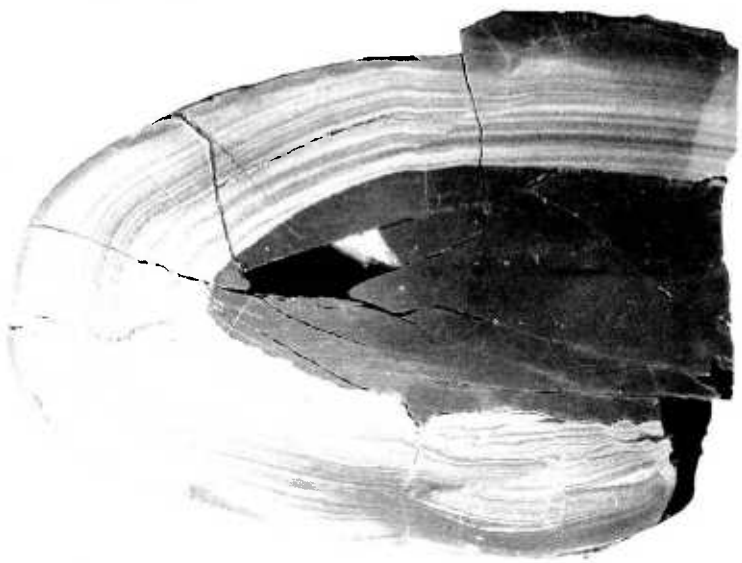


FIGURE 4.50 see below



FIGURES 4.49/50 Folds from Unit 5 with deformed kink zones. Plots show the variation with dip of the angle between kink zones and lamination.



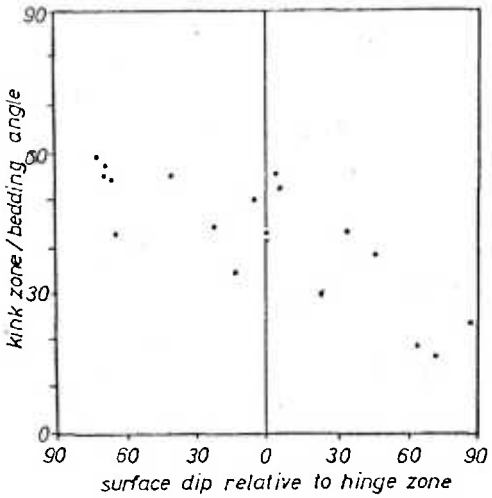


FIGURE 4.51 Fold from Unit 5 with deformed kink zones. Plots show variation with dip of the angle between kink zones and lamination.

4.10 LINEATIONS

A characteristic of most of the slumped units is a lineation on bedding and lamination surfaces (Fig. 4.10). This is most prominent in the 'laminated slumped segments' and 'segments with intrafolial folds', and is only weakly developed in the 'folded slumped segments'. Examination of the associated internal structures in thin section reveals several types.

The first, and by far the most common, type of lineation is associated with folding of the bedding laminae. This association was first described by Williams et al. (1957) from the slump units in the Elton area of the shelf succession (Sec. 7.2). A rather greater range of internal structure is present in the Cwm Blithus section. The most simple type is a true kink band development (Fig. 4.52A). This must form at a relatively early stage in the slump deformation as it is often deformed round the larger slump folds (Figs. 4.49,50,51). A



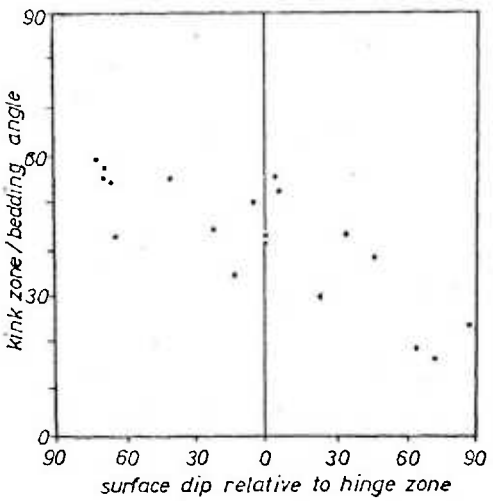


FIGURE 4.51 Fold from Unit 5 with deformed kink zones. Plots show variation with dip of the angle between kink zones and lamination.

4.10 LINEATIONS

A characteristic of most of the slumped units is a lineation on bedding and lamination surfaces (Fig. 4.10). This is most prominent in the 'laminated slumped segments' and 'segments with intrafolial folds', and is only weakly developed in the 'folded slumped segments'. Examination of the associated internal structures in thin section reveals several types.

The first, and by far the most common, type of lineation is associated with folding of the bedding laminae. This association was first described by Williams et al. (1957) from the slump units in the Elton area of the shelf succession (Sec. 7.2). A rather greater range of internal structure is present in the Cwm Blithus section. The most simple type is a true kink band development (Fig. 4.52A). This must form at a relatively early stage in the slump deformation as it is often deformed round the larger slump folds (Figs. 4.49,50,51). A

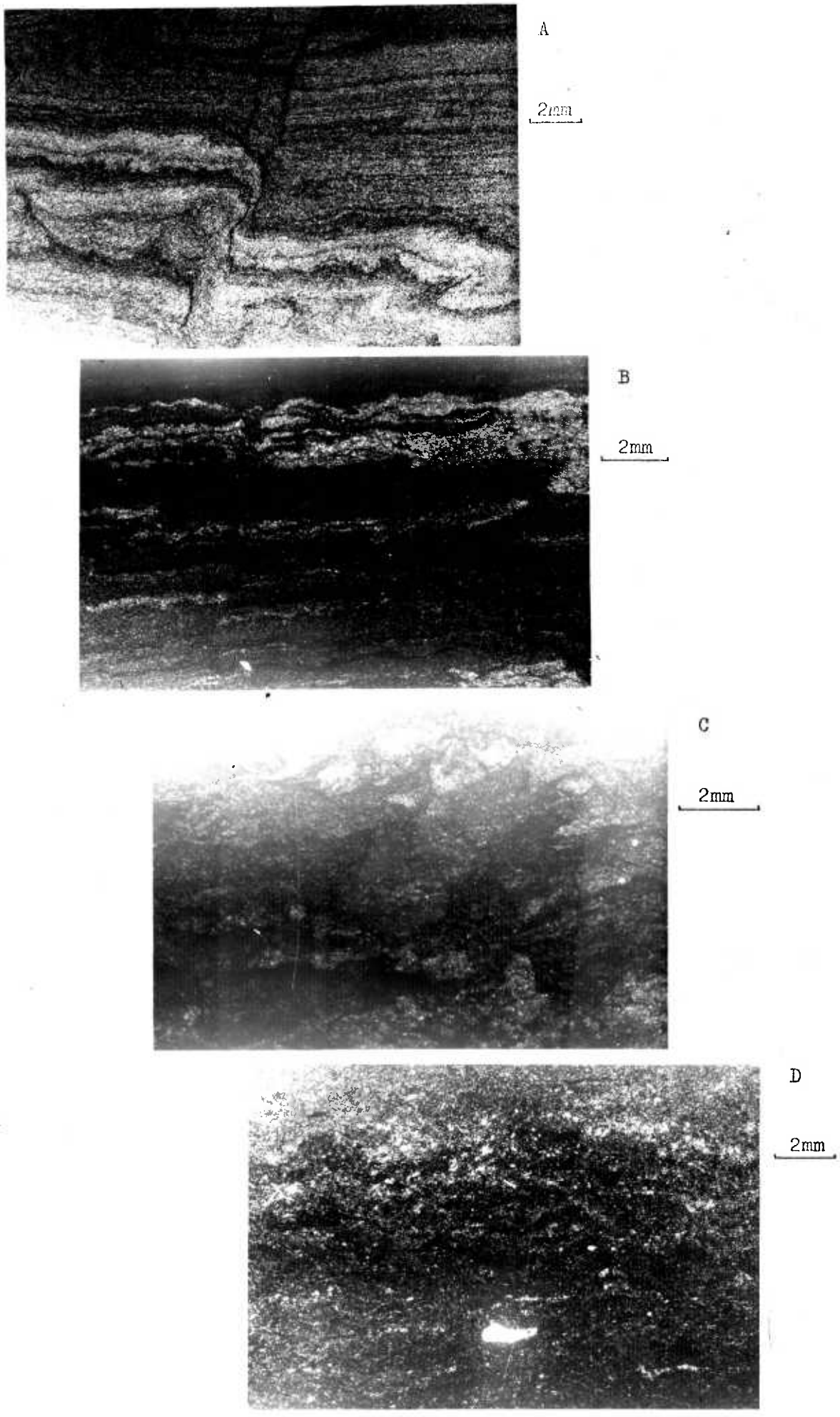


FIGURE 4.52 Four stages in the development of a 'fold' lineation, (see text).

pervasive asymmetric folding develops from the discrete kink zones (Fig. 4.52B), and this is associated with a more closely spaced lineation. Further stages in the lineation development show a gradual destruction of the bedding laminae (Fig. 4.52C), until no trace of the folding remains (Fig. 4.52D). This final type of internal structure is characteristic of the laminated segments, where bedding is destroyed on all scales.

The 'fold' type of lineation and its more extreme derivatives apparently have the same directional significance as slump folds, and all axial lineations on folded surfaces are of this type. However 'fold' lineations are sometimes oblique to, and deformed round, slump folds (Sec. 4.9). This probably indicates that slump folds do not necessarily initiate with axes normal to the bulk movement direction, a hypothesis which also explains their marked dispersion in the plane of the sheet (Sec. 8.2). A further problem in interpreting lineation orientation is the presence of two intersecting lineations on the same surface. This problem was noted by Williams et al. (1957) and further considered by Bailey (1966). In Cwm Blithus many of these situations involve the intersection of a fold lineation with one of the other two types of lineation to be described. The remaining instances represent the true superposition of two fold lineations formed at two different stages in the progressive deformation of the sheet.

The second type of lineation is usually finer than the fold lineation, and is not associated with any visible internal structure (Fig. 4.53). It is apparently a true slickensiding caused by



FIGURE 4.53 A wide spaced fold lineation (N-S) associated with kink zones, traversed by a slickenside lineation (E-W) with no associated internal structure.

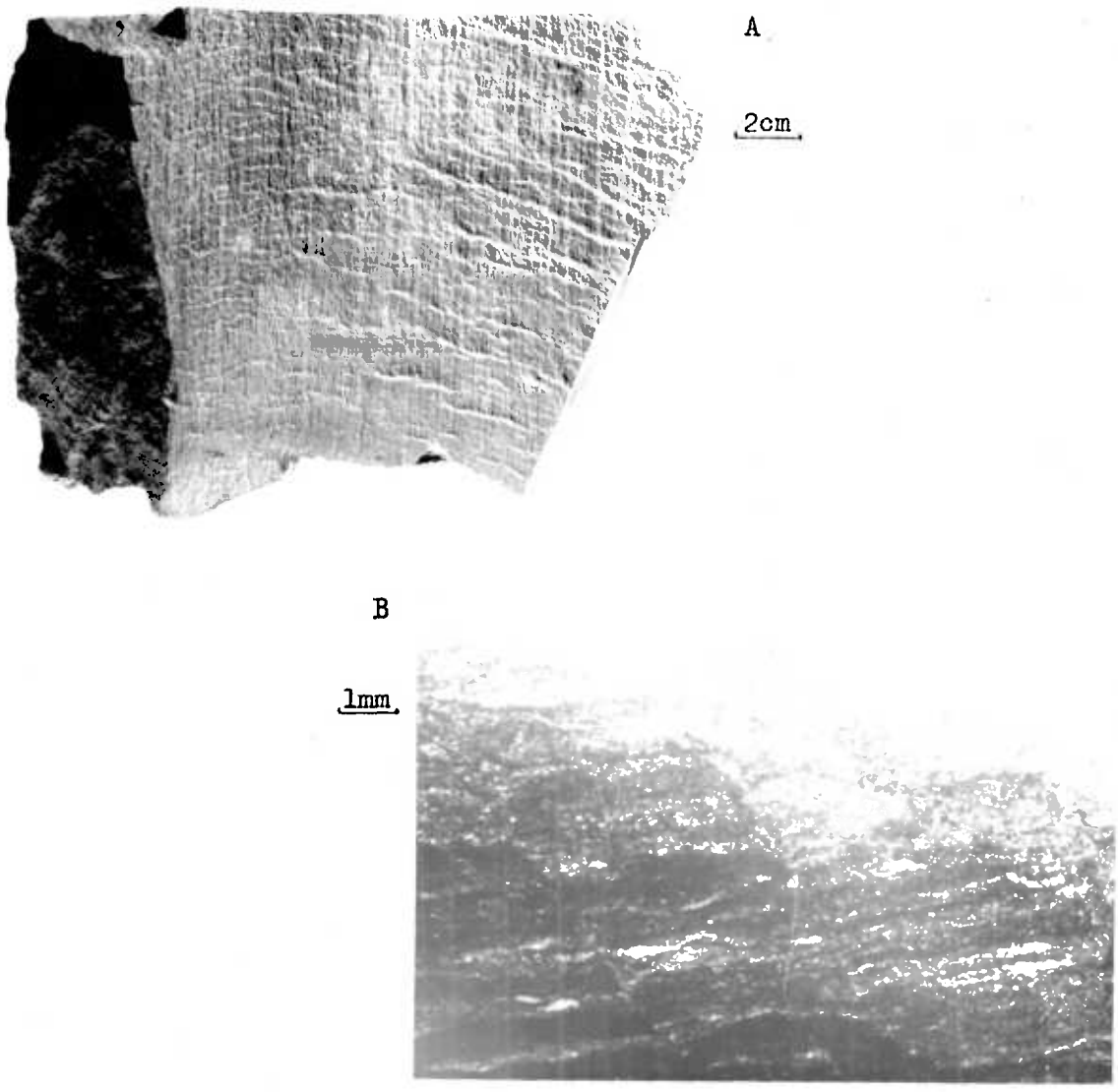


FIGURE 4.54 A) A fold lineation axial to a gentle fold (running N-S) cut by a shear lineation (running E-W). B) Internal structure associated with the shear lineation.

differential movement along discrete bedding surfaces. It either occurs at high angles to a fold lineation or approximately normal to the axes of folds. Such folds must clearly have had a component of flexural slip during their development.

The third type of lineation has an associated internal structure akin to crenulation cleavage (Fig. 4.54), the bedding being cut by discrete shear discontinuities. This structure is demonstrably later than the folding in many places (Fig. 4.54A), and gives rise to a mesoscopic cleavage in some places. Its origin will be discussed with reference to better developments seen in other areas (Sec. 6.5).

4.11 FABRICS

Some of the intrafolial folds apparently have an associated cleavage. In the field this often appears as a 'fracture' cleavage (Fig. 4.55), but on polished surfaces a more penetrative, approximately axial planar, fabric is revealed (Fig. 4.56). In thin section the fabric is seen to be due to dimensional alignment, both of elongate quartz grains and of flaky minerals, in this case dominantly muscovite and chlorite.

Associated with the dimensional orientation fabric is a magnetic anisotropy fabric. Cores were taken from the fold in Fig. 4.56 (see



FIGURE 4.55 Fold with an apparent convergent 'fracture' cleavage fan (Unit 30).



FIGURE 4.56 Fold with a penetrative axial planar fabric (clearly visible in the core). From Unit 30.

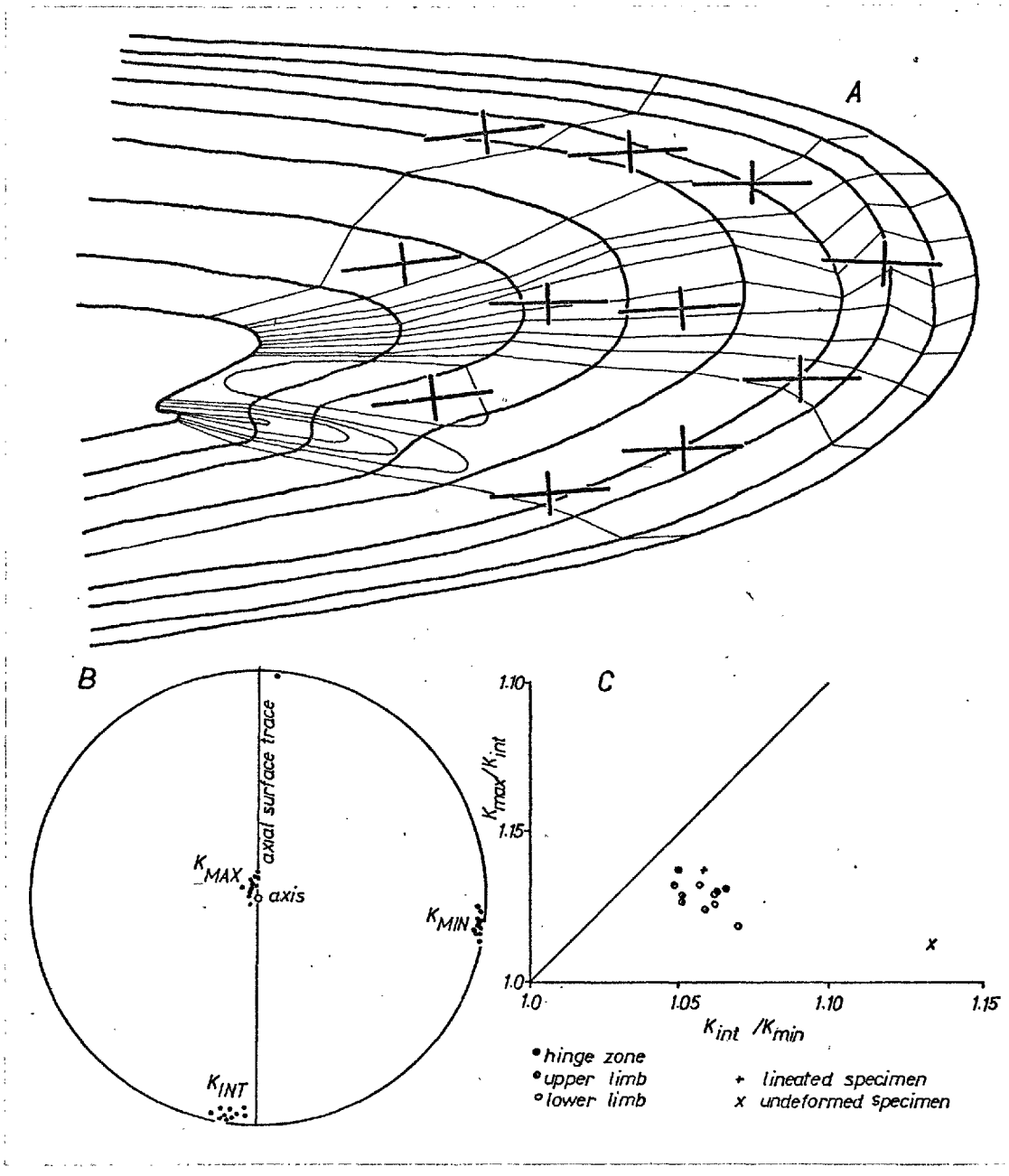


FIGURE 4.57 A) Dip isogons at 15 degree intervals on the fold profile in Fig. 4.56. Orientation of the minimum (short) and intermediate (long) principal susceptibilities is indicated.
B) Projection of the principal axes of magnetic anisotropy showing the consistent orientation throughout the fold.
C) Ratio plot of principal susceptibilities from the fold and also from a lineated and an undeformed specimen.

Fig. 4.57A), and the magnetic anisotropy was determined by Dr. W. Owens at Birmingham University. The apparatus and procedure used was that mentioned by King et al. (1962). The principal susceptibility axes have a consistent orientation throughout the fold (Fig. 4.57B), with the maximum susceptibility parallel to the fold axis and the minimum approximately normal to the axial surface. The susceptibility ellipsoids are all oblate (Fig. 4.57C), but there are slight differences in shape in different parts of the fold. The hinge zone shows a more intense oblate fabric than the two limbs. Since the source of the anisotropy is apparently paramagnetic, and almost certainly associated with the chlorite, the oblate fabric is consistent with a planar dimensional orientation of the chlorite.

The susceptibility anisotropy in two other rocks was also tested (Fig. 4.57C). A specimen from an undeformed unit showed a stronger, more oblate fabric in the plane of the bedding. A lineated specimen of 'fold' type showed an essentially similar fabric to that in the fold, with maximum susceptibility parallel to the lineation. The fabrics of the undeformed, lineated and folded specimens are summarised in Fig. 4.58.

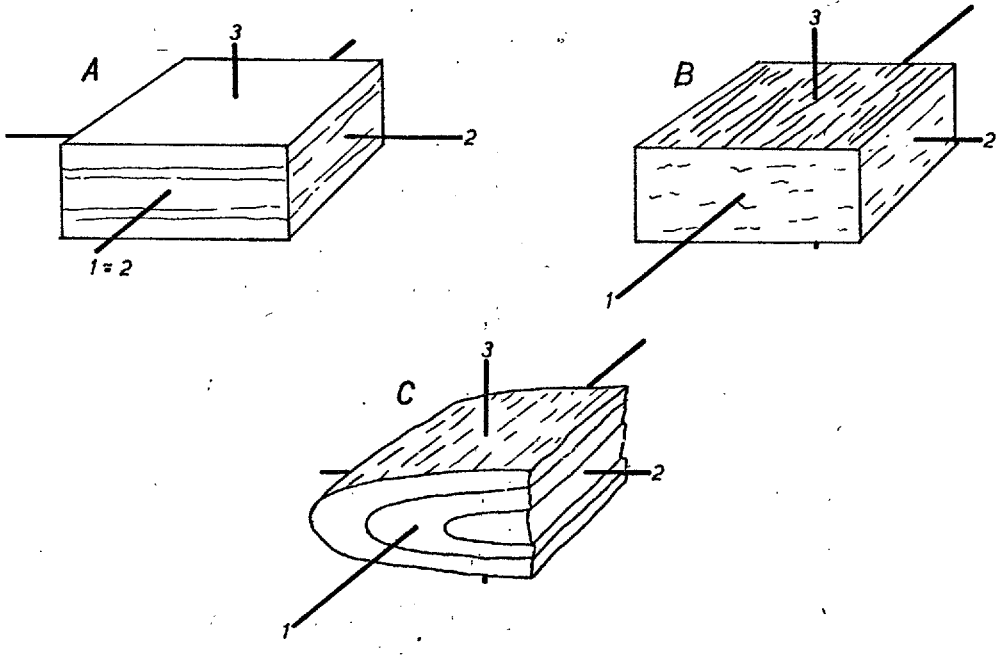


FIGURE 4.58 Summary of the relationship of magnetic anisotropy to A) an undeformed sample, B) a lineated sample and C) a fold.

There are two previously recorded examples of fabrics related to slump or soft sediment folds. Yagishita (1971) measured the dimensional orientation of quartz grains in a slump fold, and found a similarly oriented oblate fabric to that in Fig. 4.58C. He considered the fabric to have developed during simple shear parallel to the axial surface of the fold. Williams et al. (1969) also described a dimensional orientation of quartz and mica parallel to the axial surfaces of soft sediment (possibly slump) folds.

In the present case there are two possible causes of this preferred orientation: either it formed during, and as an integral part of, the folding process, or it resulted from compaction of the folds after slump deformation. Both mechanisms might produce approximately axial planar fabrics, since most folds are recumbent. Further work is required before the importance of each mechanism can be decided.

CHAPTER FIVE

THE EASTERN SEQUENCE : OTHER AREAS

5.1 THE AREA WITHIN AND TO THE WEST OF THE WYE VALLEY

The important localities in the Eastern Slump Sequence, excluding the Cwm Blithus section (see Chap. 4), will be described in this chapter, beginning with those in the southwest and working northeastwards.

Exposures to the west of the Wye valley (see Enclosure 1) are rather sporadic, and no locality provides much directional data. The exposed slump units are generally 'laminated' or 'phacoidal' with lineated lamination surfaces but few folds. Erosional upper contacts are sometimes exposed (e.g. at Llandewi'r Cwm, Fig. 2.6).

The few slump folds which are visible generally have weakly convergent isogons (Class 1C) throughout successive layers (Figs. 5.1, 5.2). However at Llanfaredd road cutting (SO 068503) occur slump folds with an unusual geometry (Fig. 5.3). There is a distinct difference in style between the lighter (more calcareous) layers, of Class 1C, and the darker (more pelitic) layers, which tend towards Class 3. This geometry indicates a significant competence difference between layers during slumping.

Throughout the area folds trend approximately NE-SW and rare asymmetric folds (e.g. Fig. 5.3) overturn towards the northwest.

At Cwm Graig Ddu (SN 965484) some units are complicated by ellipsoidal weathering. A further complication is a prominent



FIGURE 5.1 Fold with Class 1C geometry from south of Aberduhonw (SO 063505).

CHAPTER FIVE

THE EASTERN SEQUENCE : OTHER AREAS

5.1 THE AREA WITHIN AND TO THE WEST OF THE WYE VALLEY

The important localities in the Eastern Slump Sequence, excluding the Cwm Blithus section (see Chap. 4), will be described in this chapter, beginning with those in the southwest and working northeastwards.

Exposures to the west of the Wye valley (see Enclosure 1) are rather sporadic, and no locality provides much directional data. The exposed slump units are generally 'laminated' or 'phacoidal' with lineated lamination surfaces but few folds. Erosional upper contacts are sometimes exposed (e.g. at Llandewi'r Cwm, Fig. 2.6).

The few slump folds which are visible generally have weakly convergent isogons (Class 1C) throughout successive layers (Figs. 5.1, 5.2). However at Llanfaredd road cutting (SO 068503) occur slump folds with an unusual geometry (Fig. 5.3). There is a distinct difference in style between the lighter (more calcareous) layers, of Class 1C, and the darker (more pelitic) layers, which tend towards Class 3. This geometry indicates a significant competence difference between layers during slumping.

Throughout the area folds trend approximately NE-SW and rare asymmetric folds (e.g. Fig. 5.3) overturn towards the northwest.

At Cwm Graig Ddu (SN 965484) some units are complicated by ellipsoidal weathering. A further complication is a prominent



FIGURE 5.1 Fold with Class 1C geometry from south of Aberduhonw (SO 063505).



FIGURE 5.2 Folds with Class 1C geometry (tending to Class 2) from south of Middle Hall (SO 070485).



FIGURE 5.3 Alternating Class 1C and Class 3 geometry in folds from Llanfaredd road cutting (SO 068503).



FIGURE 5.4 Crenulation cleavage cutting slumped sediments, from Cwm Graig Ddu (SN 964484).



FIGURE 5.2 Folds with Class 1C geometry (tending to Class 2) from south of Middle Hall (SO 070485).



FIGURE 5.3 Alternating Class 1C and Class 3 geometry in folds from Llanfaredd road cutting (SO 068503).



FIGURE 5.4 Crenulation cleavage cutting slumped sediments, from Cwm Graig Ddu (SN 964484).

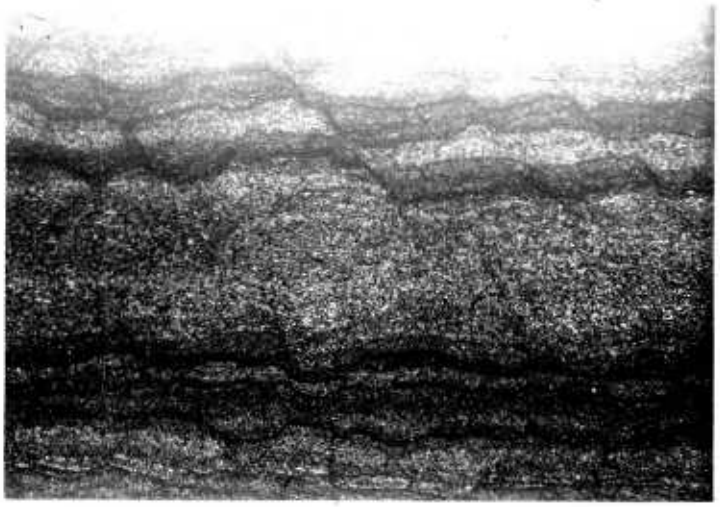


FIGURE 5.5 Conjugate normal shear discontinuities cutting lamination in slumped beds at Llanfaredd road cutting (SO 068503).

'fracture' cleavage visible in outcrop, and due to deformation along discrete shears with an apparent normal displacement sense (Fig. 5.4). At this locality the cleavage probably has a tectonic origin. A rather different cleavage occurs further east, for instance at the Llanfaredd road cutting (SO 068503). A distinct planar cleavage is not visible in outcrop, the most prominent structure being a lineation on the lamination surfaces. In thin section (Fig. 5.5) this is seen to be due to two sets of rather 'smeared' normal shears, symmetrically disposed to the lamination. This structure is possibly contemporaneous with slumping, for reasons set out in Sec. 6.5.



FIGURE 5.6 A slumped unit overlying more undisturbed beds at Hungry Green (SO 117537). Hammer head indicates the approximate contact.

5.2 THE AREA BETWEEN THE WYE VALLEY AND RADNOR FOREST

The slump sequence continues to the east of the Wye valley with little change in morphology. A typical exposure, with a slumped unit overlying an undisturbed unit, is shown in Fig. 5.6.

One locality provides directional data adequate for palaeoslope determination. This comprises exposures on the track over Rhiw Rhwstyn (SO 075519) and in the gully immediately to the south (SO 076517) (see Enclosure 1). Fold hinge lines and axial surface poles indicate a NE-SW palaeoslope (Fig. 5.7). The exposed sheets lie near the base of the sequence in this area, and show clear intercalation with undisturbed units (Fig. 5.8). A further feature, well shown here (Fig. 5.9) but common throughout the southwestern part of the Eastern sequence, is the breakdown of structures in some slump sheets to give a more massive appearance.

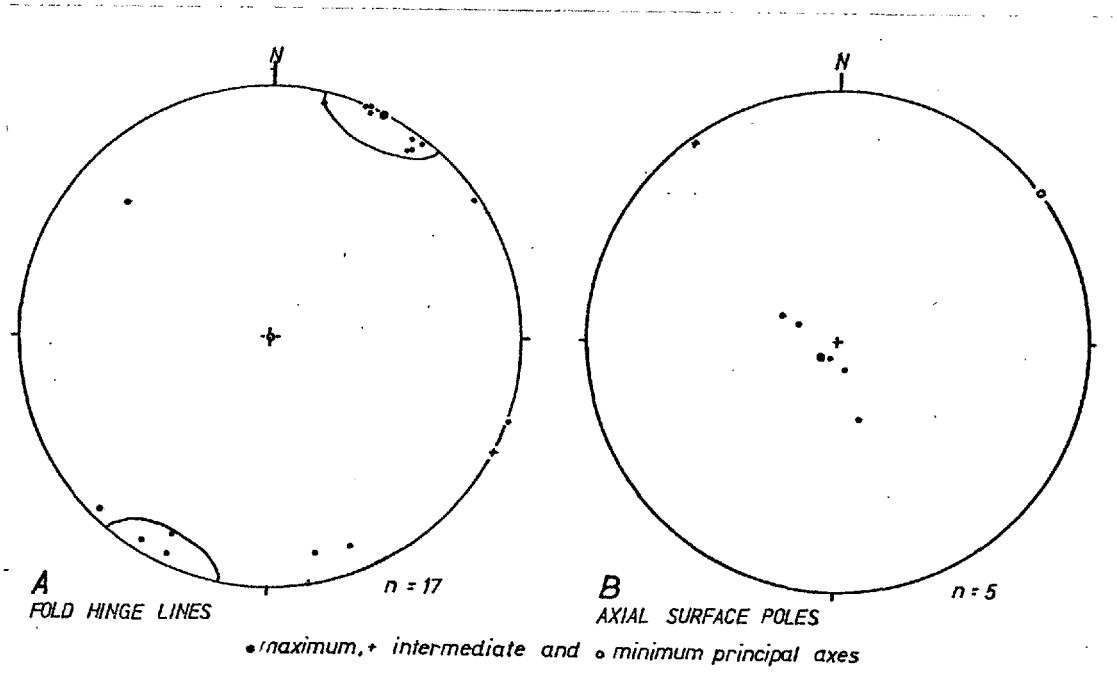


FIGURE 5.7 Projections of directional data from Aberedw Hill (SO 076518) with principal axes and 95% cones of confidence.



FIGURE 5.8 Slumped beds overlying more undisturbed beds on the Aberedw Hill road (SO 075519).



FIGURE 5.9 Slumped unit with folds and lamination barely visible, and a massive structureless appearance in places. Gully south of Rhiw Rhwstyn (SO 075517).

5.3 CWM-Y-BONT

An extensive section through the sequence is exposed in Cwm-y-bont, the valley of the Gilwern Brook, about 2 km SE of Llanfihangel-nant-Melan (Enclosure 1). The exposure has been mapped at a scale of 1:2500 (Enclosure 3). The succession dips gently to the northwest, and the valley thus provides a strike section through the sequence. The relationship of this outcrop to those further southwest is uncertain, due to poor exposure of the intervening ground. It is slightly later in time (See Fig. 3.4) but is probably part of the same diachronous sequence.

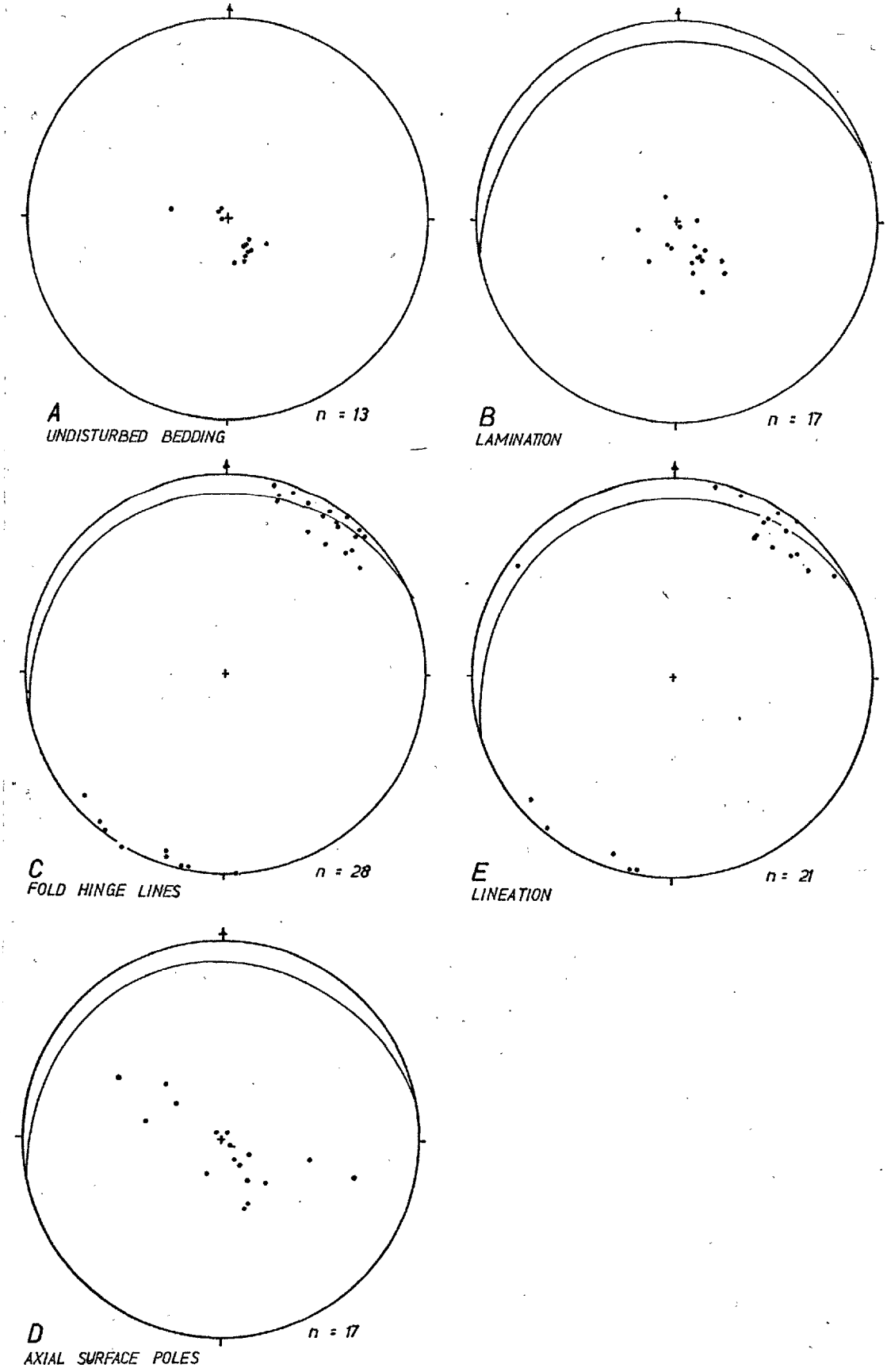


FIGURE 5.10 Projections of orientation data from Cwm-y-Bont. The mean bedding trace is marked on projections B to E.

The exposed part of the sequence is dominantly slumped, but contains two prominent undisturbed units. The slumped units are mainly 'laminated' with few intrafolial folds. The directional data are plotted in Fig. 5.10 and summarised on a principal axis plot (Fig. 5.11) and a ratio plot (Fig. 5.12). All structures have a symmetrical relationship to the depositional datum, as did those at Cwm Blithus.

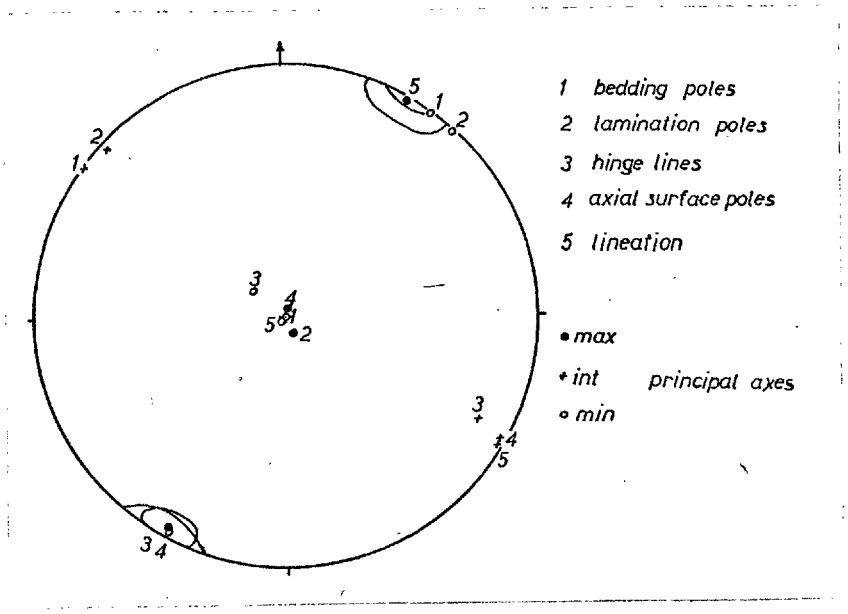


FIGURE 5.11 Plot of principal axes of the distributions in Fig. 5.10 (Cwm-y-Bont). Data are referred to the original depositional datum.

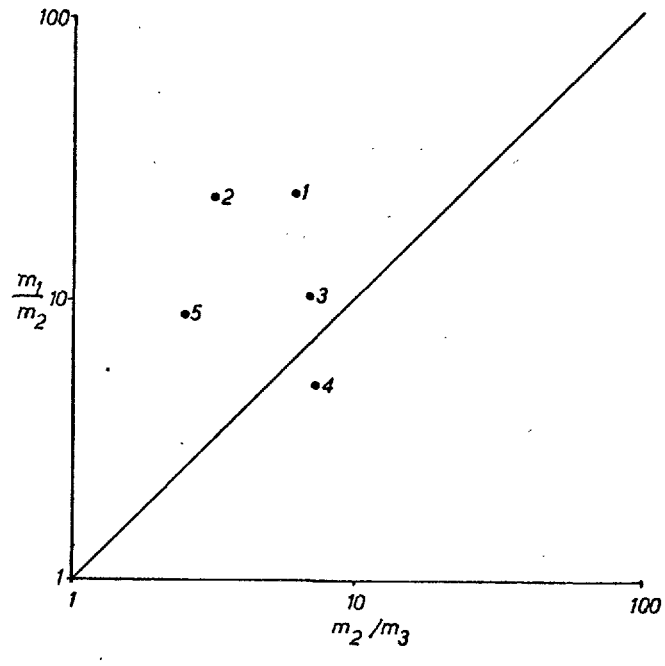


FIGURE 5.12 Plot of eigenvalue ratios from distributions in Fig. 5.10 (Cwm-y-Bont). Numbering corresponds to that in Fig. 5.11.

The lamination and bedding poles show similar distribution shapes to those at Cwm Blithus, but hinge lines and lineations form a tighter cluster within the plane of the sheets, and axial surface poles are more dispersed along a great circle girdle (Fig. 5.12 cf. Fig. 4.19).

Hinge line and lineation means, and the pole to the girdle of axial surface poles, all indicate a palaeoslope trend of about 030° ± 10°. The dominant overturning sense of folds indicates slump movement towards the northwest (Figs. 5.13, 5.14).



FIGURE 5.13 Large folds in Cwm-y-Bont with an asymmetry sense indicating northwesterly movement.

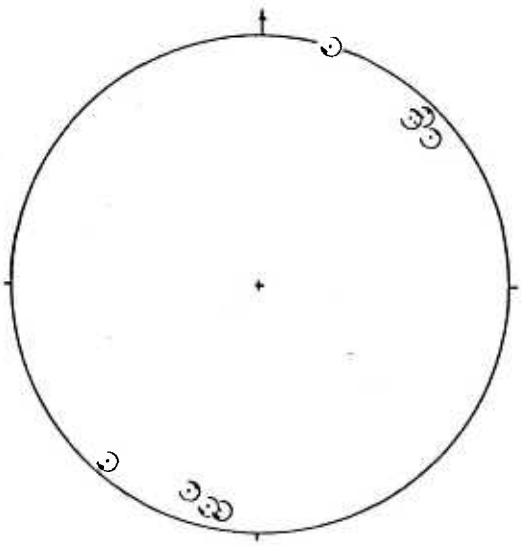


FIGURE 5.14 Sense of asymmetry of folds from Cwm-y-Bont. Data are corrected for tectonic tilt.

When compared with folds in Cwm Blithus, those in Cwm-y-Bont show a more restricted range of axial plunge, but a wider range of axial surface dip (Fig. 5.15 cf. Fig. 4.30). They do, however, show a similar range of style. Most folds have weakly convergent isogons (Class 1C) (Fig. 5.16), but a few approximate to the similar (Class 2) model (Fig. 5.17).

Lineations are mainly of the fold type. These take a variety of forms. One illustrated in Fig. 5.18 shows a tendency for 'diapiric' injection of pelitic material into the more calcareous laminae above fold crests. Shear lineations are poorly developed (Fig. 5.19), and do not generally give a visible cleavage in outcrop.

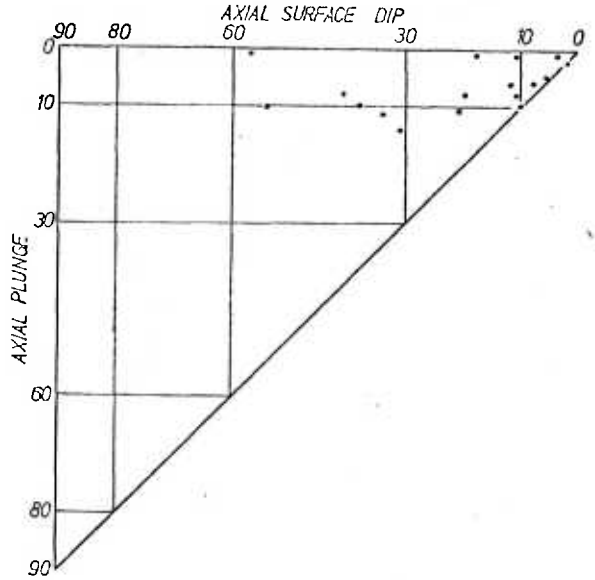


FIGURE 5.15 Plot of axial plunge against axial surface dip of folds in Cwm-y-Bont.



FIGURE 5.16 Fold with Class 1C geometry from Cwm-y-Bont.

When compared with folds in Cwm Blithus, those in Cwm-y-Bont show a more restricted range of axial plunge, but a wider range of axial surface dip (Fig. 5.15 cf. Fig. 4.30). They do, however, show a similar range of style. Most folds have weakly convergent isogons (Class 1C) (Fig. 5.16), but a few approximate to the similar (Class 2) model (Fig. 5.17).

Lineations are mainly of the fold type. These take a variety of forms. One illustrated in Fig. 5.18 shows a tendency for 'diapiric' injection of pelitic material into the more calcareous laminae above fold crests. Shear lineations are poorly developed (Fig. 5.19), and do not generally give a visible cleavage in outcrop.

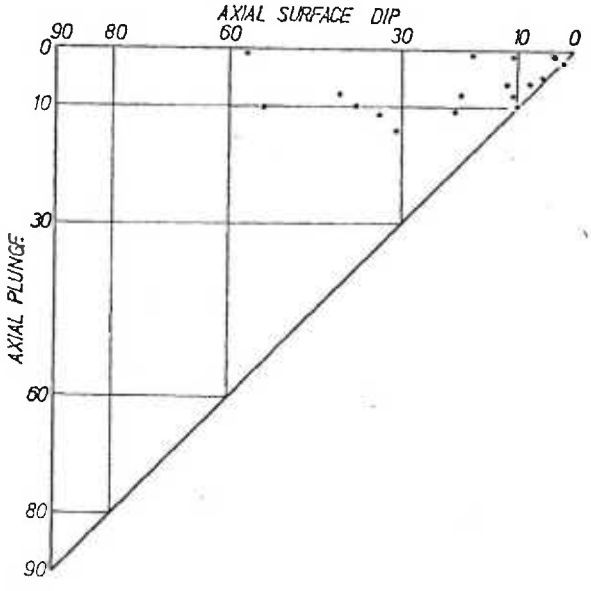


FIGURE 5.15 Plot of axial plunge against axial surface dip of folds in Cwm-y-Bont.

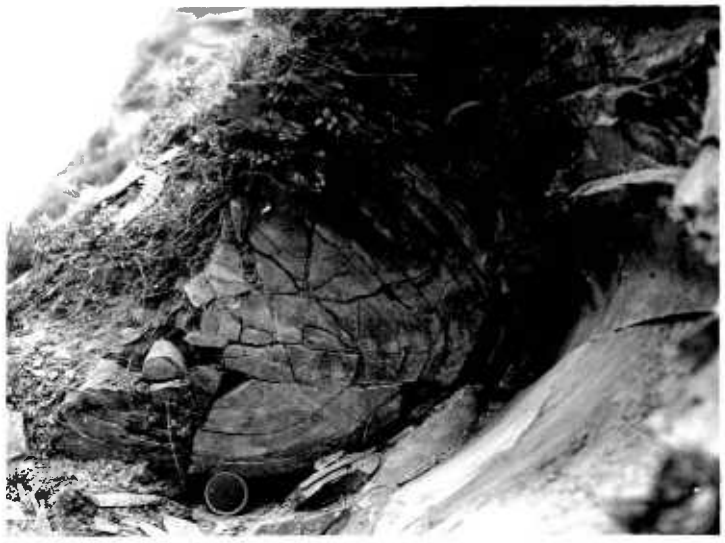


FIGURE 5.16 Fold with Class 1C geometry from Cwm-y-Bont.



FIGURE 5.17 Fold with approximate Class 2 geometry from Cwm-y-Bont.

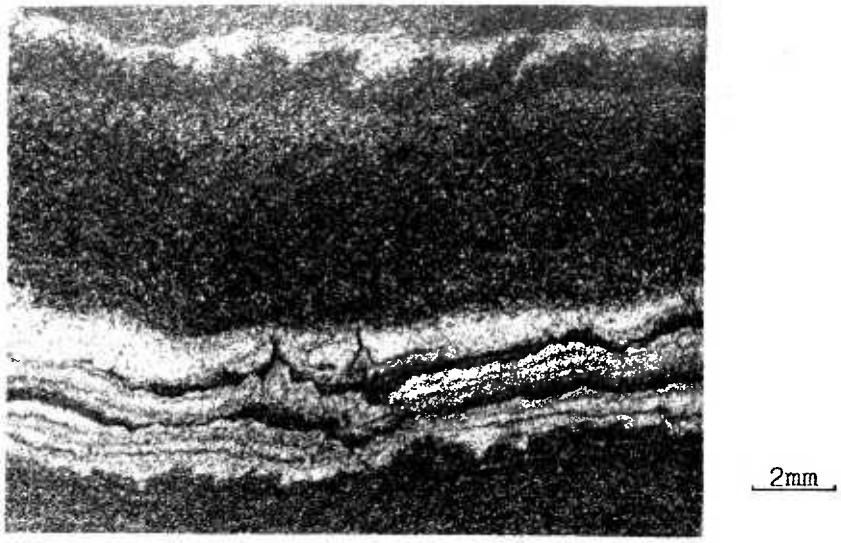


FIGURE 5.18 Profile section of a fold lineation from Cwm-y-Bont with tendency for diapiric injection of pelitic material at fold crests.

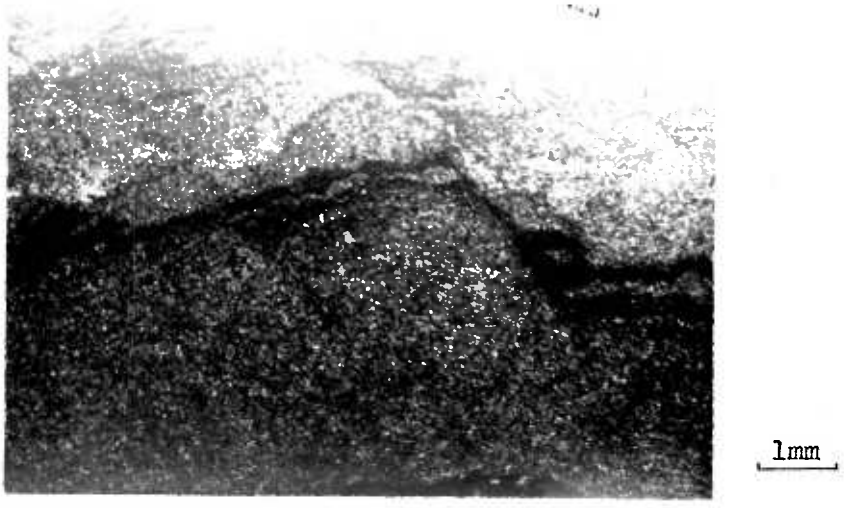


FIGURE 5.19 Normal shears associated with lineation from Cwm-y-Bont.

5.4 THE RADNOR FOREST AREA

The slump sequence exposed in Cwm Blithus (Chap. 4) can be clearly traced northwards along the western scarp of Radnor Forest, where it thins and finally disappears. To the south it is probably continuous with the main sequence of Sec. 5.2. The exposures along the southern margin of Radnor Forest, represented by exposures in Black Brook (SO 183606) and Harley Dingle (SO 200610), are probably continuous with those in Cwm-y-Bont, and correlate with those further west across a gentle syncline.

There are few informative exposures apart from those in Cwm



FIGURE 5.20 Fold with Class 1C geometry from Llanevan Dingle (SO 168617).

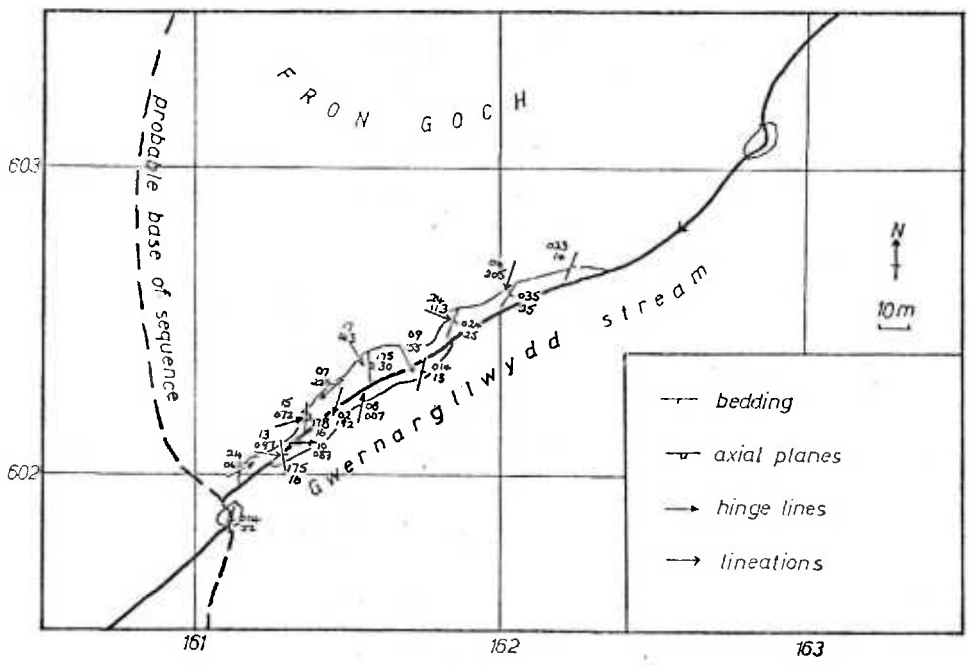


FIGURE 5.21 Map of slump exposures in the stream east of Gwernargllwydd (see Enclosure 1).

5.4 THE RADNOR FOREST AREA

The slump sequence exposed in Cwm Blithus (Chap. 4) can be clearly traced northwards along the western scarp of Radnor Forest, where it thins and finally disappears. To the south it is probably continuous with the main sequence of Sec. 5.2. The exposures along the southern margin of Radnor Forest, represented by exposures in Black Brook (SO 183606) and Harley Dingle (SO 200610), are probably continuous with those in Cwm-y-Bont, and correlate with those further west across a gentle syncline.

There are few informative exposures apart from those in Cwm



FIGURE 5.20 Fold with Class 1C geometry from Llanevan Dingle (SO 168617).

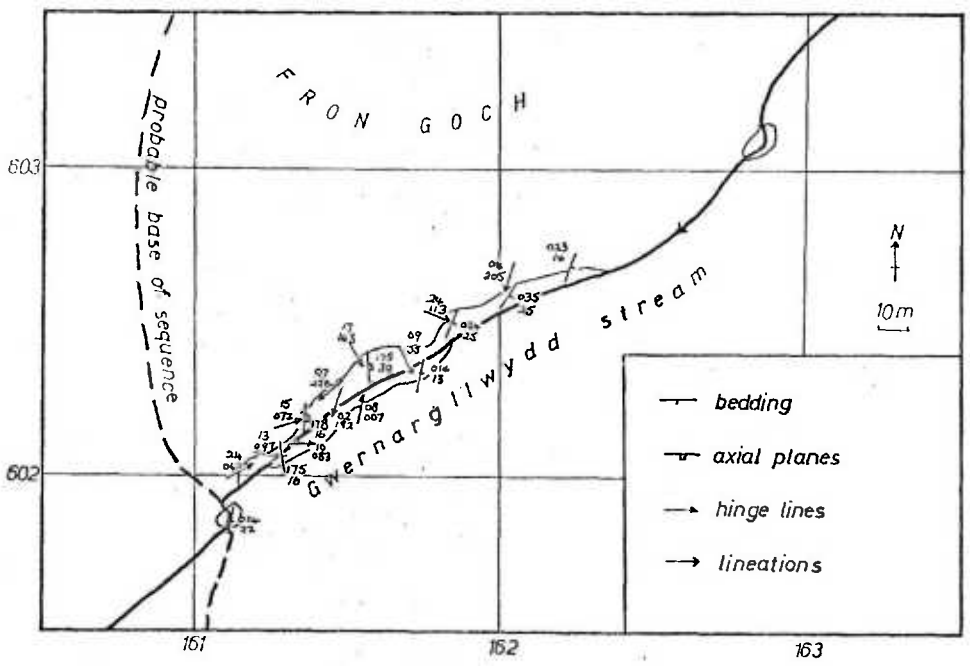


FIGURE 5.21 Map of slump exposures in the stream east of Gwernargllwydd (see Enclosure 1).

Blithus. Wherever folds are seen, however, they show orientations and styles essentially similar to those in Cwm Blithus (e.g. Fig. 5.20).

Also exposed in the Radnor Forest area are several sheets stratigraphically below the main slump sequence. An exposure in the stream east of Gwernargllwydd (SO 160602, see Enclosure 1) may be one such sheet, or may possibly be the approximate base of the main slump sequence in this area. It shows rather chaotic folding with little preferred orientation of structures (Figs. 5.21, 5.22). However, most folds show the usual weakly convergent isogon patterns in profile. Some have deformed lineations indicating a component of flexural slip during formation (Fig. 5.23).

Other features of interest in the Radnor Forest area are a well exposed upper contact to a slump sheet north of Llanfihangel-nant-Melan (SO 182586, Fig. 5.24), and a slump conglomerate south of Gwernargllwydd (SO 156597, Fig. 5.25).



FIGURE 5.22 A folded unit in the stream east of Gwernargllwydd (SO 16146022).

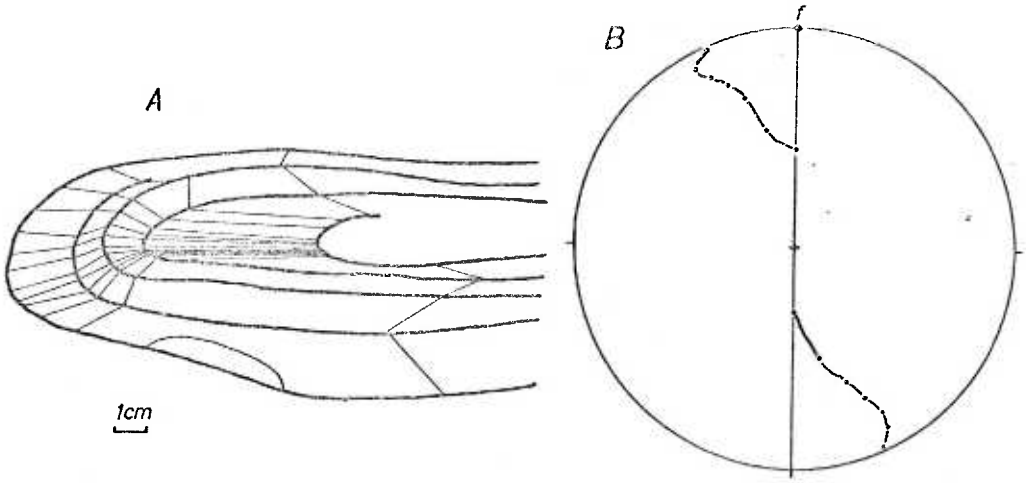


FIGURE 5.23 A) Fold profile from the Gwernargllwydd stream with dip isogons at 15 degree intervals. B) Locus of deformed lineation from outer surface of fold.

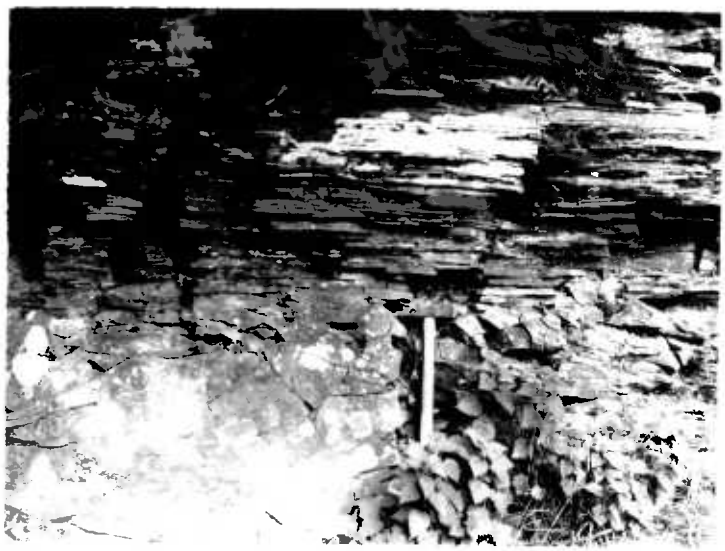


FIGURE 5.24 Upper contact to a massive slump sheet north of Llanfihangel-nant-Melan (SO 182586).



FIGURE 5.25 Slump conglomerate south of Gwernargllwydd (SO 156597).

5.5 THE BISHOPS CASTLE AREA

Further exposures of slumps formed on the eastern margin of the Montgomery Trough occur in the Bishops Castle area, some 30 km to the north of the Radnor Forest sequence. These clearly represent a local slump development unrelated to the main sequence.

The most extensive exposure is in Cwm Hopton (SO 230905) where three sheets are exposed. The few visible slump folds suggest a NNE-SSW palaeoslope trend. There is a tendency for a nodular structure to develop, especially in the cores of folds. Similar features are seen in the City Lane section (SO 212900).

Isolated exposures further east show thin slump sheets only. Allender (1959) took this to indicate increasing proximity to the shelf on the eastern margin of the trough.

CHAPTER SIX

THE WESTERN SEQUENCE

6.1 THE TEME VALLEY SECTION : INTRODUCTION

The most important section through the Western slump sequence is exposed in the valley of the River Teme, for a distance of about one and a half kilometres below its source (SO 120840 to 125830). This locality is the main subject of the present chapter. Other localities in the Western Sequence are described in Secs. 6.6 and 6.7.

The Teme valley locality was first described by Earp (1938). He showed that the exposed slump sheets lie near the top of the thickest part of the Western Slump Sequence, whose 800 metre thickness in this area is also the greatest of any Ludlovian sequence in Central Wales (Enclosure 1). The upper part of the sequence was correlated with the leintwardinensis zone, but the sequence as a whole was shown to extend downwards through the tumescens/incipiens into the scanicus zone (Fig. 3.4). Later work by Bailey (1964, 1969) showed that the slump sequence (the 'slumped siltstone facies') is replaced to the east by, and in this area is intercalated with, the contemporaneous 'silt turbidite facies' of the axial zone of the Montgomery Trough (Fig. 3.7).

For the present study the valley has been mapped at a scale of 1:1000 (Enclosure 4). It trends approximately along the strike of the eastward dipping sequence, the total exposed thickness of the succession being only between 70 and 100 metres. The exposure is mainly in steep cliffs, and the outcrop patterns of each unit are a reflection of this topography.

The sequence shows the characteristic alternation of slumped and undisturbed units. The lithologies in both types are siltstones and mudstones with occasional silt turbidite beds. In contrast to the Eastern Sequence, shelly fossils are rare in both slumped and undisturbed units. The slumped units in the Teme Valley section are dominantly of the intrafolial fold type recognised in Cwm Blithus (Sec. 4.1). Folds are invariably isolated in laminated sediments, though thick developments of exclusively laminated sediment are absent and such sediment has not been separately distinguished on the map. No examples of the low deformation 'folded' units are seen.

The lower contact of each slumped unit is invariably gradational, and the upper contact is usually so. The gradational zones tend to be thicker than those in the Eastern Slump Sequence, and the distinction



FIGURE 6.1 Erosional upper contact to a slump sheet in the Teme Valley (contact approximately at lens cap).

between undisturbed and slumped units is consequently more difficult. Several slumped units do however show clearly truncated upper contacts (Fig. 6.1), confirming the penecontemporaneous nature of the structures.

The average proportion of undisturbed units in the total sequence is about 25%, an approximately similar proportion to that determined at Cwm Blithus.

6.2 ORIENTATION OF STRUCTURES

A plot of the attitude of bedding in the undisturbed units (Fig. 6.2) reveals a gentle anticline plunging at about 10 degrees towards 030°, and with an axial surface dipping steeply northwestwards. This

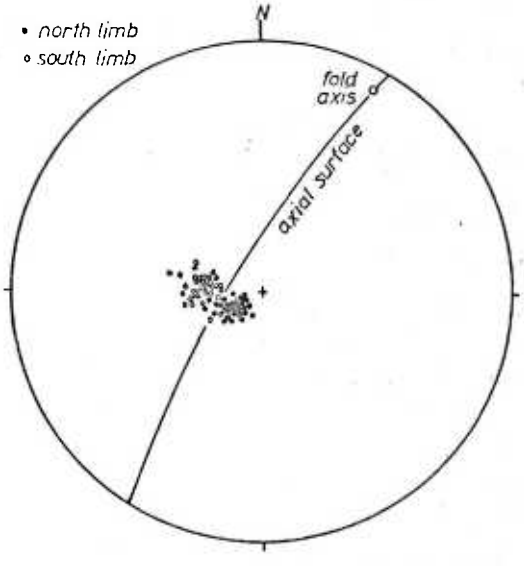


FIGURE 6.2 Plot of bedding poles from the Teme Valley section.

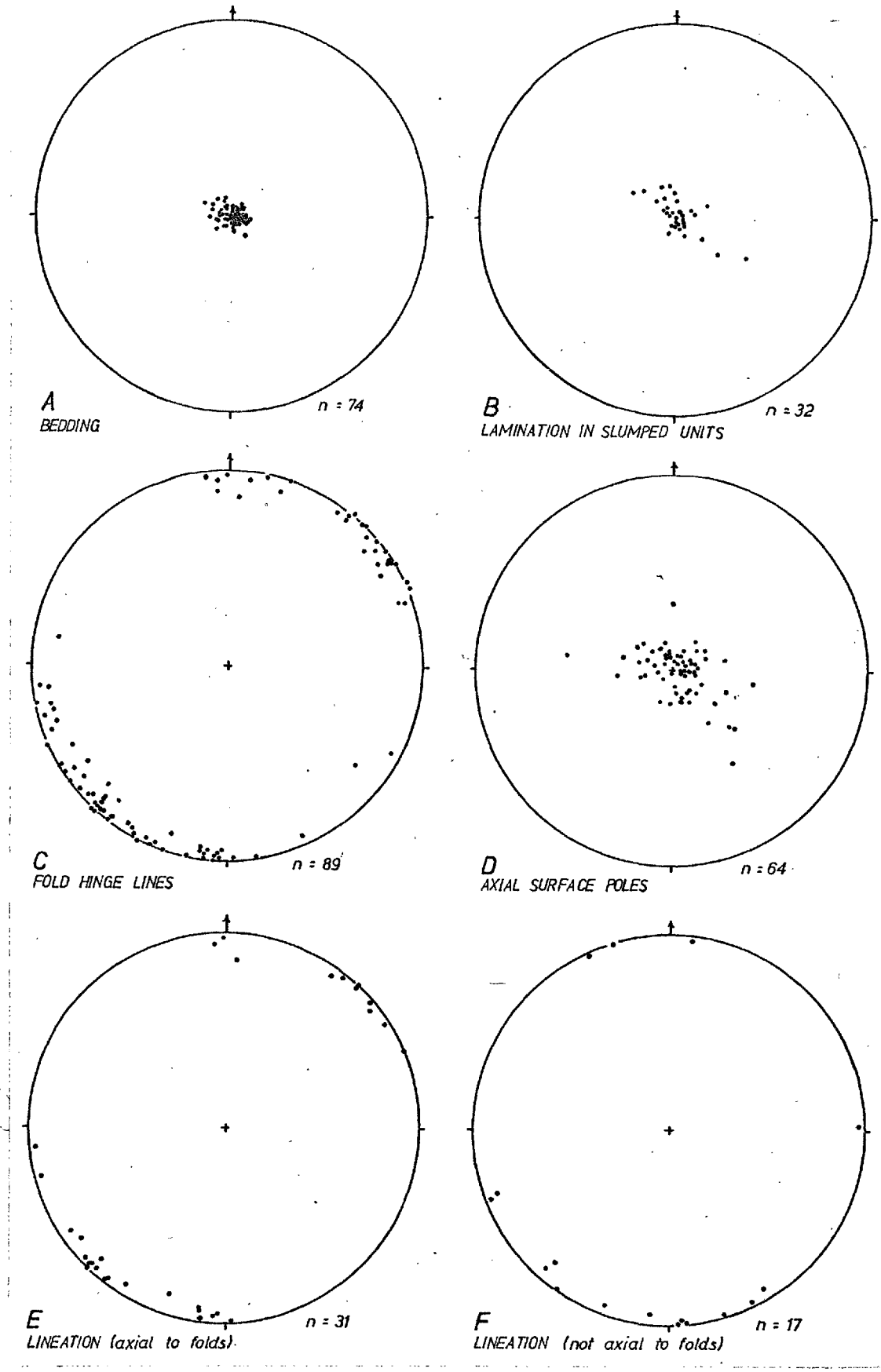


FIGURE 6.3 Projections of orientation data from the Teme Valley referred to the original depositional datum.

fold is clearly a tectonic feature contiguous to the more pronounced structures of similar trend to the north. To partially correct the slump data for the effects of this tectonic deformation, the data on each limb have been separately transformed to refer to the mean attitude of the limb; that is they have been rotated about the strike of the limb. This approximate correction is probably adequate for valid comparison of structures from all parts of the measured sequence.

The transformed data are plotted on Fig. 6.3, and these distributions are summarised on a principal axis plot (Fig. 6.4) and an eigenvalue ratio plot (Fig. 6.5). The bedding poles assume an approximately axially symmetrical distribution (Fig. 6.3A), but the poles to the lamination in the disturbed units and to the axial surfaces are partially dispersed about a NE-SW axis (Fig. 6.3B,D). The fold hinge lines and lineations are dispersed in the plane of the sheets. The hinge lines (Fig. 6.3C) have a clear NE-SW mean orientation, as do those lineations which are demonstrably axial to folds (Fig. 6.3E). However, lineations which are not clearly related to folds (Fig. 6.3F) have a N-S mean orientation, a feature which will be discussed in Sec. 6.5. Apart from these anomalous lineations, the geometry displayed in Figs. 6.3, 4, 5 is strikingly similar to that found in Cwm Blithus (Sec. 4.3), and suggests that this pattern is typical of the Central Welsh Ludlovian slumps.

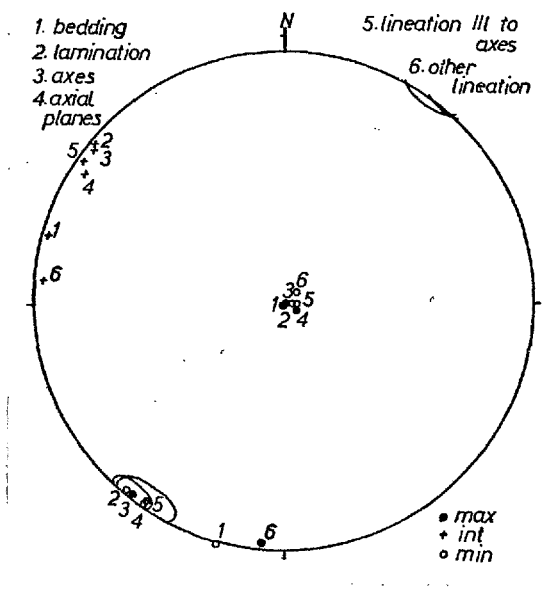


FIGURE 6.4 Synoptic plot of principal axes of distributions in Fig. 6.3, with cones of confidence at the 95% level.

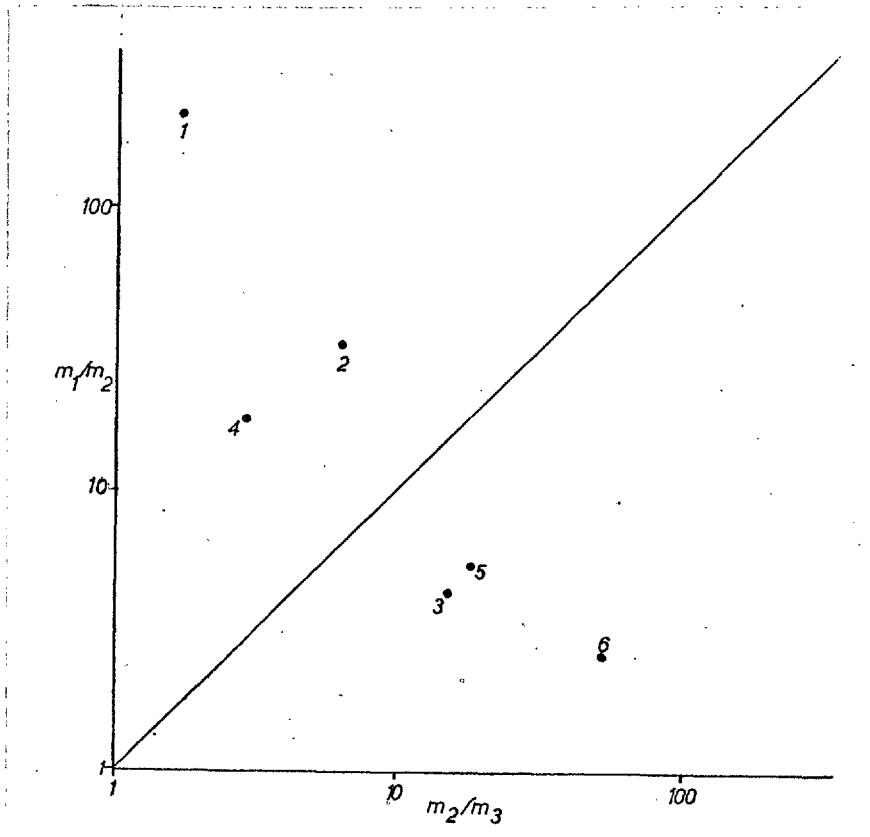


FIGURE 6.5 Ratio plot of the distributions in Fig. 6.3.

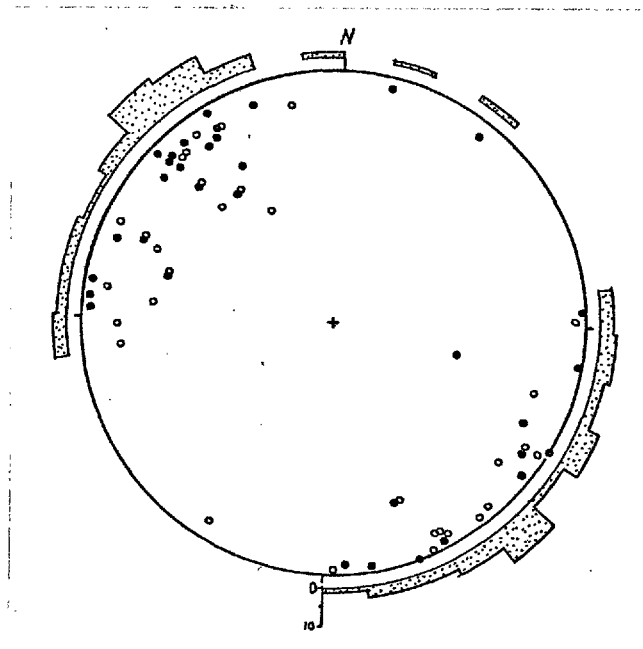


FIGURE 6.6 Projection showing fold closure directions. Closure into the plot is denoted by a solid circle, and closure out of the plot by an open circle. A circular histogram summarises the azimuthal frequencies of closure. Data are corrected for tectonic tilt.

6.3 ESTIMATION OF PALAEOSLOPE ATTITUDE

The best estimate of palaeoslope trend based on fold hinge lines, lineations and axial planes is about 037° ± 10° (see Fig. 6.4). There is no significant variation in this trend along the section. A similar estimate of the palaeoslope in this area was made by Bailey (1964).

In order to fit the Western Slump Sequence into Cummins' (1959) 'Montgomery Trough' model (Sec. 3.5), both Bailey (1969) and Cummins assumed, but did not verify, that these sheets moved southeastward down a western margin to the trough. It is possible to test this assumption by applying the techniques used in Sec. 4.5.

A plot of fold closure directions (Fig. 6.6) shows, as expected, no preferred closure sense. This further supports the conclusion of Sec. 4.5 that this method of determining movement direction has no general validity.

A few folds only have a clear sense of asymmetry (Fig. 6.7). All but one of these however overturn to the southeast (Fig. 6.8). A similarly conclusive result is obtained from the folds where facing directions could clearly be determined (Fig. 6.9). These data provide good evidence that the movement of sheets was southeasterly.

A further suggestion of southeasterly movement is provided by the consistent deviation of the 'vertical' principal axis of distributions from that of the undisturbed bedding (Fig. 6.4). As in Cwm Blithus, this imbrication is not marked enough to be statistically significant, but its accordance with other slope direction criteria suggests that it is a real effect.



FIGURE 6.7 Asymmetric fold indicating a southeasterly movement direction.

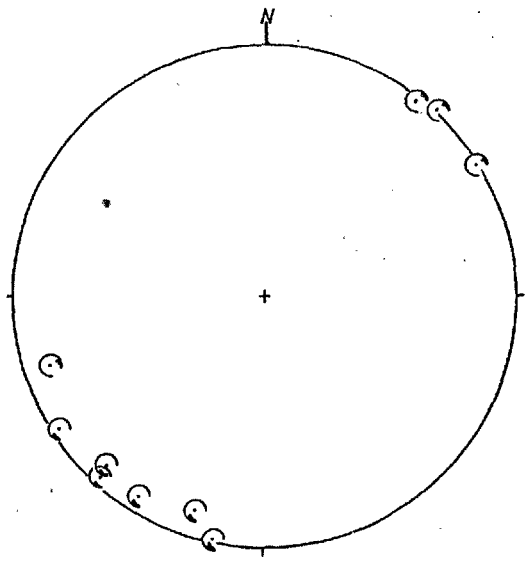


FIGURE 6.8 Projection of hinge lines of folds showing asymmetry sense. Data corrected for tectonic tilt.

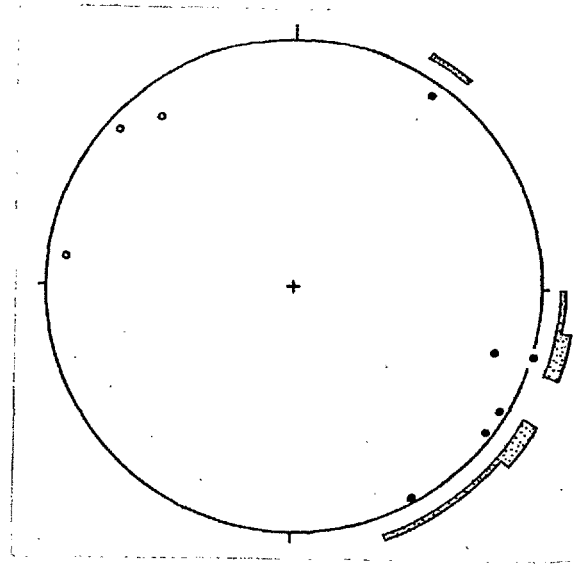


FIGURE 6.9 Projection of fold facing directions. Data corrected for tectonic tilt. Plotting conventions as Fig. 6.7.

6.4 FOLD GEOMETRY

The description of fold geometry follows the same scheme as used in Secs. 4.6, 7, 8 & 9.

Fold attitudes are summarised in Fig. 6.10. Most folds have sub-horizontal axes with recumbent or gently inclined axial surfaces, when referred to the original depositional datum.

Both the sizes of folds and their interlimb angles show broadly similar distributions and means to those in Cwm Blithus. The 'length' and 'breadth' frequency distributions (Fig. 6.11) are positively skewed, and length/breadth ratios vary between 0.5 and 7.0 (Fig. 6.12). The interlimb angle frequency distribution is also positively skewed with a mean of about 24 degrees (Fig. 6.13).

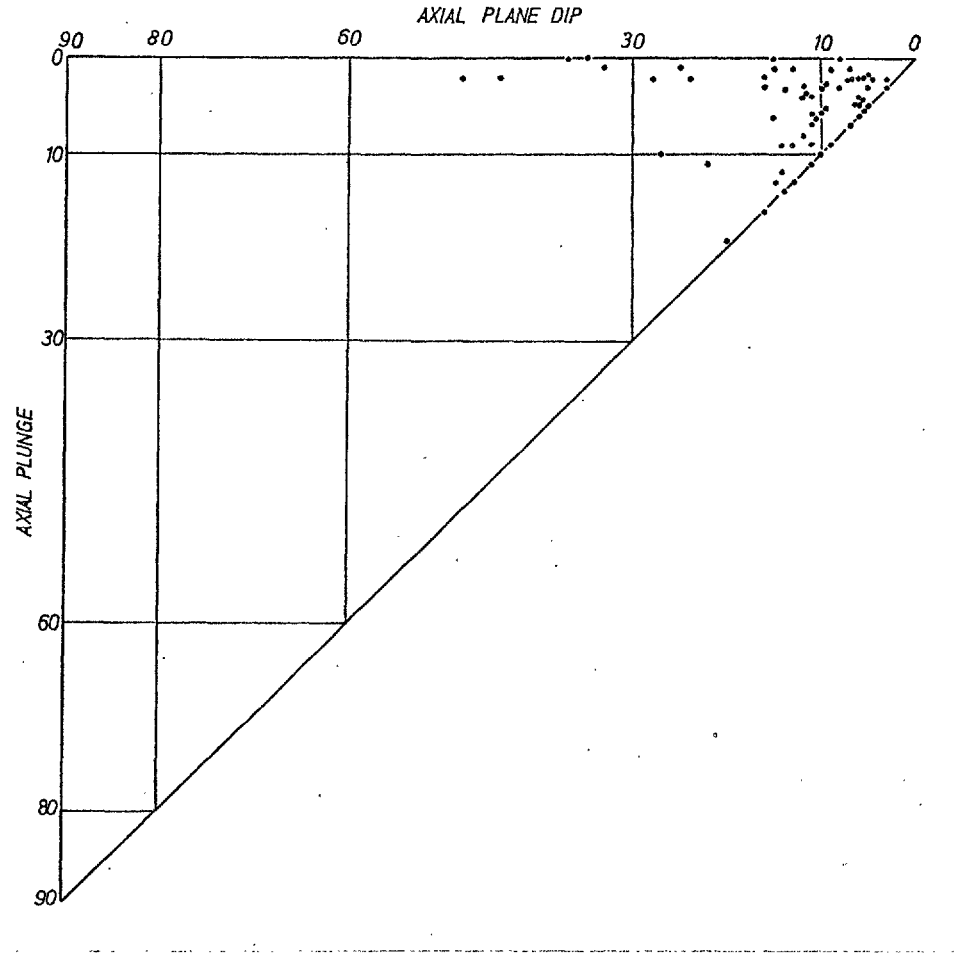


FIGURE 6.10 Plot of fold axial plunge against their axial surface dip. Data corrected for tectonic tilt.

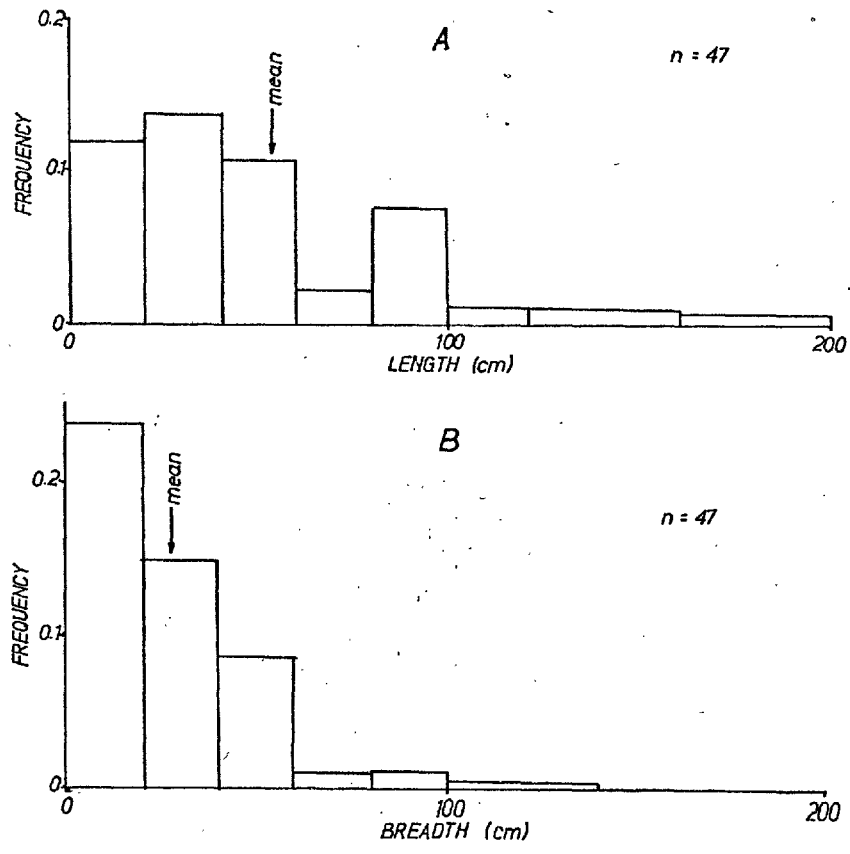


FIGURE 6.11 Histograms of fold length and breadth frequency (see Fig. 4.31A).

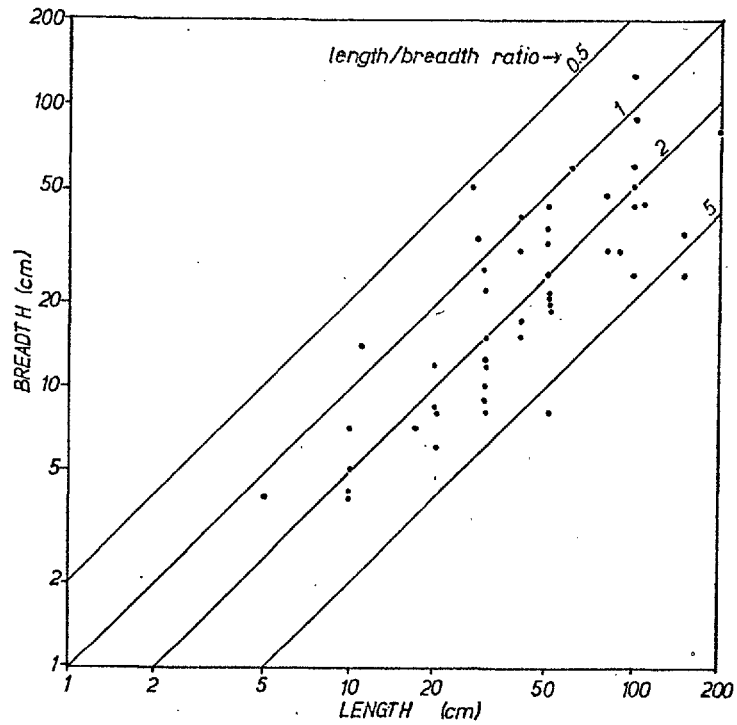


FIGURE 6.12 Plot of fold length against breadth.

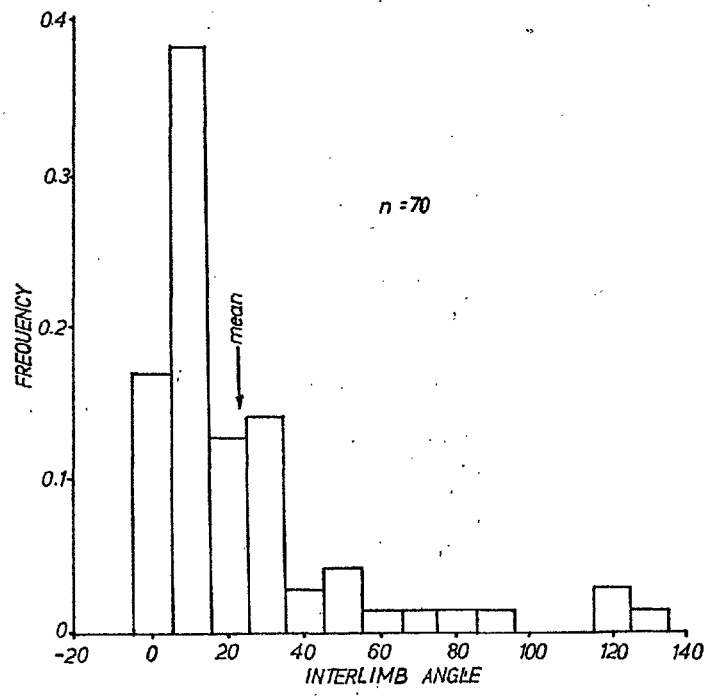


FIGURE 6.13 Frequency histogram of interlimb angle.



FIGURE 6.14 Fold with Class 1C geometry close to Class 2.



FIGURE 6.15 Fold with Class 1C geometry close to Class 2.

The folds in Figs. 6.14,15 are representative of the dominant layer geometry. Dip isogons reveal an overall Class 1C geometry which is rather closer to the Class 2 (similar)model than the typical folds in the Eastern Sequence (cf. Figs. 4.38, 39, 40). Folds with more strongly convergent isogon patterns are present but not common (Fig. 6.16). Despite the near similar styles in some of the Teme Valley folds, the absence of folds which truly fit this model suggests that there has been a significant buckling component at some stage in their formation. This is confirmed by analysis of deformed lineations. The locus of a lineation from the fold in Fig. 6.15 is shown in Fig. 6.17. The marked discontinuity in the locus on either side of the axial surfaces clearly indicates a mechanism other than simple shear alone.



FIGURE 6.14 Fold with Class 1C geometry close to Class 2.



FIGURE 6.15 Fold with Class 1C geometry close to Class 2.

The folds in Figs. 6.14,15 are representative of the dominant layer geometry. Dip isogons reveal an overall Class 1C geometry which is rather closer to the Class 2 (similar)model than the typical folds in the Eastern Sequence (cf. Figs. 4.38, 39, 40). Folds with more strongly convergent isogon patterns are present but not common (Fig. 6.16). Despite the near similar styles in some of the Teme Valley folds, the absence of folds which truly fit this model suggests that there has been a significant buckling component at some stage in their formation. This is confirmed by analysis of deformed lineations. The locus of a lineation from the fold in Fig. 6.15 is shown in Fig. 6.17. The marked discontinuity in the locus on either side of the axial surfaces clearly indicates a mechanism other than simple shear alone.

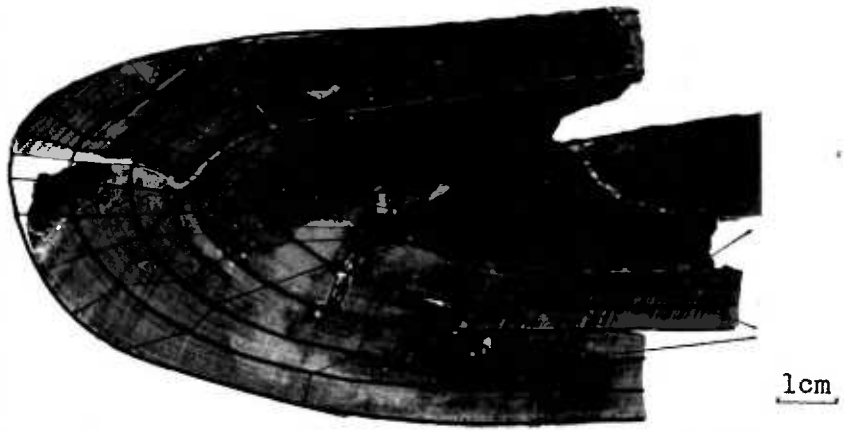


FIGURE 6.16 Fold with Class 1C geometry.

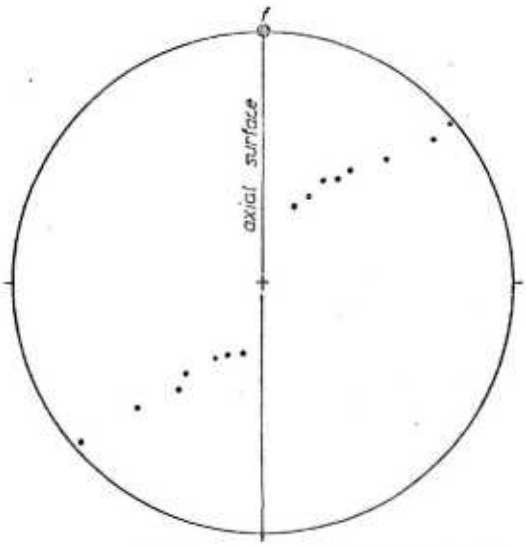


FIGURE 6.17 Lineation locus from outer surface of fold in Fig. 6.15.

6.5 LINEATION AND CLEAVAGE

The range of lineation types developed in the Teme Valley section is similar to that described for Cwm Blithus (Sec. 4.10). The 'fold' type of lineation is again the most common, showing all the typical stages of development (Fig. 4.52) except for the initial kink bands. These fold lineations are commonly axial to slump folds, and apparently have a similar directional significance (Fig. 6.3E).

Also common in this section are lineations associated with a 'crenulation cleavage'. This problematical structure is clearly seen in thin section (Fig. 6.18), and is also sporadically visible in the field (Fig. 6.19). Deformation has taken place along thin discrete zones, which have a normal sense of displacement. This displacement is seemingly a real effect, there being no evidence of removal of



FIGURE 6.16 Fold with Class 1C geometry.

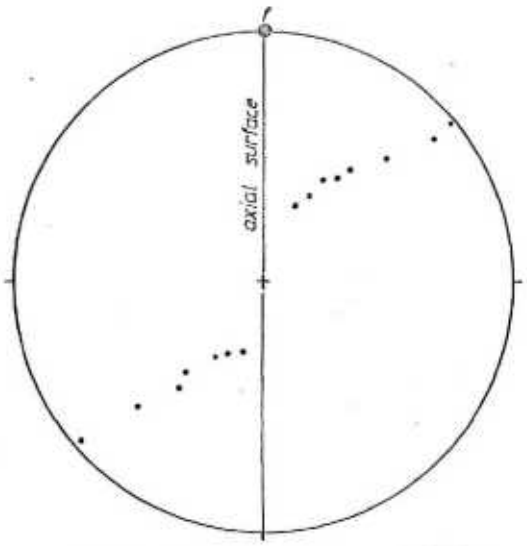


FIGURE 6.17 Lineation locus from outer surface of fold in Fig. 6.15.

6.5 LINEATION AND CLEAVAGE

The range of lineation types developed in the Teme Valley section is similar to that described for Cwm Blithus (Sec. 4.10). The 'fold' type of lineation is again the most common, showing all the typical stages of development (Fig. 4.52) except for the initial kink bands. These fold lineations are commonly axial to slump folds, and apparently have a similar directional significance (Fig. 6.3E).

Also common in this section are lineations associated with a 'crenulation cleavage'. This problematical structure is clearly seen in thin section (Fig. 6.18), and is also sporadically visible in the field (Fig. 6.19). Deformation has taken place along thin discrete zones, which have a normal sense of displacement. This displacement is seemingly a real effect, there being no evidence of removal of

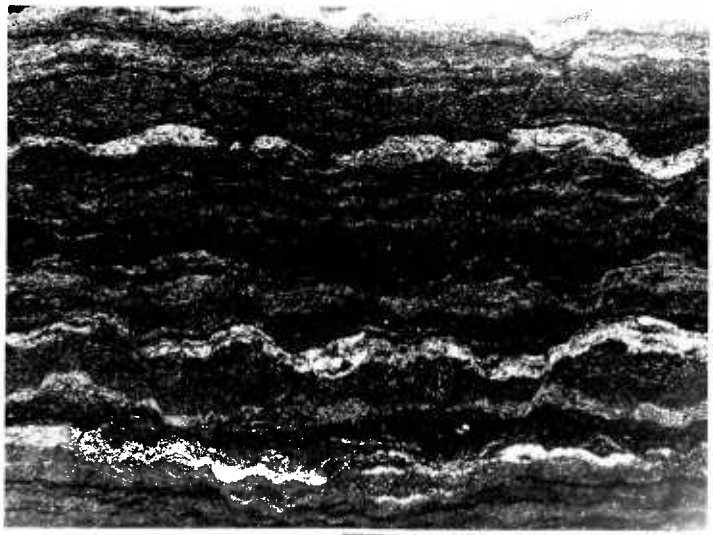




FIGURE 6.18 Two examples of conjugate normal shears associated with a slump lineation.



FIGURE 6.19 Cleavage cutting horizontal lamination. Microscopic structure is similar to that in Fig. 6.18A. Conjugate cleavages are visible in the upper part of the outcrop.

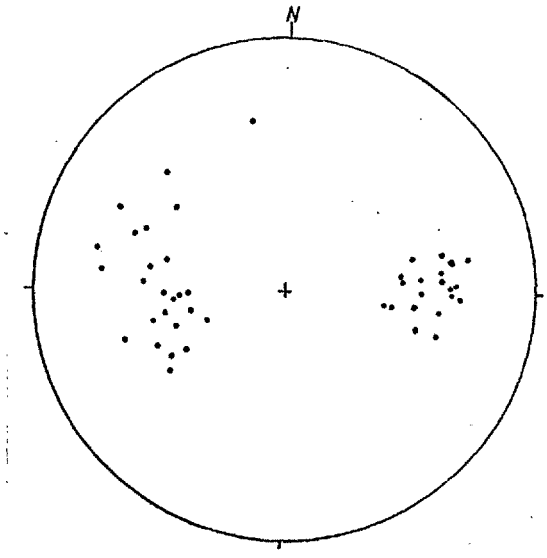


FIGURE 6.20 Projection of poles to cleavage planes.

material from the zone as in tectonically formed crenulation cleavage. Almost invariably two sets of zones are developed with a symmetrical relationship to the bedding, and inclined to it at between 40° and 60°. The structures strike fairly consistently N-S throughout the mapped section (Fig. 6.20). It is clear that the anomalous N-S trending lineations previously noted (Fig. 6.3F) are due to the intersection of these cleavages with lamination surfaces in the slumped units.

The mode of origin of the structures is uncertain. Their trend oblique to the definite slump structures might suggest a tectonic origin. They are, however, also oblique to all known tectonic structures in the area. Moreover their irregular smeared appearance, their symmetrical relationship to the bedding, and their restriction to slumped units (see also Fig. 5.2) favours a penecontemporaneous origin. They are most probably related to the compaction of the slump units under the load of later sediments. The structures indicate a bulk strain ellipsoid for this 'compaction phase' of deformation having its shortest axis normal to the bedding and its intermediate axis parallel to the intersection of the conjugate shears (Fig. 6.21). Under these conditions Cobbold et al (1971) predicted theoretically, and formed experimentally, structures of an essentially similar geometry to the compaction cleavages. Hence the compaction origin seems feasible if it can be explained (a) why the compaction strain ellipsoid should have been inequiaxial in the plane of the bedding rather than simply uniaxial and (b) why the ellipsoid was oblique to previously formed slump structures. The only explanation which suggests itself is that the slump sheets, though they moved mainly down a NNE-SSW trending slope,

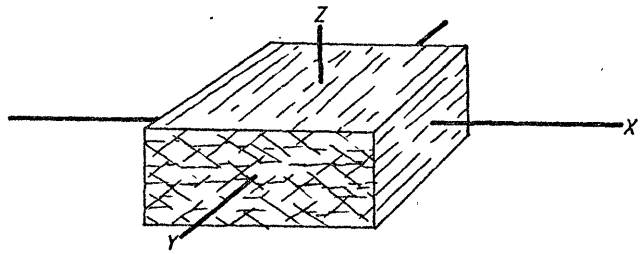


FIGURE 6.21 Relationship of conjugate normal shears to the bulk finite strain ellipsoid.

finally came to rest in the axial zone of the trough on a gentle slope trending N-S. During compaction further slight downslope adjustments in the sheets occurred, with the formation of the conjugate shears. This hypothesis of a N-S trending palaeoslope is supported by the approximately northward current directions in this area (Fig. 3.8).

6.6 OTHER LOCALITIES IN THE WESTERN SEQUENCE

The Teme Valley section is the only extensive exposure of the Western Slump Sequence. Other localities, which are indicated on the regional map (Enclosure 1), are mainly small quarries or rather poor stream valley exposures. They reveal nothing to suggest that the structures described from the Teme Valley are not representative of the sequence as a whole.

A good section is exposed in a stream gully 700 metres east of Maes Gwyn (SO 158778). A map of the exposures (Fig. 6.22A) shows the

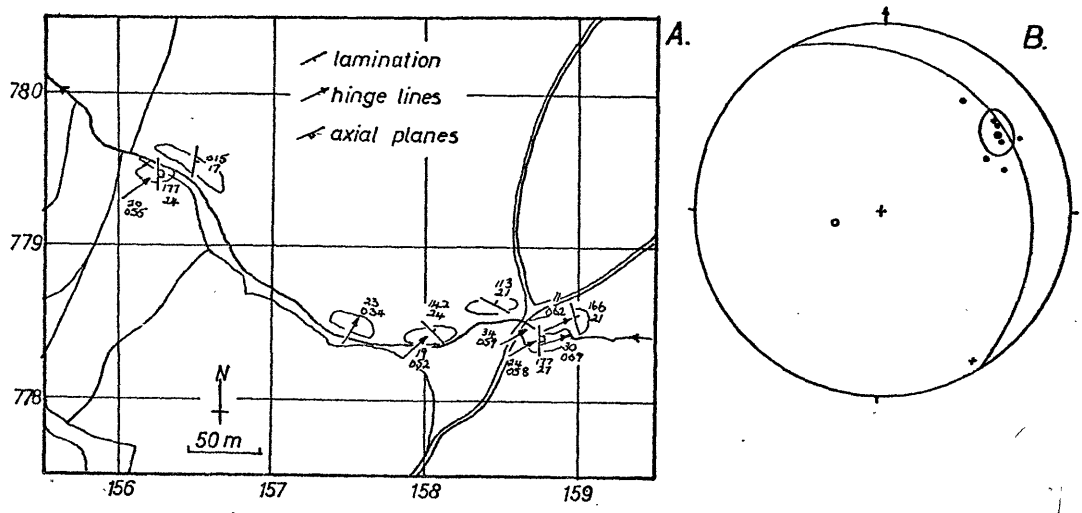


FIGURE 6.22 A) Map of exposures in gully E of Maes Gwyn (National Grid indicated). B) Plot of fold hinge lines and their principal axes.The trace of the mean lamination is indicated.



FIGURE 6.23 Fold with Class 1C geometry from Maes Gwyn gully.

rather restricted amount of data available from such sections. Nevertheless, the fold axis data are dispersed in the plane of the sheet in the usual way, and permit a fairly accurate estimate of palaeoslope trend. Folds are recumbent, tight or isoclinal, with a Class 1C geometry (Fig. 6.23).

Of the more typical exposures in the Western Sequence, the best are in the stream west of Cider House (SO 106845), the quarry north of Butterwell Farm (SO 110825, Fig. 6.24), the gully to the east of Cwm Nanty (SO 101805, Fig. 6.25), on Moelfre Hill (SO 119759) and in the Lawn Brook (SO 187760).



FIGURE 6.24 Two slump sheets with intervening undisturbed units. The hammer head marks the upper erosional contact of the lower sheet. Butterwell Farm Quarry (SO 110825).



FIGURE 6.25 Upper contact to a slump sheet in Cwm Nanty (SO 101805).

6.7 SLUMP SHEETS NEAR LLANGUNLLO

To the east of Llangunllo (SO 212713) occurs a group of slump sheet exposures which is not obviously related to either the Western or to the Eastern Sequence. The exposures are located approximately in the thickest part of the Ludlovian succession, which presumably corresponds with the axial zone of the Montgomery Trough. They are therefore of special interest, despite their limited extent.

Three slump localities have been recognised (Fig. 6.26); a quarry north of Cefnsuran Farm (SO 229712), a bank in Cefnsuran Lane (SO 227704) and a stream section above Upper Weston (SO 213703). The first of these was mentioned by Holland (1959b). The three exposures are not obviously correlated with each other, and probably represent several thin sheets.

The slump folds involve silt turbidite beds and show the typical tight recumbent geometry (Fig. 6.27). The limited amount of orientation data available suggests a NE-SW trending palaeoslope at Cefnsuran Farm, and one trending NW-SE in Cefnsuran Lane (Fig. 6.26). A northeasterly movement direction is indicated by fold asymmetry in the latter exposure. The conflicting estimates of palaeoslope trend suggest that these slumps represent minor developments in a region with no predominant palaeoslope. This is consistent with their being a separate 'axial' slump development, unrelated to the Eastern and Western marginal sequences.

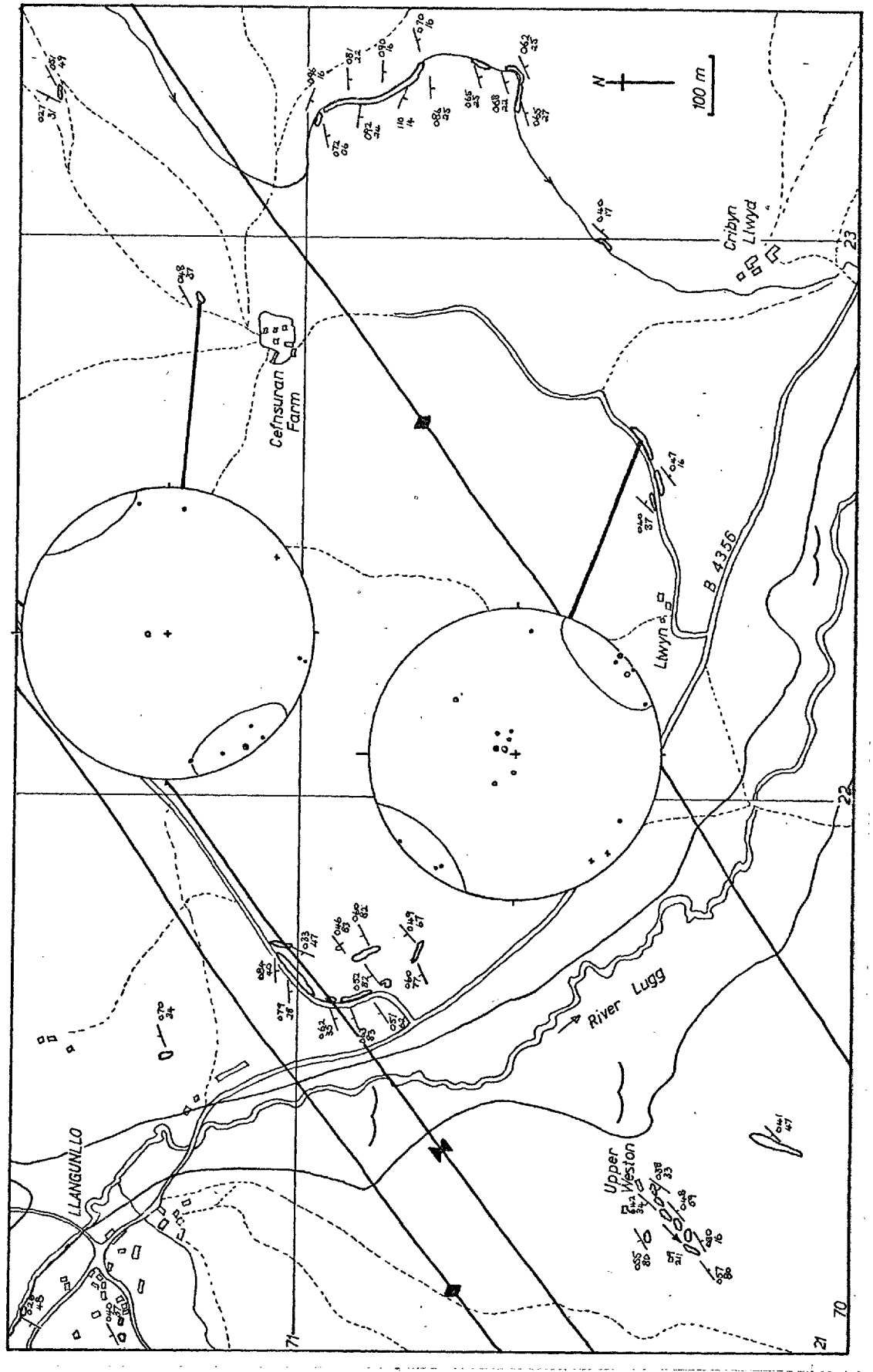


FIGURE 6.26 Map showing slump localities near Llangunllo. Inset are the distributions of fold hinge lines at two localities with their principal axes and 95% confidence limits. Axial surface poles (open circles) are included on one plot.

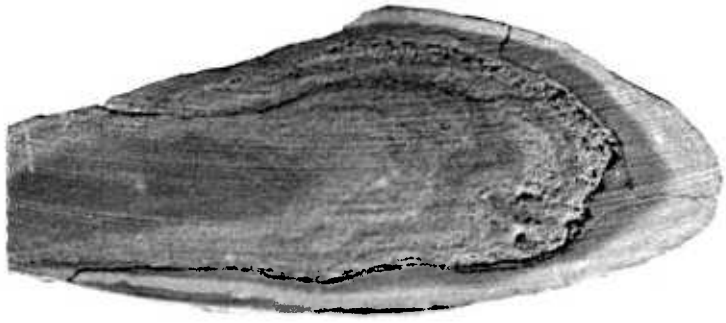


FIGURE 6.27 Fold from Cefnsuran Lane (SO 227704) showing Class 1C geometry.

CHAPTER SEVEN

THE SHELF SLUMPS

7.1 MODE OF OCCURRENCE

The descriptions of the basin slumps have shown that they typically occur as part of a slump sequence comprising a number of individual sheets. In contrast, the shelf slumps usually occur as isolated sheets. Only in the area transitional to the basin facies do thicker sequences develop (Sec. 7.2).

The best exposures of the typical shelf slumps are in the Whitcliffe (SO 508741) and Clive Cottages quarry (SO 505745), both at Ludlow, and in the quarries southeast of St. Giles Church, Downton (SO 438743). These sheets are all at the base of the Lower Whitcliffe Beds (Holland *et al.* 1963, Whitaker 1962), and show erosional upper contacts and gradational lower contacts. The internal structure of the sheets is irregular, and fold styles and orientations cannot generally be determined. Any visible folds in these and other sheets (Fig. 7.1) usually show a Class 1C geometry.

Near Leintwardine (SO 405740) occur unusual slumps, which Whitaker (1962) showed to be associated with submarine channels, possibly cut in the edge of the shelf. These slumps are very localised and are poorly exposed. They are distinguished from the slump sheets of the remainder of the shelf by their association with boulder beds.



FIGURE 7.1 Fold from the Downton Gorge (SO 428730).

7.2 THE GATLEY COPPICE SEQUENCE

The slump structures at Gatley Coppice, south of Leinthall Starkes (SO 440 695), were described by Williams et al. (1957). They are anomalous in that they occur in a sequence some 50 metres thick. This thickness may be a consequence of the position of the sequence in the transition zone between the typical shelf facies to the east and the basin facies to the west. The westward increase in intensity of deformation and thickness of the sequence may reflect this transition.

The dominant structure is a slump lineation, which Williams et al. showed to be due to 'crinkling' of the lamination. To the southwest more intense folding is developed (Fig. 7.2). Hinge lines and most



FIGURE 7.2 A slump unit at the western end of Gatley Long Coppice (SO 433685).



1mm

FIGURE 7.3 Profile section through a fold lineation from the Gatley Coppice sequence.



FIGURE 7.4 A normal shear cleavage from the Gatley Coppice sequence.

lineations trend approximately east-west, and the asymmetry of microfolds suggests a northerly movement.

Although most lineations are of the fold type originally described by Williams et al. (Fig. 7.3), some lineations are clearly associated with conjugate cleavages similar to those described in Sec. 6.5 (Fig. 7.4). These strike east-west approximately parallel to other structures. Their presence may explain some of the problematical intersecting lineations which Williams et al. noted.

CHAPTER EIGHT

SUMMARY AND DISCUSSION OF FIELD RESULTS

8.1 SUMMARY OF RESULTS

1. Slumped deposits in the Central Welsh Ludlovian occur almost exclusively as slump sheets, with a large areal extent in comparison to their thickness.
2. Some sheets are an isolated feature within a relatively large thickness of undisturbed sediments. The majority, however, are grouped into two slump sequences , one on either side of the Montgomery Trough axis.
3. Successive sheets are usually separated by a unit of autochthonous sediments. The lower contact of each sheet is always gradational, the upper contact occasionally sharp and demonstrably erosional. Composite slumped units comprising two or more slump sheets also occur, and may often go unrecognised.
4. Each slump sheet may comprise a variety of structural types, representing increasing disturbance of the original depositional structure.
5. The thickness frequency distribution of both slumped and undisturbed units approximates to a gamma distribution with a strong positive skew.
6. The attitude of all slump structures is closely related to the original depositional datum. Fold hinge lines and the associated axial lineations are dispersed in the plane of the sheet, but usually show some tendency to cluster within it. Axial surfaces tend to lie in the plane of the sheet, but also show some dispersion about the mean fold axis.
7. Palaeoslope trend can be estimated by the mean lineation or fold axis and, less reliably, from the pole to the girdle of axial plane poles. Due to the wide dispersion of structures, trend estimates have rather wide confidence limits unless large samples can be obtained.
8. The direction of slump movement is not revealed by fold closure directions, but can be reliably predicted from either fold asymmetry, lineation (microfold) asymmetry, fold facing direction, or possibly axial plane 'imbrication'.
9. Estimated palaeoslope trends are approximately NE-SW throughout

the main slump sequences, and no significant change is apparent along the length of the trough. The palaeoslope trend within one area may vary slightly with time. Slumps in the Eastern Sequence moved to the northwest and those in the Western Sequence towards the southeast.

10. More variable palaeoslope attitudes occurred on the shelf and in the axial zone of the trough.
11. Most slump folds are recumbent or gently inclined with sub-horizontal axes. They may be markedly non-cylindrical on the outcrop scale. Open folds have variable but predominantly angular shapes. Most folds are, however, tight or isoclinal and have more rounded hinge zones, sometimes double hinged.
12. Folds show an approximately lognormal size distribution within any one area. Sheets showing low deformation have a smaller mean fold size than the more deformed units.
13. Most folds have an overall Class 1C geometry and only rarely approximate to the Class 2 (similar) model. Folds are not therefore continuous for long distances along their axial surfaces, being replaced by thrusts, or by complete breakdown of the structure. Consistent variation in style between adjacent layers is uncommon, suggesting that competence differences between layers were low.
14. Deformed lineations and minor structures suggest a significant component of flexural slip or possibly tangential longitudinal strain during fold formation.
15. Some folds show a clear axial planar fabric due both to grain orientation and magnetic anisotropy.
16. Lineated lamination surfaces are characteristic of most slump deposits. The majority of lineations are due to microfolding and are often axial to the larger slump folds. Some are true slickensides.
17. Conjugate cleavages occur sporadically in some slump sheets. These are due to sets of normal shears which may have formed as a result of compaction after slumping had ceased.

8.2 THE SEQUENCE OF DEVELOPMENT OF STRUCTURES

Although the main object of Part II has been to describe the geometry of the Ludlovian slump structures, some speculation on their mode of development is appropriate.

The deformation history is more easily deduced with some knowledge of the probable stress states which existed in a deforming sheet.

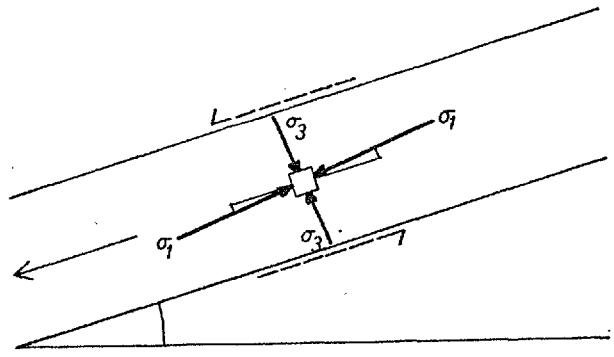


FIGURE 8.1 Probable orientation of principal stresses in a moving slump sheet (see text for explanation).

Fig. 8.1 shows one possible model for the orientation of bulk principal stresses at an early stage in sheet transport. The maximum principal (compressive) stress lies close to the plane of the sheet, and in the direction of bulk transport. This is justified by assuming that the maximum restraining influence on sheet movement is exerted at the toe (leading edge) of the sheet, resulting in an overall downslope compression. There is some evidence for this assumption from seismic reflection profiles of sheet structure (Fig. 2.22). The minimum principal stress is assumed to be approximately normal to the sheet. There will, however, be a component of simple shear in the plane of the sheet, with a downslope shear direction, resulting in slightly oblique maximum and minimum principal stress axes.

Structures have been observed on two fairly distinct scales; one set due to deformation of a fine lamination (in the order of millimetres thick) and the other to a coarser lamination (in the order of centimetres or tens of centimetres thick). The development of each set can to some extent be considered separately (Fig. 8.2A).

The apparent deformation sequence in the fine lamination has already been outlined in Sec. 4.10, and the sequence depicted in Fig. 8.2A is essentially that illustrated in Fig. 4.52. In Stage 1 the lamination buckles under a compression almost parallel to the layering. The fold style is determined by the total anisotropy of the layering rather than by the properties of any individual layer (see Cobbold *et al.* 1971). Much of the lamination on this scale has a moderately high anisotropy and develops fairly angular folds. Discrete zones of deformation propagate, mostly with the asymmetry sense appropriate to the monoclinic symmetry of the total system. The axial direction is approximately normal to the transport direction. With further

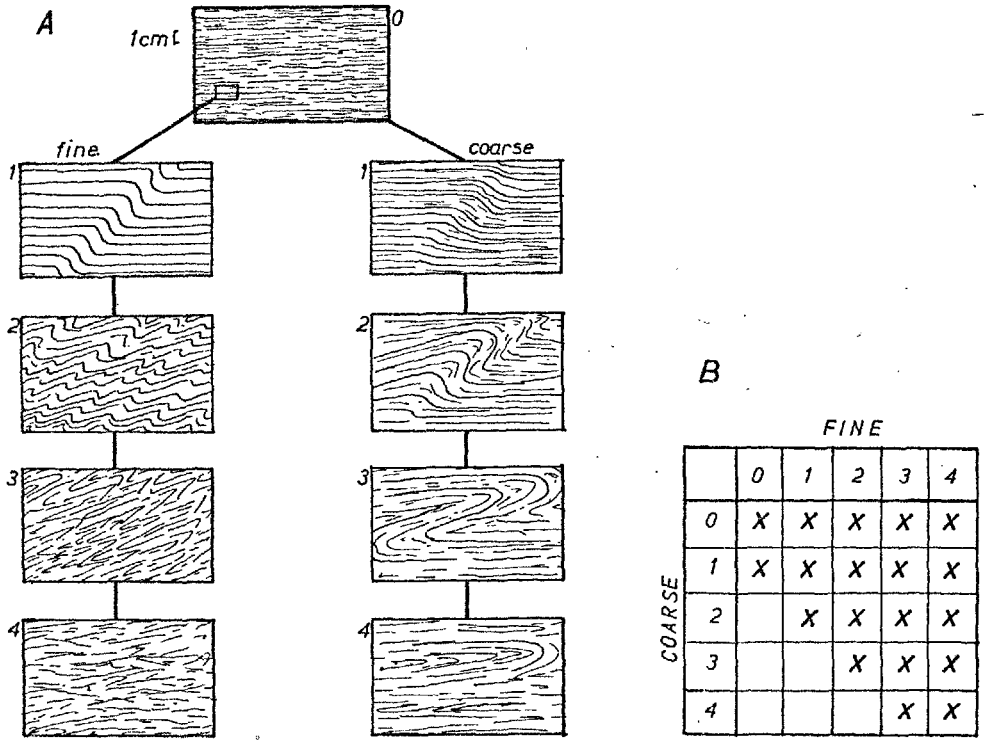


FIGURE 8.2 A) Sequence of development of structure in fine and coarse lamination. B) Table showing the coexistence of the two sequences in the field.

deformation more zones develop and the zones coalesce (Stage 2), eventually to pervade the whole system in a rather irregular way (Stage 3). The integrity of the folds may eventually be destroyed, producing a transposed lamination parallel to its original orientation (Stage 4). This sequence is associated with the development of a linear structure on lamination surfaces which changes slightly in character as deformation proceeds.

The deformation sequence on the larger scale is less well preserved. Folds may well initiate in a similar way to those in the fine lamination, though they probably have a more rounded style due to the lower effective anisotropy on this scale. Single layer buckling may also control fold styles to some extent. Folds are asymmetrical and have an axial direction approximately normal to the sheet movement. As the folds develop a more recumbent attitude the limbs start to shear out (Stage 3) until individual hinge zones become isolated as intrafolial folds (Stage 4). The evidence is that small folds are destroyed first during this sequence (see Sec. 4.6).

The structures produced by the two deformation sequences are of

course inter-related in the field, and each stage in one sequence may coexist with any one of several stages in the other sequence at the end of the deformation (Fig. 8.2B). However, the later stages in the larger scale structures never coexist with the earlier stages in the small scale sequence, but always involve more extreme minor structures. The relationships of the two sequences in time are more difficult to determine, though some clear relationships are seen such as the folding of previously formed kink bands (Fig. 4.50) and of other lineation. The overall impression is that the two sequences are essentially contemporaneous, with local conditions controlling the better development of one rather than the other.

The simplified sequence outlined above fails to account for several important features of slump geometry. The dispersion of axes in the plane of the sheet, for instance, requires that the fold axes initiate oblique to the trend of the slope, or are subsequently rotated into an oblique orientation. Either mechanism seems possible. A further complication is the presence of 'refolded folds' (Fig. 8.3). These are evidence that folds could initiate at any stage in the deformation history.

After the true slump deformation has ceased, a sheet probably undergoes further deformation in its unconsolidated state by compaction alone. The strain ellipsoid for this phase of deformation will, in the simplest case, be a uniaxial oblate type lying in the plane of the sheet. Strain is initially accommodated by intergranular movements, but at lower depths interstitial cementation and



FIGURE 8.3 A refolded isoclinal fold from Cwm-y-Bont (SO 193570).

intergranular stresses may inhibit this and there is a transition to other mechanisms, such as pressure solution. The magnitude of the strain achieved in the soft sediment state is merely a function of initial porosity and porosity at the time intergranular movements cease. The strain ratio Y/Z is then given by

$$\frac{Y}{Z} = \frac{1 - n_f}{1 - n_i} \qquad 8.1$$

where n_i and n_f are the initial and final porosities respectively. This function is plotted in Fig. 8.4 for a variety of values of initial porosity.

An estimate of probable porosity values for the Welsh sediments is difficult. However, assuming the porosity immediately after slumping was about 0.5 or 0.6 the strain/porosity gradient is sufficient to give quite appreciable strain ratios, with only low porosity decrease. This 'flattening' deformation could therefore significantly alter the geometry of folds and other slump structures and this should be considered in their description.

If the compaction strain ellipsoid is not uniaxial it may be possible to induce shear failure of the sediment, as discussed in Sec. 6.5

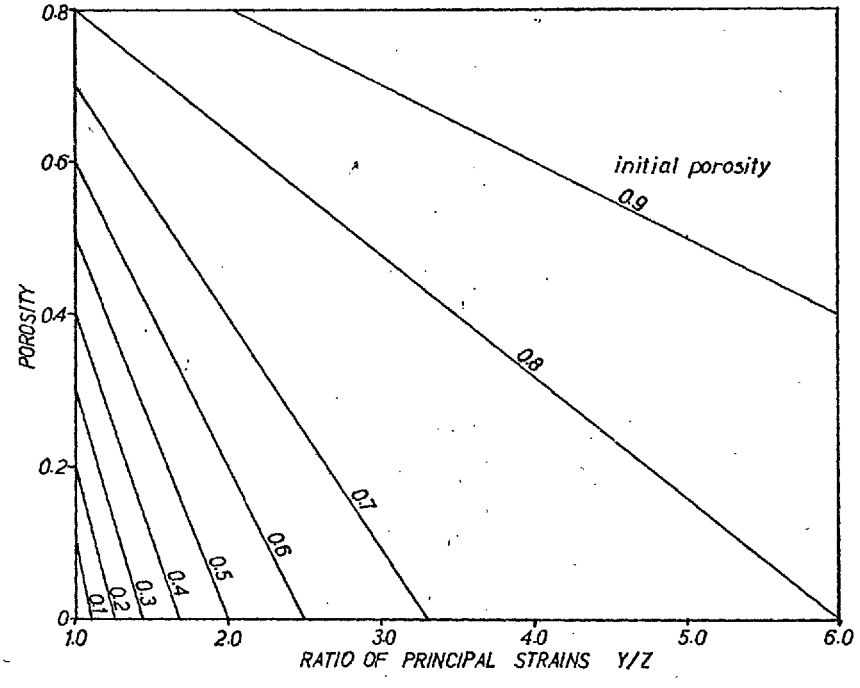


FIGURE 8.4 Graph of principal strain ratio due to compaction against porosity for various values of initial porosity.

8.3 CRITERIA FOR DISTINGUISHING SLUMP STRUCTURES FROM TECTONIC STRUCTURES

It has been tacitly assumed throughout the description of the Central Welsh structures that they were formed by slumping rather than by any tectonic process. Most of the evidence for this assumption is contained in the descriptions in Chaps. 4 to 7, but is collated in this section and compared with previously published criteria for recognition of slumping. A list of these criteria is given in Fig. 8.5, compiled from six representative accounts in which the evidence for slumping is explicitly stated. That of Rettger (1935) was intended to cover all types of soft sediment deformation.

The most reliable indicator of a slump origin is a demonstrably erosional contact above a discrete zone of deformation. This criterion was first stressed by Jones (1939) and remains the only conclusive proof of penecontemporaneous slumping . Many clear examples of such contacts occur in Central Wales, and a number have been figured (Figs. 2.6, 5.24, 6.1, 6.25). They are nevertheless atypical of upper contacts in general which are more commonly gradational or lack erosional features. Having proved a slump origin for several deformed units in a sequence, however, it is clearly parsimonious to assume the same origin for the remainder, provided that they show a similar internal structure.

All other features of slump deformation are, as Helwig (1970) observed, merely suggestive of their origin and not in themselves conclusive. It is appropriate to comment on the reliability of each criterion listed in Fig. 8.5 as it applies to the Central Welsh Ludlovian slumps.

3. The décollement form of lower contact is nowhere seen in these deposits. As with upper contacts they are usually gradational (Figs. 4.11, 5.7, 5.8).
4. The existence of faunal breaks across contacts has not been investigated. The abundant shelly fauna in the sheets of the Eastern Sequence may indicate superimposition of fauna from two contrasting environments (basin and slope), and this would be expected in general if marked translation of sheets had occurred.
5. The small size of the structures is not in itself indicative of slumping, the essential point being that these are not related to large 'lower order' structures as are most minor tectonic structures.
6. The descriptions in Chaps. 4 to 7 have shown that folds do not have a random attitude. Both their axes and their axial surfaces show

	RETTGER (1935)	JONES (1939)	FAIRBRIDGE (1947)	GRANT-MACKIE et al. (1964)	GREGORY (1969)	HELWIG (1970)
1. Deformation confined to a zone within undeformed beds	+	+	+		+	+
2. Upper contact commonly erosional		+	+	+	+	+
3. Lower contact commonly a décollement	+		+			+
4a. Contacts are faunal or stratigraphical breaks	+					
4b. Contacts are <u>not</u> faunal or stratigraphical breaks				+	+	
5. Structures are of small size	+		+		+	
6. Folds are randomly oriented				+	+	
7. Folds have curvilinear hinges						+
8. Folds have variable style but are often recumbent						+
9. Folds show no slip between layers						+
10. Folds do not have a related cleavage	+		+			
11. Folds develop into slump balls		+		+	+	+
12. Any faults are 'blurred'	+		+			+
13. No joints occur related to folds	+					+
14. Shell debris remains undeformed	+			+		
15. Folds associated with breccias			+			+
16. Structures are not directly related to tectonics	+	+	+			

FIGURE 8.5 Table of criteria for distinguishing slump structures from tectonic structures.

a statistically symmetrical relationship to the original depositional datum, and the axes form a marked, if dispersed, maximum related to the palaeoslope (e.g. Figs. 4.16, 6.3). Such dispersed distributions, though differing from the more tightly clustered distributions shown by many tectonic folds, are also associated with gravity tectonics (e.g. Cliff et al. 1971), and may be an indicator of a 'sheet' form of deformation rather than solely of slumping.

7. Curvilinear hinge lines are commonly seen, though these are also a feature of much tectonic deformation, albeit on a rather larger scale.
8. The evidence from Fourier analysis of fold shapes (Figs. 4.37, 4.38) suggests that a fairly restricted range is present, and that this range is comparable with that from one individual phase of tectonic deformation (cf. Hudleston 1973c) and from experimental studies (Hudleston 1973b). A similarly restricted range of isogon patterns occurs. The occurrence of isolated tight or isoclinal recumbent folds is however particularly characteristic of slump deformation.
9. Interlayer slip during slumping is evidenced by apparent slickensiding (Fig. 4.53), and suggested by the possible flexural slip component indicated by deformed lineations. True slickensides may in fact be more characteristic of slumping than of tectonic deformation, since in the latter interlayer slip is commonly evidenced instead by mineral fibre growth.
10. Pervasive axial plane fabrics are commonly related to the described slump folds (Sec. 4.11), and their presence does not imply tectonic deformation.
11. The presence of slump balls or folds with nodular cores is a fairly widespread feature which is strongly suggestive of slumping.
12. Small scale faulting is commonly seen and this does have a characteristic 'smeared' appearance.
13. Jointing is completely unrelated to folds in all areas.
14. The rigid behaviour of shell debris during deformation is clearly seen (e.g. Fig. 4.49), though this may also occur to a lesser extent in some tectonic environments.
15. Probable slump conglomerates are present, though they are not demonstrably related genetically to the slump sheets.
16. The complete contrast in style between the slump structures in the Central Welsh Ludlovian and definite tectonic structures in the same area persuasively advocates their contrasting origin. However,

this contrast would be less marked or obliterated in an area of greater tectonic deformation. Both slump folds and tectonic folds have a similar Caledonoid trend in this area. This common near-coincidence of tectonic and sedimentary trends in orogenic belts will render impossible the contradistinction of slump and tectonic folds on the basis of orientation in many areas.

In conclusion therefore, it is the total assemblage of deformation features which is likely to indicate their slump origin, rather than, with the exception of an erosional contact, one individual feature. Nevertheless, if a slump sequence suffers subsequent deformation and metamorphism, especially to high grades, it may become virtually impossible to distinguish the structures from tectonic structures.

PART III

THEORETICAL STUDIES
THE TRANSLATION OF SLUMP SHEETS

CHAPTER NINE

THE INITIAL STATE OF THE SEDIMENT

9.1 VALUES OF SEDIMENT PARAMETERS

Part II of this thesis was mainly concerned with the internal structure and deformation of slump sheets, as the field studies provided very little information on their bulk translation. Some indication of their distance of travel might be obtained from field evidence by a detailed analysis of the fauna in the allochthon as compared with the autochthon, but this was beyond the scope of the present work. Part III therefore speculates on the probable bulk behaviour of the Welsh slump sheets, by applying both original and published theoretical work to conditions in the Ludlovian Montgomery Trough.

A prerequisite to such studies is some knowledge of the physical properties of the sediments, both before and during slumping. Some attributes can be directly determined from the slumped sediments in their present state. However, most were clearly modified during slumping and must be estimated from data on recent sediments of a similar type.

A list of all the sediment parameters to be used in the following chapters is given in Fig. 9.1. Other relevant parameters relating to basin geometry, sedimentation rate etc. are also included. Estimates are given of the maximum and minimum and/or the average value of each parameter for the Ludlovian sediments of the Welsh basin. Some of the 'average' estimates are necessarily subject to a large error, but this is reflected in the maximum and minimum values. The source of each estimate is cited, and further notes relating to some parameters are given in Sec. 9.2. The estimation of the 'excess pore pressure factor' requires a more lengthy discussion which is given in Sec. 9.3.

9.2 NOTES ON PARAMETER ESTIMATES

Sedimentation rates

A rough estimate of average sedimentation rates is obtained by assuming a 10my duration for the Ludlow Period and sediment thicknesses of 300, 1000, and 2000 metres for the shelf, slope and axial basin sediments respectively (thicknesses from Holland *et al.* 1963). The corresponding rates are 3, 10 and 20 cm/1000yrs. The

PARAMETER		UNITS	MINIMUM	AVERAGE	MAXIMUM	REFERENCE
Sedimentation rate - long term average.	m	cm/1000yr				
(a) shelf			2	6	10	
(b) slope			10	20	50	see Sec. 9.2
(c) basin			10	20	30	
Coeff. of consolidation	c_v	cm^2/sec	2×10^{-4}	10^{-3}	2×10^{-3}	Morgenstern (1967)
Excess pore pressure factor due to sed^n.	μ	-	0	0	0.1	see Sec. 9.3
Gradient	α	degrees				Menard(1964),
(a) shelf			-	0.1	-	Heezen et al.
(b) slope			1	5	10	(1963), and
(c) rise			0.1	1	1.5	Shephard (1963)
Friction angle	ϕ'	degrees				
(a) peak			20	28	35	Hough (1957)
(b) residual			20	25	30	
Porosity	n	-	30	60	70	Hough (1957)
Total unit weight	γ	gm/cm^3	1.5	1.7	2.2	see Sec. 9.2
Shear strength/ pressure ratio	N	-	0.2	0.3	0.4	Skempton (1957)

FIGURE 9.1 Table of assumed values of sediment and basin parameters.

rate for the slope is clearly an underestimate if a proportion of the basin succession is slope-derived sediment redeposited by slumping or turbidity flow. The slope average rate has therefore been doubled, as has the rate for the shelf. The basin rate however needs no adjustment, being the combined rate of the turbidity flows and the continuous basin deposition.

Unit Weight

The total unit weight (γ) of a water saturated sediment is given by

$$\gamma = \gamma_{solids} - n(\gamma_{solids} - \gamma_{water})$$

where n is porosity. The average unit weight of the minerals is about 2.7 gm/cm^3, being slightly higher for more calcareous sediments and slightly lower for quartzose sediments. The estimates of γ then follow from the porosity estimates in Fig. 9.1.

9.3 ESTIMATION OF EXCESS PORE PRESSURE DUE TO SEDIMENTATION

In an accumulating sediment of high permeability pore water can flow relatively freely, and hence the pore pressures will be hydrostatic at all depths. In a sediment of low permeability the escape of pore water during consolidation is more restricted and pore pressures in excess of hydrostatic may develop, depending on the rate of sedimentation. The most useful analytical solution of this situation was provided by Gibson (1958).

Sediment accumulates on an impermeable base at a constant rate of deposition m (Fig. 9.2). At time t the deposit has a thickness h, given by h = m.t. The sediment unit weight γ and the coefficient of consolidation c_v are assumed constant with time and depth. An excess

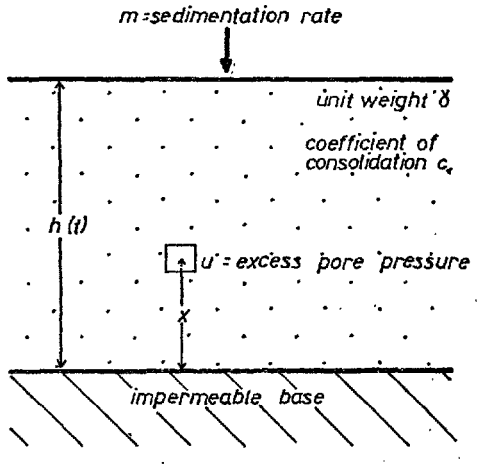


FIGURE 9.2 Definition diagram for Gibson's solution of consolidation during sedimentation.

pore pressure u is developed at height x in the sediment. This excess pore pressure may take values between 0 (i.e. hydrostatic) and $\gamma'(h - x)$, where γ' ($\simeq \gamma - 1.0$) is the 'submerged unit weight' of the sediment. The dimensionless parameter $u/\gamma'h$, denoted here by μ, is therefore a useful measure of the excess pore pressure in the sediment.

Gibson's solution for the development of the pore pressure profile with time is illustrated by plotting x/h against the factor μ, for various values of a time factor m^2t/c_v (Fig. 9.3). It is clear that the highest pore pressure factor occurs at the base of the deposit. The development of the basal pore pressure factor with increasing layer thickness is graphed in Fig. 9.4, using the maximum, average and minimum values of m and c_v given in Fig. 9.1.

If sediment with the lowest coefficient of consolidation was deposited at the highest sedimentation rate, a 100 metre thick layer would only have $\mu = 0.02$ at its base. For thinner layers, and at any other sedimentation rate or coefficient of consolidation, excess pore

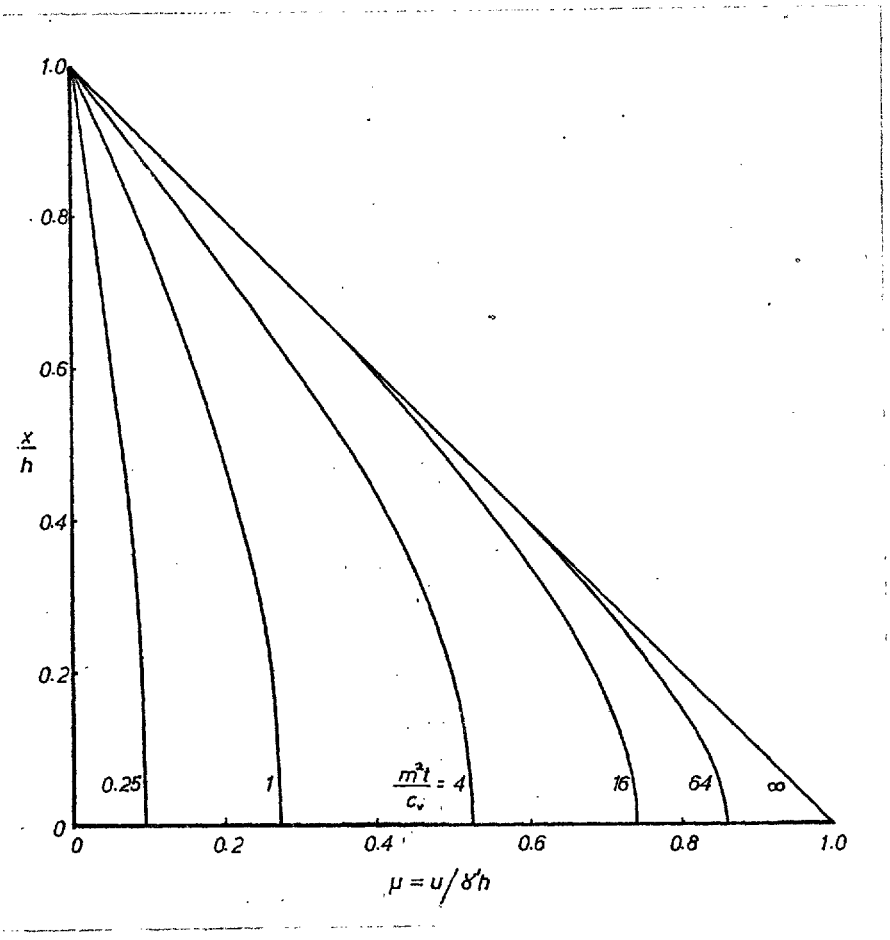


FIGURE 9.3 Graph of excess pore pressure factor μ against depth factor x/h for various values of a time factor m^2t/c_v for a consolidating layer (after Gibson 1958).

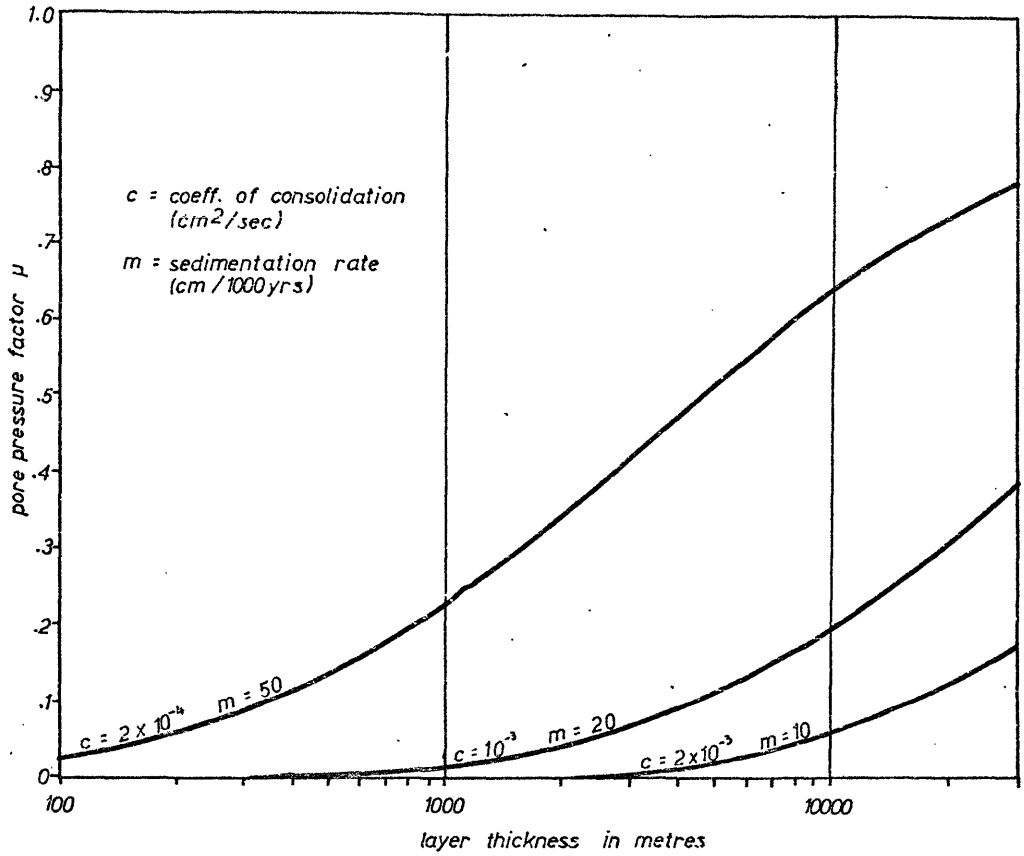


FIGURE 9.4 Graph of pore pressure factor μ at the base of a consolidating layer for various conditions of sedimentation rate and coefficient of consolidation (from data of Gibson 1958).

pressures would be virtually neglible.

Gibson's analysis does not take into account the decrease in sediment porosity and therefore permeability with depth, and hence the pore pressure values it yields may be rather low. Smith (1971) has used a model which includes these factors, and has derived a numerical solution for a shale deposited at a rate of 10 cm/1000yrs to a thickness of 320 metres. The pore pressures derived by this method are graphed in Fig. 9.5 in a form similar to Gibson's graphs. The excess pore pressure profile has a slightly different form from those derived by Gibson. However the low values predicted for this thick shale deposit indicate that excess pore pressures for a silt bed of smaller thickness would be very low indeed.

The conclusion seems justified, therefore, that virtually no excess pore pressure existed in the Ludlovian sediments before slumping occurred.

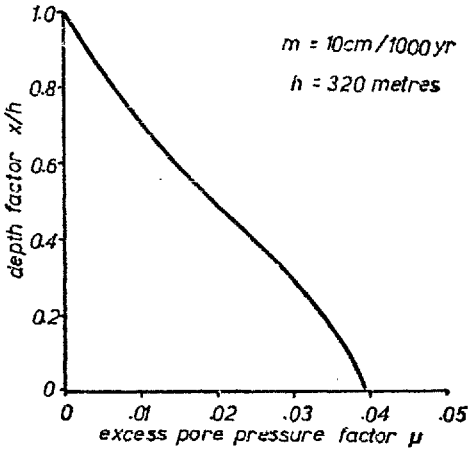


FIGURE 9.5 Graph of excess pore pressure factor against depth in a consolidating shale layer (from data of Smith 1971).

CHAPTER TEN

THE INITIATION OF SLUMPING

10.1 MODE OF SLUMP FAILURE

A mass of sediments on a slope may fail in a variety of ways (Fig. 10.1), but the evidence from the Ludlovian slumps suggests that they failed on a more or less planar surface parallel to the slope (Fig. 10.1C). In suitable exposures individual sheets can be seen to have a large horizontal extent in comparison to their (more or less uniform) thickness (e.g. Enclosure 4). There is no suggestion of any imbricate arrangement (Fig. 10.1B). The sheet mode of failure is apparently characteristic of most submarine slumping, and is also evidenced by seismic profiles of the present sea floor (Sec. 2.6).

There may, in the Ludlovian sediments, be local examples of the 'rotational' slump mode (Fig. 10.1A). The slumps in the 'submarine canyon heads' near Leintwardine (Whitaker 1962, also Sec 7.1) might be of this type, as might some other structures in the shelf facies. However sheet slumps also occur on the shelf (Sec. 7.1), and they are apparently ubiquitous in the basin facies, where the abrupt breaks of slope necessary for rotational failure were probably not present.

There is some evidence that movement may have occurred, not along a discrete plane, but on a zone of weak sediment of significant thickness. Thus the lower contacts of the Ludlovian sheets are always gradational with the underlying undisturbed sediment, and it is generally impossible to decide whether the gradational zone is primarily autochthon or allochthon. The failure criterion for such

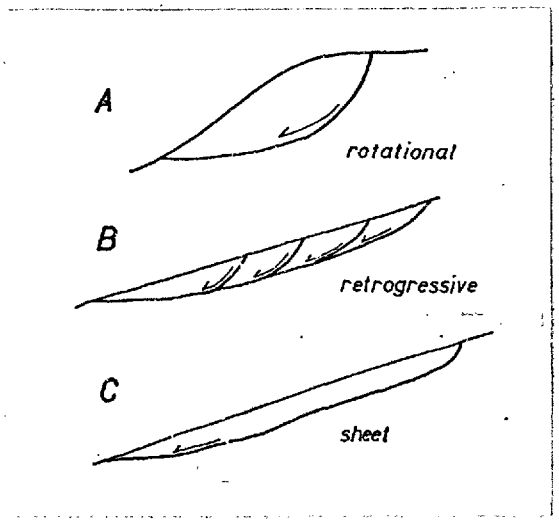


FIGURE 10.1 Three possible types of slump failure.

zones probably approximates closely to that of a discrete surface failure and will not be considered separately in this chapter. The effect on post-failure movement will be considered in Sec. 11.4.

10.2 SLOPE STABILITY

A 'sheet' slump may be approximated by a layer of constant thickness, but of infinite extent, on a constant slope. This model ignores effects at the toe, head and lateral margins of the sheet, and also assumes simultaneous failure over its whole extent. Moore (1961) and Morgenstern (1967) have previously derived failure criteria for this infinite slope model. An essentially similar derivation is given here, and its implications are developed with reference to the Ludlovian slumps.

Consider a sheet of thickness h on a slope α (Fig. 10.2). The submerged weight of a segment of horizontal length a will be $\gamma' ah/\cos\alpha$, where γ' is the submerged unit weight of the sediment. In the absence of any excess pore pressure on the failure plane, the normal and shear stresses at the base of the sheet are given by

$$\sigma' = \frac{\gamma' ah.\cos\alpha}{\cos\alpha} \cdot \frac{\cos\alpha}{a} = \gamma' h.\cos\alpha \qquad 10.1$$

$$\tau = \frac{\gamma' ah.\sin\alpha}{\cos\alpha} \cdot \frac{\cos\alpha}{a} = \gamma' h.\sin\alpha \qquad 10.2$$

If there is an excess pore pressure u at the base of the sheet the effective normal stress becomes

$$\sigma' = \gamma' h.\cos\alpha - u \qquad 10.3$$

At limiting equilibrium on the failure plane

$$\tau = c' + \gamma'.\tan\phi' \qquad 10.4$$

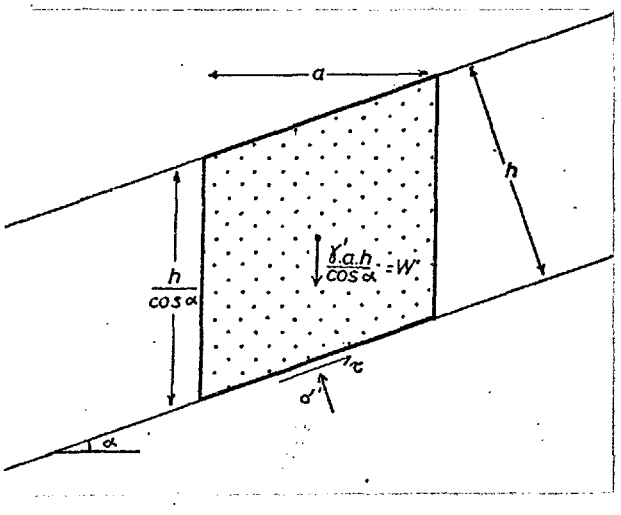


FIGURE 10.2 Definition diagram for initiation of an infinite slump sheet.

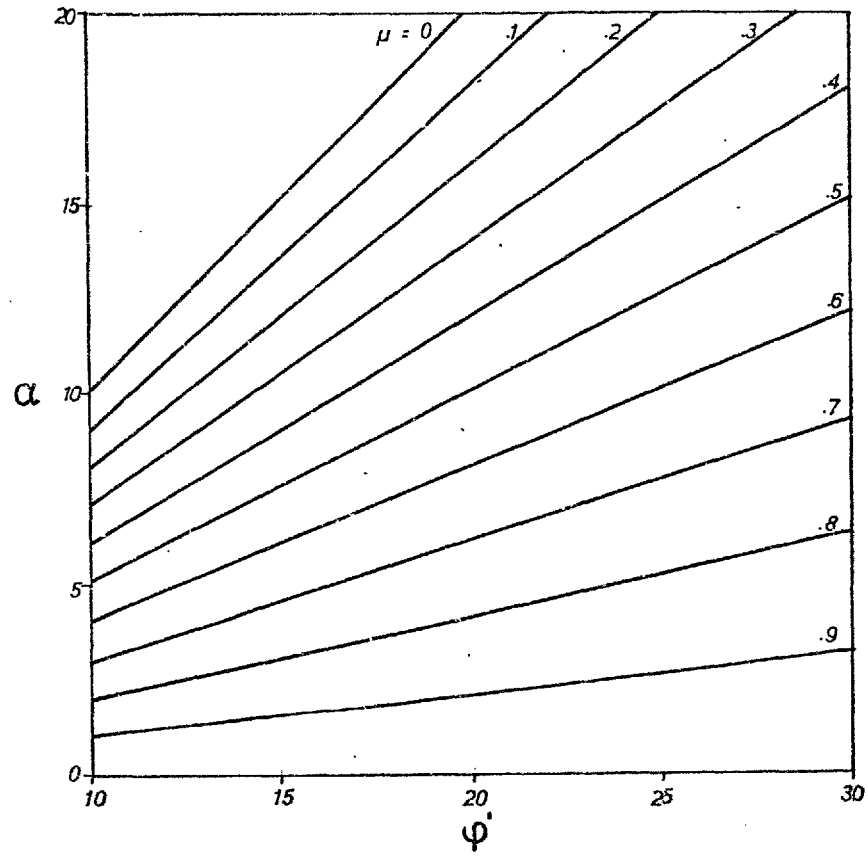


FIGURE 10.3 Plot of the excess pore pressure factor μ required for failure of a sediment of friction angle ϕ' on a slope α.

where c' and ϕ' are the cohesion and peak friction angle of the sediment. The failure criterion becomes

$$\gamma'h.\sin\alpha = c' + \gamma'h.\cos\alpha.\tan\phi' - u.\tan\phi'$$

$$\tan\alpha = \frac{c'}{\gamma'h.\cos\alpha} + \tan\phi' - \frac{u.\tan\phi'}{\gamma'h.\cos\alpha} \qquad 10.5$$

The dimensionless group $u.\cos\alpha/\gamma'h$ is analogous to the pore pressure factor μ used in Gibson's analysis of consolidation (Sec. 9.2). The failure criterion becomes

$$\tan\alpha = \frac{c'}{\gamma'h.\cos\alpha} + \left(1 - \frac{\mu}{\cos^2\alpha}\right)\tan\phi' \qquad 10.6$$

For the special case where the sediment cohesion is zero Eq. 10.6 reduces to

$$\mu = \left(1 - \frac{\tan\alpha}{\tan\phi'}\right)\cos^2\alpha \qquad 10.7$$

The graph of this relationship (Fig. 10.3) thus gives the minimum excess pore pressure factor necessary for failure. Higher values of μ will be necessary for failure of sediments having some degree of cohesion. The most favourable possible conditions for slumping in the Welsh basin are (from Fig. 9.1) $\alpha = 10^\circ$, $\phi' = 20^\circ$. At these conditions

failure would only occur at μ values higher than about 0.5. Such high values could not have been generated during sedimentation (see Sec. 9.3), suggesting that some additional factor must have been operative.

There are a restricted number of additional initiating causes of slumping. Disturbance by wave or current action is a possibility on the shelf, but would be unlikely in the slope/basin deposits. Similarly, erosional steepening of slopes could only have operated in submarine canyons or possibly on the shelf. Earthquakes are the only remaining cause of widespread slumping.

10.3 INFLUENCE OF EARTHQUAKES

The failure criterion for an infinite slump sheet during an earthquake can be estimated using the model of Morgenstern (1967) (Fig. 10.4). Excess pore pressures are neglected at this stage. The earthquake is assumed to have a horizontal acceleration component of magnitude kg. The vertical component is assumed to be neglible. There is therefore an earthquake induced horizontal body force on the block of $k.w = k.\gamma.a.h/\cos\alpha$. The resolved shear stress parallel to the base of the sheet is

$$\tau = w.\sin\alpha.\frac{\cos\alpha}{a} = kw.\cos\alpha.\frac{\cos\alpha}{a}$$

$$= \gamma' h.\sin\alpha + k\gamma h.\cos\alpha \qquad 10.8$$

Failure will occur when τ exceeds S, the total undrained shear strength of the sediment at the base of the sheet. At limiting equilibrium

$$S = \gamma' h.\sin\alpha + k\gamma h.\cos\alpha$$

$$\frac{S.\cos\alpha}{\gamma' h} = \sin\alpha.\cos\alpha + \frac{k\gamma}{\gamma'}.\cos^2\alpha \qquad 10.9$$

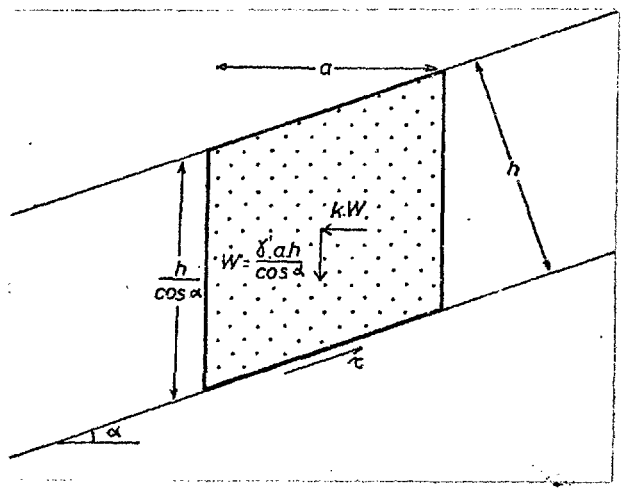


FIGURE 10.4 Definition diagram for initiation of an infinite slump sheet under the influence of earthquakes.

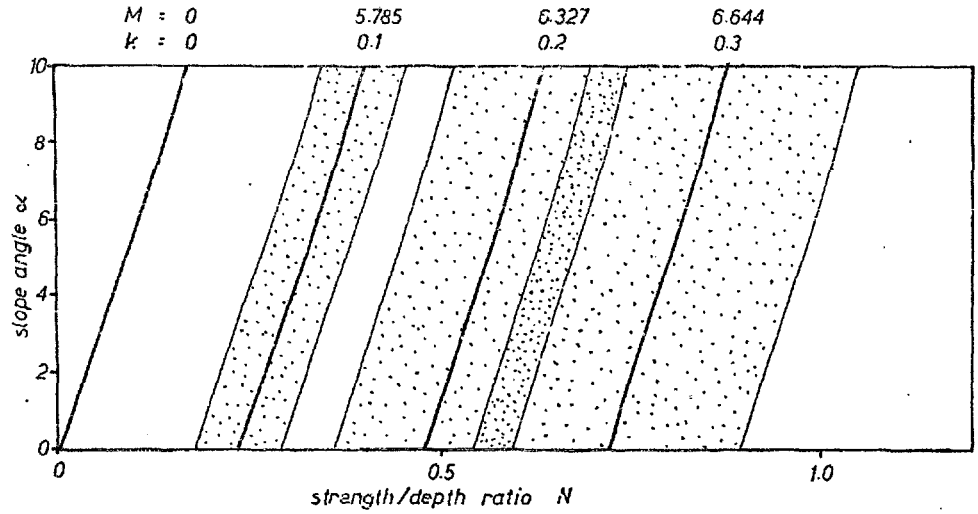


FIGURE 10.5 Plot of the failure criterion in terms of slope α and strength/depth ratio N for various earthquake magnitudes M. Bold lines are for 'average' sediment properties (see Fig. 9.1). Fine lines are for the maximum and minimum properties.

Eq. 10.9 can be simplified by replacing $S.\cos\alpha/\gamma'h$ by S/P where $P = \gamma'h/\cos\alpha$ is the vertical normal stress at the base of the sheet in the absence of earthquake loading. The ration S/P is found to be approximately constant for a given fully consolidated sediment (Skempton 1954), and in denoted by N. N is therefore a measure of the increase of undrained strength with depth. The failure criterion becomes

$$N = \sin\alpha.\cos\alpha + \frac{k\gamma}{\gamma'}.\cos^2\alpha \qquad 10.10$$

This expression is graphed in Fig. 10.5 using maximum and minimum values of γ from Fig. 9.1. The earthquake accelerations (k) have been converted to approximate magnitudes (M) using the empirical relationship

$$M = 2.2 + 1.8.\log kg \qquad 10.11$$

given by Gutenberg et al. (1942). This expression applies to the epicentral area only.

Using the values of N from Fig. 9.1 it is evident that on a 5 degree slope failure would occur at magnitudes of around 5 or 6. This suggests that, if Central Wales was a seismically active area during the Ludlow Period, earthquakes would have provided an effective trigger for slump activity.

There is a further effect of earthquake activity which may cause

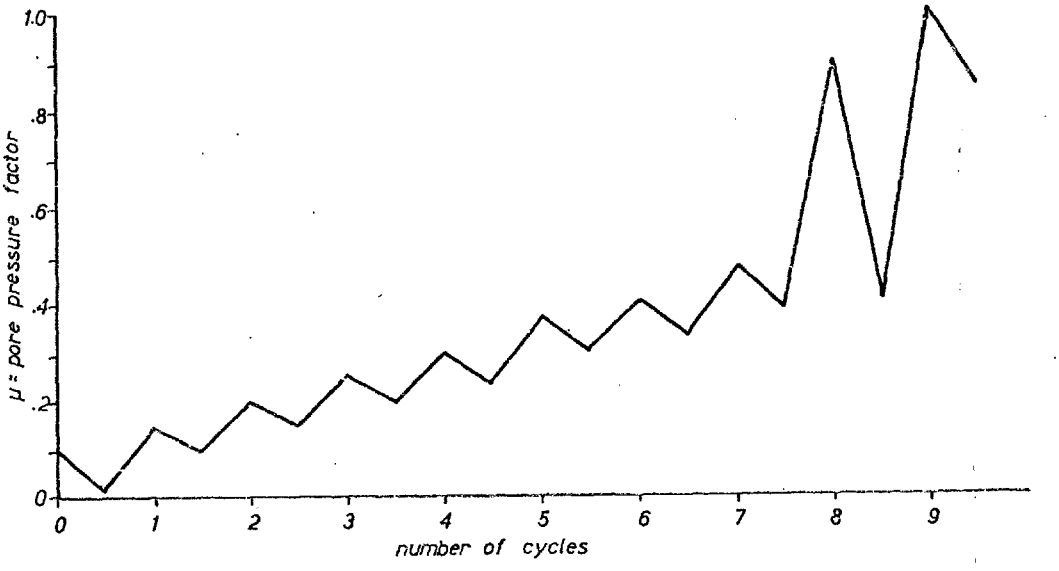


FIGURE 10.6 The change in pore pressure on cyclic loading of a loose sand. Replotted after Seed and Lee 1966.

failure, possibly at lower magnitudes than predicted in Fig. 10.5. This is the generation of excess pore pressures by cyclic loading during earthquakes, an effect which has been experimentally simulated by Seed et al. (1966). Their results are replotted in Fig. 10.6 in terms of the excess pore pressure factor μ. There was a more or less linear increase in μ, due to adjustment of the grain framework, until a critical value when the sediment failed and subsequently liquefied. These experiments used uniform fine sand which is especially susceptible to liquefaction, but the effect may well have been important in the Ludlovian silts of the Welsh basin.

10.4 FIELD EVIDENCE SUPPORTING EARTHQUAKE INITIATION

It was shown in Sec. 4.2 that thickness frequency distributions for both slumped and unslumped units at Cwm Blithus approximated to the gamma distribution

$$f(x) = \left(\frac{k}{\mu}\right)^k \cdot \frac{x^{(k-1)} \cdot e^{-kx/\mu}}{\Gamma(k)}$$

and were strongly positively skewed (Figs. 4.13,14). The significance of this observation can be deduced by considering a simple model of slump deposition in a basin (Fig. 10.7).

Slumping initiates in area A and slump sheets are transported to area B (Fig. 10.7A). In between slumping episodes normal sedimentation

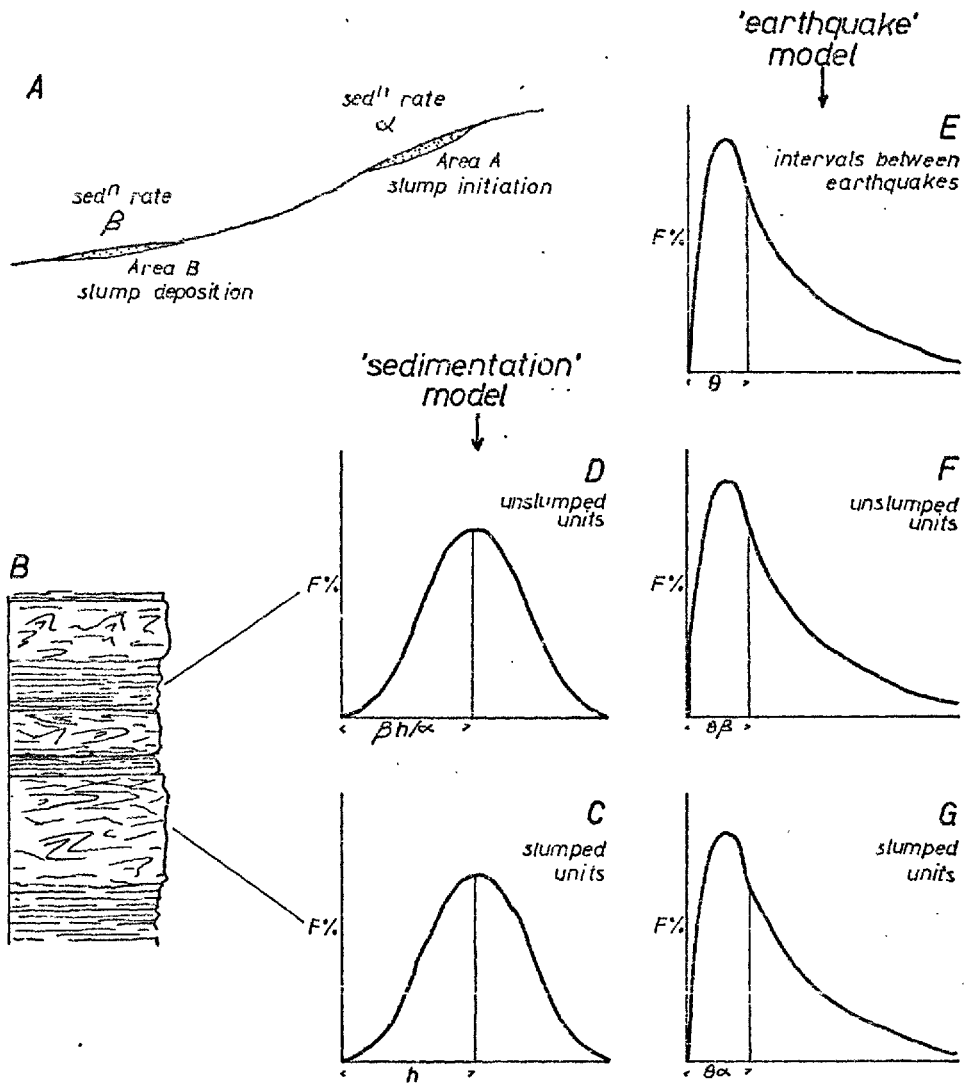


FIGURE 10.7 Two models for predicting the thickness frequency distributions of slumped and unslumped units in a sequence. See text for explanation.

continues in area B at rate β and in area A at rate α. The succession in area B thus comprises slump sheets and intervening autochthonous units (Fig. 10.7).

Assume first that slump initiation in area A is not due to earthquakes. From Eq. 10.5 it is evident that slump failure occurs after deposition of a critical sediment thickness h. This critical thickness will depend on the sediment properties and excess pore pressure gradient but, if the sedimentation rate and sediment type are constant with time, successive slump sheets will have a similar thickness. Thus, allowing for some random variations in conditions through time, and , unless significant changes in thickness occur

during sheet movement, the thickness of slump sheets in area B should show a normal distribution (Fig. 10.7C) with mean h. The mean time interval between slump episodes will be h/α during which time the thickness of normal sediments deposited in area B will be $\beta h/\alpha$. Thus the undisturbed units in area B will have thicknesses normally distributed with mean $\beta h/\alpha$ (Fig. 10.7D).

Consider now the case of earthquake initiation. Slump failure will occur whenever area A is subjected to an earthquake stronger than a critical magnitude M determined by slope angle and sediment strength/depth ratio (Fig. 10.5). Little is known concerning the recurrence intervals of large earthquakes in one area. From the evidence of low magnitude shocks, and of aftershocks of large earthquakes, it is probable that they are more or less randomly distributed in time. For truly random events the time intervals between events show an exponential distribution. If events have some degree of periodicity a gamma distribution results. Assuming, therefore, that time intervals between large shocks in area A have a gamma distribution with mean θ (Fig. 10.7E), the thicknesses of autochthonous units in area A will show a similar gamma distribution with mean $\theta\beta$ (Fig. 10.7F). The distribution of slump sheet thicknesses is more difficult to predict because for constant N (strength/depth ratio) there is no critical sheet thickness at failure (Eq. 10.10). If sediment accumulates on an essentially rigid substratum in area A, failure will probably occur at the base of the 'new' sediment layer. The slump thickness is then only determined by the time interval between earthquakes, and has a gamma distribution with mean $\theta\alpha$ (Fig. 10.7G). However it seems certain that in reality slump thickness will also be a function of earthquake magnitude, and may well be critically dependent on minor irregularities in the strength/depth gradient. No reliable estimate can therefore be made of the slump sheet thickness distribution for this model.

Comparison of the field data from Cwm Blithus (Figs. 4.13, 14) with the predicted distributions reveals a better agreement with the earthquake model than with the sedimentation model. As noted in Sec. 4.2, failure to subdivide 'composite' slump sheets in the field will have resulted in a skewness 'k' value which is, for the unslumped distribution, too large, and, for the slumped distribution, too small. Correction of any such errors would still support the earthquake model.

The model developed in this section is clearly too naive to use

quantitatively, or to provide conclusive proof of the earthquake initiation of the Welsh slumps. However, taken in conjunction with the conclusions of Secs. 10.2, 3 the field evidence provides strong support for such a hypothesis. Further support is provided by Fitch et al. (1964) who estimate a Ludlow date for the start of the Caledonian orogeny in Wales. This may well have been accompanied by abnormally strong seismic activity.

CHAPTER ELEVEN

POST-FAILURE MOVEMENT OF A SLUMP SHEET

11.1 EQUATIONS OF MOTION

The equations of motion for an infinite slump sheet after failure are derived by resolving forces parallel to the slope for one segment of the slump (Fig. 10.2) (e.g. Moore 1961, Morgenstern 1967). The downslope body force is

$$\frac{\gamma' ah.\sin\alpha}{\cos\alpha} = \gamma' ah.\tan\alpha$$

and assuming cohesion is totally destroyed along the failure plane the frictional force on the base is

$$\left(\frac{\gamma' ah.\cos\alpha}{\cos\alpha} - \frac{ua}{\cos\alpha}\right)\tan\phi'$$

or

$$\left(\gamma' h - \frac{u}{\cos\alpha}\right)a.\tan\phi'$$

The net downslope force is therefore

$$P = \gamma' ah\ (\tan\alpha - \tan\phi') + \frac{ua.\tan\phi'}{\cos\alpha} \qquad 11.1$$

Since the total mass of this segment of the sheets is $\gamma ah/g.\cos\alpha$, the acceleration (f) of the slump is given by

$$f = P.\frac{g.\cos\alpha}{\gamma ah}$$

$$f = \frac{\gamma'}{\gamma}.g.\cos\alpha\left(\tan\alpha - \tan\phi' + \frac{u.\tan\phi'}{h\gamma'.\cos\alpha}\right) \qquad 11.2$$

or by putting $\mu = u.\cos\alpha/\gamma' h$

$$f = \frac{\gamma'}{\gamma}.g.\cos\alpha\left(\tan\alpha - \tan\phi' + \frac{\mu.\tan\phi'}{\cos^2\alpha}\right) \qquad 11.3$$

Assuming the slope and sediment properties remain constant, the acceleration will be constant and velocities and distances of travel can be obtained by the standard formulae.

The limiting condition for movement is obtained by putting f = 0 in Eq. 11.3. Then

$$\tan\phi' - \tan\alpha = \frac{\mu.\tan\phi'}{\cos^2\alpha}$$

$$\mu = \left(1 - \frac{\tan\alpha}{\tan\phi'}\right)\cos^2\alpha \qquad 11.4$$

This condition is identical to the failure criterion for a cohesionless sediment (Eq. 10.7), which is graphed in Fig. 10.3. The graph shows that, even under the most favourable conditions ($\alpha = 10°$, $\phi' = 20°$), the Welsh slumps would not have moved unless the pore pressure factor

μ was higher than 0.5. A value of 0.8 would be necessary for movement under more probable conditions ($\alpha = 5°$, $\phi' = 25°$). It is clear that, in the absence of high pore pressures developed during sedimentation, movement could only have occurred if their was a dramatic increase in pore pressure at or about the time of failure. One possible cause of such an increase is cyclic loading by earthquakes as mentioned in Sec. 10.3. A more general consideration of the problem is given in the next section.

11.2 CRITICAL POROSITY

Deformation of granular aggregates at low confining pressures takes place mainly by intergranular movement, and consequently the state of grain packing has a major effect on the stress/strain characteristics of a sediment. Tight grain packing inhibits intergranular slip, while loose packing allows the grains to move more freely. In a dry sediment, or a water saturated sediment under drained conditions, this effect causes volume changes during the initial stages of deformation. A dense sediment must increase in volume (i.e. assume a looser packing) in order to deform, while a loose sediment may decrease in volume (i.e. assume a denser packing) (Fig. 11.1). A sediment with a particular critical packing density (corresponding to a critical porosity) will deform with no bulk volume change. In water saturated sediments under undrained conditions volume changes are inhibited and instead packing changes induce changes in the pore pressure (Fig. 11.2). Again there is a critical porosity at which a sediment may deform with little overall change in pore pressure.

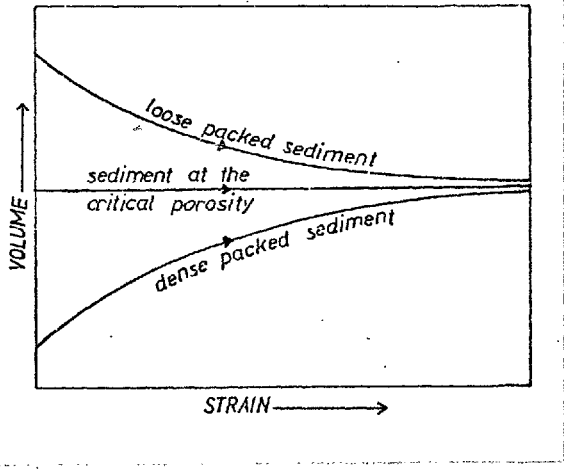


FIGURE 11.1 Volume changes in drained or dry sediments during deformation.

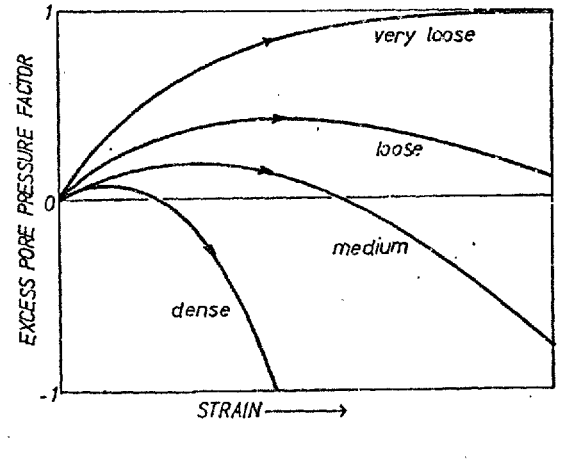


FIGURE 11.2 Pore pressure changes in undrained sediments during deformation.

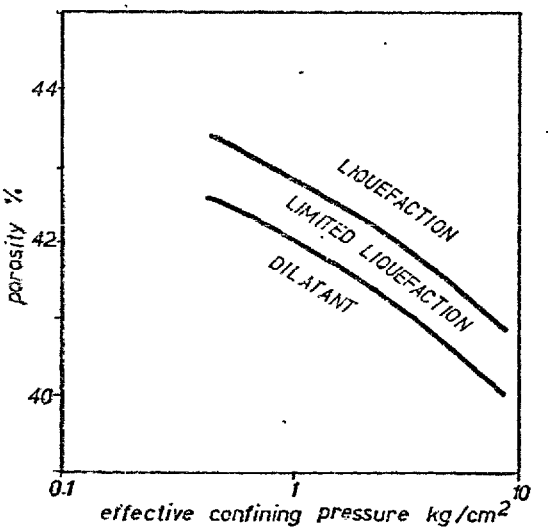


FIGURE 11.3 Fields of liquefaction and 'limited liquefaction' in terms of porosity and confining pressure for a fine sand (after Castro 1969).

The concept of critical porosity was introduced by Casagrande (1936), who recognised its importance in all sediments with a significant granular fraction. He showed that sediments with porosities higher than critical often develop pore pressures high enough to cause liquefaction of the sediment. Castro (1969) has shown that there is a significant range of porosity close to the critical value in which only limited liquefaction occurs (Fig.11.3).

The initial porosity of a slumped sediment probably has an important influence on the post-failure behaviour of a sheet. If the porosity is below critical no excess pore pressures can be generated along the failure plane in the early stages of deformation. From Fig. 10.3 it is clear that, with $\mu \simeq 0$, no downslope transport of the sheet can occur in situations similar to those in the Welsh basin. At porosities above critical, however, pore pressures can increase during deformation, possibly to the high values necessary for large scale sheet transport (Fig. 10.3). There is, therefore, a limiting porosity value at which sheet transport is possible because the necessary pore pressures can be generated. The limiting value is dependent on the slope, density and friction angle, but is always higher than the critical porosity for the sediment (Fig. 11.4).

If the porosity of a sediment is very high, the pore pressure factor can increase to unity. At this condition the effective normal stress on the grain framework reduces to zero, and the sediment

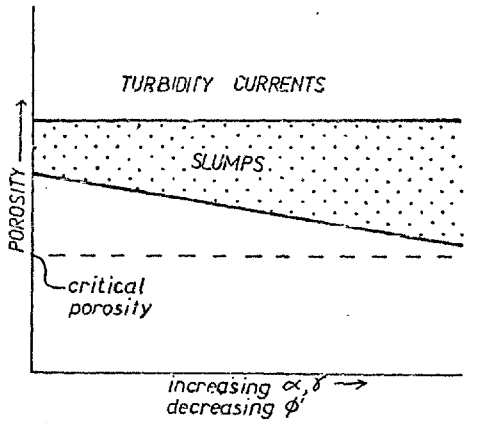


FIGURE 11.4 Diagram showing the field in which slumping is the dominant mechanism immediately after failure.

undergoes liquefaction. If failure has occurred on a discrete plane, liquefaction will initially occur here. However a liquefaction front will spread quickly to all parts of the sheet, and there will be a change from a true slump mechanism to a grainflow or turbidity flow mechanism. Thus the porosity at which liquefaction can first occur probably marks an upper limit to the slump mechanism (Fig. 11.4).

The two porosity limits discussed bound a region of sediment porosities in which slumping is likely to be the dominant mechanism shortly after failure (Fig. 11.4). There is, however, the possibility that some slump sheets may subsequently reach a velocity sufficient to transform into a turbidity current, say by sediment mixing at their upper surface. The condition necessary for the formation of a turbidity current will be discussed in Sec. 11.3.

Neither the values of the porosity limits for the Welsh sediments, nor their actual values at the time of slumping, can be accurately predicted. Castro (1969) showed that for fine sands 'limited liquefaction' occurred over a porosity range of only about 2%, but at porosity values anywhere between 40% and 60% (Fig. 11.3). The critical zone for clayey silts probably covers a larger porosity range than that for fine sands. Nevertheless small variations in porosity prior to slumping of the Welsh sediments could have critically determined the post-failure pore pressures generated. If the porosity was close to the lower limit of the critical zone the small excess pore pressures generated would have resulted in limited sliding only. A porosity only a few per cent higher might have been near the upper critical limit, and have resulted in almost total liquefaction. Consequently the value of the pore pressure factor (μ) after failure is unpredictable, and a wide range of acceleration is therefore predicted theoretically by the equation of motion (Eq. 11.3).

11.3 DEVELOPMENT OF THE RIGID SHEET MODEL

Despite the difficulty of predicting the probable pore pressures in a failed slump sheet, the equation of motion (Eq. 11.3) can still usefully be applied to the Welsh slumps. The relationship of acceleration to the pore pressure factor μ has been plotted in Fig. 11.5 for the maximum, average and minimum values of γ, α, ϕ' indicated in Fig. 9.1. The large influence of the pore pressure on the acceleration is clearly shown. Though values of acceleration up to 100 cm/sec^2 are possible values below 50 cm/sec^2 are more likely.

Of particular interest are the probable velocities attained by a sheet, and its probable distance of travel. A distance/velocity graph (Fig. 11.6) drawn for the average conditions in Fig. 9.1 ($\gamma = 1.7$, $\alpha = 5.0°$, $\phi' = 25°$) shows the high velocities which are theoretically possible with high pore pressures. However, it is generally accepted that, at sufficiently high velocities, a turbidity current will develop from a slump sheet by mixing at its upper surface. The conditions for this transformation are poorly understood, and will clearly be a function of time as well as velocity. However, in the absence of any better estimate, the transformation can be assumed to occur at approximately the velocity predicted by a Chezy-type equation for a flow of similar thickness and density (e.g. Morgenstern 1967). Velocities predicted for flows of various thickness are superimposed on Fig. 11.6. An equation of the form

$$v = \sqrt{\frac{8gh.\sin\alpha}{F} \cdot \frac{\gamma'}{\gamma_w}} \qquad 11.5$$

has been used (Allen 1970), where h is the flow thickness and F a

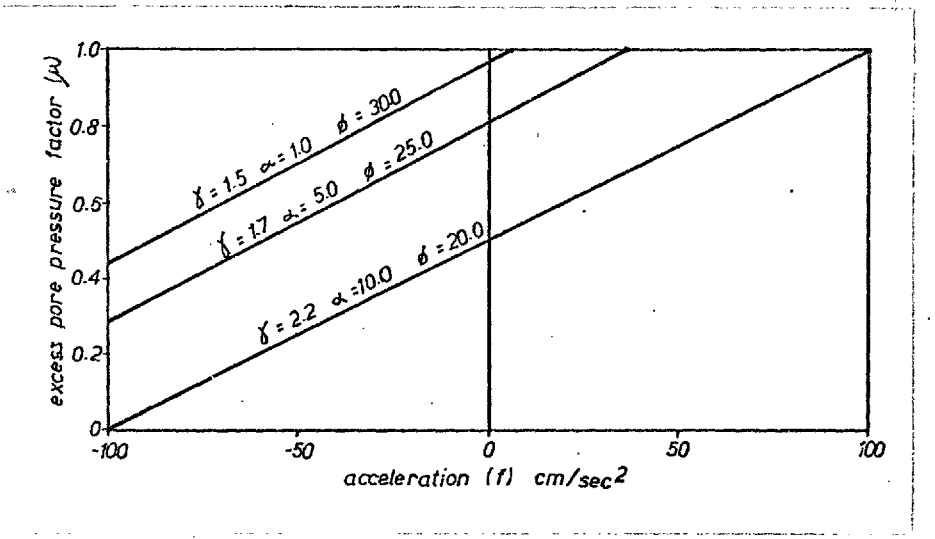


FIGURE 11.5 Plot of an acceleration of a slump sheet against excess pore pressure factor for the average and extreme parameters for the Welsh sediments.

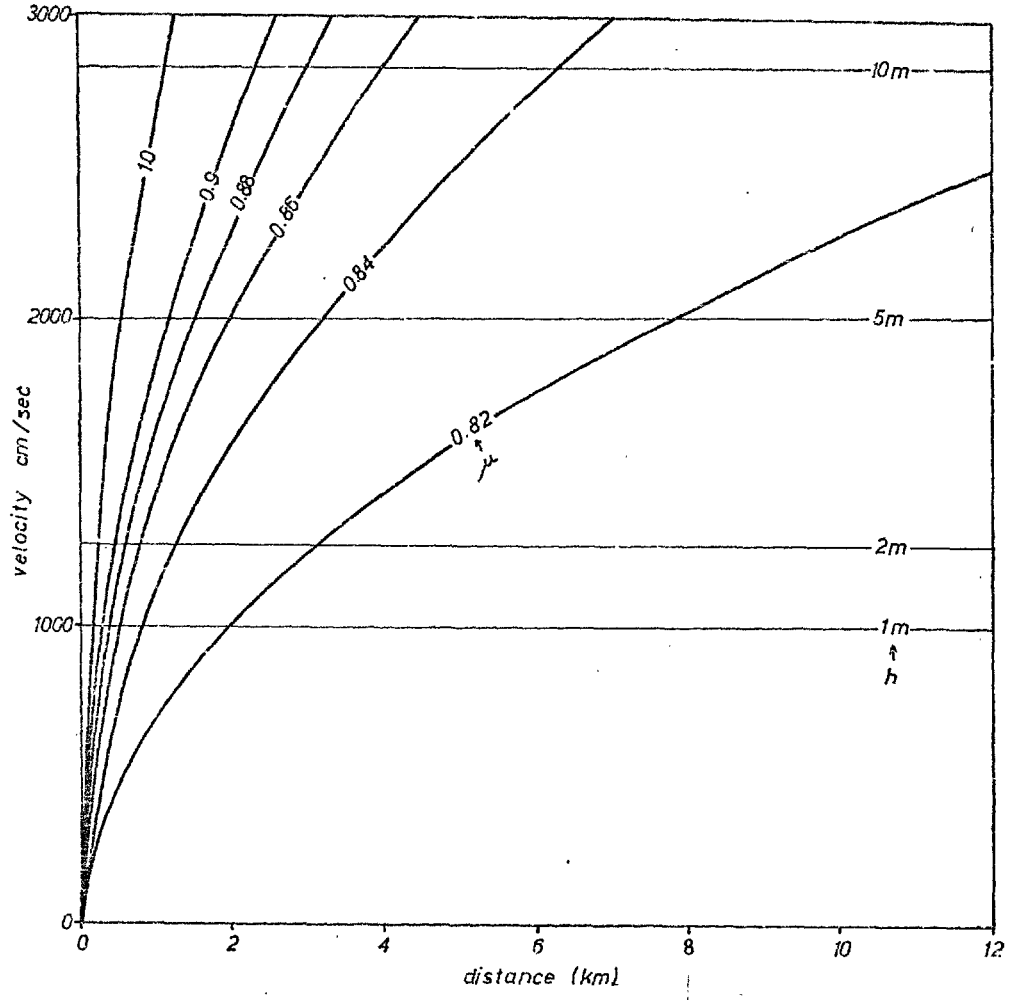


FIGURE 11.6 Distance/velocity graph for slump sheets with various excess pore pressures (μ). The Chezy equation condition is superimposed for flows of various thicknesses (h).

frictional resistance coefficient. A value of 0.06 has been used for F (see Middleton 1966).

If the velocities predicted by Eq. 11.5 are even approximately correct it is clear that most slumps with a high pore pressure will transform into turbidity currents in a relatively short distance. If pore pressures are interpreted in terms of the initial porosity of the sediment (Fig. 11.7) the range of sediments which is likely to give rise to preserved slump sheets rather than turbidites is seen to be very restricted. This may well be a partial explanation of the volumetric predominance of turbidites over slump sheets in a typical basin.

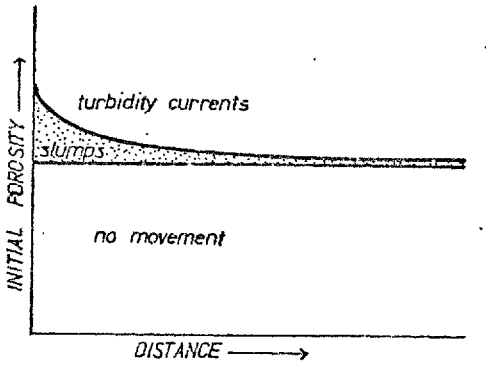


FIGURE 11.7 Porosity/distance diagram showing the field in which slumping is the dominant mechanism.

11.4 CRITICISM OF THE RIGID SHEET MODEL

The conclusions of this and the last chapter have been based on a 'rigid infinite sheet' model, which is clearly a simplification of the true mechanism. The probable complications of the natural mechanism are examined in this section to consider their effect on the results already derived and to test the usefulness of any more refined models. Two main complications can be recognised:-

(a) Real sheets have finite dimensions, their behaviour being influenced by effects at their head, toe, and lateral margins.

(b) Sheets are unlikely to be strictly rigid, but will show some degree of viscous behaviour.

The marginal effects will clearly be most important where the length of margins is high compared to the area of the sheet; that is for small sheets or those with an irregular or elongate shape. A schematic section through a sheet (Fig. 11.8) would show a rapid fall off in basal pore pressure towards the margins. At failure the

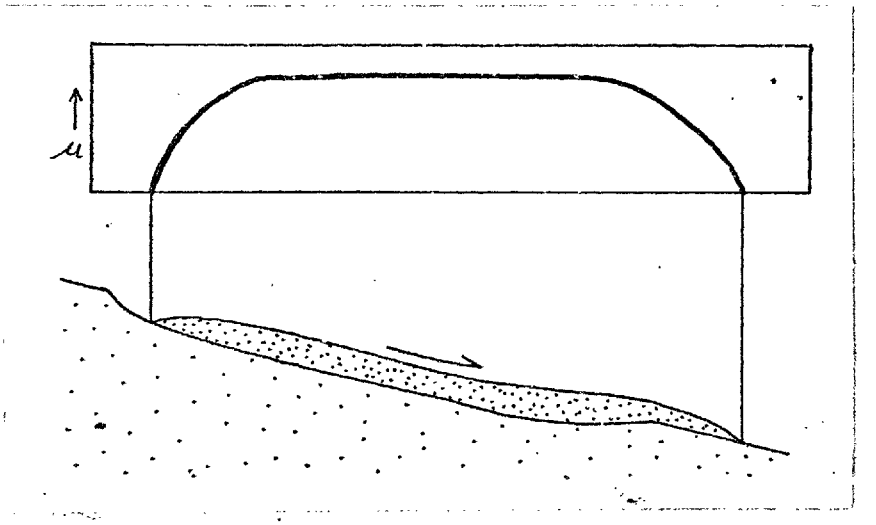


FIGURE 11.8 Probable distribution of excess pore pressure along a hypothetical slump sheet soon after initiation.

resultant restraining effect of the margins is probably neglible for large sheets. However post-failure acceleration of the sheet may well be considerably reduced below that predicted in Sec. 11.3. Of critical importance will be the behaviour of the slump at its toe. If the zone of low pore pressure at the toe is short the toe may be pushed ahead of the advancing slump (Fig. 11.9A). Sediment probably disperses both in suspension and along the slide plane, and the low pore pressure zone will 'eat back' into the sheet. If however the low pore pressure zone is initially long, or becomes so during sliding, the sheet may thrust over the toe (Fig. 11.9B). This behaviour is clearly seen in seismic profiles of a recent slump figured by Lewis (1971) (see Fig. 2.22). Thrusting at the toe will severely reduce the possible distances of travel of slump sheets.

Morgenstern (1967) has derived velocities for a visco-frictional model of a slump sheet, and found that maximum velocities in the sheet were similar to those in the rigid sheet model, especially in the early stages of transport. It is probable, therefore, that the viscous effects have less influence on the bulk transport of a slump sheet than do effects at the sheet margins. Viscous effects are clearly important in determining the internal deformation of sheets.

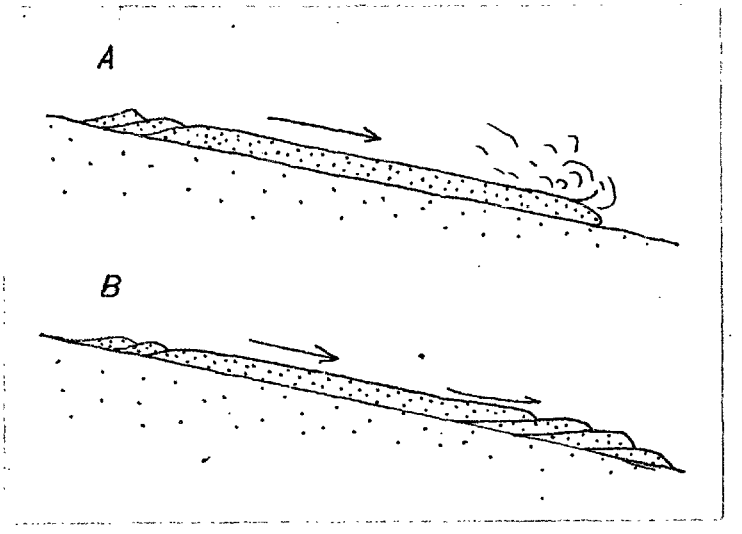


FIGURE 11.9 Two possible effects at the toe of a moving slump sheet (see text).

CHAPTER TWELVE

THE FINAL POSITION OF THE SHEETS

12.1 INTRODUCTION

It follows from the analysis of slump failure in Chap. 10 that, unless sediment properties vary markedly over a region, or unless earthquakes are localised in one specific area, most slumps will be initiated in the areas of greatest slope. Thus most of the Central Welsh Ludlovian slumps were probably initiated on the marginal slopes of the Montgomery Trough. Their present position, however, marks the area, not where they were initiated, but where they finally came to rest. This could have been further down the marginal slope, or at or beyond the base of the slope if any.

An important factor in predicting the final position of the sheets is the assumed slope profile across the trough. Bailey (1962,1969) assumed that the turbidites in the axial zone of the Montgomery Trough (see Fig. 3.7) mark the extent of a 'floor' to the trough which was practically horizontal in profile section, but which probably had a slight axial plunge to the north. The level floor was flanked by marginal slopes on which turbidites, presumed to be axially transported, could not be deposited. Bailey inferred that the observed interdigitation of slump sheets and turbidites was due to sheets moving out considerable distances over the floor of the trough (Bailey 1967). The following section investigates theoretically the behaviour of a slump sheet in a trough with the slope/floor profile envisaged by Bailey.

12.2 DISTANCE OF TRAVEL FOR THE SLOPE/FLOOR PROFILE MODEL

The post-failure motion of an infinite rigid slump sheet, in a trough with a constant marginal slope and a level floor can be considered in two phases; an acceleration phase on the slope and a deceleration on the floor. The equation of motion (Eq. 11.3) is valid for both situations if the slopes are constant, and can be used to predict the distance of travel on the floor. Effects at the sheet margins (Sec. 11.4) will in reality decrease the acceleration of the sheet on the slope, and increase its deceleration on the floor. The distances predicted from the 'infinite' model are therefore the maximum possible distances for real sheets.

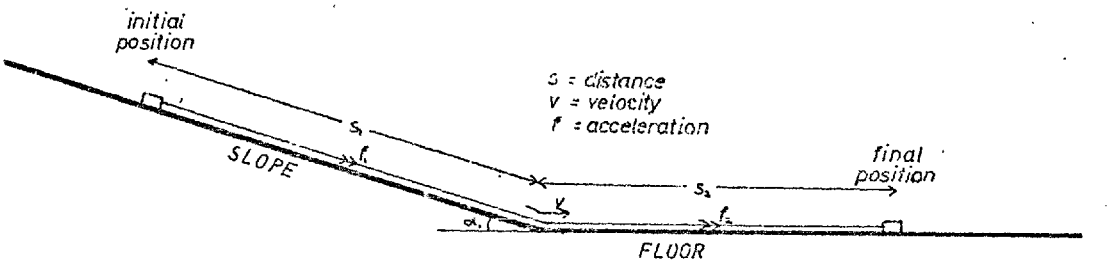


FIGURE 12.1 Definition diagram for transport of a sheet from basin slope to floor.

The problem is defined in Fig. 12.1. A sheet fails on a slope α_1, at a distance s_1 up from the base of the slope. It moves downslope with acceleration f_1 and at the base of the slope has attained a velocity v. On the floor, which has slope α_2 (taken here to be zero), it acquires acceleration f_2. This will be negative and thus the sheet will eventually come to rest at distance s_2 from the base of the slope. It is assumed that the sediment properties ϕ' and γ are constant and that the maximum pore pressure factor μ is attained immediately after failure and is constant thereafter.

The distance travelled on the floor is given by

$$s_2 = -v^2/2f_2$$

Ignoring the inevitable small change in velocity across the slope/floor junction, v is given by

$$v^2 = 2f_1 s_1$$

i.e.
$$\frac{s_2}{s_1} = \frac{-f_1}{f_2} \qquad 12.1$$

From Eq. 11.3

$$\frac{f_1}{f_2} = \frac{(\gamma'/\gamma).g.\cos\alpha_1\,(\tan\alpha_1 - \tan\phi' + \mu.\tan\phi'/\cos^2\alpha_1)}{(\gamma'/\gamma).g.\cos\alpha_2\,(\tan\alpha_2 - \tan\phi' + \mu.\tan\phi'/\cos^2\alpha_2)}$$

If $\alpha_2 = 0$ this becomes

$$\frac{f_1}{f_2} = \frac{\cos\alpha_1}{(\mu - 1)} \cdot \left(\frac{\tan\alpha_1}{\tan\phi'} + \frac{\mu}{\cos^2\alpha_1} - 1\right) \qquad 12.2$$

From Eqs. 12.1 and 12.2

$$\frac{s_2}{s_1} = \frac{\cos\alpha_1}{(1 - \mu)} \cdot \left(\frac{\tan\alpha_1}{\tan\phi'} + \frac{\mu}{\cos^2\alpha_1} - 1\right) \qquad 12.3$$

This expression will however only be valid if the velocities reached during transport never at any time exceed those at which a transition

to a turbidity flow mechanism would be expected (Sec. 11.3). Using the Chezy equation (Eq. 11.5) the critical velocities are estimated by

$$v^2_{crit} = \frac{8gh.\sin\alpha_1.\gamma'/\gamma_w}{f} \qquad 12.4$$

where γ_w is the density of the sea water, and F is a frictional resistance coefficient. The critical velocities are just reached at the base of the slope if

$$s_1 = v^2_{crit}/2f_1 \qquad 12.5$$

Eq. 12.3 is therefore only valid when the distance travelled on the slope is less than

$$s_{1\ crit} = \frac{4gh.\sin\alpha_1.\gamma'/\gamma_w}{f_1 F} \qquad 12.6$$

By substitution for f_1 using Eq. 11.3 this condition becomes

$$s_{1\ crit} = \frac{4h.\tan\alpha_1.\gamma/\gamma_w}{F(\tan\alpha_1 - \tan\phi' + \mu.\tan\phi'/\cos^2\alpha_1)} \qquad 12.7$$

By combining Eqs. 12.7 and 12.3 and simplifying, the corresponding distance travelled on the floor is given by

$$s_{2\ crit} = \frac{4h\gamma.\sin\alpha_1}{\gamma_w(1-\mu)F.\tan\phi'} \qquad 12.8$$

The variation of distance travelled on the floor (s_2) with upslope distance of slump initiation (s_1) and pore pressure factor (μ), as calculated from Eq. 12.3, is shown by the fine lines in Fig. 12.2 for the estimated average conditions in the Montgomery Trough (Fig. 9.1). Relatively large distances of travel are predicted for high values of μ. However the condition of Eq. 12.8, superimposed on Fig. 12.2 as bold lines, severely restricts the range of conditions which would not involve a transition to a turbidity flow.

The maximum width of the eastern slope of the Montgomery Trough was probably about 15 to 20 kilometres. Of slumps initiated near the top of this slope, only those with pore pressure factors marginally above those necessary for movement could possibly have reached the trough floor without first transforming into a turbidity flow. Those that did so would be brought to a halt within a few hundred metres of the base of the slope. Essentially similar behaviour would be shown by all slumps initiated at appreciable distances above the base of the slope. The only slumps which could possibly have travelled over 1km along the floor would be thick slumps with very high pore pressures, which were initiated just above the base of the slope.

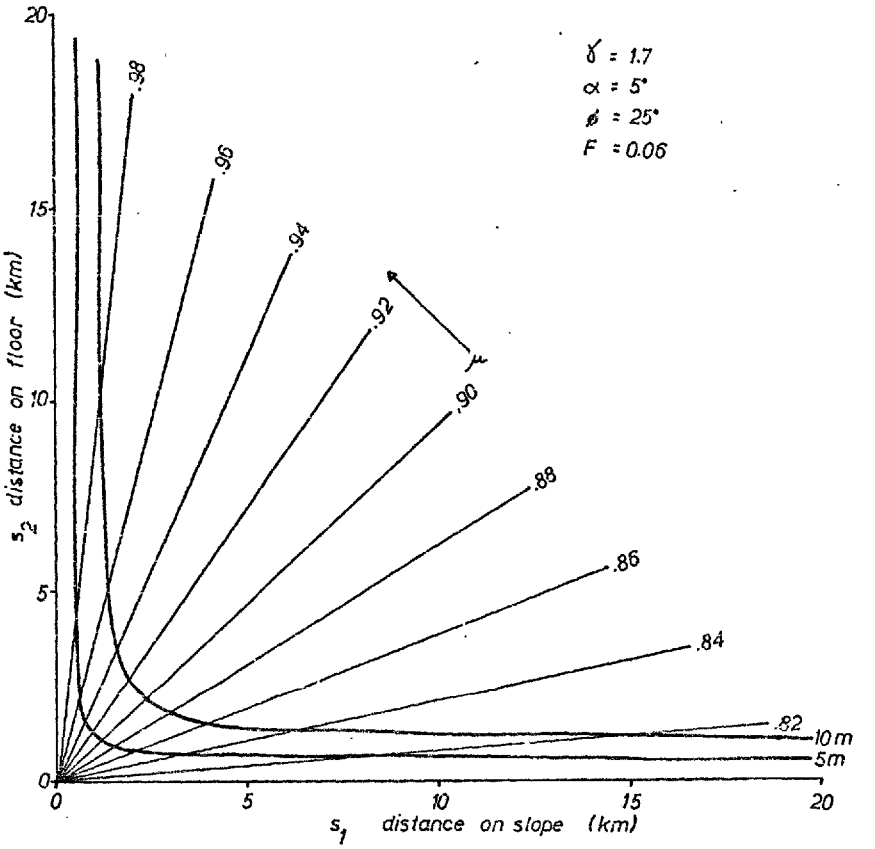


FIGURE 12.2 Plot of distance travelled on the trough floor against upslope distance of slump initiation. Bold lines are the Chezy equation condition for two flow thicknesses.

As noted in Sec. 11.4, real sheets will have a lower acceleration than predicted for the 'infinite' model because of the restraining effects at their margins. It is probable therefore that most of the lower pore pressure sheets actually come to rest on the slope, while the remainder are arrested essentially at the slope/floor junction. High pore pressure sheets are probably less restricted by toe effects and those initiated on the upper slope will all transform into turbidity currents. Some of those from the lower slope may move limited distances on to the floor, but this may also involve a partial transformation to a mudflow or similar mechanism.

12.3 TRUE PROFILE OF THE MONTGOMERY TROUGH

The discussion in the last section suggests that the lower slope and slope/floor break are the main sites of slump deposition. However, this deposition will itself modify the trough profile, with a tendency for a slump 'fan' or 'rise' to be constructed at the slope toe (Fig. 12.3). If this slope/rise/floor profile persists through

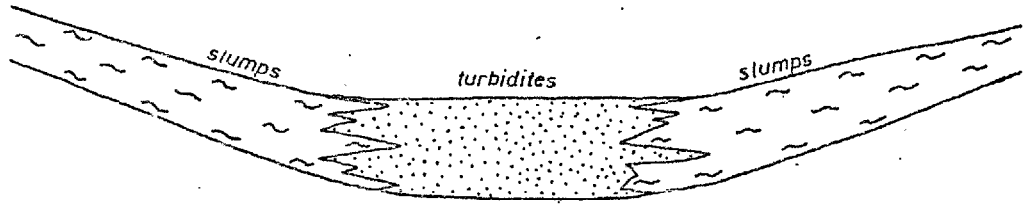


FIGURE 12.3 Profile of a hypothetical basin with interdigitation of slumps and axial turbidites.

time, most slumps will in fact be deposited on the rise rather than reaching the true floor of the trough. This has the corollary that, where slump sheets and turbidites are intercalated as in some parts of the Montgomery Trough, the axial turbidity currents must have flowed on to the rise as well as over the floor of the trough. There are two possible causes of this behaviour.

The first is if the advancing turbidity current was appreciably wider than any floor to the trough. The lateral margins of the flow would then overlap some distance on to the adjoining rise, with a concomitant increase in the flow depth in the axial zone. The width of the belt of turbidite deposition in the Montgomery Trough was generally less than 20 km. Evidence from the recent Grand Banks current (Heezen et al. 1952) suggests that a large unrestricted flow may have a width of up to 300 km on a level bottom. An individual current in the Montgomery Trough could therefore conceivably have spread over the whole width of any floor to the trough, and some distance on to the bounding rise areas.

A second possibility is that turbidity currents directed obliquely to the axis of a trough could flow some distance on to the marginal rise or slope areas before returning to the axial zone. This process must occur to some degree wherever a turbidity current is constrained to flow in a curving trough. This situation has not previously been analysed theoretically, and any exact analysis would be complex. However a rough estimate of the maximum upslope distances involved can be obtained from the model in Fig. 12.4.

A body of density ρ_1 with velocity v on a slope α moves in a fluid of density ρ_2. There is no friction between the body and either the slope or the fluid. The body is initially directed with velocity v_0 at an angle β_0 to the base of the slope. The components of

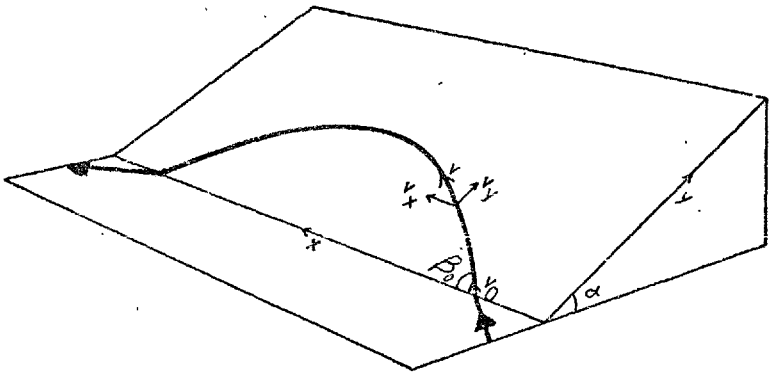


FIGURE 12.4 Trajectory of a body directed obliquely up a slope.

acceleration on the body are

$$\frac{dv_x}{dt} = 0 \qquad 12.9$$

$$\frac{dv_y}{dt} = -g.\left(\frac{\rho_1 - \rho_2}{\rho_1}\right).\sin\alpha = \frac{g.\Delta\rho.\sin\alpha}{\rho_1} \qquad 12.10$$

Using the equations of motion for constant acceleration in the x and y directions gives

$$y = v_0 \sin\beta_0 t - \frac{g\,\Delta\rho.\sin\alpha.t^2}{2\rho_1} \qquad 12.11$$

$$x = v_0 \cos\beta_0 t \qquad 12.12$$

The trajectory of the body is obtained by eliminating t from Eqs. 12.11 and 12.12

$$y = x.\tan\beta_0 - \frac{\Delta\rho}{\rho_1}.\frac{gx^2.\sin\alpha}{2v_0^2.\cos^2\beta_0} \qquad 12.13$$

The maximum upslope distance is attained by the body when dy/dx = 0, that is when

$$x = \frac{v_0^2.\sin 2\beta_0}{2g.\sin\alpha}.\frac{\rho_1}{\Delta\rho} \qquad 12.14$$

and its value is therefore

$$y_{max} = \frac{v_0^2.\sin^2\beta_0}{2g.\sin\alpha}.\frac{\rho_1}{\Delta\rho} \qquad 12.15$$

The 'range' of the body on the slope is given by y = 0, that is by

$$x_{max} = \frac{v_0^2.\sin^2\beta_0}{g.\sin\alpha}.\frac{\rho_1}{\Delta\rho} \qquad 12.16$$

The maximum upslope distances predicted by this model are plotted on Fig. 12.5. One graph is for a slope of 1 degree, representative of the rise, and the other of 5 degrees, representative of the slope.

Both graphs are plotted for $\beta_0 = 45°$. This angle gives the largest range on the slope of any angle of incidence. Greater upslope distances are attainable at higher β_0 values but are probably not applicable to the present problem. The graphs show that upslope distances are in the order of several kilometres on the rise, but are considerably reduced on the slope.

The applicability of this model to turbidity currents is uncertain. The two main complicating effects in a turbidity flow are the frictional resistance at the base and top of the flow, and the progressive decrease in mean density of the flow as sediment is deposited. On balance these

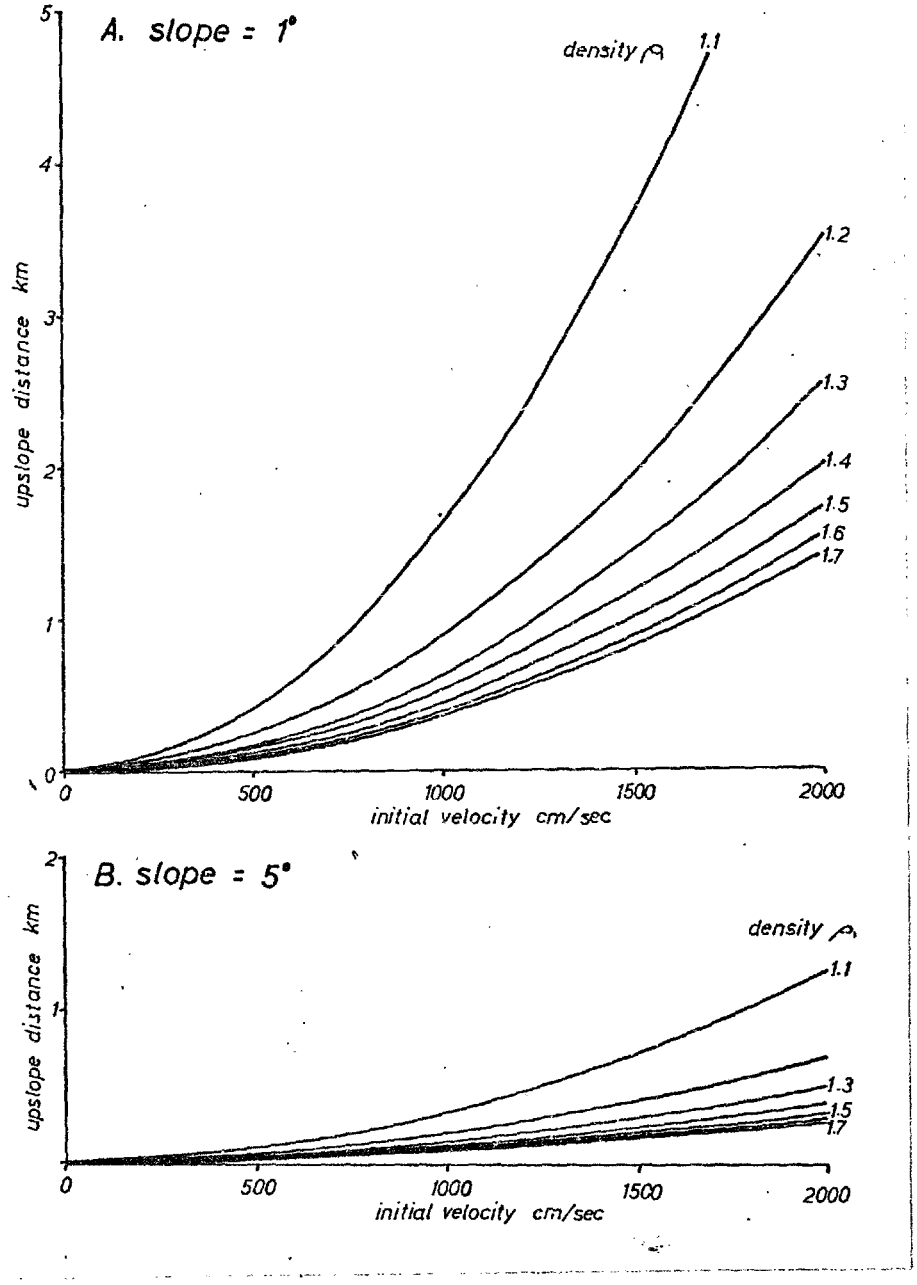


FIGURE 12.5 Upslope distance of travel of bodies of various densities on slopes of A) 1° and B) 5°.

factors will probably reduce significantly the upslope distances and range attained by a real current, below those shown in Fig. 12.5. But, even allowing for these factors, the results suggest that turbidity currents could travel significant distances up and along slopes comparable to the present continental rise, but not on those as great as the continental slope.

Returning, therefore, to the geometry of the Montgomery Trough, it seems likely that the slope/floor model is an oversimplification. The trough probably had a significant rise area beyond the toe of the marginal slope, and may have only had a narrow level floor. This revised profile is suggested by the analysis of slump deposition, and is not incompatible with turbidite deposition over the whole of the floor and rise area. The marked curvature of the trough in places (Fig. 3.5,3.9) would in fact necessitate some turbidity current flow over the rise areas in places.

CHAPTER THIRTEEN

SUMMARY OF THE THEORETICAL ANALYSIS OF SHEET MOVEMENT

13.1 SUMMARY OF RESULTS

1. It is unlikely that significant excess pore pressures existed in the Welsh Ludlovian sediments prior to slumping.
2. The sediment probably failed as a sheet with large areal extent in comparison to its thickness.
3. Due to the low pore pressure, failure could not have occurred 'spontaneously' and was probably initiated by moderately large earthquakes.
4. Earthquakes induce failure either by increasing the downslope body force on the sheet, or by increasing pore pressure by inducing packing changes in the sediment.
5. Evidence for the operation of earthquakes is provided by the near-exponential frequency distribution of interslump sediments.
6. A sheet of sediment which has failed under earthquake loading will not move an appreciable distance downslope unless there is a marked increase in pore pressure along the failure surface, at or immediately after the time of failure.
7. Marked pore pressure increases can only be induced in sediments with porosities higher than the critical porosity (Casagrande 1936). If the porosity is very high however, the sediment may liquefy and a transition to a turbidity flow or mudflow mechanism may occur. There is therefore a rather narrow porosity range in which true slumping is the dominant mechanism.
8. The value of any pore pressure rise at failure is critically dependent on the sediment properties and cannot, in general, be predicted. It is impossible therefore to predict accurately the post-failure acceleration of a slump sheet.
9. In a basin with a marginal slope and a flat 'floor' most sheets from the upper region of the slope would transform into turbidity currents before reaching the base of the slope. Any remaining sheets from the upper slope, and most sheets from the lower slope, would come to rest actually on the lower slope, or within a narrow zone beyond its base. Very few sheets could travel appreciable distances on to the floor.
10. The true profile of the Montgomery Trough probably had a very

narrow 'floor' bounded by a sloping rise, and the marginal slopes. This implies that turbidity currents were not restricted to the floor, but could flow appreciable distances on to the rise. There is some theoretical justification for this hypothesis.

APPENDICES

APPENDIX ONE

THE ACCURACY OF FIELD ORIENTATION MEASUREMENTS

A1.1 INTRODUCTION

There are five different types of measurement which are used to fix the attitude of structures in the field; strike and dip of planar structures, and trend, plunge and pitch of linear structures. When taken using a compass and clinometer they are subject to errors because of a) defects in the instrument, b) inaccurate reading of the instrument scale and c) incorrect positioning of the instrument with respect to the measured structure. Errors from a) and b) should normally be less than $\pm$ 2 degrees. Errors from c) however, may be rather large in certain situations (e.g. the measurement of strike on gently dipping surfaces).

The accuracy of each type of measurement can be predicted theoretically by assuming a model for the way in which the errors are generated. The analysis (Sec. A1.2) predicts that large errors may occur in some situations. These predictions can be checked by practical tests (Sec. A1.3).

A1.2 THEORETICAL DETERMINATION OF ACCURACY

Each of the five types of orientation measurement is considered separately in the subsequent sections. The surface of the clinometer which is vertical during use is referred to as the clinometer plane, and similarly the horizontal surface of the compass is called the compass plane. The datum line refers to the line within the compass or clinometer plane which is aligned with the measured structure. The analyses assume that a) the recorded reading on the clinometer is the angle between the datum line and the line of greatest slope in the clinometer plane, and b) the recorded reading on the compass is the angle between the datum line and the line trending north-south within the compass plane. The following sections use lower hemisphere stereographic projections to illustrate the geometry of the systems analysed. Spherical trigonometry is then used to derive the expressions for errors.

Plunge errors

A correct measure ment of the plunge of a lineation contained within a plane surface is obtained with the clinometer plane vertical

and the datum line aligned with the lineation. The errors introduced by incorrectly positioning the clinometer can be resolved into two components :-

1. Those due to non-verticality of the clinometer plane.
2. Those due to non-coincidence of the datum line and the lineation.

Component 1 :- In Fig. A1.1 point A represents a lineation with plunge β. DC is the plane perpendicular to the lineation. The clinometer datum line is aligned with the lineation, and therefore also plots at A. The correct attitude of the clinometer plane is ABC. In this case the recorded plunge (as previously defined) is given by angle BC, and is equal to β. If the compass plane is rotated about the datum line by an angle δ it takes up a position AB'C'. The recorded plunge is then given by angle B'C' (denoted by β').

By solution of the spherical triangle ACC' (noting that angle A $= \delta$ and angle C $= 90°$) we obtain

$$\tan \beta' = \frac{\tan \beta}{\cos \delta} \qquad \text{A1.1}$$

This expression is recorded graphically in Fig. A1.2 in the form of plunge error $(\beta' - \beta)$ against true plunge β for various values of deviation from vertical δ.

The maximum value of the angle δ depends on the sensitivity of the operator to non-verticality of the clinometer plane, and is probably less than 10°. The graph shows that even at this value of δ the error is clearly small enough to be neglected.

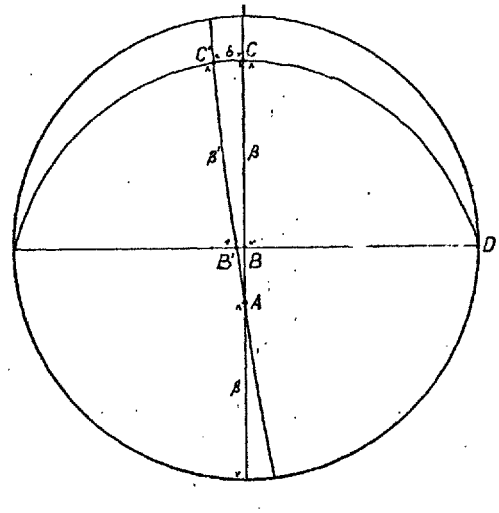


FIGURE A1.1 Stereographic projection defining parameters for calculation of plunge errors due to non-verticality of the clinometer plane.

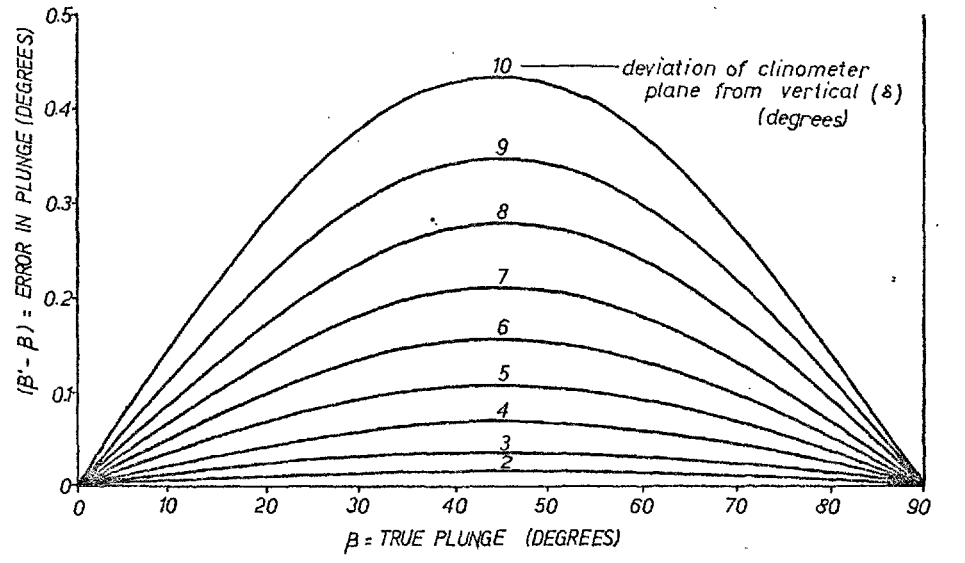


FIGURE A1.2 Graph of errors in plunge reading due to non-verticality of the clinometer plane.

Component 2 :- In Fig. A1.3 A is a lineation with plunge β, contained within a plane BA with dip α. Solution of the triangle BAC gives

$$\sin \gamma = \frac{\sin \beta}{\sin \alpha} \qquad \text{A1.2}$$

where γ is the pitch of the lineation.

The correct attitude of the clinometer plane is in plane DAC, with the datum line plunging towards A. The recorded plunge is then β. If however the datum line is positioned in the plane BA, but at an angle ϵ to the lineation, the clinometer plane takes up position DA'C', and the recorded plunge is angle A'C' (denoted by β'). Solution of triangle BA'C' gives

$$\sin \beta' = \sin \alpha . \sin(\gamma + \epsilon) \qquad \text{A1.3}$$

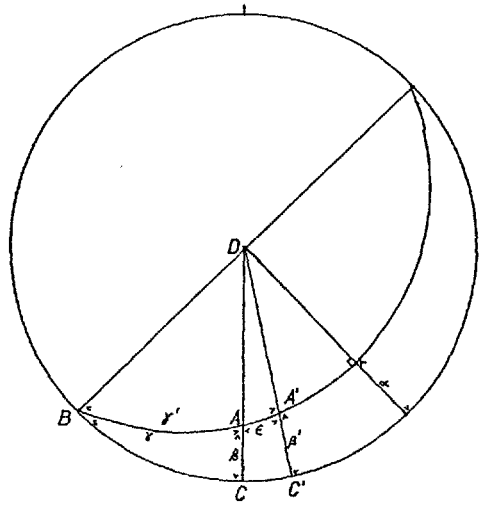


FIGURE A1.3 Projection defining parameters for calculation of plunge errors due to misalignment of clinometer.

Eliminating γ by substituting Eq. A1.2 gives

$$\sin\beta' = \sin\beta.\cos\epsilon + (\sin^2\alpha - \sin^2\beta)^{\frac{1}{2}}.\sin\epsilon \qquad \text{A1.4}$$

If the deviation ϵ is defined as positive when the pitch of the datum line is greater than that of the lineation, then a positive deviation gives a positive error in plunge (i.e. the recorded plunge is greater than the true plunge) and vice versa.

Eq. A1.4 is plotted in Fig. A1.4 in the form of plunge error as a proportion of deviation $(\beta'-\beta)/\epsilon$ against true plunge β, for various values of surface dip α. Two solid lines are plotted for each value of dip, the outer one corresponding to a negative value of ϵ, and the inner one to a positive value. The fine solid line joins points where the surface dip equals the plunge of the lineation.

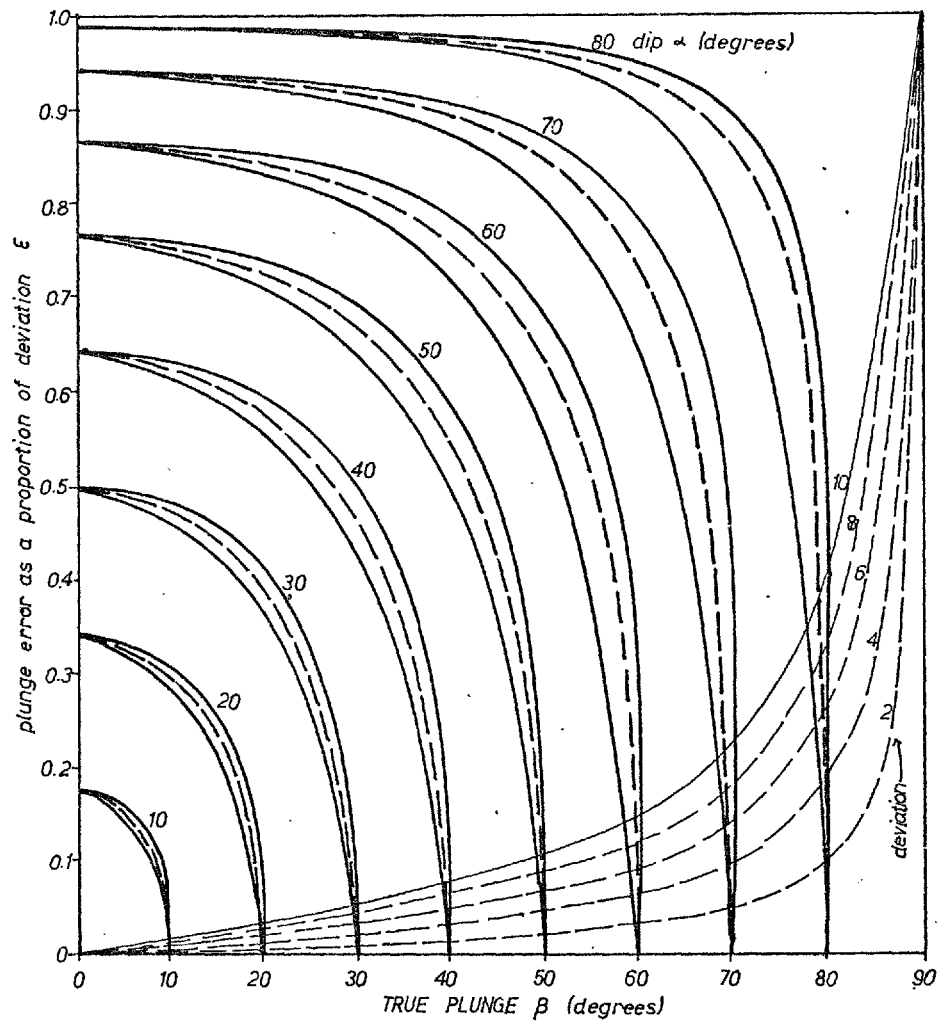


FIGURE A1.4 Graph of errors in plunge due to misalignment of the clinometer with a lineation (see text for explanation).

The solid lines in Fig. A1.4 are plotted for a value of $\epsilon = 10°$. The form of the plot is essentially similar at other ϵ values, but shows slight changes in detail. At lower values of ϵ the pairs of lines for each dip value are closer together and at $\epsilon = 0°$ both coincide with the bold dashed line shown. The $\alpha = \beta$ line alters position as shown by the fine dashed lines.

The graphs show that the largest errors in recorded plunge occur when a lineation plunges gently in a steeply dipping surface. However, the error can never be greater than ϵ - the angular error made in aligning the clinometer with the lineation. Since lineations are usually well-defined 'visible' structures in the surface (as opposed to strike and dip direction which are 'imaginary' lines) the value of ϵ will be small. Significant errors in plunge readings would only occur where the linear structure was feint.

Dip errors

The dip of a planar surface is correctly measured when the clinometer plane is vertical and the datum line coincides with the line of greatest slope in the surface. The possible errors comprise the same two components as for the measurement of plunge, of which the effect of non-verticality of the clinometer plane is similarly negligible.

The effect of wrongly positioning the datum line with respect to the line of greatest slope is shown in Fig. A1.5. A is the line of greatest slope within a surface DAE with dip α. The correct attitude of the clinometer plane is in CBA. The recorded dip is given by the angle CB and is equal to the true dip α. If the datum line is misplaced by an angle ϵ within the surface, it will take up a position

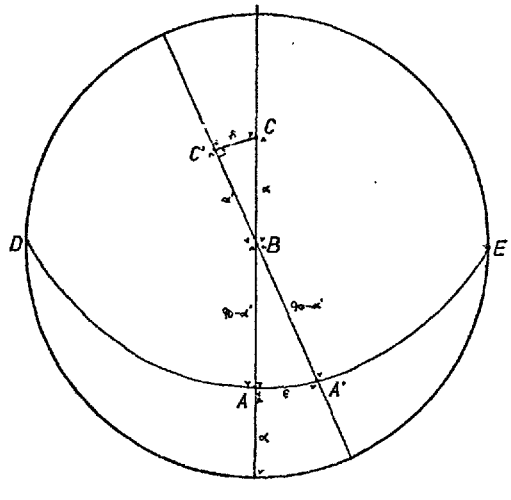


FIGURE A1.5 Projection defining parameters for calculating dip errors.

A', with the compass plane in C'BA'. The recorded dip is then given by angle C'B (denoted by α'). Solution of triangle ABA' gives

$$\sin \alpha' = \sin \alpha . \cos \epsilon \qquad \text{A1.5}$$

This result may also derived by putting $\beta = \alpha$ in Eq. A1.4, since dip measurement corresponds to the case of plunge measurement where the lineation plunge is equal to the surface dip.

Eq. A1.5 is represented by the fine lines in Fig. A1.6, where the error in recorded dip $(\alpha' - \alpha)$ is plotted against true dip α for a range of values of deviation ϵ. The line of greatest slope has no physical marking, therefore ϵ may take large values, especially for low dipping surfaces, where the line of greatest slope is difficult to determine.

Eq. A1.5 embodies the constraint that the clinometer plane is held vertically. However, another constraint during dip measurement

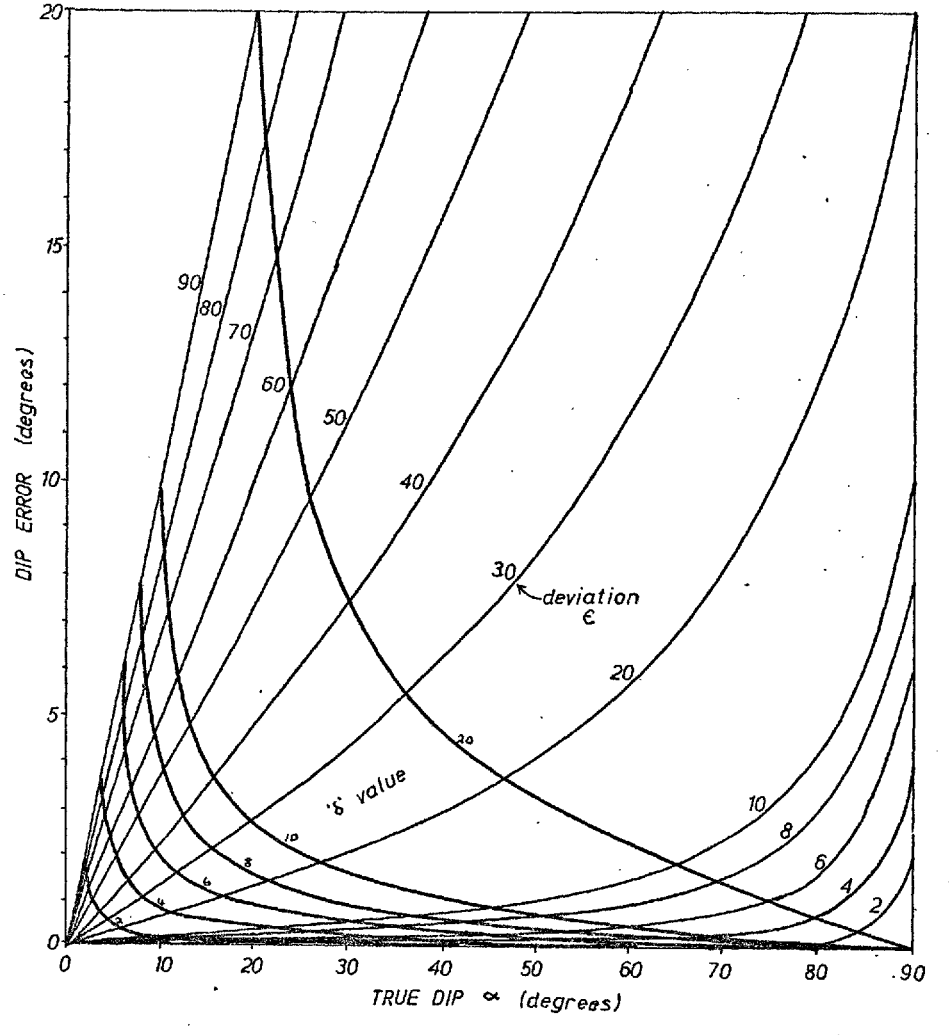


FIGURE A1.6 Graph of errors in dip (see text for explanation).

is that the clinometer plane should contain the surface normal. This constraint restricts the maximum deviation (ϵ) value at any dip value. In Fig. A1.5, CC' (denoted by δ) is the angle between the clinometer plane and the surface normal. Solution of the triangle BCC' gives

$$\cos\delta = \frac{\cos\alpha}{\cos\alpha'} \qquad \text{A1.6}$$

Eliminating α' by substituting Eq. A1.5 gives

$$\tan\delta = \tan\alpha.\sin\epsilon \qquad \text{A1.7}$$

This equation gives the maximumvalue of ϵ which can be allowed if the clinometer plane is to be within angle δ of the surface normal. Eq. A1.7 is represented by the bold lines in Fig. A1.6 for various values of δ. The operator will probably detect departures from the surface normal of more than 10°.

The graph shows that significant errors are only possible when δ is high, and then only for a restricted range of dips.

Strike errors

A correct measurement of the strike of a plane surface is obtained with the compass plane horizontal, and the datum line in contact with the surface. Errors are introduced by wrongly positioning the compass in either or both of two ways :-

1. By rotating the compass plane about the datum line so that it is non-horizontal.
2. By misplacing the datum line itself, so that it is non-horizontal.

Component 1:- The size of this error can be calculated in an analogous way to Component 1 in the measurement of plunge. Even if the compass plane deviates from the horizontal by 10°, the maximum error in strike reading is less than 1°, and is therefore negligible.

Component 2:- In Fig. A1.7 ABC is a plane with strike η and dip α.

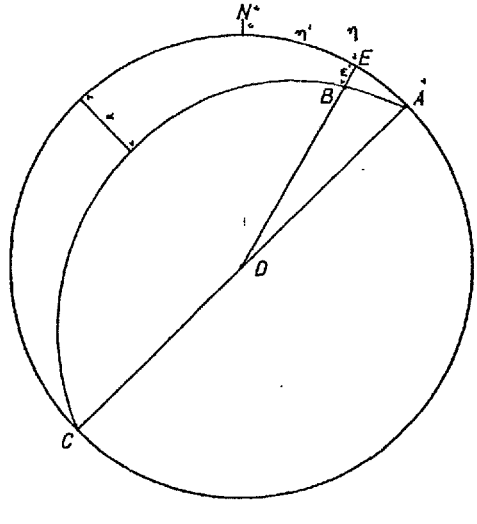


FIGURE A1.7 Projection defining parameters for calculation of strike errors.

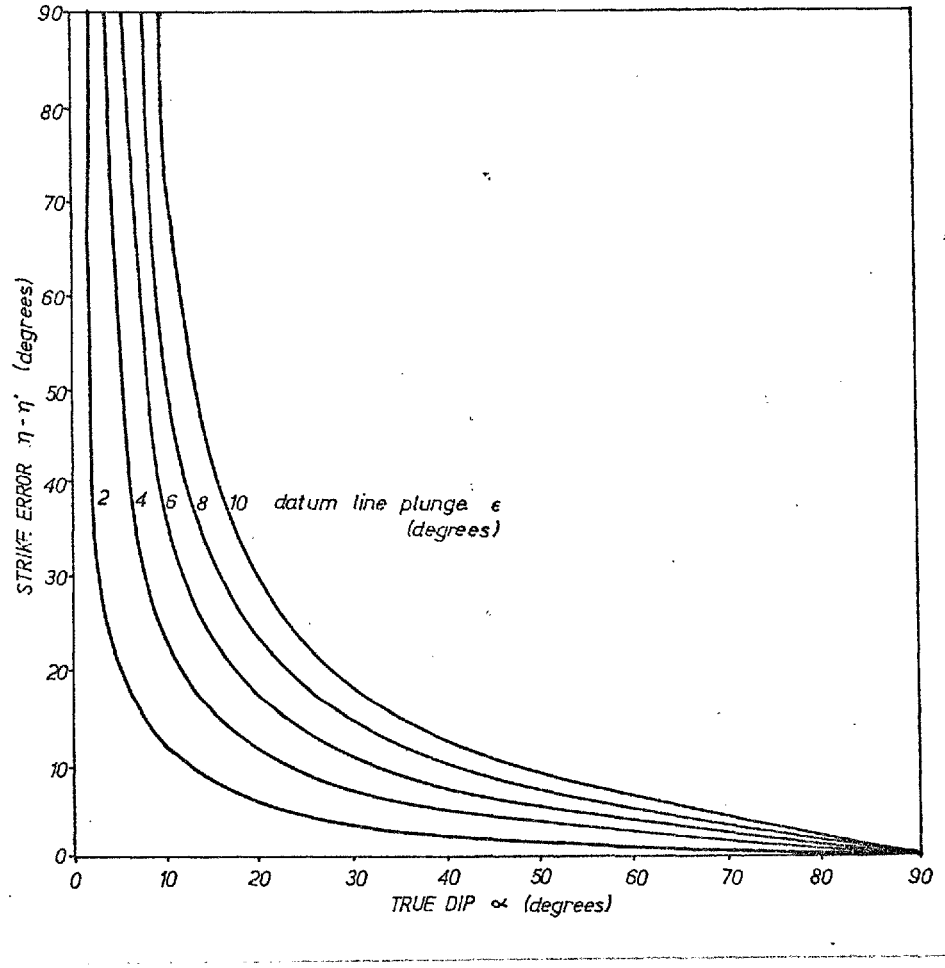


FIGURE A1.8 Graph of errors in strike caused by incorrect positioning of the compass datum line.

A is the correct position of the datum line and B is its actual position. The datum line thus has a trend η' and a plunge ϵ. The error in the recorded strike is $(\eta - \eta')$, which by solution of triangle AEB is given by

$$\sin(\eta - \eta') = \frac{\tan \epsilon}{\tan \alpha} \qquad \text{A1.8}$$

The plot of this function (Fig. A1.8) shows that possible errors are rather large on low dipping surfaces. The exact magnitude of the maximum errors depends on the value of ϵ - the maximum datum line plunge which might go uncorrected by the operator. This is investigated experimentally in Sec. A1.3.

Trend errors

The trend of a lineation contained in a plane surface is correctly measured by aligning the compass datum line with the horizontal projection of the lineation. Fig. A1.9 shows a lineation C with pitch

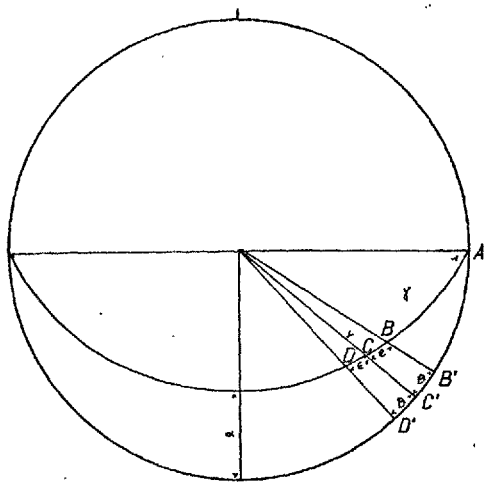


FIGURE A 1.9 Projection defining parameters for calculation of trend errors.

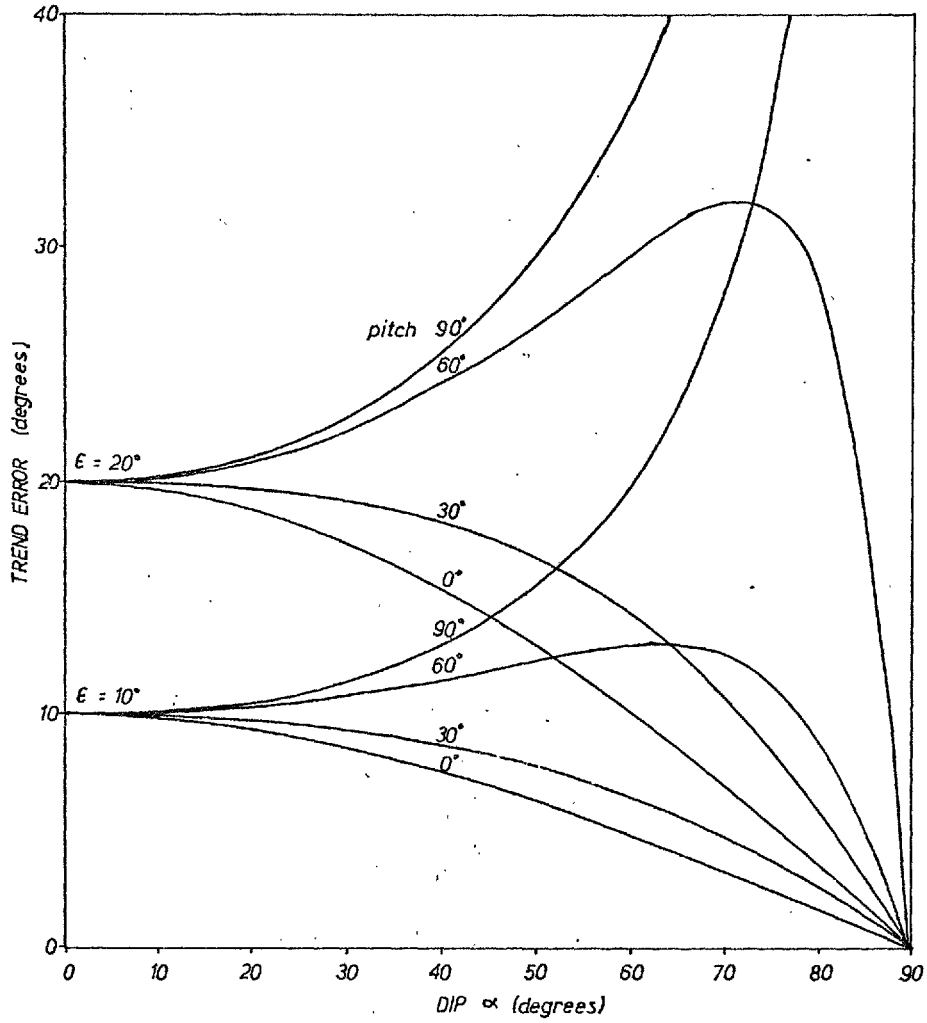


FIGURE A1.10 Graph of errors in trend for two different values of 'pitch uncertainty' in a lineation (see text).

in a plane ABCD of dip α. There is an angular uncertainty ϵ in the pitch of the lineation. The maximum error θ in the trend reading is taken as the horizontal projection of this uncertainty.

From solution of triangle ADD'

$$\tan AD' = \cos\alpha.\tan(\gamma + \epsilon) \qquad \text{Al.9}$$

and from triangle ACC'

$$\tan(AD' - \theta) = \tan\gamma.\cos\alpha$$

expanding this and substituting Eq. Al.9

$$\tan\gamma.\cos\alpha = \frac{\cos\alpha.\tan(\gamma + \epsilon) - \tan\theta}{1 + \cos\ .\tan(\ +\ ).\tan}$$

whence

$$\tan\theta = \frac{\cos\alpha(\tan(\gamma + \epsilon) - \tan\gamma)}{1 + \tan\gamma.\tan(\gamma + \epsilon).\cos^2\alpha} \qquad \text{Al.10}$$

Eq. Al.10 is plotted in Fig Al.10 for ϵ values of 10° and 20°. A similar set of curves can be plotted for any value of ϵ, depending on the 'pitch uncertainty' of the lineation.

At low surface dips, the maximum errors are similar to the 'pitch uncertainty'. At higher dips the maximum error depends markedly on the pitch of the lineation. Lineations with high pitch values may be subject to high errors at medium or high surface dips.

The pattern of errors in Fig. Al.10 has been checked experimentally in Sec. Al.3.

Pitch Errors

The pitch of a lineation in a surface is measured by the angle between the lineation and the horizontal line within the surface. The main error arises in fixing the position of the horizontal line. If the estimated 'horizontal' line plunges at angle β, an error is introduced equivalent to the pitch γ of the line. The relationship between pitch, plunge and surface dip α is given by Eq. Al.2

$$\sin\ = \frac{\sin}{\sin}$$

This function is plotted in Fig. Al.11, and shows that high errors are possible when pitch is measured on gently dipping surfaces.

Al.3 PRACTICAL TESTS OF ACCURACY

Introduction

The theoretical analysis in Sec. Al.2 predicted that high errors might occur in the measurement of strike, trend and pitch. The predicted error values are checked experimentally in this section. The errors in pitch measurement are not checked separately however, since these arise in essentially the same way as in strike measurement.

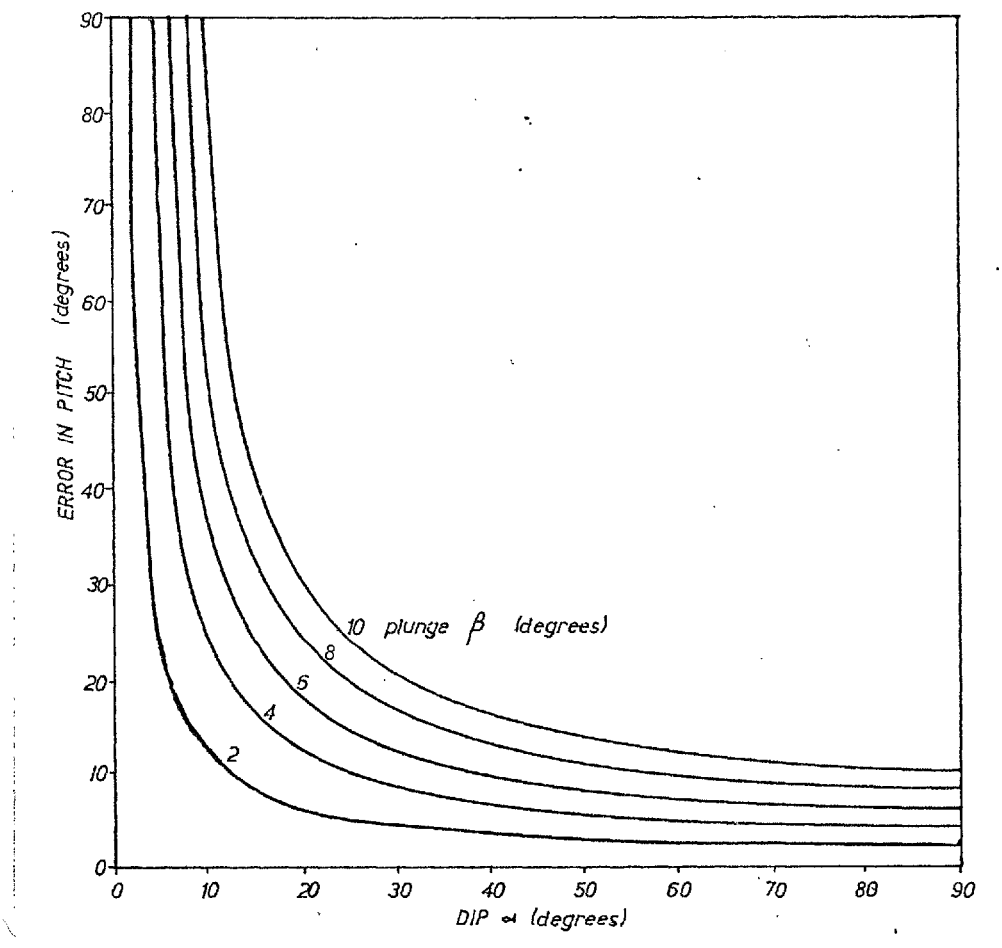


FIGURE A1.11 Graph of errors in pitch for a lineation of plunge β on a surface of dip α.

The tests of strike measurement were carried out on bedding surfaces of large loose blocks of Carboniferous sandstone in a quarry near Hathersage, Derbyshire. The trend measurement tests were done in the laboratory on a slab of lineated schist.

Strike measurement

A series of surfaces were chosen, showing a wide range of dip values. Four strike measurements were taken on each surface, using a compass without any spirit level facility. Each of the four measurements was taken from a different position with respect to the surface. The 'true' dip and strike of each surface was accurately measured with the aid of a spirit level. The error in each strike reading was found by subtracting the true strike reading for that surface. These error values are plotted in Fig. A1.12, ignoring the sign of the error.

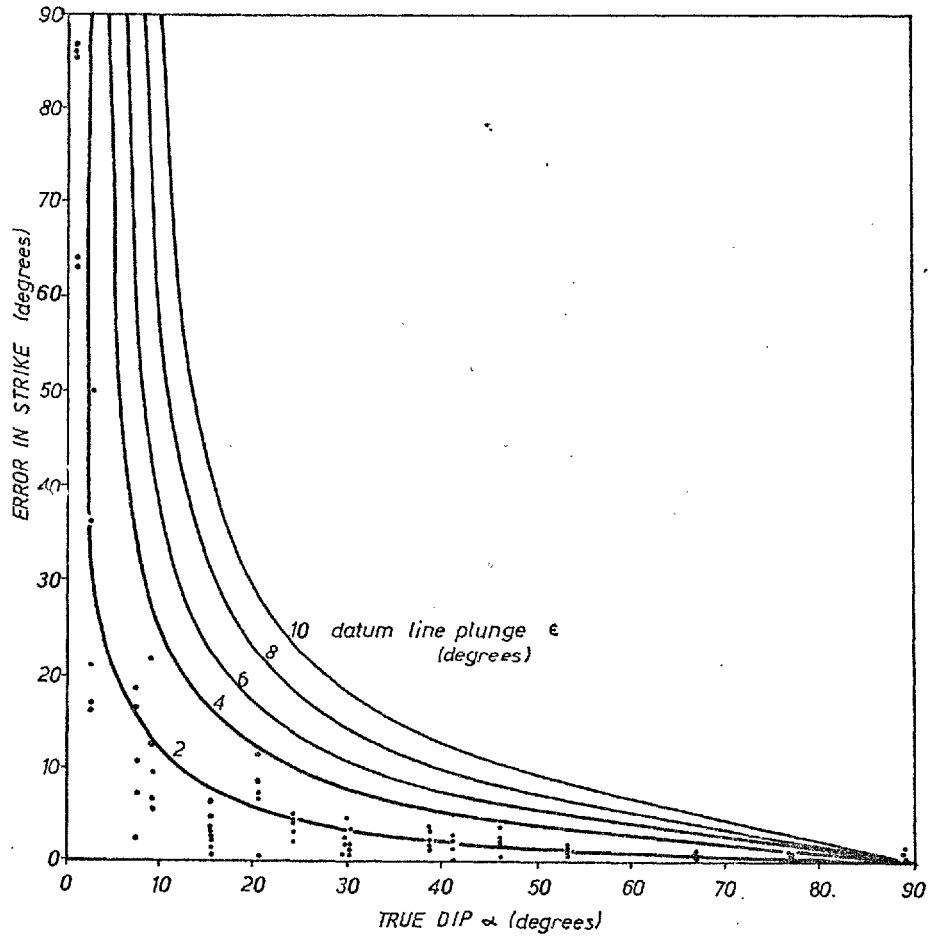


FIGURE A1.12 Plot of the field determination of the accuracy in strike measurement.

Large errors occur on surfaces of low dip. The form of the maximum errors shows a general correspondence to the theoretically determined curves, taken from Fig. A1.8. In particular the curve for 4° maximum datum line plunge approximately envelopes the observed errors. The maximum plunge of the compass datum line which went uncorrected by the operator (i.e. the ϵ value) was about 4°.

Trend measurement

A lineated surface of rock was arranged so that it could be rotated about a horizontal axis within the surface. The lineation was set at an accurately known pitch value and measurements of its trend were taken, with the surface dipping at a range of values from 0° to 90°. Six values of trend were taken from a variety of positions with respect to the surface. The true trend of the lineation was calculated from its pitch and the surface attitude, and the error in

each reading determined.

The maximum error value (ignoring sign) of the trend reading at each dip is plotted in Fig. A1.13, for lineations pitching at 25° and 80°. These errors show some correspondence to the theoretically derived curves for these pitch values, taking a pitch uncertainty of 6°. The model assumed in the theoretical analysis is probably broadly correct, though there are clearly other factors which are important

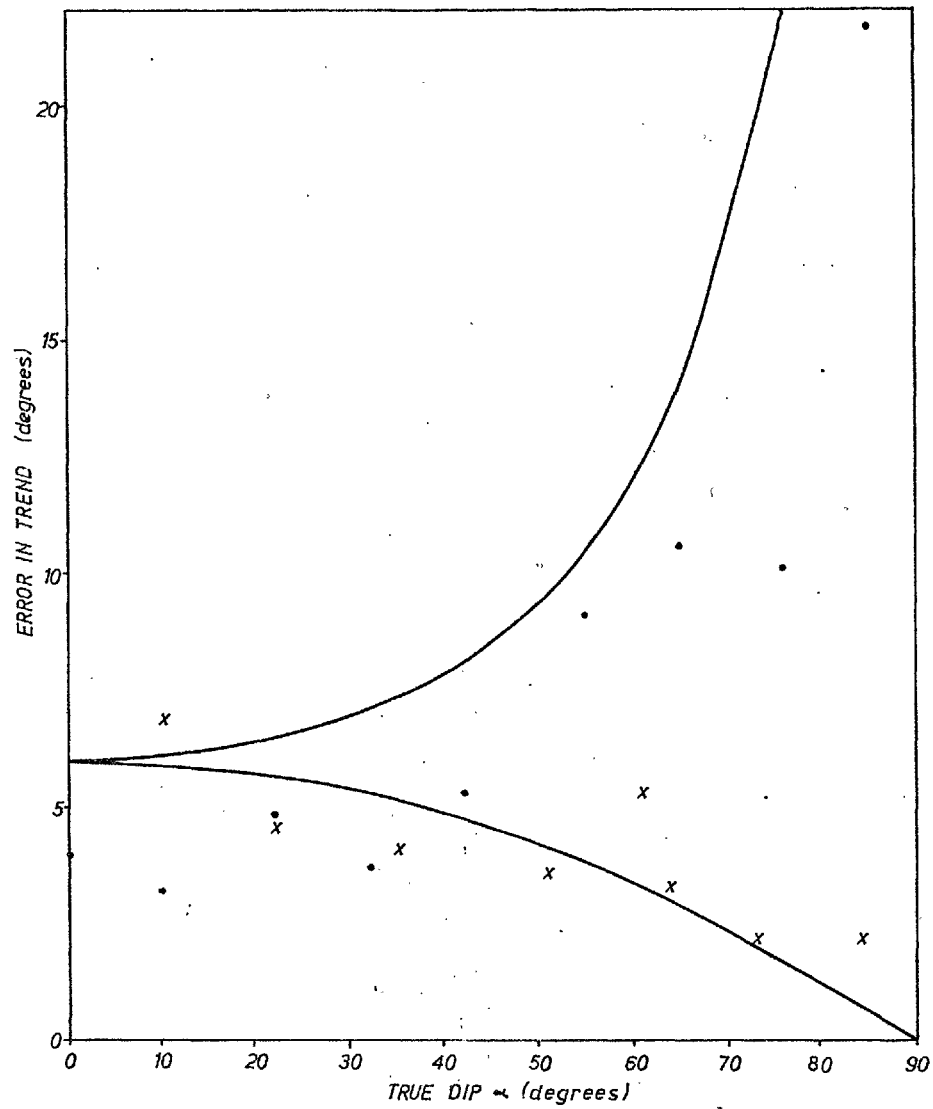


FIGURE A1.13 Plot of experimental determinations of errors in trend measurement.

A1.4 CONCLUSION

No large errors are to be expected in the measurement of plunge or dip.

Measurements of strike or pitch are subject to large errors on gently dipping surfaces. The magnitude of the errors depends on the accuracy of estimating the horizontal line within the surface. Using a compass without a levelling mechanism, this accuracy is low enough to produce significant error (greater than 5°) on any surface dipping at less than 40°. Use of a spirit level greatly reduces this error.

Trend measurements taken by sighting along a lineation may be very inaccurate, particularly for lineations pitching at high angles in surfaces of medium to high dip. These errors are not reduced by use of a compass with a levelling device. Accurate trend measurements can only be obtained in these situations by measuring the pitch of the lineation and the attitude of the containing surface.

In most studies large errors in trend and strike readings will have little effect on the interpretation of field data, because the strike of gently dipping surfaces, and the trend of steeply plunging lineations are relatively unimportant components in determining the total attitude of the structures. Only in especially accurate studies will these errors become significant.

APPENDIX TWO

GRAPHICAL REPRESENTATION OF ORIENTATION DATA

A2.1 INTRODUCTION

Three-dimensional orientation data are most commonly summarised on a stereographic projection where each line or the pole to each plane is represented by a plotted point. Large numbers of points can be plotted to give a scatter diagram, or they can be summarised by contouring. Such techniques are usually adequate for analysing, and displaying the pattern of, data within an area. Some regions, however, show a marked change in orientation pattern between separate subareas. This can be represented by producing separate plots for each subarea, but, though this may be adequate for analysing the changing pattern, the large number of stereograms involved is a cumbersome means of visually displaying the data.

A method has been devised whereby the essential features of large numbers of stereograms can be summarised on just two synoptic diagrams. One plot shows the orientation of each distribution, and the other plot summarises the distribution pattern. The method is based on the technique for statistical analysis of orientation data described in the following section.

A2.2 THE WATSON METHOD

Watson (1966) outlined a method of statistical analysis which can be used for any type of orientation data.

The data, initially in the form of azimuth and plunge values, are expressed as direction cosines l, m, n. The cross-products of the direction cosines are then summed over all the observations to form the cross-products matrix

$$\begin{bmatrix} \Sigma l^2 & \Sigma ml & \Sigma nl \\ \Sigma lm & \Sigma m^2 & \Sigma nm \\ \Sigma ln & \Sigma mn & \Sigma n^2 \end{bmatrix}$$

and the eigenvalues and eigenvectors of this matrix are determined. A routine for performing these computations is included in the computer program descibed in Appendix 3.

To illustrate the significance of the eigenvalues and eigenvectors the Watson method has been applied to a set of bedding poles abstracted from a map of the Ludlow anticline published by Holland et al. (1963) (Fig. A2.1). The eigenvector associated with the largest eigenvalue

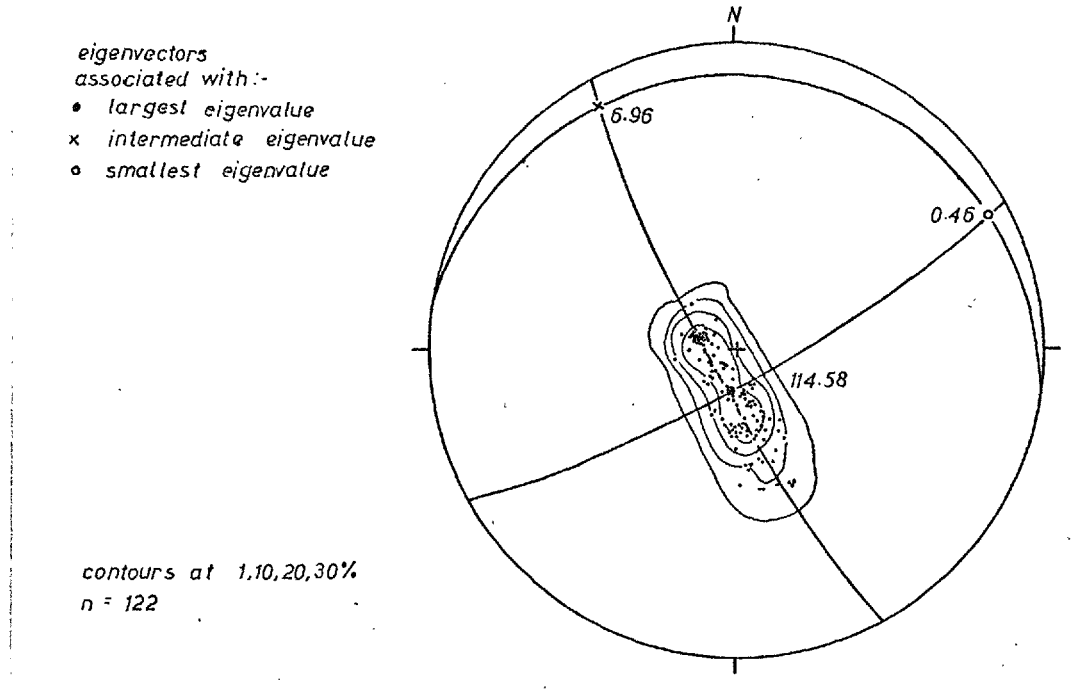


FIGURE A2.1 Bedding poles from the Ludlow Anticline, Shropshire (from data collected by Holland et al. 1963).

coincides with the vector mean of the observations, and that associated with the smallest eigenvalue coincides with the pole to the girdle of bedding poles. The eigenvectors therefore indicate the attitude of the distribution, and the eigenvalues are related in some way to the shape of the distribution.

A2.3 SYNOPTIC PLOT OF DISTRIBUTION ATTITUDE

The eigenvectors effectively indicate the principal axes of the data distribution, regardless of the distribution shape. The attitude of a distribution can therefore be unambiguously specified by plotting at least two of these principal axes on a stereographic projection. This enables large numbers of distributions to be represented on one diagram. In the hypothetical example in Fig. A2.2 the change in bedding orientation around a fold is summarised by this method.

The principal axes are fundamentally related to the mean properties of the distribution. However, they also closely reflect the modal attributes of many naturally occurring distributions. Unimodal clusters (Fig. A2.3A) and great circle girdles with or without an associated unimodal maximum (Fig. A2.3B,C) are the most common examples. The modal attributed of distributions such as double clusters (Fig. A2.3D),

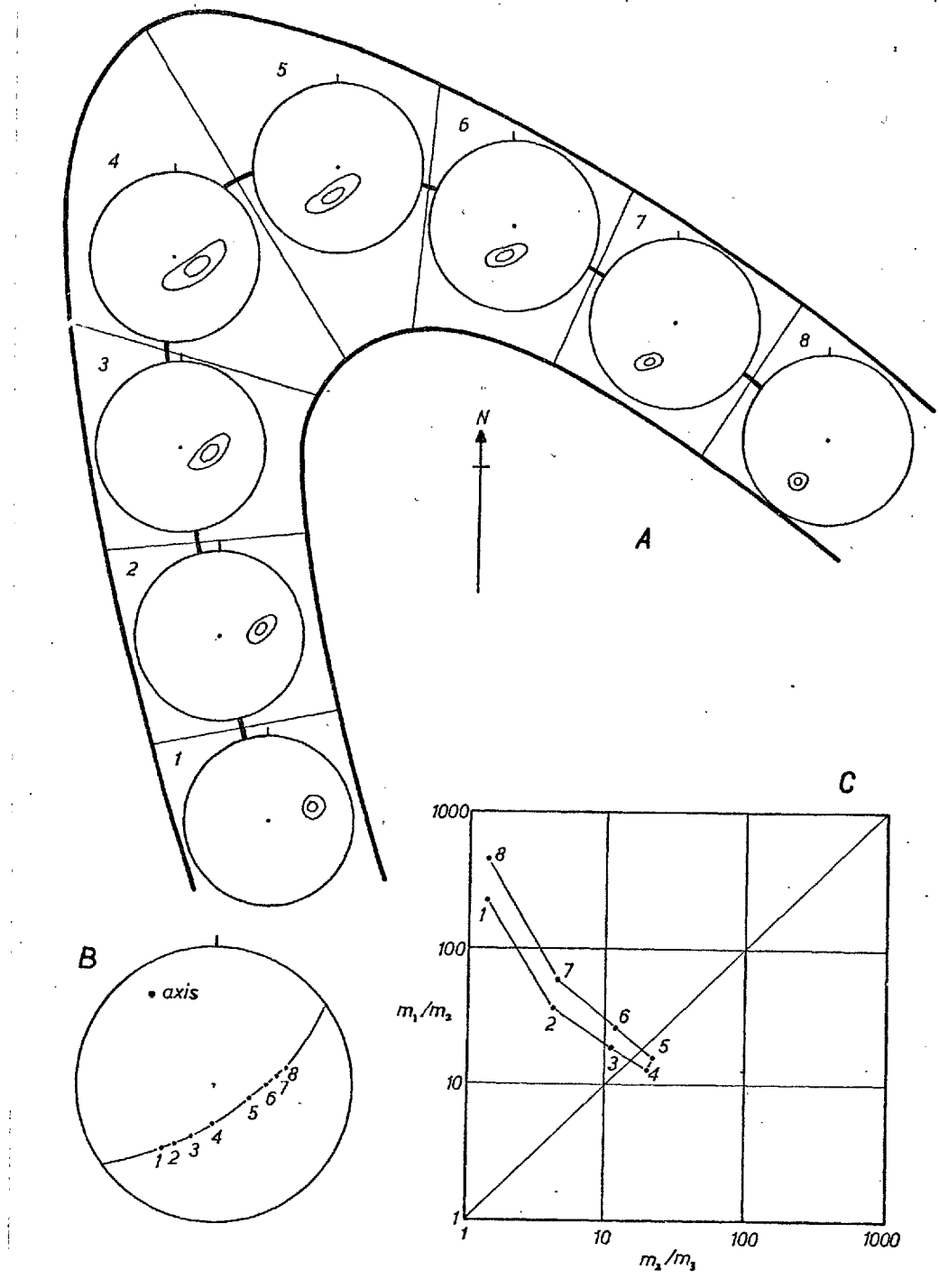


FIGURE A2.2 A) Map of a hypothetical folded area with contoured plots of poles to bedding. B) Plot of the eigenvectors corresponding to the largest eigenvalue of each distribution. C) Plot of the eigenvalue ratios in each subarea.

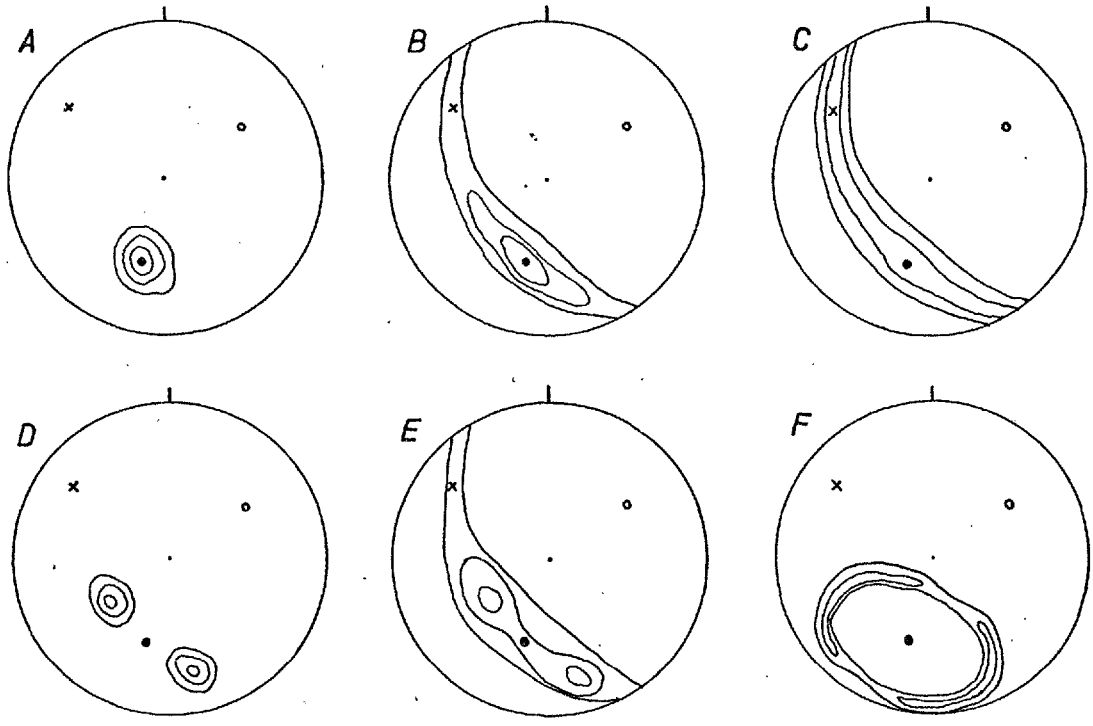


FIGURE A2.3 Hypothetical distributions with their relationship to the principal axes.

bimodal great circle girdles (Fig. A2.3E) and small circle girdles (Fig. A2.3F) are less directly related to the principal axes.

A2.4 SYNOPTIC PLOT OF DISTRIBUTION SHAPE

The eigenvalues (e_1, e_2, e_3) of the cross-products matrix have the property

$$e_1 + e_2 + e_3 = n \qquad (e_1 \geq e_2 \geq e_3) \qquad \text{A2.1}$$

where n is the number of observations summed. To compare the eigenvalues of distributions comprising different numbers of observations it is convenient to derive three parameters m_1, m_2, m_3 where

$$m_1 = e_1/n \ , \quad m_2 = e_2/n \ , \quad m_3 = e_3/n$$

and hence

$$m_1 + m_2 + m_3 = 1 \qquad (m_1 \geq m_2 \geq m_3) \qquad \text{A2.2}$$

These normalised eigenvalues are measures of the second moments of the distribution about the principal axes.

The relative sizes of m_1, m_2, m_3 are a guide to the form of the distribution. Hence, if m_1 is much greater than m_2 and m_3 the points

probably form a cluster, whereas if m_1 and m_2 are roughly equal, but both greater than m_3, a girdle is probably present. The significance of the variations in moments can better be seen by graphing the three components. The range of possible plots for representing m_1, m_2, m_3 in many ways corresponds to that for representing the shapes of strain ellipsoids (Ramsay 1967, pp. 134-9).

The most convenient method is to plot the ratio $m_1/m_2 = a$ as ordinate, and the ratio $m_2/m_3 = b$ as abscissa (Fig. A2.4). Unlike the analogous plots of Zingg (1935) for pebble shapes and of Flinn (1962) for strain ellipsoids, this two-dimensional graph involves no loss of information since, from Eq. 2.2, only two of the three components m_1, m_2, m_3 are mutually independent.

Fig. A2.4 shows the plot position of various distributions from the continuum embracing unimodal clusters and great circle girdles with or without a unimodal maximum. Most natural distributions have a and b values less than 1000. Axially symmetrical clusters plot along the line $b = 1$, and axially symmetrical great circle girdles along the line $a = 1$. The fields between the lines $b = 1$ and $a = b$, and between $a = b$ and $a = 1$, are occupied respectively by partially dispersed clusters and by great circle girdles with a partial maximum. The line $a = b$ thus marks the transition from girdles to clusters.

An alternative way of specifying the position of a distribution on the ratio plot is to use the parameters $c = m_1/m_3$ and $k = (a - 1)/(b - 1) = m_3(m_1 - m_2)/m_2(m_2 - m_3)$ (Fig. A2.4). The parameter k is a measure of the 'girdle' or 'cluster' tendency of the distribution, whereas c measures the strength of the preferred orientation. Hence girdles with axial symmetry have $k = 0$, and axially symmetrical clusters $k = \infty$. The transition from girdles to clusters occurs at $k = 1$.

Distributions with poor cluster or girdle development plot near the point (1,1) and therefore have a low value of c. At the point (1,1) would plot a distribution with perfect spherical symmetry. 'Spherical symmetry' is perhaps a misleading term when, as with many structural observations, the data have no directional sense and are thus plotted in one hemisphere only. However, a feature of the Watson method is that similar eigenvalues are derived from (a) a distribution in the lower hemisphere, (b) its transformation about a centre of symmetry into the upper hemisphere, and (c) a spherical distribution combining (a) and (b). Thus a full spherically symmetrical distribution has the same eigenvalues as 'half' the same distribution plotted in the lower hemisphere only, and occupies the same position on

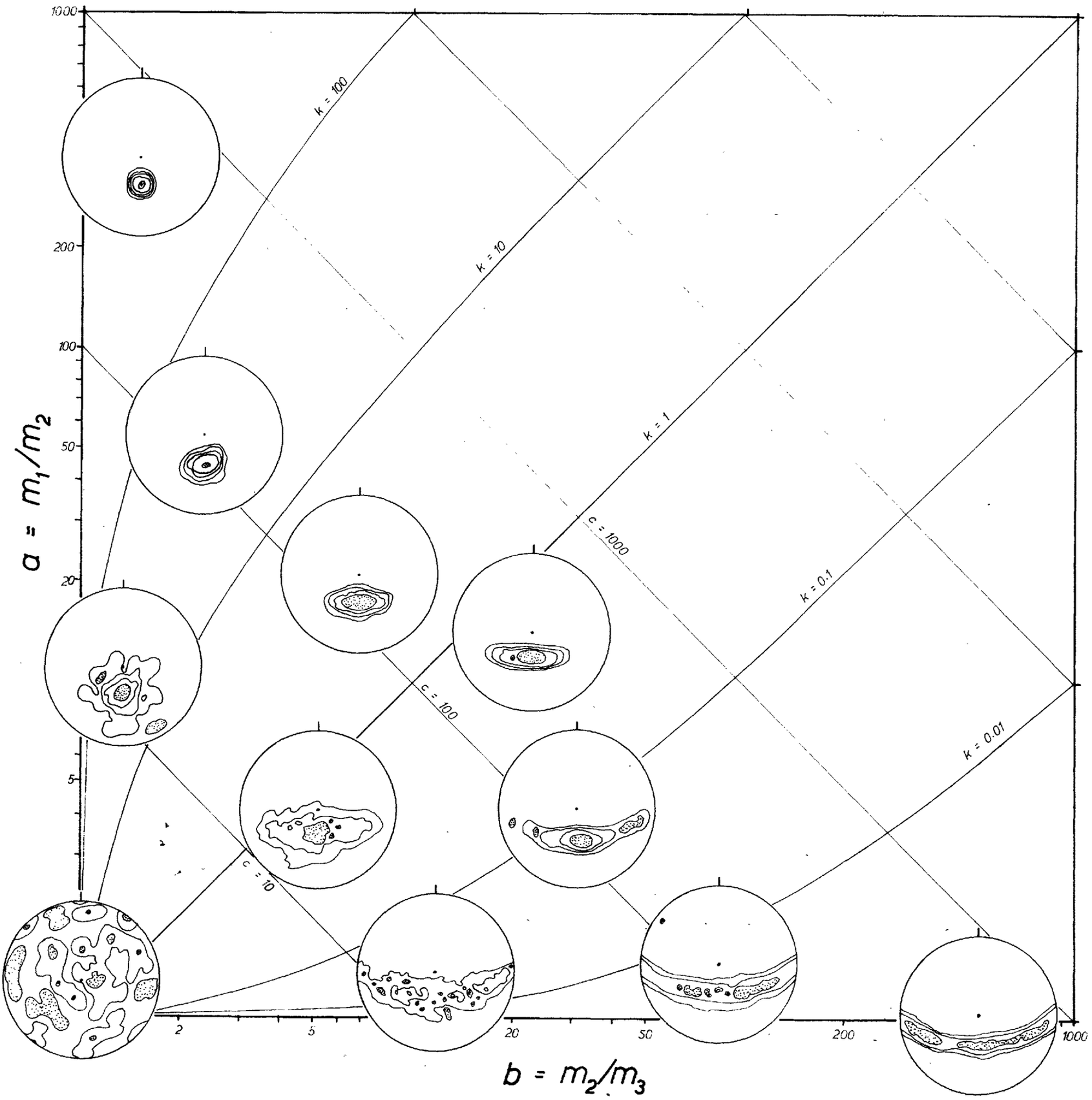


FIGURE A2.4 Graph of eigenvalue ratios showing the plot positions of a variety of distributions. The maxima in each distribution are stippled.

the ratio plot. For this reason also the plot position of a given distribution is independent of its orientation.

Several problems arise when distributions other than the unimodal or great circle types are plotted.. For instance, distributions with two clusters may plot in the 'cluster' or 'girdle' fields depending on their angular separation.

Small circle girdles present a furthe anomaly. Small circles with perfect axial symmetry fall on the a = 1 or b = 1 lines, those with half-apical angles of less than about 55° plotting as 'clusters' and the remainder as 'girdles' (Fig. A2.5). These patterns, and those without axial symmetry which plot off the graph axes, cannot be distinguished from unimodal distributions on the basis of eigenvalues.

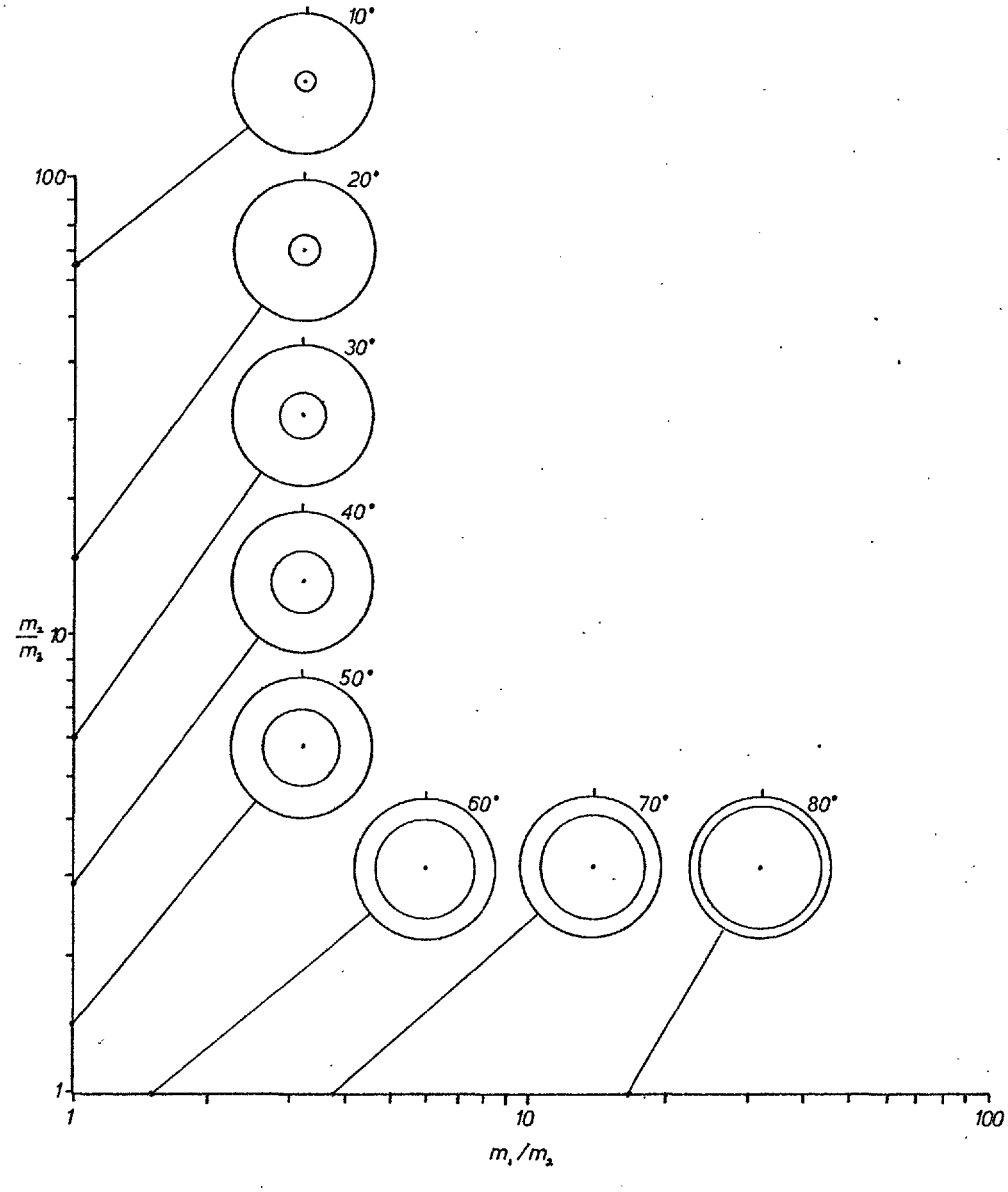


FIGURE A2.5 Position of spherically symmetrical small circle distributions on the ratio plot.

Despite the anomalies mentioned, the ratio plot provides a useful method of summarising distributions from several areas, especially where these are of a simple cluster or great circle type. An example of its use is shown in Fig. A2.2C..

APPENDIX THREE

THE DATA ANALYSIS PROGRAM - STATIS

A3.1 PROGRAM CAPABILITY

STATIS is a FORTRAN IV computer program for analysis of field orientation data. It will process one or more data sets, each comprising either planar or linear elements. Data sets may be generated by (a) punch card input, or (b) combination of data sets previously read in. The basic output for each data set is generated on the line printer and comprises (a) a list of the input data, (b) results of a statistical analysis using the method of Watson (19 6), (c) results of a statistical analysis assuming a Fisher distribution (a particular unimodal cluster, see Fisher 1953), and (d) an optional contoured equal area plot of the input data.

In addition, any set of data may be rotated in accordance with specified Euler angles. These angles may be specified on card input or calculated from the principal axes of any one data set. The possible output for each rotated data set is (a) a list of the rotated data and statistics, (b) an optional contoured plot of the rotated data, and (c) optional punch card output of the rotated data.

After analysis of all data sets, the statistics of each set may be compared using an F-test.

The statistical techniques employed in the program are all described in Koch et al. (1971), where the origin of each technique is cited. The FORTRAN routines used, however, have been newly written, except for the PLOT routine and that part of the WATSON routine which derives eigenvalues and eigenvectors. The former is a modified routine from Warner (1969) and the latter was written by M. Casey of Imperial College.

A rather more complex data analysis program, which has some features in common with STATIS, was published by Loudon (1964).

A3.2 PROGRAM DESIGN

Program operation is controlled by the main routine STATIS. Six primary subroutines (SETUP, WATSON, FISHER, PLOT, ROTATE, COMPAR) are called from STATIS to process the data and generate the output (Fig. A3.1). Three secondary subroutines (CHANGE, INVERT, TRANSF) are called from the various primary subroutines to perform standard matrix operations and other basic functions.

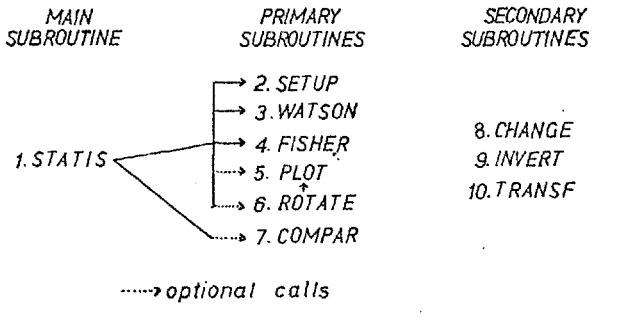


FIGURE A3.1 Diagram showing intercommunication between routines.

The purpose and logic of each routine is outlined in the program listing (Sec. A3.5).

A3.3 DATA INPUT INSTRUCTIONS

The complete data deck comprises three parts as listed below. Superscripts refer to the notes below the list. Asterisks denote columns which may be left blank where appropriate.

	COLUMN	FORMAT	VARIABLE NAME	
PART I	one initial data card			
	1-5	I5	NUM	number of data sets to be processed[1].
	6-10	I5	NCOM	number of comparisons between sets.
	11-15	F5.2	CONLEV	confidence level for statistics[2].
	*16-20	I5	IROT	set number in which Euler angles are to be computed[3].
	*21-25	I5	IEVROT	rank (1, 2, or 3) of eigenvector corresponding to the pole of the rotated projection plane[3].
PART II	one or more data sets each comprising the following			
card 1	1-80	20A4	TITLE	any alphanumeric title for this set.
card 2	1-5	I5	N	number of values in this set[1].
	6-10	I5	JA	1 if data are lines from card input, 2 if data are planes from card input, 3 if data are derived from combining earlier data sets.
	*11-15	I5	IOPT	output option[4].

	*16-20	I5	IPUN	1 if rotated data is to be punched on to card output.
	*21-30	F10.5	THETA	Euler angles for rotation of set.
	*31-40	F10.5	PSI	
	*41-50	F10.5	PHI	
card 3 onward	(a) if data are lines			
	1-5	I5	IPLU	Plunge value
	6-9	I4	IAZ	Azimuth value
	(b) if data are planes			
	1-5	I5	IST	Strike value
	6-8	I3	IDIP	Dip value
	10	A1	IDIR	either N or S indicating dip direction[5].
	(c) if data are derived			from previous sets
	1-5	I5	LB	number of each set to be combined[6].
last card	1-5	I5	-	99999
PART III	(optional) cards giving details of any comparisons of sets			
card 1	1-5	I5	JCA	numbers of sets to be compared.
	6-10	I5	JCB	
last card	1-5	I5		99999

Notes

1. The program as listed in Sec. A3.5 is dimensioned for 10 data set each of 200 elements.
2. Confidence level throughout this thesis is 0.95.
3. No entries are punched here if data are not to be rotated, or if Euler angles are given on the card input for each data set instead.
4. Output options 0 to 5 give the following combinations of output for each set :-

see overleaf

OPTION	0	1	2	3	4	5
Unrotated data list and statistics	+	+	+	+	+	+
Rotated data list			+	+	+	+
Unrotated plot		+		+		+
Rotated plot					+	+

5. An orientation 000/20E should be punched as 000/20S and 180/20E as 180/20N.
6. More than two sets may be combined.

A3.4 STORAGE AND TIME REQUIREMENTS

The program has been running on a CDC 6400 machine. It requires less than 25K storage. The running time depends mainly on the number of data points processed by the PLOT routine (Fig. A3.2).

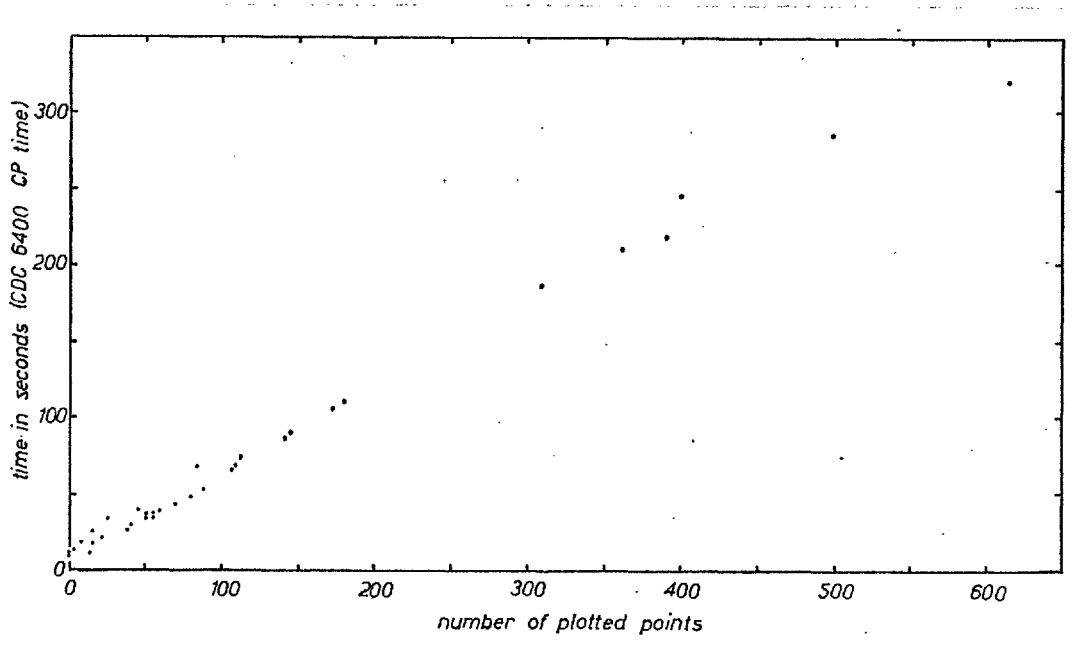


FIGURE A3.2 Running times of STATIS on the CDC 6400.

A3.5 PROGRAM LISTING

```
      PROGRAM STATIS(INPUT,OUTPUT,TAPE5=INPUT,TAPE6=OUTPUT
     1,PUNCH,
C          MAIN ROUTINE TO CONTROL PROGRAM OPERATION
      DIMENSION CTPC(57,95),DASHS(33),DC(3),DCM(3,200,10),
     1  EVCM(3,3,10),JA(25),JS(10),N(10),PREC(10),
     2  TITLE(20,10),V(3),W(3,3)
      COMMON AZ,CONLEV,CTPC,DASHS,DC,DCM,EVCM,IOPT,IROT,
     1  JA,JCA,JCB,JS,K,N,NCOM,PHI,PHIB,PL,PREC,PSI,
     2  PSIB,THETA,THETAB,TITLE,V,W,IPUN
      DATA DASH /1H-/
C          FORM LINE OF DASHES FOR TITLES
      DO 100 IA = 1,33
  100 DASHS(IA) = DASH
C          READ AND WRITE THE NUMBER OF DATA SETS ETC.
      READ (5,1000)NUM,NCOM,CONLEV,IROT,IEVROT
 1000 FORMAT (2I5,F5.2,2I5)
      WRITE (6,2000) NUM,CONLEV
 2000 FORMAT (1H1,18HTHIS RUN PROCESSES,I3, 6H DATA ,
     1  4HSETS//1H ,19HCONFIDENCE LEVEL IS,F5.2)
      CALL PLOT(1)
C          TAKE EACH SET IN SUCCESSION
      DO 102 K = 1,NUM
C          READ INITIAL DATA FOR SET AND WRITE HEADING
      READ (5,1001) (TITLE(I,K),I=1,20)
 1001 FORMAT (20A4)
      READ (5,1002) N(K),JA(K),IOPT,IPUN,THETA,PSI,PHI
 1002 FORMAT (4I5,3F10.5)
      WRITE (6,2001) (DASHS(I),I=1,11),K,(TITLE(I,K),
     1  I=1,20),(DASHS(I),I=1,11)
 2001 FORMAT (1H1,11A1/1H ,8HDATA SET,I3,2X,20A4/1H ,
     1  11A1)
C          SET UP DATA ARRAY FOR THIS SET
      CALL SETUP
C          COMPUTE STATISTICS FOR THIS SET
      CALL WATSON
      CALL FISHER
C          CHECK IF EULER ANGLES ARE TO BE COMPUTED FROM
C          EIGENVECTORS OF THIS SET
      IF (K .NE. IROT) GO TO 11
      WRITE (6,2002) (DASHS(I),I=1,21)
 2002 FORMAT (1H0,4X,21HCOMPUTED EULER ANGLES/1H ,4X,
     1  21A1)
C          CHECK FOR INDETERMINATE EIGENVECTORS
      IF (JS(K) .EQ. 0) GO TO 10
      WRITE (6,2003)
 2003 FORMAT (1H ,32H**COMMENT**EULER ANGLES NOT COMP,
     1  37HUTED SINCE EIGENVECTORS INDETERMINATE)
      GO TO 11
C          COMPUTE AND WRITE EULER ANGLES
   10 DO 101 IA = 1,3
      DC(IA) = EVCM(IA,IEVROT,K)
  101 CONTINUE
      CALL CHANGE(2)
      THETAB = 90.0 - PL
      PSIB = AZ
      PHIB = 360.0 - AZ
      WRITE (6,2004) IEVROT,THETAB,PSIB,PHIB
 2004 FORMAT (1H ,8X,30HFOR ROTATION ABOUT THE STRIKE ,
     1  12HOF THE PLANE/1H ,8X,19HWHOSE POLE IS EIGEN,
```

```
     2   11HVECTOR RANK,I2/1H ,8X,7HTHETA =,F7.2,
     3   7H, PSI =,F7.2,7H, PHI =,F7.2)
C          CHECK IF UNROTATED PLOT IS REQUIRED
   11  IIOPT = IOPT + 1
       GO TO (102,12,13,12,13,12),IIOPT
   12  WRITE (6,2005) (TITLE(I,K),I=1,20),N(K)
 2005  FORMAT (1H1,33HEQUAL AREA PLOT OF UNROTATED DATA,
     1   3H - ,20A4/1H ,3X,I3,7H POINTS)
       CALL PLOT(2)
C          CHECK IF DATA ARE TO BE ROTATED
   13  IF (IOPT .GE. 2) CALL ROTATE
C          CONTINUE TO NEXT DATA SET
  102  CONTINUE
C          COMPARE DATA SETS
       CALL COMPAR
       WRITE (6,2006)
 2006  FORMAT (1H1)
       STOP
       END
```

```
      SUBROUTINE SETUP
C          ROUTINE TO SET UP DIRECTION COSINE MATRIX
C          FOR EACH DATA SET
      DIMENSION LB(5)
      DIMENSION CTPC(57,95),DASHS(33),DC(3),DCM(3,200,10),
     1  EVCM(3,3,10),JA(25),JS(10),N(10),PREC(10),
     2  TITLE(20,10),V(3),W(3,3)
      COMMON AZ,CONLEV,CTPC,DASHS,DC,DCM,EVCM,IOPT,IROT,
     1  JA,JCA,JCB,JS,K,N,NCOM,PHI,PHIB,PL,PREC,PSI,
     2  PSIB,THETA,THETAB,TITLE,V,W,IPUN
      DATA  IDIRS,IDIRN/1HS,1HN/
C          WRITE SECTION HEADING
      WRITE (6,2000) (DASHS(I),I=1,14)
 2000 FORMAT (1H0,4X,14HUNROTATED DATA/1H ,4X,14A1)
C          TEST IF SET COMPRISES INPUT LINES,INPUT
C          PLANES OR DATA DERIVED FROM PREVIOUS SETS
      JJA = JA(K)
      GO TO (10,12,14),JJA
C          INPUT ROUTINE FOR LINES
C          WRITE HEADINGS
   10 WRITE (6,2001) N(K)
 2001 FORMAT (1H ,7X,I3,22H LINES FROM CARD INPUT/1H ,
     1  8X,2HNO,22X,4HLINE,6X,1HL,7X,1HM,7X,1HN)
C          READ AND CHECK EACH ELEMENT IN SUCCESSION
      KT = 0
   11 READ (5,1000) IPLU,IAZ
 1000 FORMAT (I5,I4)
      IF (IPLU .EQ. 99999) GO TO 24
      KT = KT + 1
      JB = 1
      IF (IPLU .LT. 0 .OR. IPLU .GT. 90) JB = 2
      IF (IAZ .LT. 0 .OR. IAZ .GT. 359) JB = 2
      AZ = IAZ
      PL = IPLU
C          CONVERT TO DIRECTION COSINES AND WRITE THESE
C          PLUS INPUT DATA
      CALL CHANGE(1)
      DO 100 IB = 1,3
  100 DCM(IB,KT,K) = DC(IB)
      WRITE (6,2002) KT,IPLU,IAZ,(DCM(I,KT,K),I=1,3)
 2002 FORMAT (1H ,7X,I3,21X,I2,1H/,I3,3F8.4)
      IF (JB .EQ. 1) GO TO 11
      WRITE (6,2003)
 2003 FORMAT (1H+,7H**ERROR)
      GO TO 11
C          INPUT ROUTINE FOR PLANES
C          WRITE SECTION HEADING
   12 WRITE (6,2004) N(K)
 2004 FORMAT (1H ,7X,I3,23H PLANES FROM CARD INPUT/1H ,
     1  8X,2HNO,12X,5HPLANE,5X,4HPOLE,6X,1HL,7X,1HM,7X,
     2  1HN)
C          READ AND CHECK EACH ELEMENT IN SUCCESSION
      KT = 0
   13 READ (5,1001) IST,IDIP,IDIR
 1001 FORMAT (I5,I3,1X,A1)
      IF (IST .EQ. 99999) GO TO 24
      KT = KT + 1
      JB = 1
      IF (IST .LT. 0 .OR. IST .GT. 179) JB = 2
```

```
      IF (IDIP .LT. 0 .OR. IDIP .GT. 90) JB = 2
      IF (IDIR .NE. IDIRS .AND. IDIR .NE. IDIRN) JB = 2
C          FIND POLE TO PLANE
      IF (IDIP .EQ. IDIRS) IAZ = IST - 90
      IF (IDIR .EQ. IDIRN) IAZ = IST + 90
      IF (IAZ .LT. 0) IAZ = IAZ+ 360
      IPLU = 90 - IDIP
      AZ = IAZ
      PL = IPLU
C          CONVERT POLE TO DIRECTION COSINES AND WRITE
C          THESE PLUS INPUT DATA
      CALL CHANGE(1)
      DO 101 IB = 1,3
  101 DCM(IB,KT,K) = DC(IB)
      WRITE (6,2005) KT,IST,IDIP,IDIR,IPLU,IAZ,
     1   (DCM(I,KT,K),I=1,3)
 2005 FORMAT (1H ,7X,I3,10X,I3,1H/,I2,1X,A1,3X,I2,1H/,
     1   I3,3F8.4)
      IF (JB .EQ. 1) GO TO 13
      WRITE (6,2003)
      GO TO 13
C          ROUTINE TO COMBINE DATA SETS
C          FIND WHICH SETS ARE TO BE COMBINED AND TEST
C          FOR ERRORS IN SET-UP INSTRUCTIONS
   14 KNT = 0
      IFLAG = 1
   15 KNT = KNT + 1
      READ (5,1002) LB(KNT)
 1002 FORMAT (I5)
      IF (LB(KNT) .EQ. 99999) GO TO 16
      IF (LB(KNT) .GE. K) WRITE (6,2006) LB(KNT)
 2006 FORMAT (1H ,14H**COMMENT**SET,I3,13H DOES NOT YET,
     1   6H EXIST)
      LLB = LB(KNT)
      IF (KNT .EQ.1) ITEST = JA(LLB)
      IF(ITEST .NE. JA(LLB)) IFLAG = 2
      GO TO 15
C          WRITE INITIAL MESSAGES
   16 KNT = KNT - 1
      JA(K) = ITEST
      WRITE (6,2007) N(K) ,(LB(I),I=1,KNT)
 2007 FORMAT (1H ,7X,I3,27H ELEMENTS DERIVED FROM DATA,
     1   5H SETS,5I3)
      IF (IFLAG .NE.  2) GO TO 17
      WRITE (6,2008)
 2008 FORMAT (1H ,33H**COMMENT**DATA SET CONTAINS BOTH,
     1   17H LINES AND PLANES)
      JA(K) = 2
   17 JJA = JA(K)
      GO TO (18,19) , JJA
C          WRITE HEADING FOR LINES
   18 WRITE (6,2009)
 2009 FORMAT (1H ,8X,2HNO,22X,4HLINE,6X,1HL,7X,1HM,
     1   7X,1HN)
      GO TO 20
C          WRITE HEADING FORPLANES
   19 WRITE (6,2010)
 2010 FORMAT (1H ,8X,2HNO,11X,5HPLANE,6X,4HPOLE,6X,1HL,
     1   7X,1HM,7X,1HN)
```

```
C          TAKE EACH SET IN TURN
   20 KT = 0
      DO 104 IA = 1,KNT
      IF (LB(IA) .GE. K) GO TO 104
      LC = LB(IA)
      NLC = N(LC)
C          TAKE EACH ELEMENT IN TURN
      DO 103 IB = 1,NLC
      KT = KT + 1
      DO 102 IC = 1,3
      DCM(IC,KT,K) = DCM(IC,IB,LC)
  102 DC(IC) = DCM(IC,KT,K)
C          CHANGE TO AZIMUTH AND PLUNGE
      CALL CHANGE(2)
      IAZ = AZ + 0.5
      IPL = PL + 0.5
C          IF DATA ARE LINES , WRITE
      IF (JA(LC) .NE. 1) GO TO 21
      WRITE (6,2002) KT,IPL ,IAZ,(DCM(I,KT,K),I=1,3)
      GO TO 103
C          IF DATA ARE PLANES , FIND PLANE AND WRITE
   21 IDP = 90 - IPL
      IF (IAZ .GE. 90 .AND. IAZ .LT. 270) GO TO 22
      IDIR = IDIRS
      IST = IAZ + 90
      IF (IST .GE. 360) IST = IST - 360
      GO TO 23
   22 IDIR = IDIRN
      IST = IAZ - 90
   23 WRITE (6,2005) KT,IST,IDP,IDIR,IPL,IAZ,
     1   (DCM(I,KT,K),I=1,3)
  103 CONTINUE
  104 CONTINUE
   24 IF (KT  .EQ. N(K)) RETURN
      WRITE (6,2011) KT ,N(K),KT
 2011 FORMAT (1H ,11H**COMMENT**,I3,15H ELEMENTS READ ,
     1   10HINSTEAD OF,I3/1H , 4X,17HSTATISTICS CALCUL,
     2   8HATED FOR,I3,9H ELEMENTS)
      N(K) = KT
      RETURN
      END
```

```
      SUBROUTINE WATSON
C          ROUTINE TO DERIVE STATISTICS FROM THE WATSON
C          METHOD. INCORPORATES A ROUTINE TO DERIVE
C          EIGENVALUES AND EIGENVECTORS OF A SYMMETRIC
C          MATRIX, WRITTEN BY M. CASEY
      DIMENSION CTPC(57,95),DASHS(33),DC(3),DCM(3,200,10),
     1  EVCM(3,3,10),JA(25),JS(10),N(10),PREC(10),
     2  TITLE(20,10),V(3),W(3,3)
      COMMON AZ,CONLEV,CTPC,DASHS,DC,DCM,EVCM,IOPT,IROT,
     1  JA,JCA,JCB,JS,K,N,NCOM,PHI,PHIB,PL,PREC,PSI,
     2  PSIB,THETA,THETAB,TITLE,V,W,IPUN
      DIMENSION CPM(3,3),DPM(3,3),EVAL(3),VIM(3,3),
     1  IEVAZ(3),IEVPL(3),SMOM(3)
C          WRITE SECTION HEADING
      WRITE (6,2000) (DASHS(I),I=1,30)
 2000 FORMAT (1H0,4X,30HRESULTS FROM THE WATSON METHOD/
     1  1H ,4X,30A1)
C          DERIVE MATRIX OF SUMS OF CROSS PRODUCTS OF
C          DIRECTION COSINES, AND FORM DISPERSION MATRIX
      M = N(K)
      RN = N(K)
      DO 100 IA = 1,3
      DO 100 IB = 1,3
      CPM(IA,IB) = 0.0
      DO 100 IC=1,M
      CPM(IA,IB)= CPM(IA,IB)+DCM(IA,IC,K)*DCM(IB,IC,K)
  100 DPM(IA,IB) = CPM(IA,IB)/RN
C          DERIVE EIGENVALUES AND EIGEN VECTORS OF CPM
C          BY THE JACOBI METHOD
C          SET VIM TO THE IDENTITY MATRIX
      DO 101 I = 1,3
      DO 101 J = 1,3
      IF(I.EQ.J)GO TO 10
      VIM(I,J) = 0.0
      GO TO 101
   10 VIM(I,J) = 1.0
  101 CONTINUE
C          COMPUTE INITIAL NORM
      INDIC=0
      SUM=0.0
      DO 102 I = 1,2
      M=I+1
      DO 102 J = M,3
  102 SUM = SUM + CPM(I,J)**2
      TEST=SQRT(SUM)
C          COMPUTE FINAL NORM
      TESTF=TEST*1.0E-9
C          COMPUTE NEW NORM
   11 TEST=TEST/3.0
C          START SEARCH FOR OFF-DIAGONAL ELEMENT
C          GREATER THAN NORM
   12 J = 2
   13 I = 1
   14 IF(ABS(CPM(I,J)) .LT. TEST) GO TO 15
      INDIC=1
C          COMPUTE SINE THETA-R1 AND COSINE THETA-R2
      PH   = -CPM(I,J)
      THET   = (CPM(I,I) - CPM(J,J)) * 0.5
      ZETA=PH / SQRT(THET **2+PH **2)
```

```
      IF (THET  .LT.0.0) ZETA = -ZETA
      R1=ZETA/ SQRT(2.0*(1.0+ SQRT(1.0-ZETA**2)))
      R2= SQRT(1.0-R1**2)
C          TRANSFORM CPM TO MAKE CPM(I,J) ZERO
      DO 103 L = 1,3
      X = CPM(L,I) * R2 - CPM(L,J) * R1
      CPM(L,J) = CPM(L,I) * R1 + CPM(L,J) * R2
  103 CPM(L,I) = X
      CPM(I,I) = CPM(I,I) * R2 - CPM(J,I) * R1
      X = CPM(I,J) * R1 + CPM(J,J) * R2
      CPM(I,J) = CPM(I,J) * R2 - CPM(J,J) * R1
      CPM(J,J) = X
      DO 104 L = 1,3
      CPM(I,L) = CPM(L,I)
  104 CPM(J,L) = CPM(L,J)
C          COMPUTE NEW TOTAL ROTATION MATRIX
      DO 105 L = 1,3
      X = VIM(L,I) * R2 - VIM(L,J) * R1
      VIM(L,J) = VIM(L,I) * R1 + VIM(L,J) * R2
  105 VIM(L,I) = X
C          CHECK FOR END OF SWEEP
   15 IF(I.EQ.J-1)GO TO 16
      I=I+1
      GO TO 14
   16 IF(J.EQ.3)GO TO 17
      J=J+1
      GO TO 13
C          CHECK WHETHER A TRANSFORMATION HAS OCCURRED
C          SINCE SWEEP STARTED.  IF SO SWEEP AGAIN
   17 IF(INDIC.NE.1)GO TO 18
      INDIC=0
      GO TO 12
C          CHECK FOR END OF ITERATION
   18 IF(TEST.GE.TESTF)GO TO 11
C          END OF JACOBI ROUTINE
C          ARRANGE EIGENVALUES IN ORDER OF SIZE.
      DO 108 IA = 1,3
      CMAX = 0.0
      DO 106 IB = 1,3
      IF (CPM(IB,IB) .LT. CMAX) GO TO 106
      CMAX = CPM(IB,IB)
      IJK = IB
  106 CONTINUE
      EVAL(IA) = CPM(IJK,IJK)
      DO 107 IB = 1,3
      DC(IB) = VIM(IB,IJK)
  107 EVCM(IB,IA,K) = VIM(IB,IJK)
      CPM(IJK,IJK) = 0.0
C          DERIVE 2ND MOMENT FROM EIGENVALUE
      SMOM(IA) = EVAL(IA)/RN
C          CONVERT EIGENVECTORS TO PLUNGE AND AZIMUTH
      CALL CHANGE(2)
      IEVAZ(IA) = AZ + 0.5
      IEVPL(IA) = PL + 0.5
  108 CONTINUE
C          WRITE EIGENVALUES AND VECTORS ETC.
      WRITE (6,2001)
 2001 FORMAT (1H ,8X,30HEIGENVALUES  2ND MOM  ATTITUDE,
     1  6X,12HEIGENVECTORS)
```

```
      DO 109 IA = 1,3
  109 WRITE (6,2002) IA,EVAL(IA),SMOM(IA),IEVPL(IA),
     1  IEVAZ(IA),(FVCM(I,IA,K),I = 1,3)
 2002 FORMAT (1H ,8X,I1,F10.5,F9.5,3X,I2,1H/,I3,3F8.4)
C          TEST FOR INDETERMINATE EIGENVECTORS
      JS(K) = 0
      IF (IEVPL(1) .EQ. IEVPL(2) .AND. IEVAZ(1) .EQ.
     1  IEVAZ(2)) JS(K) = 1
      IF (IEVPL(2) .EQ. IEVPL(3) .AND. IEVAZ(2) .EQ.
     1  IEVAZ(3)) JS(K) = 1
      IF (IEVPL(3) .EQ. IEVPL(1) .AND. IEVAZ(3) .EQ.
     1  IEVAZ(1)) JS(K) = 1
      IF (JS(K) .EQ. 1) WRITE(6,2003)
 2003 FORMAT(1H ,28H**COMMENT**EIGENVECTORS ARE ,
     1  13HINDETERMINATE)
      WRITE (6,2004)
 2004 FORMAT (1H )
C          COMPUTE AND WRITE EIGENVALUE RATIOS
      DO 110 IA=1,3
      IB = IA + 1
      IF (IA .EQ.3) IB=1
      IF(EVAL(IB) .LE. 0.0) GO TO 19
      EVR = EVAL(IA)/EVAL(IB)
      WRITE ( 6,2005) IA,IB,EVR
 2005 FORMAT (1H ,32X,4HRANK,I2,5H/RANK,I2,2H -,F14.4)
      GO TO 20
   19 WRITE (6,2006) IA,IB
 2006 FORMAT (1H ,32X, 4HRANK,I2,5H/RANK,I2,2H -,
     1  6X,8HINFINITE)
   20 IF (IA .EQ. 1) WRITE (6,2007)
 2007 FORMAT (1H+,8X,23HRATIOS OF EIGENVALUES -)
      IF (EVAL(IA) .LE. 0.0) GO TO 21
      EVR = EVAL(IB)/EVAL(IA)
      WRITE (6,2005) IB,IA,EVR
      GO TO 110
   21 WRITE (6,2006) IB,IA
  110 CONTINUE
C          COMPUTE AND WRITE K-PARAMETER
      WRITE ( 6,2008)
 2008 FORMAT (1H ,8X,22HVALUE OF K-PARAMETER -)
      IF (EVAL(2) .GT. 0.0) GO TO 22
      WRITE (6,2009)
 2009 FORMAT (1H+,53X,8HINFINITE)
      RETURN
   22 IF(EVAL (3) .GT. 0.0)GO TO 23
      RKPAR = 0.0
      GO TO 24
   23 RKPAR = (EVAL (1)/EVAL(2)-1.0)/(EVAL(2)/EVAL(3)-1.0)
   24 WRITE  (6,2010) RKPAR
 2010 FORMAT (1H+,50X,F11.4)
      RETURN
      END
```

```
      SUBROUTINE FISHER
C          ROUTINE TO DERIVE STATISTICS FROM THE FISHER
C          METHOD. DATA ARE DIRECTION COSINES
      DIMENSION CTPC(57,95),DASHS(33),DC(3),DCM(3,200,10),
     1  EVCM(3,3,10),JA(25),JS(10),N(10),PREC(10),
     2  TITLE(20,10),V(3),W(3,3)
      COMMON AZ,CONLEV,CTPC,DASHS,DC,DCM,EVCM,IOPT,IROT,
     1  JA,JCA,JCR,JS,K,N,NCOM,PHI,PHIB,PL,PREC,PSI,
     2  PSIB,THETA,THETAB,TITLE,V,W,IPUN
      DIMENSION SDC(3)
      DATA RD,IDIRS,IDIRN/57.29578,1HS,1HN/
C          WRITE SECTION HEADING
      WRITE (6,2000) (DASHS(I), I=1,30)
 2000 FORMAT (1H0,4X,30HRESULTS FROM THE FISHER METHOD/
     1  1H ,4X,30A1)
C          TEST FOR ONLY ONE DATA POINT
      IF (N(K) .GT. 1) GO TO 9
      WRITE (6,2001)
 2001 FORMAT (1H ,31H**COMMENT**ONLY ONE DATA POINT.,
     1  22HNO STATISTICS COMPUTED)
      RETURN
C          TEST FOR INDETERMINATE EIGENVECTORS
    9 IF (JS(K) .NE. 1) GO TO 10
      WRITE (6,2002)
 2002 FORMAT (1H ,34H**COMMENT**EIGENVECTORS INDETERMIN,
     1  41HATE THEREFORE DATA NOT ROTATED,STATISTICS/
     1  1H ,11X,23HBELOW MAY BE UNRELIABLE)
      GO TO 11
C          FORM THE ROTATION MATRIX FROM THE EIGENVECTORS
   10 DO 100 IA=1,3
      SDC(IA) = 0.0
      DO 100 IB=1,3
      IC = 4-IB
  100 W(IA,IB) = EVCM(IA,IC,K)
C          ROTATE EACH ELEMENT IN TURN (IF EIGENVECTORS
C          ARE KNOWN) AND DERIVE CUMMULATIVE SUM OF
C          DIRECTION COSINES
   11 M = N(K)
      DO 102 IA = 1,M
      DO 101 IB = 1,3
  101 V(IB) = DCM(IB,IA,K)
      IF (JS(K) .NE. 1) CALL TRANSF
      DO 102 IB = 1,3
      SDC(IB) = SDC(IB) + V(IB)
  102 CONTINUE
C          DERIVE R SQUARED
      RS = 0.0
      DO 103 IA = 1,3
  103 RS = RS + SDC(IA) * SDC(IA)
C          COMPUTE R AND DIRECTION COSINES OF MEAN
      R    = SQRT(RS)
      DO 104 IA = 1,3
  104 V(IA) = SDC(IA)/R
C          ROTATE THE MEAN TO TRUE POSITION IF NECESSARY
      IF (JS(K) .EQ. 1) GO TO 12
      CALL INVERT
      CALL TRANSF
   12 DO 105 IA = 1,3
  105 DC(IA) = V(IA)
```

```
C           CONVERT MEAN TO AZIMUTH AND PLUNGE,AND WRITE
      CALL CHANGE(2)
      IAZ = AZ + 0.5
      IPL = PL + 0.5
      WRITE (6,2003) IPL,IAZ
 2003 FORMAT (1H ,8X,23HPREDICTED SAMPLE MEAN -,20X,I5,
     1  1H/,I3)
C           IF DATA WERE PLANES CALCULATE THE MEAN PLANE
      IF (JA(K) .NE. 2) GO TO 15
      IDP = 90 - IPL
      IF (IAZ .GE. 90 .AND. IAZ .LT. 270) GO TO 13
      IDIR = IDIRS
      IST = IAZ + 90
      IF (IST .GE. 360) IST = IST - 360
      GO TO 14
   13 IDIR = IDIRN
      IST = IAZ - 90
   14 WRITE (6,2004) IST,IDP,IDIR
 2004 FORMAT (1H+,61X,3HOR ,I3,1H/,I2,A1)
C           CALCULATE AND WRITE CONE OF CONFIDENCE
   15 RN = N(K)
      WRITE (6,2005)
 2005 FORMAT (1H ,8X,27HCONE OF CONFIDENCE FOR THE ,
     1  6HMEAN -)
      TEMP = (1.0/(1.0-CONLEV))**(1.0/(RN-1.0)) - 1.0
      COSCC = 1.0 - ((RN - R)/R) * TEMP
      IF (COSCC .GT. 1.0 .OR. COSCC .LT. -1.0) GO TO 16
      CC = ACOS(COSCC) * RD
      WRITE (6,2006) CC
 2006 FORMAT (1H+,53X,F6.2,8H DEGREES)
      GO TO 17
   16 WRITE (6,2007)
 2007 FORMAT (1H+,53X,24HGREATER THAN 180 DEGREES)
C           CALCULATE AND WRITE PRECISION
   17 PREC(K)  = (RN - 1.0)/(RN - R)
      WRITE (6,2008) PREC(K)
 2008 FORMAT (1H ,8X,26HESTIMATE OF PRECISION FOR ,
     1  14HDISTRIBUTION -,3X,F8.2)
C           CALCULATE AND WRITE ANG. STANDARD. DEVIATIONS
      IF ((RN-R) .LT. 0.0) RETURN
      DELTA = ACOS(R   /RN) * RD
      EPSIL = DELTA * (1.0/RN**0.5)
      WRITE (6,2009) DELTA,EPSIL
 2009 FORMAT (1H ,8X,27HANGULAR STANDARD DEVIATION ,
     1  16HABOUT THE MEAN -,2X,F6.2,8H DEGREES/1H ,8X,
     2  40HANGULAR STANDARD DEVIATION OF THE MEAN -,
     3  5X,F6.2,8H DEGREES)
      RETURN
      END
```

```
      SUBROUTINE PLOT (IND)
C          ROUTINE TO GIVE EQUAL AREA CONTOURED PLOT
C          ON THE LINE PRINTER. ROUTINE IS PART OF A
C          PROGRAM WRITTEN BY J.WARNER (1969),KANSAS
C          STATE GEOL. SURV.COMPUTER CONTRIBS., NO. 33
      DIMENSION IM(75),JM(75),DUMMY(40)
      DIMENSION CTPC(57,95),DASHS(33),DC(3),DCM(3,200,10),
     1  EVCM(3,3,10),JA(25),JS(10),N(10),PREC(10),
     2  TITLE(20,10),V(3),W(3,3)
      COMMON AZ,CONLEV,CTPC,DASHS,DC,DCM,EVCM,IOPT,IROT,
     1  JA,JCA,JCB,JS,K,N,NCOM,PHI,PHIB,PL,PREC,PSI,
     2  PSIB,THETA,THETAB,TITLE,V,W,IPUN
      DATA (DUMMY(I),I=1,40)/1H ,1H-,1H0,1H1,1H2,1H3,
     1  1H4,1H5,1H6,1H7,1H8,1H9,1HA,1HB,1HC,1HD,1HE,
     2  1HF,1HG,1HH,1HI,1HJ,1HK,1HL,1HM,1HN,1HO,1HP,
     3  1HQ,1HR,1HS,1HT,1HU,1HV,1HW,1HX,1HY,1HZ,1H*,1H /
      DATA (JM(I),I=1,71)/95,1,3*48,47,46,45,44,43,42,
     1  41,40,39,38,38,37,36,35,34,33,2*32,31,30,29,
     2  2*28,27,26,2*25,24,23,2*22,21,20,19,18,
     3  17,16,15,14,13,12,11,11,10,10,9,8,7,7,6,6,5,5,
     4  4,4,3*3,3*2,5*1/
      DATA (IM(I),I=1,71)/3*29,57,11*1,7*2,5*3,4*4,4*5,
     1  3*6,7,7,8,8,9,2*10,2*11,2*12,2*13,14,15,2*16,
     2  2*17,18,19,2*20,21,2*22,23,2*24,25,26,27,28/
      DATA (IM(I),JM(I),I=72,74)/3*1,2,2,1/
      GO TO (10,11),IND
C          IF IND = 1 PRINT SYMBOL TABLE
   10 WRITE (6,2000)(DUMMY(I),I=1,4)
 2000 FORMAT (28H0 SYMBOLS ON STEREO NET MEAN//  5X,
     1  6HSYMBOL,7X,13HPERCENT RANGE//8X,A1,9X,5H0 OR ,
     2  4HLESS/8X,A1,9X,1H0,3X,3H1/2/8X,A1,8X,3H1/2,4X,
     3  A1)
      DO 100 I = 4,37
      MBO = I - 3
      MTO = I - 2
  100 WRITE (6,2001)DUMMY(I),MBO,MTO
 2001 FORMAT (8X,A1,8X,I2,4X,I2)
      WRITE (6,2002)DUMMY(38)
 2002 FORMAT (8X,A1,8X,14H35 AND GREATER)
      RETURN
C          IF IND = 2 START PLOTTING ROUTINE
   11 NK = N(K)
      XN = N(K)
C          ZERO CTPC MATRIX
      DO 101 I = 1,57
      DO 101 J = 1,95
  101 CTPC(I,J) = 0.0
C          PERFORM POINT COUNT AND FILL CTPC MATRIX WITH
C          PERCENT POPULATION PER UNIT AREA
      DO 103 I = 1,57
      YI = (58-I)*2 - 58
      YI = YI * 0.01785714
      DO 103 J = 1,95,2
      XI = J*2 - 96
      XI = XI * 0.01063829
      COUNT = 0.0
      RD = SQRT(XI*XI + YI*YI)
      IF (RD .GT. 1.01) GO TO 12
      AZ = ATAN2(XI,YI)
```

```
      ROE = ASIN(RD/SQRT(2.0)) * 2.0
      ZP = COS(ROE)
      ROSN = SIN(ROE)
      XP = SIN(AZ) * ROSN
      YP = COS(AZ) * ROSN
      DO 102 NN = 1,NK
      DOTP = ABS(XP*DCM(2,NN,K) + YP*DCM(1,NN,K) +
     1   ZP * DCM(3,NN,K))
      ANG = ACOS(DOTP)
      IF (ANG .LE. 0.16) COUNT = COUNT + 1.0
  102 CONTINUE
   12 CTPC(I,J) = COUNT * 100.0 / XN
  103 CONTINUE
C          PUT CIRCLE ON CTPC MATRIX
      XXX = -999.9
      DO 104 I = 1,5
      L = IM(I)
      M = JM(I)
      IF (CTPC(L,M) .LE. 0.0) CTPC(L,M) = XXX
  104 CONTINUE
      DO 105 I = 6,74
      I1 = IM(I)
      I2 = 58 - I1
      J1 = JM(I)
      J2 = 96 - J1
      IF (CTPC(I1,J1) .LE. 0.0) CTPC(I1,J1) = XXX
      IF (CTPC(I1,J2) .LE. 0.0) CTPC(I1,J2) = XXX
      IF (CTPC(I2,J2) .LE. 0.0) CTPC(I2,J2) = XXX
      IF (CTPC(I2,J1) .LE. 0.0) CTPC(I2,J1) = XXX
  105 CONTINUE
C          CONVERT CTPC MATRIX TO PRINT SYMBOLS
      DO 106 I = 1,57
      DO 106 J = 1,95
      IF (CTPC(I,J) .LE. (-999.9)) GO TO 15
      IF (CTPC(I,J) .LE. 0.0) GO TO 16
      IF (CTPC(I,J) .LE. 0.5) GO TO 17
      M = 3
   13 MM = M-2
      XMM = MM
      IF (CTPC(I,J) .LT. XMM) GO TO 14
      M = M+1
      IF (M .LE. 37) GO TO  13
      CTPC(I,J) = DUMMY(38)
      GO TO 106
   14 CTPC(I,J) = DUMMY(M)
      GO TO 106
   15 CTPC(I,J) = DUMMY(39)
      GO TO 106
   16 CTPC(I,J) = DUMMY(1)
      GO TO 106
   17 CTPC(I,J) = DUMMY(2)
  106 CONTINUE
C          PRINT AND ZERO MATRIX
      WRITE (6,2003)
 2003 FORMAT (1H ,51X,1H*)
      DO 107 I = 1,57
      WRITE (6,2004)(CTPC(I,J),J=1,95)
 2004 FORMAT (5X,95A1)
      DO 107 J = 1,95
```

```
      CTPC(I,J) = 0.0
  107 CONTINUE
      RETURN
      END
```

```
      SUBROUTINE ROTATE
C          ROUTINE TO ROTATE DATA ACCORDING TO
C          SPECIFIED EULER ANGLES
      DIMENSION CTPC(57,95),DASHS(33),DC(3),DCM(3,200,10),
     1  EVCM(3,3,10),JA(25),JS(10),N(10),PREC(10),
     2  TITLE(20,10),V(3),W(3,3)
      COMMON AZ,CONLEV,CTPC,DASHS,DC,DCM,EVCM,IOPT,IROT,
     1  JA,JCA,JCB,JS,K,N,NCOM,PHI,PHIB,PL,PREC,PSI,
     2  PSIB,THETA,THETAB,TITLE,V,W,IPUN
      DIMENSION STORE (3,200)
      DATA IDIRS,IDIRN/1HS,1HN/
      WRITE (6,2000) (DASHS(I),I=1,16)
 2000 FORMAT (1H1,4X,16HROTATION DETAILS/1H ,4X,16A1/
     1  1H ,8X,16HEULER ANGLES ARE)
C          TEST FOR SOURCE OF EULER ANGLES
      IF (IFIX(THETA) .EQ. 0 .AND. IFIX(PSI) .EQ. 0 .AND.
     1  IFIX(PHI) .EQ. 0) GO TO 10
      WRITE (6,2001)
 2001 FORMAT (1H+,25X,23HDERIVED FROM CARD INPUT)
      GO TO 12
   10 WRITE (6,2002) IROT
 2002 FORMAT (1H+,25X,21HTHOSE COMPUTED IN SET,I3)
C          TEST FOR NO EULER ANGLES
      IF (IROT .NE. 0 .AND. IROT .LE. K .AND. JS(IROT)
     1  .EQ. 0) GO TO 11
      WRITE (6,2003)
 2003 FORMAT (1H ,33H**COMMENT**EULER ANGLES NOT AVAIL,
     1  25HABLE,NO ROTATION POSSIBLE)
      RETURN
   11 THETA = THETAB
      PSI = PSIB
      PHI = PHIB
C          WRITE EULER ANGLES
   12 WRITE (6,2004) THETA,PSI,PHI
 2004 FORMAT (1H ,8X,7HTHETA =,F7.2,7H, PSI =,F7.2,
     1  7H, PHI =,F7.2)
C          DERIVE ROTATION MATRIX
      CONFAC = 3.1415926535898/180.0
      THETA = THETA * CONFAC
      PSI = PSI * CONFAC
      PHI = PHI * CONFAC
      STH = SIN(THETA)
      CTH = COS(THETA)
      SPS = SIN(PSI)
      CPS = COS(PSI)
      SPH = SIN(PHI)
      CPH = COS(PHI)
      W(1,1) = CPS * CTH * CPH - SPS * SPH
      W(2,1) = SPS * CTH * CPH + CPS * SPH
      W(3,1) = -STH * CPH
      W(1,2) = -CPS * CTH * SPH - SPS * CPH
      W(2,2) = -SPS * CTH * SPH + CPS * CPH
      W(3,2) = STH * SPH
      W(1,3) = CPS * STH
      W(2,3) = SPS * STH
      W(3,3) = CTH
C          WRITE ROTATION MATRIX AND NEW AXES
      WRITE (6,2005)
 2005 FORMAT (1H ,8X,15HROTATION MATRIX,9X,4HAXIS,6X,
```

```
     1   1HL,7X,1HM,7X,1HN)
         DO 102 IA = 1,3
         DO 101 IB = 1,3
         DC(IB) = W(IB,IA)
  101 CONTINUE
         CALL CHANGE(2)
         IAZ = AZ + 0.5
         IPL = PL + 0.5
         WRITE (6,2006) IPL,IAZ,(W(I,IA),I=1,3)
 2006 FORMAT (1H ,31X,I2,1H/,I3,3F8.4)
  102 CONTINUE
C            DERIVE ROTATED DATA
         WRITE (6,2007) (DASHS(I),I=1,12)
 2007 FORMAT (1H0,4X,12HROTATED DATA/1H ,4X,12A1)
         IF (JA(K) .EQ. 2) WRITE (6,2008)
 2008 FORMAT (1H ,8X,2HNO,11X,5HPLANE,6X,4HPOLE,6X,1HL,
     1   7X,1HM,7X,1HN)
         IF (JA(K) .EQ. 1) WRITE (6,2009)
 2009 FORMAT (1H ,8X,2HNO,22X,4HLINE,6X,1HL,7X,1HM,
     1   7X,1HN)
C            TAKE EACH ELEMENT IN SUCCESSION
         NN = N(K)
         DO 105 IA = 1,NN
C            STORE UNROTATED DATA IN ARRAY STORE
         DO 103 IB = 1,3
         V(IB) = DCM(IB,IA,K)
         STORE (IB,IA) = DCM(IB,IA,K)
  103 CONTINUE
C            ROTATE ELEMENT AND CHANGE TO AZIMUTH AND
C            PLUNGE
         CALL TRANSF
         DO 104 IB = 1,3
         DCM (IB,IA,K) = V(IB)
         DC(IB) = V(IB)
  104 CONTINUE
         CALL CHANGE(2)
         IAZ = AZ + 0.5
         IPL = PL + 0.5
C            IF ELEMENTS ARE LINES,WRITE
         IF (JA(K) .NE. 1) GO TO 13
         WRITE (6,2010) IA,IPL,IAZ,(DCM(I,IA,K),I=1,3)
 2010 FORMAT (1H ,7X,I3,21X,I2,1H/,I3,3F8.4)
         IF (IPUN .GT. 0) PUNCH 3000,IPL,IAZ
 3000 FORMAT (I5,I4)
         GO TO 105
C            IF DATA ARE PLANES,FIND PLANE AND WRITE
   13 IDP = 90 - IPL
         IF (IAZ .GE. 90 .AND. IAZ .LT. 270) GO TO 14
         IDIR = IDIRS
         IST = IAZ + 90
         IF (IST .GE. 360) IST = IST - 360
         GO TO 15
   14 IDIR = IDIRN
         IST = IAZ - 90
   15 WRITE (6,2011) IA,IST,IDP,IDIR,IPL,IAZ,
     1   (DCM(I,IA,K),I=1,3)
 2011 FORMAT (1H ,7X,I3,10X,I3,1H/,I2,1X,A1,3X,I2,1H/,
     1   I3,3F8.4)
         IF (IPUN .GT. 0) PUNCH 3001,IST,IDP,IDIR
```

```
 3001 FORMAT(I5,I3,1X,A1)
  105 CONTINUE
C          DERIVE AND WRITE ROTATED EIGENVECTORS
      WRITE (6,2012) (DASHS(I),I=1,20)
 2012 FORMAT (1H ,4X,20HROTATED EIGENVECTORS/1H ,4X,
     1   20A1)
      WRITE (6,2009)
      DO 108 IA = 1,3
      DO 106 IB = 1,3
      V(IB) = EVCM(IB,IA,K)
  106 CONTINUE
      CALL TRANSF
      DO 107 IB = 1,3
      DC(IB) = V(IB)
  107 CONTINUE
      CALL CHANGE(2)
      IAZ = AZ + 0.5
      IPL = PL + 0.5
      WRITE (6,2010) IA,IPL,IAZ,DC
  108 CONTINUE
C          CHECK IF ROTATED PLOT IS REQUIRED
      IF(IOPT .LT. 4) GO TO 16
      WRITE (6,2013) (TITLE(I,K),I=1,20),N(K)
 2013 FORMAT (1H1,31HEQUAL AREA PLOT OF ROTATED DATA,
     1   3H - ,20A4/1H ,3X,I3,7H POINTS)
      CALL PLOT(2)
C          RESTORE UNROTATED DATA TO DCM ARRAY
   16 DO 110 IA = 1,NN
      DO 109 IB = 1,3
      DCM(IB,IA,K) = STORE (IB,IA)
  109 CONTINUE
  110 CONTINUE
      RETURN
      END
```

```
      SUBROUTINE COMPAR
C          COMPARES THE MEANS AND PRECISIONS OF PAIRS OF
C          DISTRIBUTIONS BY DERIVING AN F-STATISTIC.
      DIMENSION CTPC(57,95),DASHS(33),DC(3),DCM(3,200,10),
     1  EVCM(3,3,10),JA(25),JS(10),N(10),PREC(10),
     2  TITLE(20,10),V(3),W(3,3)
      COMMON AZ,CONLEV,CTPC,DASHS,DC,DCM,EVCM,IOPT,IROT,
     1  JA,JCA,JCB,JS,K,N,NCOM,PHI,PHIB,PL,PREC,PSI,
     2  PSIB,THETA,THETAB,TITLE,V,W,IPUN
      DIMENSION SDC(3,2),RR(2)
      IF (NCOM .LT. 1) RETURN
C          WRITE PAGE HEADING
      WRITE (6,2000)(DASHS(I),I=1,25),(DASHS(I),I=1,25),
     1  CONLEV
 2000 FORMAT (1H1,25A1/1H ,25HCOMPARISONS OF STATISTICS/
     1  1H ,25A1/1H ,4X,19HCONFIDENCE LEVEL IS,F6.3)
      NNCOM = 0
C          TAKE EACH PAIR OF DISTRIBUTIONS IN TURN
C          READ IN NUMBERS OF SETS TO BE COMPARED AND
C          WRITE HEADING FOR THIS SECTION
   10 READ (5,1000) JCA,JCB
 1000 FORMAT (2I5)
      IF (JCA .EQ. 99999) GO TO 13
      NNCOM = NNCOM + 1
      WRITE (6,2001) JCA,JCB,(DASHS(I),I=1,19),JCA,
     1  (TITLE(I,JCA),I=1,20),JCB,(TITLE(I,JCB),I=1,20)
 2001 FORMAT (1H0,4X,9HDATA SETS,I3,4H AND,I3/1H ,4X,
     1  19A1/1H ,6X,3HSET,I3,3H - ,20A4/1H ,6X,3HSET,
     2  I3,3H - ,20A4)
C          CHECK FOR INDETERMINATE EIGENVALUES
      IF (JS(JCA) .NE. 1 .AND.JS(JCB) .NE. 1) GO TO 11
      WRITE (6,2002)
 2002 FORMAT (1H0,34H**COMMENT**NO COMPARISON POSSIBLE./
     1  1H ,11X,35HONE DISTRIBUTION HAS INDETERMINATE ,
     2  12HEIGENVECTORS)
      GO TO 10
C          FORM THE ROTATION MATRIX FROM THE
C          EIGENVECTORS OF ONE SET,AND ZERO SDC
   11 DO 101 IA = 1,3
      DO 100 IB = 1,3
      IC = 4-IB
  100 W(IA,IB) = EVCM(IA,IC,JCA)
      SDC(IA,1) = 0.0
  101 SDC(IA,2) = 0.0
C          TAKE THE DIRECTION COSINE ARRAY OF EACH
C          SET IN TURN
      DO 105 IA = 1,2
      JC = JCA
      IF (IA .EQ. 2) JC = JCB
      NN = N(JC)
C          TAKE EACH ELEMENT IN TURN
      DO 103 IB = 1,NN
C          ROTATE THE ELEMENT
      DO 102 IC = 1,3
  102 V(IC) = DCM(IC,IB,JC)
      CALL TRANSF
C          ADD TO THE SUM OF DIRECTION COSINES
      DO 103 IC = 1,3
      SDC(IC,IA) = SDC(IC,IA) + V(IC)
```

```
  103 CONTINUE
C           DERIVE R VALUE
      RS = 0.0
      DO 104 IB = 1,3
  104 RS = RS + SDC(IB,IA) * SDC(IB,IA)
      RR(IA) = SQRT(RS)
  105 CONTINUE
C           DERIVE AND WRITE STATISTICS FOR MEANS
      RTS = 0.0
      DO 106 IA = 1,3
  106 RTS = RTS + (SDC(IA,1) + SDC(IA,2)) ** 2
      RT = SQRT(RTS)
      RNA = N(JCA)
      RNB = N(JCB)
      F = (RNA+RNB-2.0)*(RR(1)+RR(2)-RT)/(RNA+RNB-RR(1)
     1  -RR(2))
      DFD = 2.0*(RNA + RNB - 2.0)
      WRITE (6,2003) F,DFD
 2003 FORMAT (1H0,8X,20HVALUE OF F-STATISTIC FOR THE ,
     1  6HMEAN -,9X,F8.4/1H ,8X,19HDEGREES OF FREEDOM ,
     2  14HIN NUMERATOR -,13X,3H2.0/1H ,8X,8HDEGREES ,
     3  27HOF FREEDOM IN DENOMINATOR -,9X,F5.1)
C           DERIVE AND WRITE STATISTICS FOR PRECISIONS
      F = PREC(JCA)/PREC(JCB)
      DFL = 2.0*(RNA - 1.0)
      DFS = 2.0*(RNB - 1.0)
      IF (F .GE. 1.0) GO TO 12
      F = 1.0/F
      TEMP = DFS
      DFS = DFL
      DFL = TEMP
   12 WRITE (6,2004) F,DFL,DFS
 2004 FORMAT (1H0,8X,25HVALUE OF F-STATISTIC FOR ,
     1  12HPRECISIONS -,7X,F8.4/1H ,8X,11HDEGREES OF ,
     2  28HFREEDOM - LARGER PRECISION -,5X,F5.1/1H ,
     3  8X,40HDEGREES OF FREEDOM - SMALLER PRECISION -,
     4  4X,F5.1)
      GO TO 10
   13 IF (NNCOM .EQ. NCOM) RETURN
      WRITE (6,2005) NNCOM,NCOM
 2005 FORMAT (1H0,11H**COMMENT**,I3,13H COMPARISONS ,
     1  15HMADE INSTEAD OF,I3)
      RETURN
      END
```

```
      SUBROUTINE CHANGE(IND)
C          ROUTINE TO CONVERT AZIMUTH AND PLUNGE TO
C          DIRECTION COSINES (FOR IND = 1) OR VICE VERSA
C          (FOR IND = 2).
C          INPUT VARIABLES ARE AZ = AZIMUTH AND PL =
C          PLUNGE, OR DC(3) = DIRECTION COSINES (REFERRED
C          TO AXES X = NORTH, Y = EAST, AND Z = DOWN).
C          INPUT VALUES MAY FALL IN UPPER OR LOWER
C          HEMISPHERES, BUT OUTPUT VALUES ARE ADJUSTED
C          TO FALL IN LOWER HEMISPHERE ONLY.
      DIMENSION CTPC(57,95),DASHS(33),DC(3),DCM(3,200,10),
     1  EVCM(3,3,10),JA(25),JS(10),N(10),PREC(10),
     2  TITLE(20,10),V(3),W(3,3)
      COMMON AZ,CONLEV,CTPC,DASHS,DC,DCM,EVCM,IOPT,IROT,
     1  JA,JCA,JCB,JS,K,N,NCOM,PHI,PHIB,PL,PREC,PSI,
     2  PSIB,THETA,THETAB,TITLE,V,W,IPUN
      DATA  RD/57.29578/
C          SELECT APPROPRIATE CONVERSION.
      GO TO (10,11),IND
C          FOR IND = 1, TEST FOR PLUNGE = 90 DEGREES
C          THEN CALCULATE DIRECTION COSINES.
   10 IF (PL .EQ. 90.0 .OR. PL .EQ. -90.0) AZ = 0.0
      AR = AZ/RD
      PR = PL/RD
      COSP = COS(PR)
      DC(1) = COSP * COS(AR)
      DC(2) = COSP * SIN(AR)
      DC(3) = SIN(PR)
C          ADJUST DIRECTION COSINES FOR LOWER HEMISPHERE
C          IF NECESSARY, THEN RETURN.
      IF (DC(3) .GE. 0.0) RETURN
      DO 100 IA = 1,3
  100 DC(IA) = -DC(IA)
      RETURN
C          FOR IND = 2, ADJUST DIRECTION COSINES FOR
C          LOWER HEMISPHERE IF NECESSARY.
   11 IF (DC(3) .GE. 0.0) GO TO 12
      DO 101 IA = 1,3
  101 DC(IA) = -DC(IA)
C          CHECK THAT DC(3) IS LESS THAN 1.0
   12 IF (DC(3) .LT. 1.0) GO TO 13
      WRITE (6,2000) DC(3)
 2000 FORMAT (1H ,34H**COMMENT**CHANGE RECEIVED A DC(3),
     1  9H VALUE OF,F14.9,25H WHICH WAS CHANGED TO 1.0)
      AZ = 0.0
      PL = 90.0
      RETURN
C          CHECK THAT DC(1) IS NOT ZERO
   13 IF (DC(1) .NE. 0.0) GO TO 14
      IF (DC(2) .GT. 0.0) AZ = 90.0
      IF (DC(2) .LT. 0.0) AZ = 270.0
      GO TO 16
C          CHECK THAT DC(2) IS NOT ZERO
   14 IF (DC(2) .NE. 0.0) GO TO 15
      IF (DC(1) .GT. 0.0) AZ = 0.0
      IF (DC(1) .LT. 0.0) AZ = 180.0
      GO TO 16
C          CALCULATE THE AZIMUTH AND PLUNGE THEN RETURN
   15 AZ = RD * ATAN2(DC(2),DC(1))
```

```
16 PL = RD * ASIN(DC(3))
   IF (AZ .LT. 0.0) AZ = AZ + 360.0
   IF (AZ .EQ. 360.0) AZ = 0.0
   RETURN
   END
```

```
      SUBROUTINE INVERT
C           COMPUTES THE INVERSE OF A 3 BY 3 MATRIX (W)
      DIMENSION CTPC(57,95),DASHS(33),DC(3),DCM(3,200,10),
     1  EVCM(3,3,10),JA(25),JS(10),N(10),PREC(10),
     2  TITLE(20,10),V(3),W(3,3)
      COMMON AZ,CONLEV,CTPC,DASHS,DC,DCM,EVCM,IOPT,IROT,
     1  JA,JCA,JCB,JS,K,N,NCOM,PHI,PHIB,PL,PREC,PSI,
     2  PSIB,THETA,THETAB,TITLE,V,W,IPUN
      DIMENSION CFM(3,3)
C           FIND COFACTORS OF W
      CFM(1,1) = W(2,2)*W(3,3) - W(2,3)*W(3,2)
      CFM(1,2) = W(2,3)*W(3,1) - W(2,1)*W(3,3)
      CFM(1,3) = W(2,1)*W(3,2) - W(2,2)*W(3,1)
      CFM(2,1) = W(3,2)*W(1,3) - W(3,3)*W(1,2)
      CFM(2,2) = W(3,3)*W(1,1) - W(3,1)*W(1,3)
      CFM(2,3) = W(3,1)*W(1,2) - W(3,2)*W(1,1)
      CFM(3,1) = W(1,2)*W(2,3) - W(1,3)*W(2,2)
      CFM(3,2) = W(1,3)*W(2,1) - W(1,1)*W(2,3)
      CFM(3,3) = W(1,1)*W(2,2) - W(1,2)*W(2,1)
C           FIND DETERMINANT OF W
      DET = 0.0
  101 DET = DET + W(1,IA) * CFM(1,IA)
C           FIND INVERSE OF W
      DO 102 IA=1,3
      DO 102 IB = 1,3
  102 W(IA,IB) = CFM(IB,IA)/DET
      RETURN
      END
```

```
      SUBROUTINE TRANSF
C          ROUTINE TO TRANSFORM A 3 ELEMENT ROW
C          VECTOR (V) CONTAINING DIRECTION COSINES, BY
C          A 3 BY 3 ROTATION MATRIX (W). THE FIRST
C          INDEX OF W IS THE ROW NUMBER AND THE SECOND
C          THE COLUMN NUMBER.
C          THE TRANSFORMED VECTOR (V) IS ADJUSTED TO
C          FALL IN THE LOWER HEMISPHERE
      DIMENSION CTPC(57,95),DASHS(33),DC(3),DCM(3,200,10),
     1  EVCM(3,3,10),JA(25),JS(10),N(10),PREC(10),
     2  TITLE(20,10),V(3),W(3,3)
      COMMON AZ,CONLEV,CTPC,DASHS,DC,DCM,EVCM,IOPT,IROT,
     1  JA,JCA,JCB,JS,K,N,NCOM,PHI,PHIB,PL,PREC,PSI,
     2  PSIB,THETA,THETAB,TITLE,V,W,IPUN
      DIMENSION U(3)
C          TRANSFER V TO U
  100 U(IA) = V(IA)
C          CARRY OUT TRANSFORMATION
      DO 101 IA = 1,3
      V(IA) = 0.0
      DO 101 IB = 1,3
  101 V(IA) = V(IA) + U(IB) * W(IB,IA)
C          CHECK LOWER HEMISPHERE POSITION
      IF (V(3) .GE. 0.0) RETURN
      DO 102 IA = 1,3
  102 V(IA) = -V(IA)
      RETURN
      END
```

LIST OF REFERENCES

ALEXANDER, F.E.S. 1936. The Aymestry Limestone of the main outcrop. Q. Jl geol. Soc. Lond. 92, 103-115.

ALLEN, J.R.L. 1960. The Mam Tor Sandstones: A 'turbidite' facies of the Namurian deltas of Derbyshire, England. J. Sedim. Petrol. 30, 193-208.

---- 1963. Depositional features of Dittonian rocks: Pembrokeshire compared with the Welsh Borderland. Geol. Mag. 100, 385-400.

---- 1970. Physical processes of sedimentation. George Allen & Unwin, 248pp.

---- & BANKS, N.L. 1972. An interpretation and analysis of recumbent-folded deformed cross bedding. Sedimentology 19, 257.

ALLENDER, R. 1959. On the stratigraphy and structure of an area of Ludlovian and Lower Downtonian rocks near Bishops Castle, Shropshire. Ph.D. Thesis, Univ. of Wales.

----, HOLLAND, C.H., LAWSON, J.D., WHITAKER, J.H.McD. & WALMSLEY, V.G. 1960. The summer field meeting at Ludlow. Proc. geol. Ass. 71, 209-32.

ANDRESEN, A. & BJERRUM, L. 1967. Slides in subaqueous slopes in loose sand and silt. In 'Marine Geotechnique' ed. Richards, A., Univ. Ill. Press.

AUDLEY-CHARLES, M.G. 1965. A Miocene gravity slide deposit from Eastern Timor. Geol. Mag. 102, 267-276.

BAILEY, E.B., COLLET, L.W. & FIELD, R.M. 1928. Palaeozoic submarine landslips near Quebec City. J. Geol. 36, 577-614.

---- & WEIR, J. 1932. Submarine faulting in Kimmeridgian times - East Sutherland. Trans. R. Soc. Edinb. 57, 429-454.

BAILEY, R.J. 1962. Sedimentation and facies change in the Ludlovian of South Cehtral Wales and the adjacent Borderland. Ph.D. Thesis., Univ. of Birmingham.

---- 1964. A Ludlovian facies boundary in South Central Wales. Geol. J. 4, 1-19.

---- 1966. Note on crinkle marks as palaeoslope indicators. Bull. Ludlow Res. Gp 13, 10-11.

---- 1967. Palaeocurrents and palaeoslopes: A discussion. J. sedim. Petrol. 37, 1252-5.

---- 1969. Ludlovian sedimentation in South Central Wales. In 'The Precambrian and Lower Palaeozoic rocks of Wales' ed. Wood, A.

BALDRY R.A. 1938. Slip planes and breccia zones in the Tertiary rocks of Peru. Q.Jl geol. Soc. Lond. 94, 347-58.

BALLANCE, P.F. 1964. The sedimentology of the Waitemata Groupin the Takapuna section, Auckland. N.Z. Jl Geol. Geophys. 7, 466-99.

BALLARD, J.A. 1966. Structure of the lower continental rise hills of the Western North Atlantic. Geophysics 31, 506-23.

BARANOWSKI, Z. 1971. Gravity submarine mass movements in the epimetamorphic complex of the Kaczawa Mts. Bull. Acad. pol. Sci. Sér. Sci. géol. géogr. 19, 277-9.

BASSETT D.A. 1963. The Welsh Palaeozoic geosyncline: A review of recent work on stratigraphy and sedimentation. In 'The British Caleconodes' ed. Johnson, M.R.W. et al. 35-39.

BEETS, C. 1946. Miocene submarine disturbances of strata in Northern Italy. J. Geol. 54, 229-45.

---- 1953. Slumping in Miocene deposits at Hurghada, Red Sea district Egypt. Geologie Mijnb. 15, 321-5.

BELDERSON, R.H. & STRIDE, A.H. 1969. The shape of submarine canyon heads revealed by Asdic. Deep Sea Res. 16, 104.

BLANC, J.J. 1972. 'Slumpings' et figures sedimentaires dans la Cretacé superieur du bassin du Beausset, France. Sed. geol. 7, 47-64.

BOSWELL, P.G.H. 1926. The geology of the eastern part of the Denbighshire moors. Q. Jl geol. Soc. Lond. 82, 556-85.

---- 1928. The Salopian rocks and tectonics of the district southwest of Ruthin (Denbighshire). Q. Jl Geol. Soc. 83, 689-710.

---- 1932. On the occurrence and significance of an area of imbrication in the Ludlow rocks of the Denbighshire moors. Proc. Lpool geol. Soc. 16, 18-32.

---- 1935a. The geology of North-western Denbighshire. Proc. geol. Ass. 46, 152-86.

---- 1935b. Report of Easter Field Meeting, 1935, North-western Denbighshire. Proc. geol. Ass. 46, 193-202.

---- 1937. The tectonic problems of an area of Salopian rocks in N.W. Denbighshire. Q. Jl geol. Soc. Lond. 93, 284-321.

---- 1942. The Wenlock and Ludlow rocks of the district around Gwytherin, NW. Denbighshire. Proc. Lpool. geol. Soc. 18, 86-100.

---- 1943. The Salopian rocks and geological structure of the country around Eglwys-fach and Glan Conway, N.W. Denbighshire. Proc. geol. Ass. 54, 93-112.

---- 1949. The middle Silurian rocks of North Wales. Edward Arnold, London. 448pp.

---- 1953. The alleged subaqueous sliding of large sheets of sediment in the Silurian rocks of North Wales. Lpool Manchr geol. J. 1, 148-152.

---- 1961. The case against a Lower Palaeozoic geosyncline in Wales. Lpool Manchr geol. J. 2, 612-625.

---- & DOUBLE, I.S. 1938. The Ludlow rocks and structure of the country in the neighbourhood of Llanfair Talhaiarn and Llansannan, Denbighshire. Proc. Lpool geol. Soc. 17, 277-311.

---- & ---- 1940. The geology of an area of Salopian rocks west of the Conway Valley in the neighbourhood of Llanrwst, Denbighshire. Proc. Geol. Ass. 51, 151-187.

BRADLEY, W.H. 1931. Origin and microfossils of the Oil Shale of the Green River formation of Colorado and Utah. Prof. Pap. U.S. geol. Surv. 168.

BROWN, C.B. 1938. On the theory of gravitational sliding applied to the Tertiary of Ancon, Equador. Q. Jl geol. Soc. 94, 359-70.

BROWN, T.C. 1913. Notes on the origin of certain Palaeozoic sediments, illustrated by the Cambrian and Ordovician rocks of Center County, Pennsylvania. J. Geol. 21, 232-5.

CASAGRANDE, A. 1936. Characteristics of cohesionless soils affecting the stability of slopes and earth fills. J. Boston Soc. civ. Engrs. 21, 276-83.

CASTRO, G. 1969. Liquefaction of sands. Ph.D. Thesis, Harvard Univ.

CHAMBERLAIN, T.K. 1964. Mass transport of sediment in the heads of Scripps submarine canyon, California. In 'Papers in Marine Geology', ed. Miller, R.L., 42-64.

CHENOWETH, P.A. 1952. Statistical methods applied to Trentonian stratigraphy in New Yory. Bull. geol. Soc. Am. 63, 521-60.

CLIFF, R.A., NORRIS, R.J., OXBURGH, E.R., & WRIGHT, R.C. 1971. Structural, Metamorphic and Geochronological studies in the Reisseck and southern Ankogel groups, the Eastern Alps. Jb. geol. Bundesanst., Wien. 114, 121-272.

CLINE, L.M. & LAURY, R.L. 1968. Preservation of rotational slump blocks in the Pennsylvanian of Southern Iowa. Abstracts Geol. Soc. Am., Spec. Pap. 121, 391.

COBBOLD, P.R., COSGROVE, J.W. & SUMMERS, J.M. 1971. Development of internal structures in deformed anisotropic rocks. Tectonophysics. 12, 23-53.

COCKS, L.R.M., HOLLAND, C.H., RICKARDS, R.B. & STRACHAN, I. 1971. A correlation of Silurian rocks in the British Isles. Jl. geol. Soc. Lond. 127, 103-36.

CORBETT, K.D. 1973. Open-cast slump sheets and their relationship to sandstone beds in an upper Cambrian flysch sequence, Tasmania. J. sedim. Petrol. 43, 147-159.

COULTER, H.W. & MIGLIACCIO, R.R. 1966. Effects of the earthquake of March 27, 1964 at Valdez, Alaska. Prof. Pap. U.S. geol. Surv. 542C.

COX, D.R. & LEWIS, P.A.W. 1966. The statistical analysis of a series of events. Methuen, London. 285pp.

CROWELL, J.C. 1957. Origin of pebbly mudstone. Bull. geol. Soc. Am. 68, 993-1010.

----, HOPE, R.A., KAHLE, J.E., OVENSHINE, A.T. & SAMS, R.H. 1966. Deep-water sedimentary structures, Pliocene Pico Formation, Santa Paula Creek, Ventura Basin, California. Spec. Rep. Calif. St. Min. Bur. 89, 40pp.

CUMMINS, W.A. 1957. The Denbigh Grits; Wenlock greywackes in Wales. Geol. Mag. 94, 433-51.

---- 1959a. The Nantglyn Flags; Mid-Salopian basin facies in Wales. Lpool Manchr geol. J. 2, 159-67.

---- 1959b. The Lower Ludlow Grits in Wales. Lpool Manchr geol. J. 2, 168-79.

---- 1969. Patterns of sedimentation in the Silurian rocks of Wales. In 'Precambrian and Lower Palaeozoic rocks Wales' Ed. Wood, A. Univ. of Wales Press, Cardiff. 461pp.

CURRAY, J.R. 1965. Structure of the continental margin off Central California. Trans. N.Y. Acad. Sci. (II) 27, 794-801.

DALEY, B. 1972. Slumping and micro-jointing in an Oligocene lagoonal limestone. Sediment. Geol. 7, 35-46.

DEAN, W.T. 1964. The geology of the Ordovician and adjacent strata in the southern Caradoc district of Shropshire. Bull. Br. Mus. nat. Hist. A9, 259-256.

DE LA BECHE, H.T. 1846. On the formation of the rocks of South Wales and South Western England. Mem. geol. Surv. U.K. i.

DE TERRA, H. 1931. Structural features of gliding strata. Am. J. Sci. (5) 21, 204-13.

DILL, R.F. 1964. Sedimentation and erosion in Scripps submarine canyon head. In 'Papers in Marine Geology' Ed. Miller, R.L. 23-41.

DIMITRIJEVIC, M.N. & DIMITRIJEVIC, M.D. 1970. Bed disturbances in the Pcinja Paleogene Formation, Southern Serbia. Acta geol. Hung. 14, 325-34.

DORREEN, J.M. 1951. Rubble bedding and graded bedding in the Talara Formation of Northwestern Peru. Bull. Am. Ass. Petrol. Geol. 35, 1829-49.

DOTT, R.H. 1955. (Abs) Eocene submarine slumping and graded bedding at Coos Bay, Oregon. Bull. geol. Soc. Am. 66, 1552.

---- 1963. Dynamics of subaqueous gravity depositional processes. Bull. Am. Ass. Petrol. Geol. 47, 104-28.

DUNNINGTON, H.V. 1945. Contemporaneous submarine slumping in the Embsay Limestone Series of the Skipton Anticline. Proc. Yorks. geol. Soc. 25, 239-47.

DZULYNSKI, S. 1963. Directional studies in Flysch. Studia geol. pol. 12, 136pp.

---- & SLACZKA, A. 1958. Directional structures and sedimentation of the Krosno beds (Carpathian Flysch). Roczn. pol. Tow. geol. 28, 205-60.

---- & WALTON, E.K. 1965. Sedimentary features of flysch and greywackes. Devs. in Sedimentology 7.

EARP, J.R. 1938. The higher Silurian rocks of the Kerry district, Montgomeryshire. Q. J. geol. Soc. Lond. 94, 125-60.

---- 1940. The geology of the south western part of Clun Forest. Q. J. geol. Soc. Lond. 96, 1-11.

EMERY, K.O. & TERRY, R.D. 1956. A submarine slope off southern California. J. Geol. 64, 271-80.

EWING, J., EWING, M. & LEYDEN. 1966. Seismic profiler survey of Blake Plateau. Bull. Am. Ass. Petrol. Geol. 50, 1948-71.

FAIRBRIDGE, R.W. 1947. Possible causes of intraformational disturbeances in the Carboniferous varve rocks of Australia. J. Proc. R. Soc.N. S.W. 81, 99-121.

FERM, J.C. & HUDDLE, J.W. 1955. (Abs) Slumps and mudflows in rocks of Pennsylvanian age in the Appalachian Plateau. Bull. geol. Soc. Am. 66, 1557.

FISHER, R.A. 1953. Dispersion on a sphere. Proc. R. Soc. A 217, 295-305.

FISHER, R.V. 1971. Features of coarse grained, high concentration fluids and their deposits. J. sedim. Petrol. 41, 916-27.

FITCH, F.J., MILLER, J.A. & BROWN, P.E. 1964. Age of Caledonian metamorphism and orogeny in Britain. Nature,Lond. 203, 275-8.

FLEUTY, M.J. 1964. The description of folds. Proc.geol. Ass. 75, 461-92.

FLINN, D. 1962. On folding during three-dimensional progressive deformation. Q. J. geol. Soc. Lond. 118, 385-443.

GEALY, B.L. 1955. Topography of the continental slope in Northwest Gulf of Mexico. Bull. geol. Soc. Am. 66, 203-28.

GIBSON, R.E. 1958. The progress of consolidation in a clay layer increasing in thickness with time. Géotechnique 8, 171-82.

GRABAU, A.W. 1913. Principles of stratigraphy. Seiler & Co. N.Y. 1185pp.

GRANT-MACKIE, J.A. & LOWRY, D.C. 1964. Upper Triassic rocks of Kiritehere, S.W. Auckland, New Zealand: Part I; Submarine slumping of Norian strata. Sedimentology 3, 296-317. *

GRAY, H.H. & ARNOLD, D.E. 1952. Penecontemporaneous erosional slump structure near Mineral City, Ohio. Ohio J. Sci. 52, 261-6. *

GREGORY, M.R. 1969. Sedimentary features and penecontemporaneous slumping in the Waitemata Group, Whangaparaoa Peninsula, North Auckland, New Zealand. N.Z. Jl Geol. Geophys. 12, 248-82. *

GREIG, D.C., WRIGHT, J.E., HAINS, B.A. & MITCHELL, G.H. 1968. Geology of the country around Church Stretton, Craven Arms, Wenlock Edge and Brown Clee. Mem. geol. Surv. U.K. 166.

GRIFFIN, J.R. 1970. Prelithification slump structures in Middle Silurian rocks of Central Maine (Abs). Abs. geol. Soc. Am. 2(7), 562. *

GRZYBEK, K. & HALICKI, B. 1958. Submarine slides in the Podhale Flysch (Carpathians). Acta geol. pol. 8, 411-50. *

GUTENBERG, B. & RICHTER, C.F. 1942. Earthquake magnitude, intensity, energy and acceleration. Bull. seism. Soc. Am. 32, 163-91.

HAAF, E. TEN. 1959. Graded beds of the Northern Appenines. Ph.D. Thesis. Univ. of Groningen 102pp.

HADDING, A. 1931. On subaquoues slides. Geol. För. Stockh. Förh. 53, 377-93.

HAHN, F.F. 1913. Untermeerische Gleitung bei Trenton Falls (Nordamerika) und ihr Verhältnis zu ähnlichen Storungsbildern. Neues Jb. Miner. Geol. Paläont. Beil Bd. 36, 1-41.

HALLAM, A. 1960. The White Lias of the Devon Coast. Proc. geol. Ass. 71, 47-60. *

HANSEN, E. 1965. Methods of deducing slip line orientations from the geometry of folds. Yb. Carnegie Instn Wash. 65, 387-405.

---- 1971. Strain Facies. George Allen & Unwin, London and Springer-Verlag, Berlin. 207pp.

HEEZEN, B.C. & DRAKE, C.L. 1964. Grand banks slump. Bull. Am. Ass. Petrol. Geol. 48, 221-5.

---- & EWING, J. 1952. Turbidity currents and submarine slumps, and the 1929 Grand Banks earthquake. Am. J. Sci. 250, 849-73.

HEIM, A. 1908. Ueber Rezente und Fossile Subaquatische Rutschungen und deren Lithologische Bedeutung. Neues Jb. Miner. Geol. Paläont. Abh. 2, 136-57.

HELWIG,J. 1970. Slump folds and early structures. J. Geol. 78, 172-87. *

HENDERSON, S.M.K. 1935. Ordovician submarine disturbances in the Girvan district. Trans. R. Soc. Edinb. 58, 487-509.

HOLLAND, C.H. 1959a. The Ludlovian and Downtonian rocks of the Knighton district, Radnorshire. Q. Jl geol. Soc. Lond. 114, 449-82.

---- 1959b. On convolute bedding in the lower Ludlovian rocks of NE Radnorshire. Geol. Mag. 96, 230-7.

---- 1969. The Welsh Silurian geosyncline in its regional context. In 'The Precambrian and Lower Palaeozoic rocks of Wales'. Ed. Wood, A. 203-17.

---- & LAWSON, J.D. 1963. Facies patterns in the Ludlovian of Wales and the Welsh Borderland. Lpool Manchr geol. J. 3, 269-88.

----, ---- & WAIMSLEY, V.G. 1963. The Silurian rocks of the Ludlow district, Shropshire. Bull. Br. Mus. nat. Hist. A 8, 95-171.

HOORN, B. VAN. 1970. Sedimentology and palaeogeography of an Upper Cretaceous turbidite basin in the South Central Pyrenees, Spain. Leid. geol. Meded. 45, 73-154. *

HORNE, G.S. 1969. Early Ordovician chaotic deposits in the Central Volcanic Belt of Northeastern Newfoundland. Bull. geol. Soc. Am. 80, 2451-64. *

---- 1970. Complex volcanic-sedimentary patterns in the Magog belt of Northeastern Newfoundland. Bull. geol. Soc. Am. 81, 1767-88. *

HOUGH B.K 1957 Basic Soils Engineering - Ronald Press N.Y

HUBBARD, W.F. & SHERIDAN, D.J.R. 1965. The Lower Carboniferous stratigraphy of some coastal exposures in Co. Sligo, Ireland. Scient. Proc. R. Dubl. Soc. A 2, 189-195. *

HUBERT, J.F. 1966. Sedimentary history of Upper Ordovician geosynclinal rocks, Girvan, Scotland. J. sedim. Petrol. 36, 677-99. *

---- 1968. Currents and slopes in flysch basins : a discussion. J. sedim. Petrol. 38, 1390-3.

HUDLESTON, P.J. 1973a. Fold morphology and some geometrical implications of theories of fold development. Tectonophysics 16, 1-46.

---- 1973b. An analysis of single layer folds developed experimentally in viscous media. Tectonophysics 16, 189-214.

---- 1973c. An analysis and interpretation of minor folds in the Moine rocks of Monar, Scotland. Tectonophysics 17, 89-132.

HUDSON, R.G.S. & DUNNINGTON, H.V. 1940. Slip bedding in the Elland Flags. Naturalist, Hull Nov 1940, 265-9.

IRVING, E. 1964. Palaeomagnetism. Wiley N.Y. 379pp.

JAMES, D.M.D. 1972. Sedimentation across an intrabasinal slope; The Garnedd-wen Formation (Ashgillian) West Central Wales. Sediment. Geol. 7, 291-307.

JOHNSON, M.A. 1964. Turbidity Currents. Oceanogr. mar. Biol. Ann. Rev. (Ed. Barnes, H.) 2, 31-43.

JONES, B.G. 1969. Sedimentology of the Waitemata Group in the Stanley Point-Devonport area, Auckland, New Zealand. N.Z. Jl Geol. Geophys. 12, 215-47.

JONES, O.T. 1927. The foundations of the Pennines. J. Manchr geol. Ass. 1, 5-14.

---- 1936. (Abstract and discussion) On the sliding or slumping of submarine sediments in Denbighshire, N. Wales, during the Ludlow Period. Abstr. Proc. geol. Soc. Lond. 1315, 110-5.

---- 1937. On the sliding or slumping of submarine sediments in Denbighshire, N. Wales, during the Ludlow period. Q. Jl geol. Soc. Lond. 93, 241-282.

---- 1938. On the evolution of a geosyncline. Q. Jl geol. Soc. Lond. 94, lx-cx.

---- 1939. The geology of the Colwyn Bay district : Astudy of submarine slumping during the Salopian period. Q. Jl. geol. Soc. Lond. 95, 335-82.

---- 1943. A comment on a new area of slumped beds in Denbighshire. Geol. Mag. 80, 66-8.

---- 1947. The geology of the Silurian rocks west and south of the Carneddau Range, Radnorshire. Q. Jl geol. Soc. Lond. 103, 1-36.

---- 1953a. On submarine slumping in the Lower Ludlow rocks of North Wales. Geol. Mag. 90, 220-1.

---- 1953b. The use of graptolites in geological mapping. Lpool Manchr geol. J. 1, 246-60.

---- 1954. The characteristics of some lower Palaeozoic marine sediments. Proc. R. Soc. A 222, 327-332.

---- 1956. The geological evolution of Wales and the adjacent areas. Q. Jl geol. Soc. 111, 323-51.

KELLING, G. & WILLIAMS, B.P.J. 1966. Deformation structures of sedimentary origin in the Lower Limestone shales (Basal Carboniferous) of south Pembrokeshire, Wales. J. sedim. Petrol. 36, 927-939.

---- & WOOLLANDS, M.A. 1969. The stratigraphy and sedimentation of the Llandovery rocks of the Rhayader district. In 'The Precambrian and lower Palaeozoic rocks of Wales' Ed. Wood,A.

KENT, P.E. 1945. Contmeporaneous disturbances in lacustrine beds in * Kenya. Geol. Mag. 82, 130-5.

KING, P.B. 1948. Geology of the southern Guadalupe Mountains, Texas. * Prof. Pap. U.S. geol. Surv. 215.

KING, R.F. & REES, A.I. 1962. The measurement of the anisotropy of magnetic susceptibility of rocks by the Torque method. J. geophys. Res. 67, 1565-72.

KIRK, N.H. 1947. Geology of the anticlinal disturbance of Breconshire and Radnorshire : Port Faen to Presteigne. Ph. D. Thesis, Cambridge.

---- 1951. The Silurian and Downtonian rocks of the anticlinal disturbance of Breconshire and Radnorshire ; Port Faen to Presteigne. Proc. geol. Soc. 1474, 72-3.

---- 1952. The tectonic structure of the anticlinal disturbance of Breconshire and Radnorshire ; Port Faen to Presteigne. Proc. geol. Soc. 1485, 87-91.

KLEIN, G.DeV., DEMELO, U., & FAVERA, J.C.della. 1972. Subaqueous gravity processes on the front of Cretaceous deltas, Reconcavo basin Brazil. Bull. geol. Soc. Am. 83, 1469-92.

KOCH, G.S. & LINK, F. 1971. Statistical analysis of geological data. Vol. 2.

KOPPEJAN, A.W., WAMELAN, B.M. & WEINBERG, L.J.H. 1948. Coastal flow slides in the Dutch province of Zeeland. Proc.2nd Int. Conf. Soil. Mech. 5, 89-96.

KSIAZKIEWICZ, M. 1958. Submarine slumping in the Carpathian Flysch. * Roczn. pol. Tow. geol. 28, 123-150.

KUENEN, P.H. 1948. Slumping in the Carboniferous rocks of Pembroke- * shire. Q. Jl. geol. Soc. 104, 365-85.

---- 1952. Estimated size of the Grand Banks turbidity current. Am. J. Sci. 250, 874-884.

---- 1956. The difference between sliding and turbidity flow. Deep Sea Res. 3, 134-9.

LAIRD, M.G. 1968. Rotational slumps and slump scars in Silurian rocks * Western Ireland. Sedimentology 10, 111-20.

LAJOIE, J. 1972. Slump fold axis orientations : An indication of palaeoslope ?. J. sedim. Petrol. 42, 584-6.

LAMONT, A. 1936. Palaeozoic seismicity. Nature Lond. 138, 243-4.

---- 1936b. Reinterpretation of the Bray Series at Howth, Irish Free State. Geol. Mag. 73, 546-50.

---- 1938. Contemporaneous slumping and other problems at Bray Series, Ordovician and Lower Carboniferous horizons in Co. Dublin. Proc. R. Ir. Acad. 45b 1.

---- 1941. Irish submarine disturbances. Quarry Mgrs' J. 24, 123-7, 150-1.

LAWSON,J.D., STRAW, S.H., WALMSLEY, V.G., HOLLAND, C.H. & PRICE, J.H. 1956. The Ludlovian rocks of the Welsh Borderland. Advmt Sci., Br. Ass. 12, 563-70.

LEITCH, E.C. & MAYER, W. 1969. Mass movement phenomena in an Upper * Carboniferous greywacke argillite sequence in North-eastern New South Wales. N.Z. Jl Geol. Geophys. 12, 156-71.

LEWIS, K.B. 1971. Slumping on a continental slope inclined at 1° - 4°. Sedimentology 16, 97-110.

LINDSAY, J.F. 1966. Carboniferous subaqueous mass-movement in the * Manning-Macleay Basin, Kempsey NSW. J. sedim. Petrol. 36, 719-32.

LOGAN, W. 1863. Geology of Canada. Rep. Prog. Can. geol. Surv. 983pp.

LOUDON, T.V. 1964. Computer analysis of orientation data in structural geology. Tech. Rep. NWest Univ. 13, 129pp.

MARSCHALKO, R. 1961. Sedimentologic investigation of marginal litho- * facies in flysch of Central Carpathians. Geol. Pr. Bratisl. 60, 197-230.

---- 1964. Sedimentary structures and palaeocurrents in the marginal lithofacies of the Central Carpathian flysch. In 'Turbidites' Ed. Bouma, A.H. et al. 106-26.

---- 1970. The origin of disturbed structures in Carpathian turbidites.* Sediment. Geol. 4, 5-18.

MATTHEWS, P.E. 1961. Slump structures in the Table Mountain Series of * Natal. Trans. geol. Soc. S. Afr. 64, 55-71.

McBRIDE, E.F. 1962. Flysch and associated beds of the Martinsburg * Formation (Ordovician), Central Appalachians. J. sedim. Petrol. 32, 39-91.

McGEE, W.J. 1891. The Pleistocene history of northeastern Iowa. Rep. U.S. geol. Surv. 11, 199-571.

MENARD, H.W. 1964. Marine geology of the Pacific. McGraw Hill, N.Y.

MIDDLETON, G.V. 1966. Experiments on density and turbidity cuurents: I Motion of the head., II Uniform flow of density currents. Can. J. earth Sci. 3, 523-46, 627-37.

MIKULENKO, K.N. (1967) Submarine slump structures in Palaeocene and Eocene deposits. Int. Geol. Rev. 9, 1353-64.

MILLER, W.J. 1908. Slightly folded between non-folded strata at Trenton Falls, New York. J. Geol. 16, 428-33.

---- 1915. Notes on the intraformational contorted strata at Trenton Falls. Bull. N.Y. St. Mus. 177, 135-43.

---- 1922. Intraformational corrugated rocks. J. Geol. 30, 587-610.

MILNE, J. 1897. Suboceanic changes. Geogr. J. 10, 129-46, 259-85.

MOORE, D.G. 1961. Submarine slumps. J. sedim. Petrol. 31, 343-57.

---- & CURRAY, J.R. 1963. Sedimentary framework of sedimentary margin off Norfolk, Virginia and Newport, Rhode Island. Bull. Am. Ass. Petrol. Geol. 47, 2051-4.

MORGENSTERN, N.R. 1967. Submarine slumping and the initiation of turbidity currents. In 'Marine Geotechnique' Ed. Richards, A.F. Univ. Illonois Press. 189-220.

MORRIS, R.C. 1971. Classification and interpretation of disturbed bedding types in Jackfork flysch rocks (Upper Missisipian) Ouachita Mntns, Arkansas. J. sedim. Petrol. 41, 410-24.

MURCHISON, R.I. 1839. The Silurian System. London.

MURPHY, M.A. & SCHLANGER, S.O. 1962. Sedimentary structures in Ilhas and Sao Sebastio Formations (Cretaceous), Reconcavo Basin, Brazil. Bull. Am. Ass. Petrol. Geol. 46, 457-77.

NAGTEGAAL, P.J.C. 1963. Convolute laminations, metadepositional ruptures and slumping in an exposure near Pobla de Segur, Spain. Geologie Mijnb. 42, 363-74.

NEWELL, N.D., RIGBY, J.K., FISCHER, A.G., WHITEMAN, A.J., HICKOX, J.E. & BRADLEY, J.S. 1953. The Permian reef complex of the Guadalupe Mountains Region, Texas and New Mexico. Freeman S.F. 236pp.

NICHOLS, D.R. 1960. Slump structures in Pleistocene lake sediments, Copper River basin, Alaska. Prof. Pap. U.S. geol.Surv. 400B, 353-4.

NORTON, W.H. 1917. Studies for students - A classification of breccias. J. Geol. 25, 160-194.

PRENTICE, J.E. 1962. The sedimentation history of the Carboniferous in Devon. In 'Some aspects of the Variscan Fold Belt' Ed. Coe, K. 93-108.

PUGH, W.J. 1950. Recent work on the Lower Palaeozoic rocks. Advmt Sci., Br. Ass. 6, 203-12.

RADOMSKI, A. 1958. The sedimentological character of the Podhale flysch. Acta geol. pol. 8, 336-409.

RADWANSKI, A. & RONIEWICZ, P. (1962) Submarine slumping in the Famenian of the Holy Cross Mtns (Central Poland). Acta geol. pol. 12, 295-305.

RAMSAY, J.G. (1967) Folding and fracturing of rocks. McGraw Hill 568pp.

REIS, O.M. 1909. Beobachten ueber Schichter-Folge und Gesteins-ausbildungen in der Fränkischen Unteren und Mittleren Trias. I. Muschelkalk und Untere Lettenkohle. Geogn. Jh. 22, 1-285.

RETTGER, P.E. 1935. Experiments on soft-rock deformation. Bull. Am. Ass. Petrol. Geol. 19, 271-92.

RICE, R.C. 1939. Contorted bedding in the Trias of N.W. Wirral. Proc. Lpool geol. Soc. 17, 361-70.

RICE, R.J. 1969. Contorted drift at Blaby Brickpit, Leicestershire. Proc. geol. Ass. 80, 283-91.

RICH, J.L. 1950. Flow markings, groovings and itrastratal crumplings for recognition of slope deposits, with illustrations from Silurian rocks of Wales. Bull. Am. Ass. Petrol. Geol. 34, 717-41.

RIGBY, J.K. 1958. Mass movements in Permian rocks of Trans-Pecos, Texas. J. sedim. Petrol. 28, 298-315.

ROBERSON, M.I. 1964. Continuous seismic profiler survey of Oceanographer, Gilbert and Lydonia submarine canyons, Georges Bank. J. geophys. Res. 69, 4779-89.

ROBERTS, D.G. 1972. Slumping on the eastern margin of the Rockall Bank, North Atlantic Ocean. Mar. geol. 13, 225-37.

---- & STRIDE, A.H. 1968. Late Tertiary slumping on the continental slope of Southern Portugal. Nature, Lond. 217, 48-50.

ROBINSON, E. 1967. Submarine slides in White Limestone Group, Jamaica. Bull. Am. Ass. Petrol. Geol. 51, 569-78.

ROSS, D.A. & SHOR, G.G. 1965. Reflection profiles across the middle America Trench. J. Geophys. Res. 70, 5551-72.

ROWA, P.E. & CLAY, C.S. 1967. Stratigraphy and structure along a continuous seismic reflection profile from Cape Hatteras, North Carolina, to the Bermuda Rise. J. geophys. Res. 72, 2107-30.

RYAN, W.B.F. & HEEZEN, B.C. 1965. Ionian Sea submarine canyons and the 1908 Messina turbidity current. Bull. geol. Soc. Am. 76, 915-32.

SANDERS, J.E. 1965. Primary sedimentary structures formed by turbidity currents and related resedimentation mechanisms. Spec. Publs. Soc. econ. Palaeont. Miner., Tulsa. 12, 192-219.

SCHOLL, D.W., BUFFINGTON, E.C. & HOPKINS, D.M. 1966. Exposure of basement rock on the continental slope of the Bering Sea. Science. N.Y. 153, 992-4.

SCOTT, K.M. 1966. Sedimentology and dispersal pattern of a Cretaceous flysch sequence, Patagonian Andes, southern Chile. Bull. Am. Ass. Petrol. Geol. 50, 72-107.

----- & DOTT, R.H. 1962. Eocene Palaeocurrent patterns in southwestern Oregon (Abs). Spec. Pap. geol. Soc. Am. 73, 236-7.

SEED, H.B. & LEE, K.L. 1966. Liquefaction of saturated sands during cyclic loading. Proc. Am. Soc. civ. Engrs. 92, SM6, 105-34.

SHACKLETON, R.M. & HARPER, J.C. 1940. An occurence of slumping in the Carboniferous Limestone at Lisnakea, Co, Fermanagh, N. Ireland. Proc. R. Ir. Acad. 46B, 22-4.

SHAWA, M.S. 1970. Upper Cretaceous depositional pattern, Coalinga Area, California. Bull. Am. Ass. Petrol. Geol. 54, 1296-1305.

SHEPHARD, F.P. 1951. Mass movements in submarine canyon heads. Trans. Am. geophys. Un. 32, 405-18.

SHERIDAN, D. 1972. Upper Old Red Sandstone and Lower Carboniferous of * the Slieve Beagh Syncline and its setting in the Northwest Carboniferous basin Ireland. Spec. Pap. geol. Surv. Irl. 2.

SKEMPTON, A.W. 1954. discussion on The structure of inorganic soil. Proc. Am. Soc. civ. Engrs. 80 (no. 478), .19. Proc. Inst. Civ. Engrs · 7 , 305-7

---- 1957. discussion on the planning and design of new Hong Kong airport

SMITH, D.B. 1970. Submarine slumping and sliding in the Lower Magnesian * Limestone of Northumberland and Durham. Proc. Yorks. geol. Soc. 38, 1-36.

SMITH, J.E. 1971. The dynamics of shale compaction and evolution of pore fluid pressures. J. Int. Ass. Math. Geol. 3, 239-63.

SPRENG, A.C. 1967. Slump structures, Fayetteville formation, North- * western Arkansas. J. sedim. Petrol. 37, 804-17.

STAUFFER, P.H. 1967. Grain-flow deposits and their implications. * Santa Inez Mountains, California. J. sedim. Petrol. 37, 487-508.

STRAATEN, L.M.J.U. VAN. 1950. Occurrence in Finland of structures due * to subaqueous sliding of sediments. Bull. Commn géol. Finl. 25, no. 144, 9-18.

STRAW, S.H. 1937. The higher Ludlovian rocks of the Builth district. * Q. Jl geol. Soc. Lond. 93, 406-56.

---- 1953. The Silurian succession at Cwm Craig Ddu (Breconshire). Lpool Manchr geol. J. 1, 208-19.

STRIDE, A.H., CURRAY, J.R., MOORE, D.G. & BELDERSON, R.H. 1969. Marine geology of the Atlantic continental margin of Europe. Phil. Trans. R. Soc. A 264, 31-75.

STURM, E. 1971. Subaqueous slump structures. Bull. geol. Soc. Am. 82, 481-3.

SUSSMILCH, C.A. & DAVID, T.W.E. 1920. Sequence, glaciation and correlation of the Carboniferous rocks of the Hunter River district NSW. J. Proc. R. Soc. N.S.W. 53, 246-338.

SZULCZEWSKI,M. 1968. Slump structures and turbidites in Upper Devonian * Limestones of the Holy Cross Mountains. Acta geol. pol. 18, 303-24.

TERZAGHI, K. 1957. Varieties of submarine slope failure. Pub. Norwn. Geotech. Inst. 25.

TYLER, J.H. 1972. Pigeon Point Formation : An Upper Cretaceous * shoreline succession, Central Californian coast. J. sedim. Petrol. 42, 537-57.

UCHUPI, E. 1967. Slumping on the continental margin SE of Long Island, New York. Deep Sea Res. 14, 635-9.

---- 1968. Seismic profiling survey of the East Coast submarine canyons. Part I. Wilmington, Baltimore, Washington and Norfolk Canyons. Deep Sea Res. 15, 613-6.

VAN DER LINGEN, G.J. 1969. The turbidite problem. N.Z. J. Geol. Geophys. 12, 7-50.

WALKER, R.G. 1970. Review of the geometry and facies organisation of turbidites and turbidite bearing basins. Spec. Pap. Geol. Ass. Can. 7, 219-251.

WALTHALL, B.H. 1967. Stratigraphy and structure, part of Athens * Plateau, Southern Ouachitas, Arkansas. Bull. Am. Ass. Petrol. Geol. 51, 504-28.

WARNER, J. 1969. FORTRAN IV program for construction of Pi diagrams with the Univac 1108 computer. Computer Contribs. Kansas. St. geol. Surv. 33.

WATERHOUSE, J.B. & BRADLEY, J. 1957. Redeposition and slumping in the * Cretaceo-Tertiary strata of S.E. Wellington. Trans. R. Soc. N.Z. 84, 519-48.

WATSON, G.S. 1966. The statistics of orientation data. J. Geol. 74, 786-97.

WEDD, C.B., SMITH, B. & WILLS, L.J. 1927. The geology of the country around Wrexham. Part I. Mem. geol. Surv. G.B. 121.

WHITAKER, J.H.McD. 1962. Geology of the country around Leintwardine, Herefordshire. Q. Jl geol. Soc. 118, 319-51.

WILLIAMS, B.J. & PRENTICE, J.E. 1957. Slump structures in the Ludlovian * rocks of North Herefordshire. Proc. geol. Ass. 68, 286-93.

WILLIAMS, E.G., GUBER, A.L. & JOHNSON, A.M. 1965. Rotational slumping * and the recognition of disconformities. J. Geol. 73, 534-7.

WILLIAMS, P.F., COLLINS, A.R. & WILTSHIRE, R.G. 1969. Cleavage and penecontemporaneous deformation structures in sedimentary rocks. J. Geol. 77, 415-425.

WILLS, L.J. & SMITH, B. 1922. The Lower Palaeozoic rocks of the Llangollen district, with special reference to the tectonics. Q. Jl geol. Soc. 78, 176-226.

WOOD, E.M.R. 1900. The Lower Ludlow formation and its graptolite fauna. Q. Jl geol. Soc. 56, 415-92.

WRIGHT, W.H. 1969. Phases of folding in the slate belt of West-central Vermont. Abs. geol. Soc. Am. 1, 64.

YAGISHITA, K. 1971. On microfabrics of slump fold of the Saukowa Anticline in Northern Fossa Magna, Central Japan. J. geol. Soc. Japan. 77, 779-90.

ZIEGLER, A.M. 1970. Geosynclinal development of the British Isles during the Silurian period. J. Geol. 78, 445-79.

ZINGG, T. 1935. Beitrag zur Scholteranalyse. Scweiz. miner. petrogr. Mitt. 15, 39-140.

MAP OF EAST CENTRAL WALES AND THE BORDERLAND SHOWING SLUMP SEQUENCES AND SLUMP LOCALITIES

SLUMP LOCALITIES

POST-SILURIAN (mainly Devonian)

LUDLOW SLUMP SEQUENCES

SILURIAN

LUDLOW

WENLOCK

LLANDOVERY

PRE-SILURIAN (mainly Ordovician)

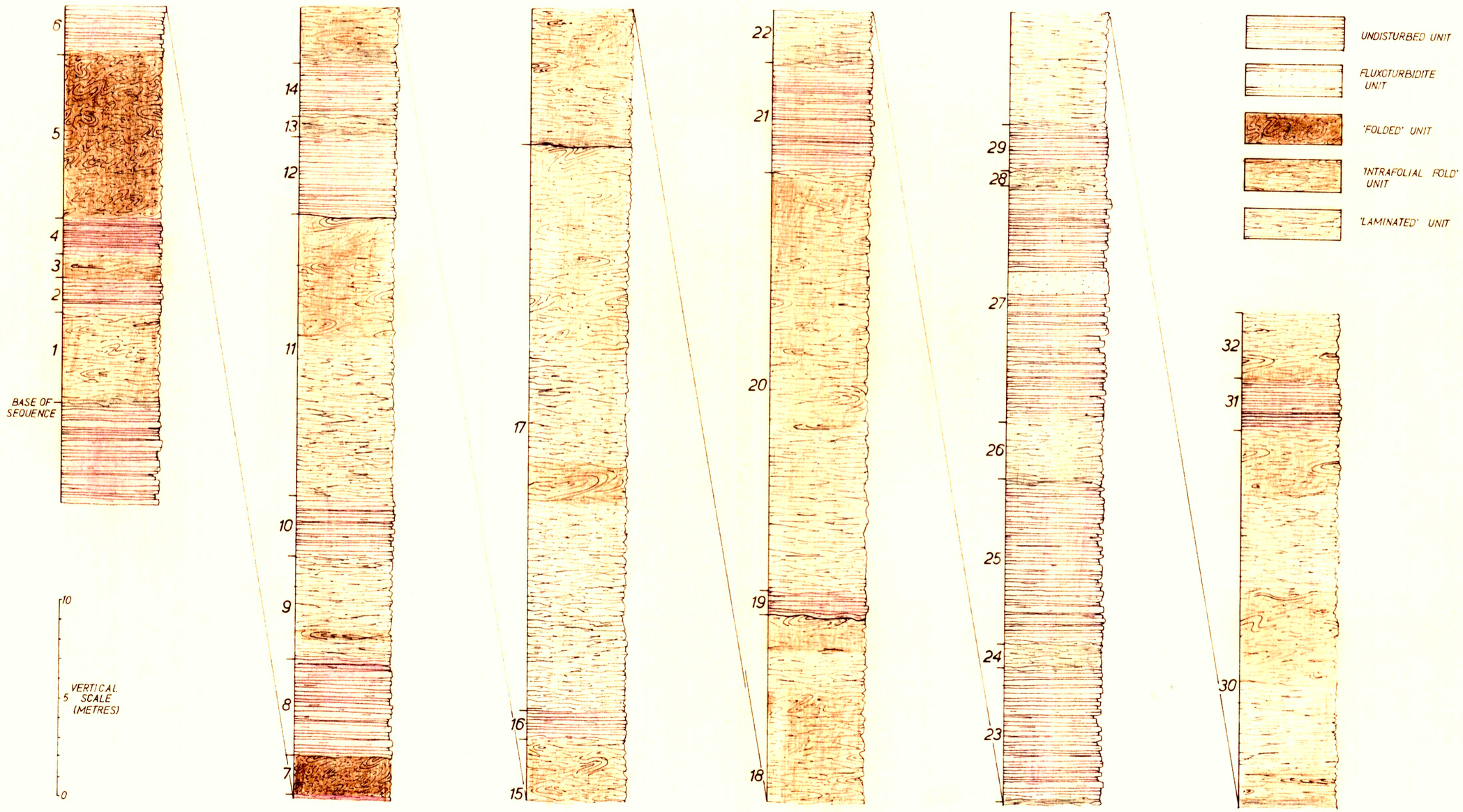
N

SCALE (kilometres)

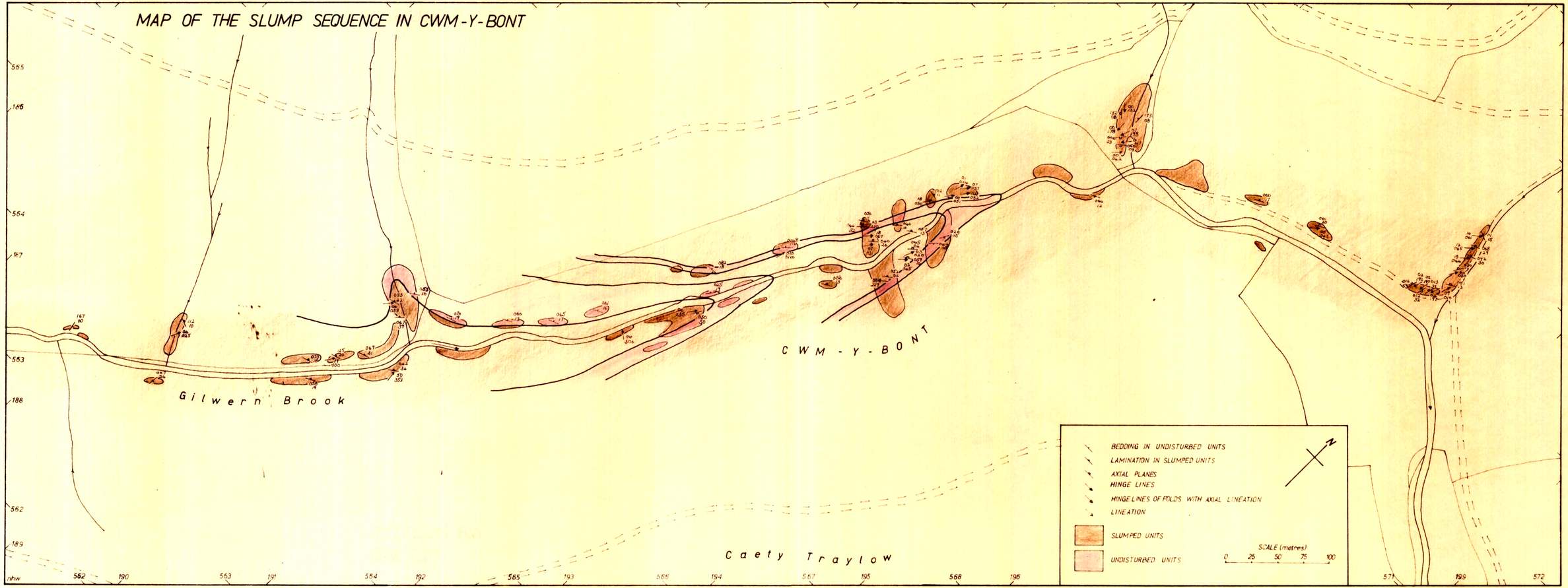
0 1 2 3 4 5

NEWTOWN
CAERWS
LLANDINAM
LLANIDLOES
CHURCH STOKE
BISHOPS CASTLE
CHURCH STRETTON
CRAVEN ARMS
LUDLOW
LEINTWARDINE
NEWCASTLE
CLUN
FELINDRE
BEGUILDY
LLANBADARN FYNYDD
LLANBISTER
LLANGUNLLO
KNIGHTON
RHAYADER
LLANDRINDOD WELLS
NEWBRIDGE ON WYE
BUILTH WELLS
NEW RADNOR
PRESTEIGNE
WIGMORE
BRIMFIELD
LEOMINSTER
KINGTON
SN 00 SO

SECTION THROUGH THE SLUMP SEQUENCE IN CWM BLITHUS



nhw


MAP OF THE SLUMP SEQUENCE IN CWM-Y-BONT
Gilwern Brook
CWM-Y-BONT
Caety Traylow
BEDDING IN UNDISTURBED UNITS
LAMINATION IN SLUMPED UNITS
AXIAL PLANES
HINGE LINES
HINGE LINES OF FOLDS WITH AXIAL LINEATION
LINEATION
SLUMPED UNITS
UNDISTURBED UNITS
SCALE (metres)
0 25 50 75 100
N


MAP OF THE SLUMP SEQUENCE IN THE TEME VALLEY
BEDDING IN UNDISTURBED UNITS
LAMINATION IN SLUMPED UNITS
AXIAL PLANES
HINGE LINES
HINGE LINES OF FOLDS WITH AXIAL LINEATION
LINEATION
SLUMPED UNITS
UNDISTURBED UNITS
SCALE (metres)
0 10 20 30 40 50
Cilfaesty Hill
River Teme
Ring Hole
Ddol